University of Alberta

Ubiquitin Activation by the *S. cerevisiae* Ubiquitin Activating Enzyme

By

J. Torin Huzil

A thesis submitted to the Faculty of Graduate Studies and Research in partial fulfillment of the requirements for the degree of Doctor of Philosophy

Department of Biochemistry

Edmonton, Alberta

Fall, 2003

Your file Votre référence
ISBN: 0-612-87994-1
Our file Notre référence
ISBN: 0-612-87994-1

University of Alberta

Library Release Form

Name of Author:	J. Torin Huzil
Title of Thesis:	Ubiquitin Activation by the *S. cerivisiae* Ubiquitin Activating Enzyme
Degree:	Doctor of Philosophy
Year this Degree Granted:	2003

J. Torin Huzil
415 Cricket Court
Edmonton, Alberta, Canada
T5T-2B2

Sept 29, 2003

University of Alberta

Faculty of Graduate Studies

The undersigned certify that they have read, and recommend to the Faculty of Graduate Studies and Research for acceptance, a thesis entitled Ubiquitin Activation by the *S. cerivisiae* Ubiquitin Activating Enzyme by J. Torin Huzil in partial fulfillment of the requirements for the degree of Doctor of Philosophy.

Supervisor: Dr. Michael J.Ellison

Dr. Hans J. Vogel

Dr. Mark Glover

Dr. Andrew MacMillan

Dr. D. Alan Underhill

Dated: Thursday, September 25, 2003

"Six by nine? Forty-two?
You know,
I've always felt that there was something fundamentally wrong with the Universe."

(Arthur Dent, 2 million BC)

Things on a small scale behave like nothing you have any direct experience about.
They do not behave like waves. They do not behave like particles.
They do not behave like clouds or billiard balls or weights on springs
or like anything you have ever seen.

(Richard Feynman, 1918-1988)

For Boo

Abstract

Proteins destined for degradation by the proteasome must first become tagged with chains of the small protein ubiquitin (Ub). This occurs through the covalent attachment of Ub to a lysine residue within the target protein. Ubiquitin activating enzyme (E1 or Uba1) is responsible for the initial, ATP-dependent, activation of Ub. This activation provides the required energy for Ub to become bound to the target protein through the action of Ub conjugating enzymes (E2s). The focus of this work was to explore the mechanism of Ub activation and the role of Uba1 in chain formation.

We have modeled the *S. cerevisiae* Uba1 active site domain, using the recently published structures of the Uba1 homologues *E. coli* MoeB and *H. sapiens* Uba3 as scaffolds. In addition, *in situ* NMR data of the interaction between the E2, Ubc1 and Ub was used to create a model of an E2~Ub thiolester. Using the Uba1 active site model and the Ubc1~Ub thiolester structure, we have examined the mechanism of Ub activation using dynamics and docking simulations.

To biochemically examine the role of the Uba1 active sites in Ub activation and its transfer to E2, we created mutations in Uba1 that correspond to the sites of Ub activation by ATP and Ub thiolester formation. These mutants and the model of the Uba1 active site, have allowed us to confirm the positions of the residues involved in ATP binding and thiolester formation and demonstrate the catalytic role that Uba1 may play in the formation of Ub chains.

Acknowledgements.

I would like to thank The Chemical Computing Group for supplying me with the Molecular Operating Environment and enough Demo keys to see me through my molecular modeling studies.

I would also like to thank the Medical Research Council of Canada for funding the first five years of my studies and Michael Ellison for the last. Thanks to Mark Glover and Andrew MacMillan for being a part of my committee throughout the years.

A huge thanks to Raj Pannu for the immeasurable assistance, numerous conversations and invigorating adventures, see you in NYC.

Most of all I would like to thank Tara McCready for all of her encouragement to finish this document and sticking by me while I did. Finally I would like to thank Marcia Craig and Christopher Ptak, without their help this thesis would have never been completed.

Table of Contents

List of Tables

List of Figures

Abbreviations

α	alpha
Å	angstrom
β	beta
Δ	deletion
°C	degrees Celsius
Ala or A	alanine
AMP	adenosine monophosphate
APC	anaphase promoting complex
APF-1	ATP dependent Proteolysis Factor 1
APF-2	ATP dependent Proteolysis Factor 2
Arg or R	arginine
Asn or N	asparagine
Asp or D	aspartic acid
ATP	adenosine triphosphate
BSA	bovine serum albumin
CBC	cullin-2 elongin complex
Cdc	cell division cycle
cdk	cyclin dependent kinases
cpm	counts per minute
CUP	copper inducible promoter
CYC	transcriptional terminator
Cys or C	cysteine
DNA	deoxyribonucleic acid
DTT	dithiothreitol
E. coli	*Escherichia coli*
E2	Ubiquitin Conjugating Enzyme
E3	Ubiquitin Protein Ligase
EDTA	ethylenediaminetetraacetic acid
FOA	5-fluoro-orotic acid
FPLC	fast performance liquid chromatography
G1	first growth phase of the cell cylcle
G2	second growth phase of the cell cycle
Gln or Q	glutamine
Glu or E	glutamic acid
Gly or G	glycine
HECT	Homologous to the E6-AP Carboxyl Terminus
HEPES	4-(2-hydroxyethyl)-1-piperazineethanesulfonic acid
His	histidine
HMCSA	hybrid Monte Carlo simulated annealing
hr	hour
HSQC	Heteronuclear Single Quantum Coherence
HTC	cultured hepatoma cells

Ile or I	isoleucine
INEPT	Insensitive Nuclei Enhanced by Polarization Transfer
K	kelvin
kCal	kilocalorie
kDa	kilodalton
k_{eq}	equilibrium constant
L	liter
LB	Luria-Bertani broth
Leu or L	leucine
Lys or K	lysine
μg	microgram
mg	milligram
min	minute
mL	millilitre
μM	micromolar
mM	millimolar
mol	mole
MSD	mean squared displacement
nM	nanomolar
NMR	Nuclear Magnetic Resonance Spectroscopy
PAGE	polyacrylamide gel electrophoresis
PCR	polymerase chain reaction
PEST	proline, glutamic acid, serine, threonine containing motif
pH	potential of hydrogen
PMSF	phenyl methyl sulfonyl fluoride
PPi	Inorganic Pyrophosphate
Pro or P	proline
ps	picosecond
RMSD	root mean squared deviation
rpm	revolutions per minute
S. cerevisiae	*Saccharomyces cerevisiae*
SCF	Skp1 Cdc53(cullin) F-box complex
SCR	structurally conserved regions
SD	synthetic defined
SDS	sodium dodecylsulfate
Ser or S	serine
Sumo	small Ubiquitin like modifier
TAT	tyrosine transaminase
TCA	trichloroacetic acid
Thr or T	threonine
Tris	tris(hydroxymethyl)aminoethane
Trp or W	tryptophan
tRNA	transfer ribonucleic acid
ts	temperature sensitive

Ub	ubiquitin
Uba1	ubiquitin activating enzyme
Uba1~Ub	Uba ubiquitin thiolester
Ubc	Ubiquitin Conjugating Enzyme
Ubc1~Ub	Ubc ubiquitin thiolester
Ubc1-Ub	Ubc ubiquitin conjugate
UBI4	ubiquitin gene
UBL	ubiquitin like protein
URA	uracil requiring
Val of V	valine
VDW	van der Waals
VR	variable regions

Software

ANAREA	Software which is incorporated in VADAR (Chapter 5).
BLAST	An internet server for performing homology searches (Chapter 2).
DISCOVER	Energy minimization and molecular dynamics program (Chapters 2, 3 and 5).
GETAREA	A program for determining molecular surface area (Chapter 2).
GRAMM	A program for performing rigid body docking (Chapter 2).
GRASP	A program for creating molecular surface representations (Chapter 3).
InsightII	A program for general visualization and molecular manipulation (Chapters 2, 3 and 5).
MacVector	A program for performing multiple sequence alignments (Chapter 2).
MOE	A program for general visualization and molecular manipulation (Chapters 2, 3 and 5).
Procheck	A protein structure analysis program (Chapter 2).
PyMol	A program for molecular visualization (Chapters 2, 3 and 5).
Swiss Model	An internet server for performing homology modeling (Chapters 2 and 5).
VADAR	A program for determining general properties of protein structures (Chapter 5).

Chapter 1

Selective Protein Degradation by the Ubiquitin-Proteasome Pathway

It is well established that proteins no longer required for normal cellular functions must be inhibited or eliminated in order for cell cycle progression to proceed. This occurs via a number of tightly regulated post-translational processes that can block the function of a protein during periods when it is not required, or can result in removal of the protein by degradation. This chapter will review the multiple mechanisms by which protein silencing and degradation are achieved within eukaryotic cells, and will focus on the biology and biochemistry of one specific mechanism known as protein ubiquitination.

Proteolysis

Proteolysis is the term given to the process by which peptide bonds within proteins are catalytically cleaved by the action of cellular enzymes called proteases. Proteolysis serves numerous roles in the biology of the eukaryotic cell, the simplest and most common being the catalytic removal of the translation initiating amino terminal methionine. This residue is cleaved from newly translated proteins by the eukaryotic methionine aminopeptidase (Wigle and Dixon, 1970; Wilson and Dintzis, 1970; Yoshida *et al.*, 1970). Analogous but more complicated mechanisms include post-translational removal of inhibitory sequences from enzymes, leading to their subsequent activation. Examples are the proteolytic activation of proteases themselves during apoptosis (Sarin *et al.*, 1993; Smyth *et al.*, 1994; Squier *et al.*, 1994; Williams and Henkart, 1994), and

the "compartmentalized" removal of signal peptides from certain proteins targeted for specific intracellular destinations (Reviewed by: Neurath, 1986).

1.1 Proteases

Cleavage of the peptide bond is catalyzed by a family of enzymes known as proteases. Each protease type, or subfamily, is distinct with respect to substrate specificity and mechanism (Reviewed by: Lopez-Otin and Overall, 2002). The proteases recognize a particular sequence of amino acid residues, a motif that defines their substrate specificity, and will catalyze the hydrolysis of any protein that contains such a motif. Sub-families include serine, cysteine, aspartate, and zinc proteases, in which the main differences are substrate specificity, based upon recognition motif, and the mechanism of peptide bond hydrolysis (For a review of the proteases see: Jones, 1991; Maurizi, 1992).

The reactive group in serine proteases is, as the name would suggest, serine. There are a number of different serine proteases within this sub-family, each having slightly different substrate specificity. For example, chymotrypsin prefers an aromatic side chain on the residue whose carbonyl carbon is part of the peptide bond to be cleaved, while trypsin prefers to cleave peptide bonds where this side chain is positively charged (Belleau and Chevalier, 1968). Substrate preference is determined, both by the general topology of the active site, along with its underlying chemical environment. Interactions between proteins, leading to the catalysis of proteolysis, can be facilitated by hydrophobic or charged pockets on the protein surface. Clefts and pockets on the surface of a protease accept specific side chains, positioning the target peptide bond close to the reactive serine residue on the protease (Figure 1.1).

The largest known protease in eukaryotes is the proteasome, a complex of proteases regulated by proteins contained within the complex itself (see Section 1.7). The proteasome is composed of serine-like proteases and recognizes proteins tagged with the small protein modifier ubiquitin (Ub) (see Section 1.5.1).

Following Ub recognition, the proteases within the proteasome catalyze the hydrolysis of peptide bonds in the target protein, resulting in the release of small peptide fragments and free Ub into the cytoplasm.

Mechanism of Peptide Bond Hydrolysis

Proteases catalyze a hydrolysis reaction that results in the cleavage of the peptide bond. Hydrolysis of the peptide bond by the serine proteases involves a nucleophilic attack by the hydroxyl oxygen of the protease reactive serine residue, at the carbonyl carbon of the peptide bond that is to be cleaved (Figure 1.2). This reaction results in the transient formation of a tetrahedral intermediate that immediately collapses to give an acyl-enzyme, releasing the amino terminal fragment of the peptide bond. The acyl-enzyme then undergoes hydrolysis to form the enzyme-product complex and the carboxy portion of the peptide is released from the enzyme. Repetition of this process at alternate recognition sites within the protein results in the production of small peptide fragments. These fragments can then become degraded by additional proteases, to produce individual amino acids for use in the translation of new proteins.

1.2 Regulation of Cellular Protein Levels by Proteolysis

The steady state level of a protein within a eukaryotic cell is determined by its rate of synthesis and its rate of degradation. Initial experiments demonstrated that hormones applied externally to cultured rat liver (HTC) cells, significantly increased the gross protein content in these cells (Schimke *et al.*, 1965). Upon removal of this stimulus, an exponential decrease in protein level was observed. More detailed experiments demonstrated a specific increase in levels of tryptophan pyrrolase, an enzyme found in the liver, in response to the applied stimulus. At this time, it was not known if the higher level of protein was due to enhanced synthesis or to a decrease in the degradation of tryptophan pyrrolase. Interestingly, a link between the cellular concentration of any protein and the rate of its degradation was postulated by Lee *et al.*, (1956) and Dubnoff *et al.*, (1959) almost a decade prior to the results with tryptophan pyrrolase. However, the

results in HTC cells demonstrated that specifically controlling a protein's rate of synthesis and rate of degradation could regulate its overall cellular concentration.

This link between protein synthesis and degradation was also observed by Grossman and Mavrides, (1967) and Granner *et al.*, (1968) during their studies of the liver protein tyrosine transaminase (TAT), which normally exists at a constant level in HTC cells. Following steroid treatment of HTC cells, the concentration of TAT rapidly increased, followed by a rapid decrease back to its steady state level following removal of the steroid. However, when protein synthesis inhibitors such as cyclohexamide or puromycin were introduced immediately following steroid treatment, the concentration of TAT did not decrease as expected. Interestingly, the stabilization of protein levels, following treatment with translational inhibitors, was also observed with many other liver proteins, but a large number still became degraded.

With protein synthesis blocked, a net decrease in protein level is expected, due to the normal cellular degradation of proteins. Then, why was there a selective inhibition of protein degradation upon blocking protein synthesis? A possible explanation is that proteins involved in degradation are not being synthesized upon addition of the translational inhibitors. With regard to the degradation of TAT, this could not be true because its rapid degradation following steroid treatment could not occur if proteases were being synthesized after the target protein was identified. It was therefore hypothesized that an ever-present pool of enzymes must exist within cells, to support the rapid degradation of any given protein.

The pathways to protein degradation can be non-specific, or can be subjected to regulated temporal and spatial synchronization. A well-described example of a non-specific mechanism involves the bulk transfer of cytoplasm to the lysosome, a large intracellular protease-filled vacuole in eukaryotic cells. In contrast, an example of a highly specific process is the Ub proteolytic system. The Ub proteolytic pathway involves the conjugation of a protein signal, Ub, to a target

protein that is destined for degradation. There can be overlap of specific and nonspecific pathways. For example, the targeting of certain membrane proteins to the lysosome was recently shown to occur via a specific mechanism, beginning with their conjugation to a single molecule of Ub (Haglund *et al.*, 2002).

1.3 Protein Degradation in the Lysosome

Lysosomal protein degradation involves the transport of proteins into the lysosome for non-specific degradation by the lysosomal proteases. This transport can be selective, or can involve the bulk movement of cytoplasm into the vacuole for the controlled self-digestion of cellular structures through a process known as autophagy (Cuervo *et al.*, 2000).

The principal mechanism of protein degradation within the lysosome is thought to occur through autophagy. During autophagy, a portion of the cytoplasm becomes surrounded by two concentric membranes. Fusion of the outer membrane of this "autophagosome" with a lysosomal vesicle results in degradation of all enclosed cytoplasmic structures and macromolecules. This bulk cellular recycling makes new protein precursors available to the cell under conditions of starvation. This process enables the synthesis of new proteins when the raw amino acids are not available in the environment. Autophagy in the lysosome was thought to be the sole pathway for ATP dependent degradation of cellular proteins. However, following the discovery that lysosome free cell extracts could support ATP dependent degradation, the presence of another cytoplasmic pathway for protein degradation was postulated.

1.4 Discovery of Ubiquitin Dependent Proteolysis

In his studies of [^{35}S]-labeled methionine released from cellular protein, M.V. Simpson (1953) demonstrated that energy input was not only required for protein synthesis, but also for protein degradation. Above and beyond the requirement

for active transport of proteins into the lysosome, the requirement for ATP on the degradation of proteins was a notable discovery, since proteolysis is an exergonic, or energy liberating, chemical reaction.

Non Lysosomal Protein Degradation

The first report of a soluble, lysosome-free, ATP-dependent degradation system was reported in the late seventies (Etlinger and Goldberg, 1977). Rabbit reticulocyte lysates were subjected to high speed centrifugation, thereby removing all organelles and leaving only soluble components of the cytoplasm. Using these lysates it was demonstrated that ATP dependent degradation of bulk cytoplasmic proteins occurred in the absence of the lysosome. Furthermore, ATP synthesis inhibitors such as sodium fluoride, dramatically inhibited proteolysis in this cell free system. This suggested the presence of an alternate ATP dependent proteolytic system in cell free reticulocyte lysates and more importantly inferred a cytoplasmic ATP dependent proteolytic pathway.

Discovery of Ubiquitin

The degradation of hemoglobin in reticulocyte lysates is normally initiated by the generation of abnormal globin protein. Early experimentation on hemoglobin degradation demonstrated that the input of energy was required for protein degradation and that this energy input occurred at an early time point within the degradation process and was therefore most likely not due to the transport of hemoglobin to the vacuole for degradation (Hershko and Tomkins, 1971).

In their studies of protein degradative pathways, Ceichanover *et al.* (1978) utilized rabbit reticulocyte lysates as a model system. Using this system, they demonstrated that hemoglobin was degraded in the cell-free lysates. They then used these lysates to determine the constituents of the degradation system using the degradation of hemoglobin as an assay. Their initial experiments involved separating the crude reticulocyte lysates into two distinct fractions. It was immediately observed that neither fraction was able to support protein degradation independently, only when the two were combined could protein degradation be restored. Fraction I was found to contain an unusually heat

stable component, while Fraction II was shown to contain some component that was sensitive to exposure to high temperatures. Because of its heat sensitivity, the authors hypothesized that Fraction II must contain the ATP requiring enzymatic activities, while Fraction I contained some other, stable, ancillary factor necessary for degradation. It was also proposed that the component(s) in Fraction I may include an additional subunit of the ATP requiring component in Fraction II.

Isolation of the components in Fraction I and Fraction II led to the isolation of: 1) an ATP dependent Proteolysis Factor 1 (APF-1), 2) an ATP requiring activator of APF-1, and 3) some additional non-ATP requiring factor (Hershko *et al.*, 1979). APF-1 was initially purified from Fraction I by boiling, and reintroduction of APF-1 into crude Fraction II resulted in the restoration of ATP dependent proteolysis. This result was identical to that obtained when crude Fraction I was combined with Fraction II, indicating that APF-1 was most likely the sole component in Fraction I required for ATP dependent proteolysis. Components in Fraction II were further purified, and two additional fractions were obtained, IIA and IIB, which were assayed for their ability to support ATP dependent proteolysis. From these assays, it was concluded that Fractions IIA, IIB and APF-1 were all required for complete degradation of hemoglobin in reticulocyte lysates. The pre-incubation of any of these fractions with ATP did not result in proteolysis of hemoglobin when the other components were reintroduced sequentially. This implied that while the degradation of proteins within this system was ATP dependent, none of the components could bind ATP and cause degradation to occur in the absence of the other components. Further purification of fraction IIA yielded a protein, initially named APF-2, which when pre-incubated with ATP and APF-1 was capable of stimulating the degradation of hemoglobin upon reintroduction into Fraction IIB.

These experiments revealed a new protein degradative pathway, carried out by the initial activation of the heat stable protein APF-1 by APF-2 in an ATP requiring mechanism. APF-1, subsequently renamed ubiquitin (due to the fact that it is conserved in all eukaryotic organisms) was also identified in cellular

extracts as the component that stimulated degradation of proteins to which it became conjugated (Hershko *et al.*, 1980).

1.5 Components of the Ubiquitin System

Ub was initially described in the mid 1970's, as a protein component found in eukaryotic cells, conjugated to Histone 2A (Schlesinger *et al.*, 1975). A striking characteristic of Ub, and one that has sparked a wealth of research into its function, is its absolute conservation throughout all eukaryotic cells. The importance of Ub-dependent proteolysis is also demonstrated by the vital regulatory functions that many of its protein targets serve in the cell. Examples are the cyclins (Glotzer *et al.*, 1991; Hershko *et al.*, 1991), which are targeted by the Anaphase Promoting Complex (King *et al.*, 1995), the SCF ubiquitin-ligase complex (Feldman *et al.*, 1997; Lisztman *et al.*, 1998), and proteins involved in cell immortality, such as the tumor suppressor, p53 (Scheffner *et al.*, 1990; Ciechanover *et al.*, 1991). The Ub system is also important in the heat shock response and is involved in the rapid silencing of transcriptional machinery during periods of cell stress (Portig *et al.*, 1996; Fujimuro *et al.*, 1997; Watt and Piper, 1997). Ub also serves many other vital roles in the cell, such as mediation of stress responses, repair of damaged DNA and regulation of differential gene expression (Goldstein *et al.*, 1975; Ciechanover *et al.*, 1991).

For Ub to become ligated to a target protein, the sequential action of three enzymes is required, E1 (Uba1, previously identified as APF-2), E2 (Ubc1) and E3. First, the carboxy terminal glycine residue of Ub is activated in an ATP requiring step by a specific activating enzyme, Uba1. This step consists of the formation of ubiquitin adenylate (Ub-AMP) (Figure 1.3A), with the concomitant release of pyrophosphate, followed by the immediate transfer of Ub to a cysteine residue within Uba1 as a thiolester. Next, the activated Ub is transferred to an active site cysteine residue of a ubiquitin conjugating enzyme, Ubc1 (E2). In the third step Ub is linked by its carboxy terminus, through an amide isopeptide

linkage, to an amino group of a lysine residue in a substrate protein, either by E2 alone or in concert with a ubiquitin protein ligase (E3) (Figure 1.3B).

1.5.1 Ubiquitin

Ub is a compact, seventy six residue protein, and is highly conserved among all eukaryotes. Its compact structure makes Ub an extremely stable protein; this is illustrated by the harsh purification scheme used initially to isolate it (Hershko *et al.*, 1979). The main source of Ub in the eukaryotic cell comes from transcription of the UBI4 gene, which is composed of five identical copies of Ub linked end-to-end by their amino and carboxy termini. The most notable sequence motif found within Ub is a carboxy terminal Gly-Gly that is believed to be responsible for providing flexibility during its activation and conjugation to target proteins. The UBI4 gene produces a polypeptide that contains an additional carboxy terminal asparagine following this Gly-Gly motif. Proteins then known as Ub hydrolases catalyze the hydrolysis of the peptide bond formed between the carboxy terminal glycine of Ub and the amino terminus of the preceding Ub molecule. Once each of the Ub molecules has been processed by the Ub hydrolases, this carboxy terminal asparagine is removed, resulting in the production of five free Ub molecules (Pickart and Rose, 1985; Ozkaynak *et al.*, 1987). This post-translational processing of the carboxy terminal asparagine may play a role in preventing premature conjugation of the UBI4 polypeptide prior to proteolytic processing into individual Ub molecules.

UBI4 expression is normally up-regulated during periods of cell stress such as heat shock (Ozkaynak *et al.*, 1987; Treger *et al.*, 1988) and cells with UBI4 deletions are highly sensitive to these stresses (Finley *et al.*, 1987). The up-regulation of this one gene results in the production of five individual molecules of Ub, therefore rapidly increasing the cell's ability to conjugate Ub to target proteins during times of stress. As noted previously (see Section 1.2), translational inhibition resulted in a noticeable decrease in protein degradation, which may be a result of the inhibition of UBI4 expression. The constant production of Ub would be essential for efficient degradation of target proteins. As multiple Ub

moieties become conjugated to target proteins, the Ub pool becomes depleted rapidly in the absence of protein synthesis.

In addition to its synthesis directed by the UBI4 gene, Ub is also found in the eukaryotic genome as fusions to three separate ribosomal structural proteins (L40B, L40A and S31) (Redman and Rechsteiner, 1989; Redman and Burris, 1996). These fusion proteins remain inactive until they have been proteolyzed by Ub hydrolases, after which they can carry out their roles in the cell. It has been proposed that these Ub fusions provide translational stability or act as chaperones during folding of their fusion partners. The stable single protein domain of Ub, could act as a nucleation center for the folding of a protein to which it is attached. Stabilization of the folding of proteins conjugated to Ub has been demonstrated in artificial constructs containing Ub fused at their amino termini (Baker *et al.*, 1994). Another possible function for Ub fusions is that they may play some role in ribosome biogenesis. Alternatively, Ub fusions to ribosomal proteins may simply be an evolutionary throwback from a previous mechanism, no longer utilized in eukaryotic cells.

Ub Structure

Ub tertiary structure is arranged in a four stranded antiparallel β sheet constrained by a single α helix across its surface (Figure 1.4A). This structural fold is common in many eukaryotic and prokaryotic proteins and has been appropriately named the ubiquitin fold. It is its compact globular structure that makes Ub an extremely stable protein, readily reactivated after being denatured by chemicals or heat (Hershko *et al.*, 1979).

The carboxy terminus of Ub extends out from its globular core into aqueous space resulting in a flexible "tail" five residues in length. The α-carboxyl group of the carboxy terminal glycine (Gly 76), of the Gly-Gly motif, participates in the formation of the isopeptide bond with the amino group of a lysine side chain in a target protein (Figure 1.3B). Even conservative mutations within the carboxy terminal tail of Ub have been shown to block its ATP dependent activation (Monia *et al.*, 1990).

1.5.2 Ubiquitin Activating Enzyme

The first step in Ub dependent proteolysis involves the ATP dependent activation of Ub. This provides the energy required for the formation of an isopeptide bond between the carboxy terminus of Ub and a lysine residue on the target protein. This reaction is catalyzed by the protein that was initially identified as APF-2 (Hershko *et al.*, 1980) and was subsequently renamed Ubiquitin Activating Enzyme (Uba1 or E1).

Uba1 is a 115-125 kDa protein that has been identified in several eukaryotic species such as wheat (Hatfield *et al.*, 1990), *Homo sapiens* (Handley *et al.*, 1991) and *Saccharomyces cerevisiae* (McGrath *et al.*, 1991). Attempts have been made to create a recombinant version of Uba1, however due to its large size and specific folding requirements, eukaryotic expression systems are required for its production (Described in Chapter 2 *Experimental Procedures*) (Hatfield *et al.*, 1990). The size of Uba1 and problems with its cloning and purification has, unfortunately, prevented the acquisition of any structural information, making it difficult to define the biochemical mechanism of Ub activation.

Uba1 contains at least two well-defined sequence motifs, also found in other enzymes involved in pathways other than ubiquitination (Chapter 4, Figure 8). The first, referred to as the UBA motif (P-[LIVM]-C-T-[LIVM]-[KRH]-x-[FT]-P), contains the active site cysteine residue (C) that is responsible for accepting activated Ub. The second is a nucleotide binding domain characterized by a classic Walker fold motif (G-X-G-X-X-G) (Walker *et al.*, 1982). Uba1 also contains two putative zinc finger motifs that may contribute to coordination of the Mg^{2+} ion that is necessary for the coordination of ATP at the nucleotide binding site (Lake *et al.*, 2001). However, in the absence of either mutational or structural data on Uba1, the function of these domains is still hypothetical.

In an attempt to identify the position of the active site cysteine residue in the wheat enzyme, Hatfield and Vierstra (1992) created several mutants and tested their ability to activate Ub *in vitro*. Several temperature sensitive mutants of

Uba1 have also shed light on the mechanism of Ub activation by Uba1. For example, mouse ts85 cells containing a temperature sensitive mutation of Uba1, arrest at the G2 cell cycle phase when grown at a non-permissive temperature (Finley *et al.*, 1984). This arrest was thought to occur because of the accumulation of proteins normally tagged and degraded by the Ub system. Results from this study estimated that up to 90% of short lived proteins in the cytoplasm of eukaryotic cells may be targets for the Ub system. Other examples of Uba1 temperature sensitive mutants have been characterized, but none have been able to provide an in depth understanding of Ub activation due to the fact that the positions of these mutations was not determined (Kulka *et al.*, 1988; Deveraux *et al.*, 1990; Mori *et al.*, 1993; Ikehata *et al.*, 1997; Tongaonkar *et al.*, 1999).

Uba1 Reaction Mechanism

The activation of Ub is achieved in a two step reaction, initiated by the binding of Ub, ATP and Mg^{2+} to Uba1 (Ciechanover *et al.*, 1981; Haas *et al.*, 1982). The final product of the reaction is a Uba1~Ub thiolester, formed between the carbonyl carbon of the carboxy terminal glycine residue of Ub and an active site cysteine residue. The specific order in which substrate molecules (Ub and ATP) bind to the Uba1 active site is not known, but the products of this reaction have been well characterized.

The mechanism of Ub activation involves the hydrolysis of one molecule of ATP to form an equivalent of Ub-AMP (Ub-adenylate) (Equation 1.1; Figure 1.3A) (Haas *et al.*, 1982). Ub-AMP remains non-covalently bound to Uba1 with a relatively low dissociation constant, allowing the Uba1/Ub-AMP complex to be purified using gel-exclusion chromatography (Chapter 2). Formation of Ub-AMP is, however, transient and can only be isolated using mutant forms of Uba1, where the active site cysteine has been selectively mutated.

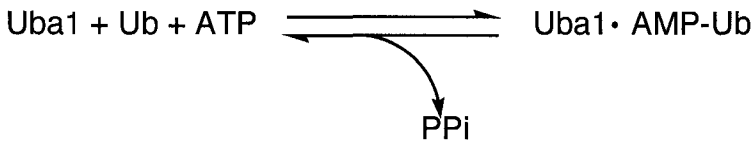

Equation 1.1

Under normal conditions, transfer of Ub to the active site cysteine of Uba1 immediately follows the formation of Ub-AMP (Haas *et al.*, 1983). Subsequent to the formation of the Ub adenylate, Ub becomes transferred to a cysteine residue, resulting in the formation of a thiolester bond, and the release of free AMP (Equation 1.2).

Equation 1.2

The release of AMP is immediately followed by a second round of ATP/Ub binding, leading to the formation of a second Ub-adenylate that remains non-covalently bound to the active site (Equation 1.3). This results the formation of a Uba1 species that contains Ub covalently bound as the thiolester, as well as Ub non-covalently bound as the adenylate poised for transfer to the active site cysteine of an E2 (See Section 1.5.3.).

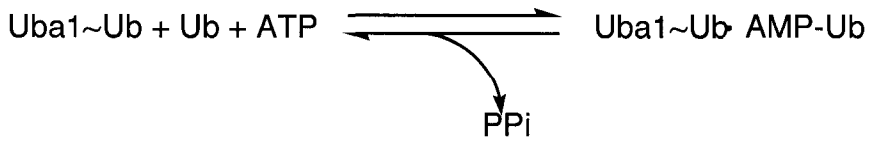

Equation 1.3

1.5.3 Ubiquitin Conjugating Enzymes

Presently, there is no evidence that Uba1 is capable of transferring Ub directly to a target protein. Uba1 must first transfer Ub to one of a family of ubiquitin conjugating enzymes (E2s), which are capable of transferring the activated Ub to a target protein. E2s appear to be key donors of Ub to specific target proteins *in vivo*, acting either as the immediate donor of Ub, or first transferring it to an ancillary ubiquitin protein ligase (E3) (See Section 1.5.4).

Thirteen distinct E2 molecules have been identified in the *S. cerevisiae* genome, many of which have had their structures solved by X-ray crystallography. All of the E2 proteins display anywhere from 35% to 90% sequence identity and range in size from 16 to 29 kDa (Seufert *et al.*, 1990; Hershko and Ciechanover, 1992). The E2 proteins contain significant structural similarities within a core catalytic domain, known as the UBC domain (Figure 1.4B). The core catalytic domain contains a conserved cysteine residue that is responsible for accepting Ub from Uba1, via a transthiolation reaction, resulting in the formation of a second thiolester bond identical in structure to that of Uba1~Ub (Equation 1.4).

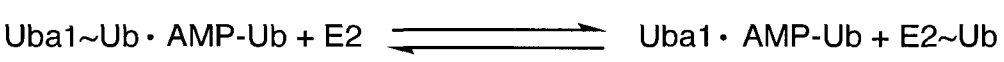

Equation 1.4

Following the transfer of Ub to an E2, a target protein becomes recognized through some yet unknown mechanism, resulting in the formation of an isopeptide bond between the carboxy terminus of Ub and an internal lysine residue within the target (Equation 1.5).

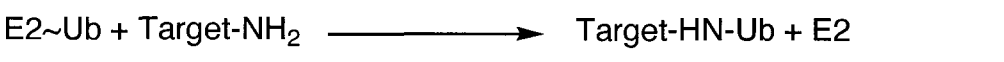

Equation 1.5

All of the E2s seem to be evolutionarily related and can be distributed into three distinct groups based on their primary sequences (Figure 1.5). The first class (Class I) is composed of E2s that contain only the core UBC domain. Class II, contains E2s with a carboxy terminal extension to the core UBC domain. These extensions can vary in their overall sequence, but tend to contain acidic residues that appear to mediate interactions with protein substrates (Liu *et al.*, 1995; Pitluk *et al.*, 1995). Class III E2s contain amino terminal extensions, the function of which is yet undetermined.

While a number of E2s are capable of conjugating Ub directly to target proteins (Haas *et al.*, 1990) and a subset have actually been shown to ubiquitinate themselves *in vitro* (Pickart and Rose, 1985; Banerjee *et al.*, 1993; Gwozd *et al.*, 1995), most require the presence of a ubiquitin protein ligase (E3) to achieve ubiquitination of a target.

1.5.4 Ubiquitin Protein Ligases

E3s, or ubiquitin protein ligases, bind target proteins, and are involved in recruiting E2s for transfer of Ub (Hershko *et al.*, 1983). Until recently the proximal donors of Ub to target proteins were thought to be Ub charged E2s and the E3s were thought to be only indirectly involved in the transfer of Ub to substrate proteins. For the main class of E3s this is indeed the case, however, there is a family of E3s that directly form thiolesters with Ub and as such become proximal donors to target proteins (Scheffner *et al.*, 1990; Huibregtse *et al.*, 1994). It is believed that the large number of distinct E2 enzymes, in combination with the numerous E3s, is responsible for conferring the high degree of target specificity on the Ub system and provides a mechanism for Ub conjugation to proteins for degradation by the proteasome.

1.6 Multi-Ub chains

While some mono-Ub protein conjugates have been shown to direct degradation via endocytosis at the lysosome (Haas *et al.*, 1990; Johnson *et al.*, 1992; Finley

et al., 1994), it is the presence of multiple Ub molecules conjugated to a target that results in their recognition by the proteasome. The first reports of Ub conjugates being targeted to the proteasome suggested that multiple Ub molecules became conjugated to multiple lysine residues within the target protein. The protein tyrosine aminotransferase was shown to contain lysine residues near its carboxy and amino termini, the presence of both were shown to be required for its normal degradation (Stellwagen, 1992). However, studies of Ub conjugation to lysozyme (Hershko *et al.*, 1984) and β -galactosidase (Bachmair *et al.*, 1986) revealed that the total number of Ub molecules conjugated to these proteins exceeded the total number of available lysine residues. The stoichiometry of Ub conjugates being higher than the available lysine side chains in lysozyme led to the hypothesis that Ub must become conjugated to itself via an internal lysine residue. When the reactive lysine side chains on Ub were methylated there was an overall decrease of Ub incorporation into the target proteins (Hershko and Heller, 1985). Later, it was observed that the length of a Ub chain is directly proportional to the Ub-appended target protein's affinity for the proteasome (Chau *et al.*, 1989; Gregori *et al.*, 1990; Deveraux *et al.*, 1994; Pickart, 1997). That is, the longer the Ub chain, the shorter the half-life of the target protein.

The current hypothesis for the formation of Ub chains on target proteins takes the form of the "bucket brigade" mechanism (Figure 1.6). In this mechanism Ub is initially activated by Uba1 and transferred to E2 (Equation 1.4). From this point, chains can be built upon the target itself, with subsequent Ub moieties added to the lysine on the preceding Ub. There are two possible modes of Ub transfer leading to the formation of a chain. The first is when the newly charged Ub is conjugated to a lysine on a Ub that already exists in the forming chain. The second is the addition of the chain to the lysine on the newly charged Ub. These two modes are termed top down and bottom up chain extensions respectively. In this way chains containing multiple Ub molecules, of anywhere between two and twenty, can be created on a target protein (Chau *et al.*, 1989).

A second, as yet uncharacterized, mechanism may also exist, involving the construction of the Ub chain prior to its conjugation to the target protein. Once Ub has formed a thiolester with E2, multiple charged E2s may act individually to pass Ub between one another with, or without, the presence of E3. Ub is passed between these proteins with newly charged Ub being conjugated to the internal lysine in an alternate Ub. Following the construction of the chain, it is then passed to the target protein and conjugated to an internal lysine residue

Ub Chain Arrangement

Ub contains a total of seven lysine residues, at least six of which are situated on its surface and may be potential targets for ubiquitination. The relative reactivity of Lys 6, 11 and 23, and to a somewhat lesser extent Lys 27, 28 48 and 63, were demonstrated by their ability to become readily acylated during Edmann degradation (Zhu *et al.*, 1986). While the number of lysine residues in Ub and the potential for linkages on each of these residues implies numerous possibilities for the formation of chains, Lys 48 seems to become ubiquitinated preferentially.

The canonical multi-Ub chain linkage at Lys 48 linkage (Figure 1.7) is believed to form the major recognition site for the proteasome (Deveraux *et al.*, 1994). Substitution of Ub Lys 48 to Arg resulted in the inability to form the multi-Ub chains normally observed in the cell (Chau *et al.*, 1989; Chau *et al.*, 1989; Gregori *et al.*, 1990). These mutant Ub molecules, while capable of forming single Ub conjugates to targets, were unable to support the formation of multiple Ub chains. The formation of alternate Ub chain linkages, such as those at Lys 63 has also been described (Hodgins *et al.*, 1996). While the linkage at Lys 63 has also been shown to be recognized by the proteasome (Baboshina and Haas, 1996), these alternate linkages are thought to confer different selectivity to targeting pathways. Some of these linkages may not be involved in protein degradation at all (Dubiel and Gordon, 1999; Mastrandrea *et al.*, 1999) and have been shown to be involved in DNA repair (Spence *et al.*, 1995) and cellular response to stress (Arnason and Ellison, 1994).

It remains to be determined if these Ub linkages form homogeneous or heterogeneous populations, and their functionality still needs to be determined. The potential variability in the connections between molecules of Ub is almost limitless if heterogeneous linkages are used in building the Ub chain, conferring even more specificity on the system. Currently only chains composed of Lys 48 linked Ub have been chemically mapped and have been definitively shown to be composed of a homogenous population and result in targeting to the proteasome (Chau *et al.*, 1989).

1.7 The Proteasome

The proteasome is composed of two main particles, a core particle and a regulatory particle. The regulatory particle is actually two separate particles that "cap" each end of the core particle. Each of the regulatory particles is made up of fourteen proteins, some of which are ATPases and others that are involved in the recognition of the Ub chain. Recognition by the regulatory particle of the Ub chain conjugated to the target protein results in unfolding of the target by the ATPases in the regulatory particle. The target protein is then translocated into the central cavity of the core particle where protease active sites on the inner surface of the core break various peptide bonds of the target protein.

The core particle is made of two separate copies of fourteen individual proteins arranged in a ring structure. Each ring is made up of seven proteins giving the proteasome a total of four of these rings. The core particle contains the proteolytic enzymes involved in cleavage of the target protein into small eight to eleven residue peptide fragments (Wenzel *et al.*, 1994). As was stated in Section 1.1, the proteasome is composed of serine like protease activities. The spacing between the catalytic residues within adjacent rings may act as a "molecular ruler" accounting for the eight to eleven residue proteasome-produced peptide fragments. Once a protein becomes tagged with a Ub chain, it indiscriminately becomes a target for degradation by the proteasome (Deveraux *et al.*, 1994; Baboshina and Haas, 1996; Beal *et al.*, 1996; Pickart, 1997). Target

selection and Ub tagging must therefore occur prior to recognition by the proteasome.

1.8 Protein Recognition and Cellular Half-Life

N-end Rule

While the components of the Ub system and the degradation of tagged substrates by the proteasome have been studied extensively, it is still not well understood what makes a protein a suitable target for Ub tagging and subsequent degradation. Initially, it was proposed that the identity of the N-terminal residue of the target protein plays a key role (Bachmair *et al.*, 1986; Varshavsky *et al.*, 1987). In this mechanism, protein substrates targeted by Ub bear a specific degradation signal, the "N-degron", which comprises two determinants: a destabilizing N-terminal residue and an internal lysine to which Ub becomes conjugated. As an example, proteins that have serine as the N-terminal amino acid are long-lived with a half-life of more than 20 hours, while proteins with aspartic acid as the amino terminal amino acid have a half-life of only 3 minutes (Bachmair *et al.*, 1986). This N-end rule pathway has been identified in all organisms, from mammals to bacteria. It is interesting to note that the N-end rule applies to protein degradation in bacteria even though they do not contain Ub (Tobias *et al.*, 1991). There appears to be specific E3 proteins that are responsible for the selection of substrates on the basis of the amino terminal residue (Bartel *et al.*, 1990). This selection occurs via some mechanism that is not dependent on the acetylation state of the amino terminus in question (Mayer *et al.*, 1989).

PEST Sequences

Certain amino acid motifs also appear to be signals for degradation. One such sequence is known as the PEST sequence because a short stretch of about eight amino acids is enriched with proline (P), glutamic acid (E), serine (S) and threonine (T). The PEST sequence is found in a multitude of proteins, many of which have half lives of less than 2 hours. For example, the protein Gcn4p has a

half-life of approximately 5 minutes under normal cellular conditions. If the PEST motif within its sequence is altered, its half-life increases approximately ten fold to 50 minutes (Kornitzer *et al.*, 1994).

Signal Masking

The motifs mentioned in this section are only viable signals for protein degradation if they are accessible to the components of the Ub system that recognize them. An additional layer of control can be attained if these sequences are hidden from the degradation machinery. For example, a recognition signal may be hidden if it is part of a protein-protein interaction. The covalent attachment of a phosphate group to the side chain of certain amino acids can also block an attack by Ub. Both of these mechanisms are reversible and allow for better control. A protein degradation signal need only be unmasked to target the protein for degradation. Such reversible masking appears to be involved in the regulation of some transcription factors and in the control of cyclin concentrations (Johnson *et al.*, 1998).

A degradation signal may also be buried in the hydrophobic core of a protein. This may be a reason why partially folded or abnormal mutant proteins are prone to degradation by the Ub system. When such proteins exist in their native state, the signals are hidden and the protein is long-lived. In a partially unfolded state, the signals become exposed to the Ub machinery, resulting in tagging of the protein by Ub.

Targets of the Ub system

Ub-dependent proteolysis is essential for at least two major cell cycle transitions, the G1 to S-phase transition and the metaphase to anaphase transition (for review see: Hershko, 1997). Key targets of the Ub proteolytic pathway at these transitions include cyclins, which are positive regulators of cyclin-dependent kinases (Cdks), and Cdk inhibitors, which are negative regulators of Cdks. Mitotic cyclins and other proteins that regulate mitosis are targeted for degradation by a cell cycle regulated E3 called the anaphase promoting complex (APC) or cyclosome (For an excellent review of the APC and its regulation see:

Page and Hieter, 1999). Utilizing electron microscopy, Gieffers *et al.* (2001) obtained a 26 Å resolution image of the three dimensional structure of the APC. This provided the first glimpse into the structure of an Ub ligase complex.

Another multi-subunit complex is the Skp1/Cdc53(cullin)/F-box (SCF) protein complex. The SCF complex is composed of a core complex and a specificity containing component acts like a modular system. The component that contributes the specificity to this complex is known as the F-box and serves as an interchangeable adapter that recruits the E2 molecule and target protein into a core complex. For example, the SCF complex that contains the F-box protein Cdc4 and E2 Cdc34 targets the Clb-Cdc28 inhibitor Sic1 for degradation (Nugroho and Mendenhall, 1994). Alternatively, the F-box protein Grr1 (Barral *et al.*, 1995; Feldman *et al.*, 1997; Li and Johnston, 1997) targets the G1 cyclin Cln2 for degradation by the proteasome. Interestingly, the SCF complex can also mediate the conjugation of the ubiquitin like protein (UBL) (UBL's are discussed in Chapter 4) Rub1 to Cdc53 using the Rub1 E2, Ubc12 (Kamura *et al.*, 1999). This observation strengthens the argument for the cooperativity of the Ub system and other protein conjugation systems. It also suggests evolutionary links between these systems.

Recently the crystal structure of the SCF complex, containing Cul1, Rbx1 Skp1 and the F-box portion of Skp2 was solved (Zheng *et al.*, 2002). This structure, along with the previously determined Skp1-Skp2 interface (Schulman *et al.*, 2000), is vital to understanding substrate specificity because the SCF complexes are the largest family of E3 Ub ligases that mediate the ubiquitination of a wide variety of regulatory and signaling proteins. This structure has provided insight into the structural relationships between the E2 and its cognate E3, in this case a multi-subunit protein complex. The structure included the Cul1, Rbx1, Skp2 and Skp1 SCF scaffold and has provided valuable insight into the spatial arrangement of the proteins in the complex and suggests likely geometries for *in vivo* interactions between E2s, E3s and their target proteins. While this structure of the SCF did not include an E2 protein, it has provided insight into how all of

the individual components of the ubiquitin system may fit into the mechanism for Ub chain formation and protein recognition.

1.9 Conclusion

The majority of work in the Ub field has focused mainly on targets of the Ub system; therefore a void exists with regard to knowledge of the mechanism of ubiquitination. The least structurally understood component of the Ub system is Uba1 and studies into the activation of Ub are limited to a biochemical understanding of the mechanism of Ub adenylation and thiolester formation. Structural relationships between active site determinants in Uba1 and how Ub is transferred between them and E2s are unknown. Structures of the Uba1 homologues, *E. coli* MoeB (Lake *et al.*, 2001) and *H. sapiens* Uba3 (Walden *et al.*, 2003), have offered some insight into the mechanism of Ub activation. The lack of mechanistic information with regards to Ub activation is interesting. While many E2s and E3s are dispensable through selective deletions, only Uba1 and Ub itself are required absolutely to maintain cellular viability (Finley *et al.*, 1987; McGrath *et al.*, 1991).

The main focus of this thesis is the study of Ub activation by Uba1 and the spatial relationship between the active sites of Uba1 and E2. Specifically, we were interested in the mechanism for Ub chain formation and what role Uba1 may play in the catalysis of this process. We suggest that Uba1 may not be simply a passive player in the Ub system as previously predicted by the "bucket brigade" model and may indeed play a key role in processes down-stream of Ub activation. Data provided in this thesis will demonstrate the positions of the active site cysteine residue and the nucleotide binding region and will suggest a direct involvement for Uba1 in the mechanism of chain formation. This was accomplished by creating a number of selective point mutations in the *S. cerevisiae* Uba1 protein. Additionally, computer modeling has been used to investigate the molecular mechanism of Ub activation. Chapters 2 and 4 deal with structural interactions between Uba1 and Ub and how these interactions

relate to the chemical activation of Ub at the Uba1 active site and the transfer of Ub to E2. Chapters 3 and 5 examine the interaction of Ub with the E2 protein Ubc1, and explore the relationship of this interaction with the structure of the larger Uba1/Ubc1/Ub complex prior to Ub transfer.

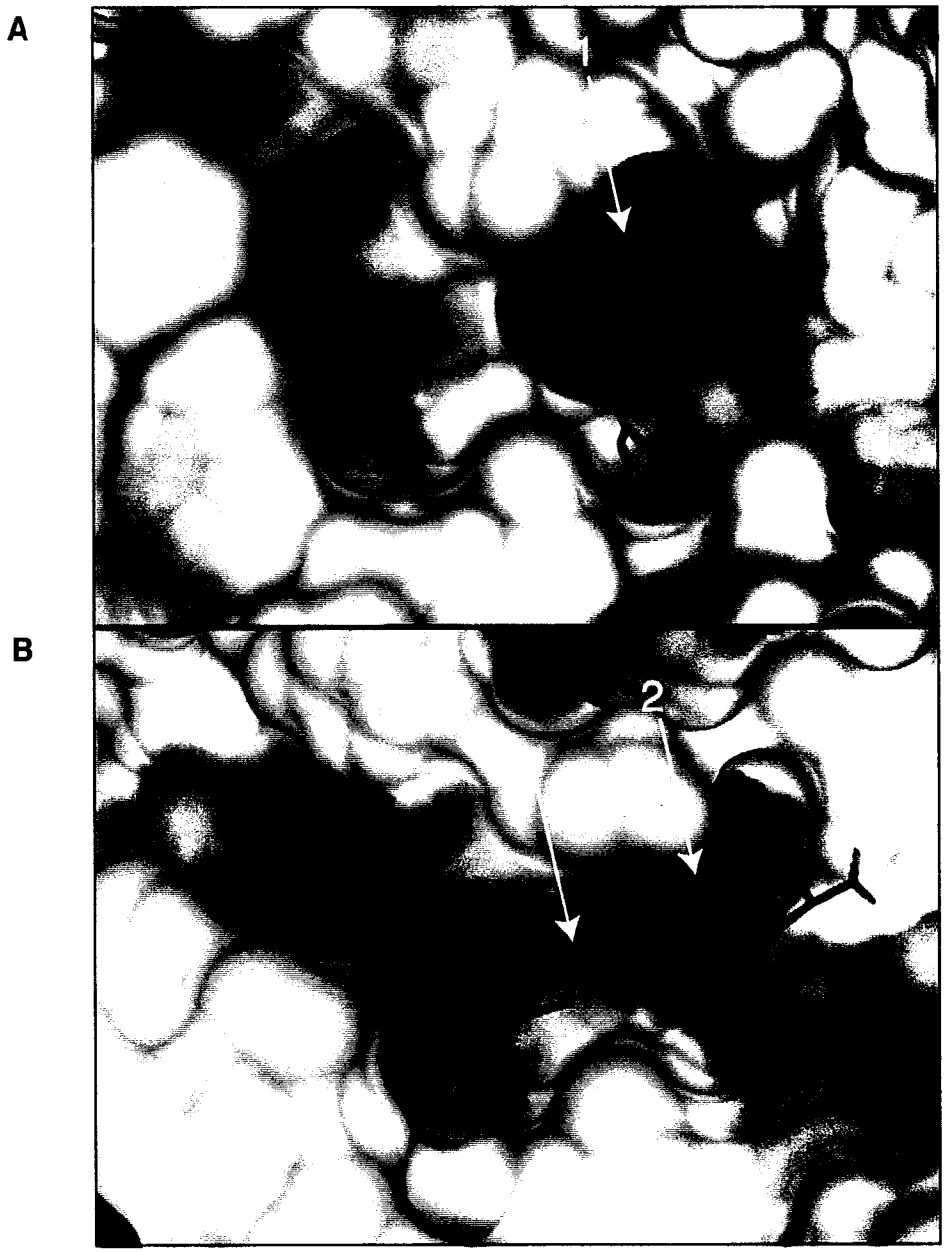

Figure 1.1. **Chymotrypsin and Trypsin Active Sites**
Solvent accessible Connelly surface representations of the Chymotrypsin and Trypsin active sites. In both cases, the surfaces are colored by pocket, with red representing hydrophobic and blue hydrophilic regions. White implies that the area is solvent exposed. **A**, Bovine γ-Chymotrypsin is shown bound with the synthetic inhibitor D-Leucyl-L-Phenylalanyl-P-Fluorobenzylamide (sticks), illustrating the position of the hydrophobic phenylalanyl group bound at its active site (**1**) (Yennawar, *et al.* 1994). **B**, Trypsin is shown bound to the Leech-derived tryptase inhibitor (sticks), illustrating the position of the lysine residue bound at its active site (**2**) and the position of the peptide bond that would normally be hydrolyzed during catalysis (**3**) (Di Marco and Priestle,1997). These two panels illustrate the similarities within these two active sites and the subtle differences that determine substrate recognition at their active sites.

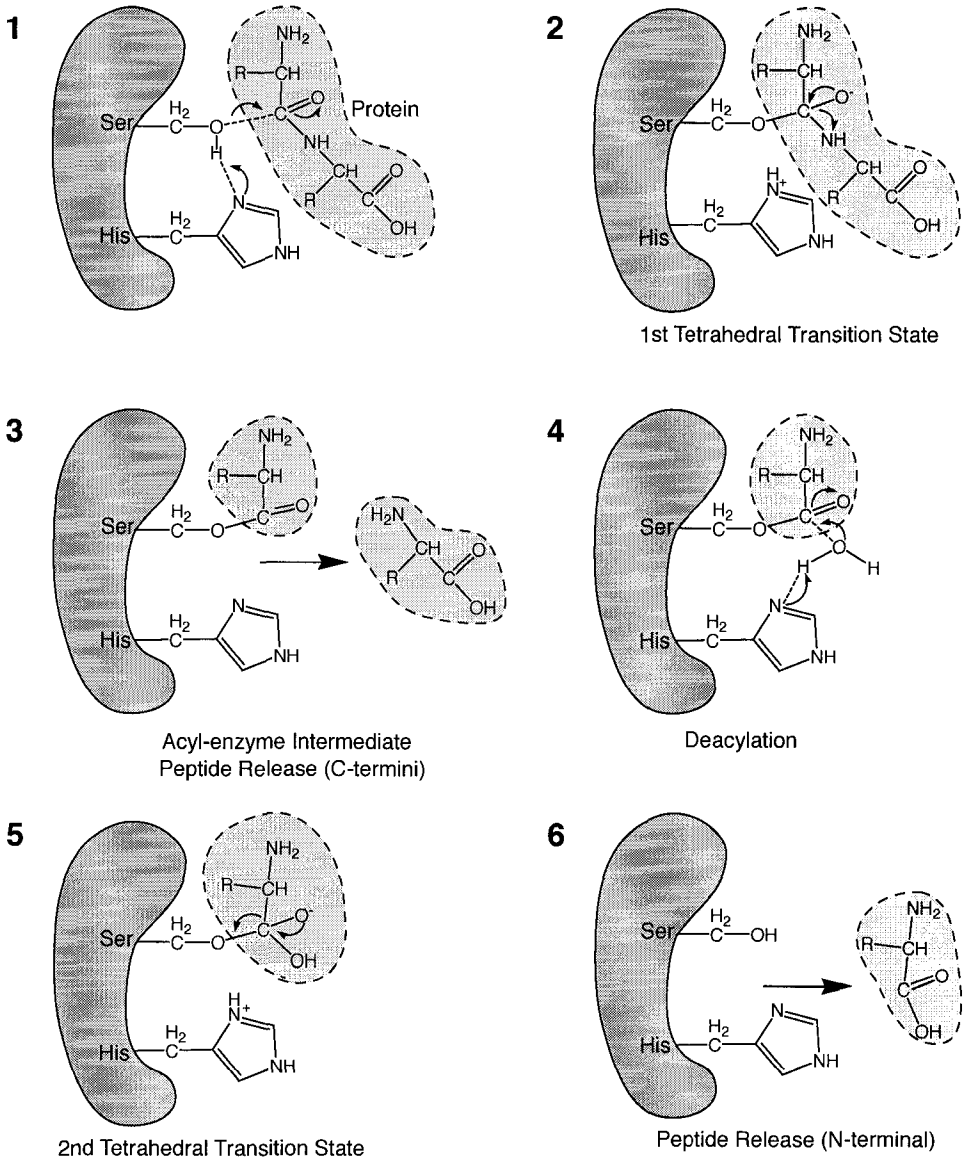

Figure 1.2. **Mechanism of Peptide bond Hydrolysis by Serine Proteases** **Step 1** involves recognition and binding of the substrate (light gray, dashed line) at the active site of the protease (dark gray solid line). The mechanism at this step involves deprotonation of the reactive serine by a catalytic histidine and formation of the tetrahedral transition state. **Step 2** involves rearrangement of the transition state. **Step 3** demonstrates the release of the carboxy terminal portion of the cleaved protein or peptide, leaving the protease acyl-enzyme intermediate. **Step 4** represents deacylation using a molecule of water and the reactive histidine at the active site. **Step 5** illustrates rearrangement of the acyl-enzyme intermediate. Finally, **step 6** ends in the release of the amino terminal fragment of the cleaved protein or peptide (Adapted: Voet & Voet, Biochemistry 2nd ed., Fig. 14-23).

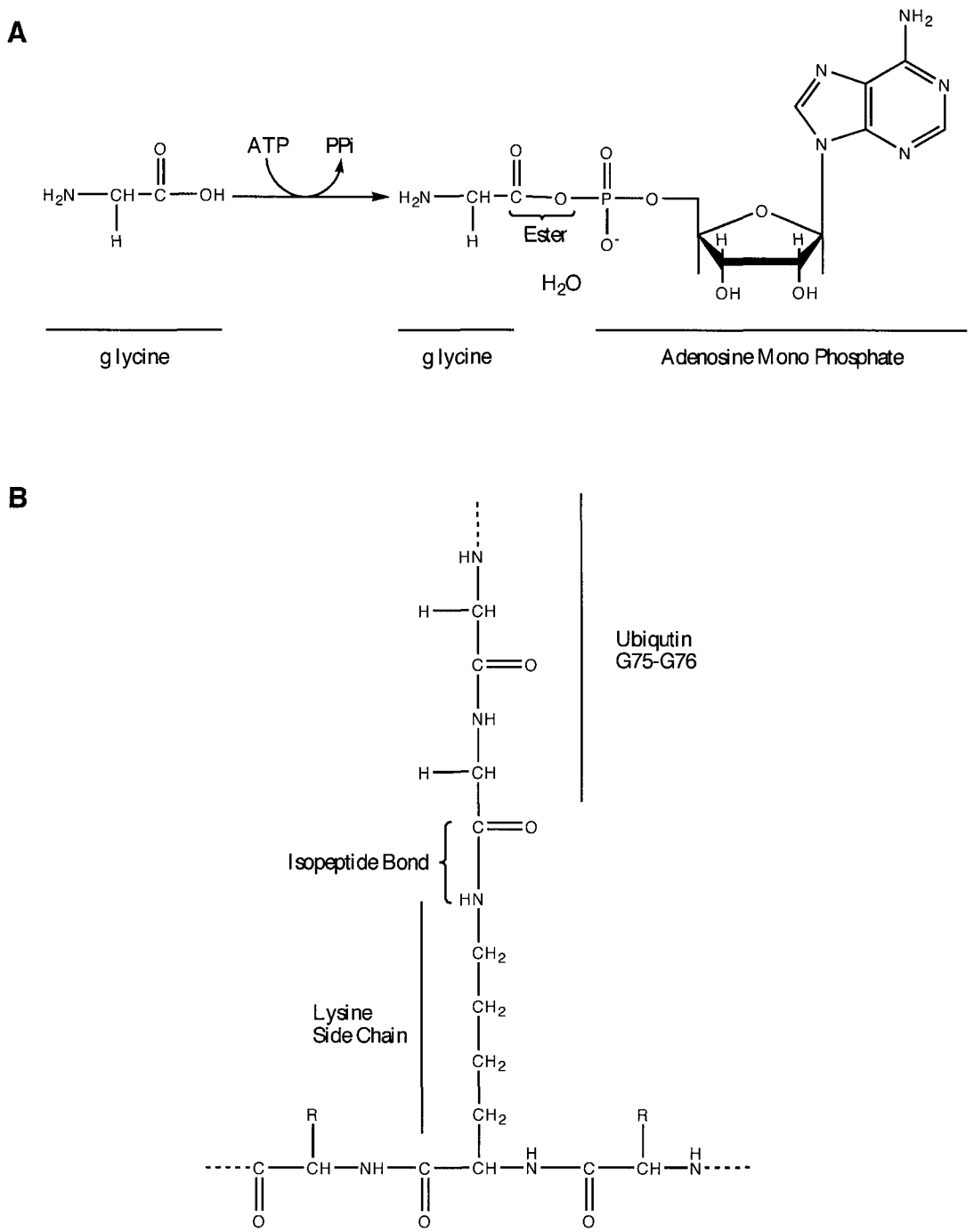

Figure 1.3. **Structures of the Ubiquitin Adenylate and Isopeptide Bond** **A**, Chemical formation of the Ub-adenylate. The initial reaction at the active site of Uba1 involves a condensation reaction between the α phosphate ATP and the carbonyl carbon of the carboxy terminal glycine residue of Ub, resulting in the formation of an ester bond. **B**, The chemical structure of the isopeptide bond formed between the carbonyl carbon of the carboxy terminal glycine of Ub and the ε amino group of a lysine within a target protein.

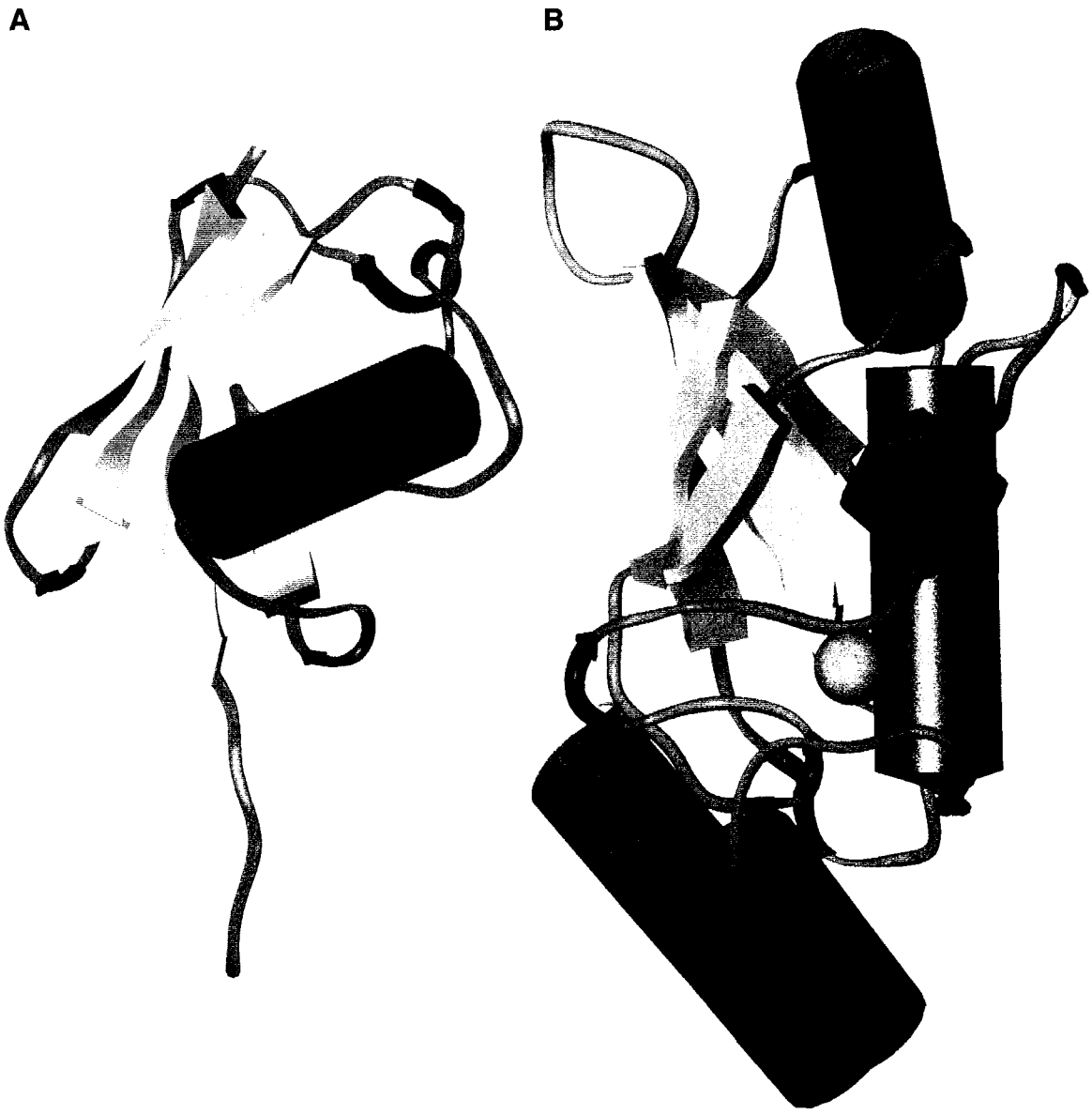

Figure 1.4. **Cartoon Representations of Ub and Ubc1Δ**
A, Ubiquitin's compact globular fold is clearly represented by the four strand anti-parallel β sheet (yellow arrows) and single α helix (red cylinder) (Vijay-Kumar, *et al.*, 1985). **B**, The Ubiquitin Conjugating Enzyme's core catalytic domain is also made of a four strand anti-parallel β sheet (yellow arrows) surrounded by α helices (red cylinders) (Hamilton, *et al.*, 2001). The active site cysteine residue of Ubc1Δ (Cys 88) is represented as an orange van der Waals sphere. Loops and random coil in both structures are represented by blue and green ribbons respectively.

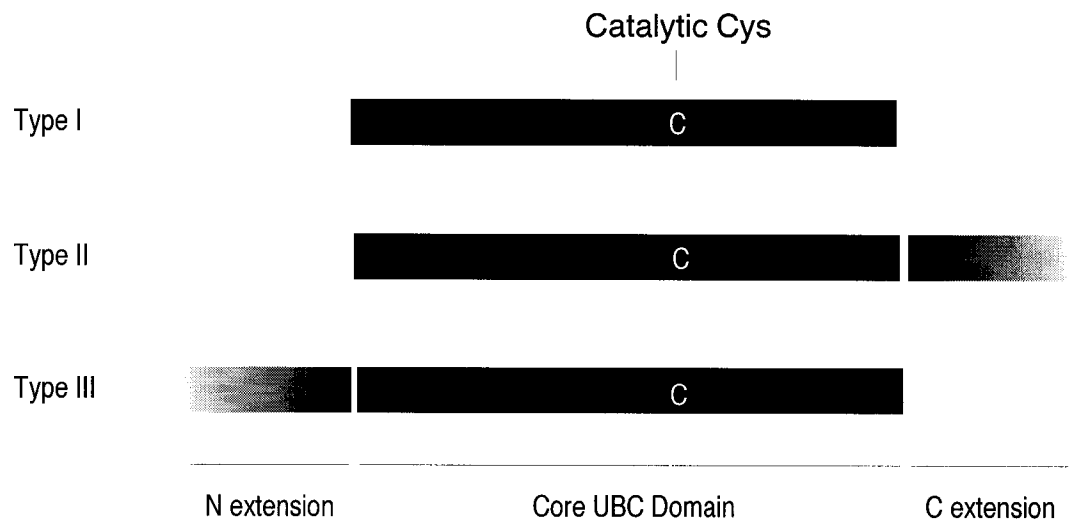

Figure 1.5. **Domains of Ubiquitin Conjugating Enzymes**
Ubiquitin Conjugating Enzymes are categorized into three types, Type I containing only the core catalytic domain (Figure 1.4), Type II having a carboxy terminal extension of varying length and Type III having an amino terminal extension of varying length. The thirteen E2 proteins that have been characterized in *S. cerevisiae* can be categorized into these categories based upon the structural alignments of Ptak, *et al.* (2001). The type I E2s include: Ubc4, Ubc5, Ubc6, Ubc7, Ubc9, Ubc11 and Ubc13, the type II E2s include: Ubc1, Ubc2, Ubc3, Ubc6 and Ubc8, while the type III E2s include Ubc10 and Ubc12. A core domain insertion is also be found in Ubc7, Ubc9, Ubc11 and Ubc13, for which the purpose has yet to be discovered.

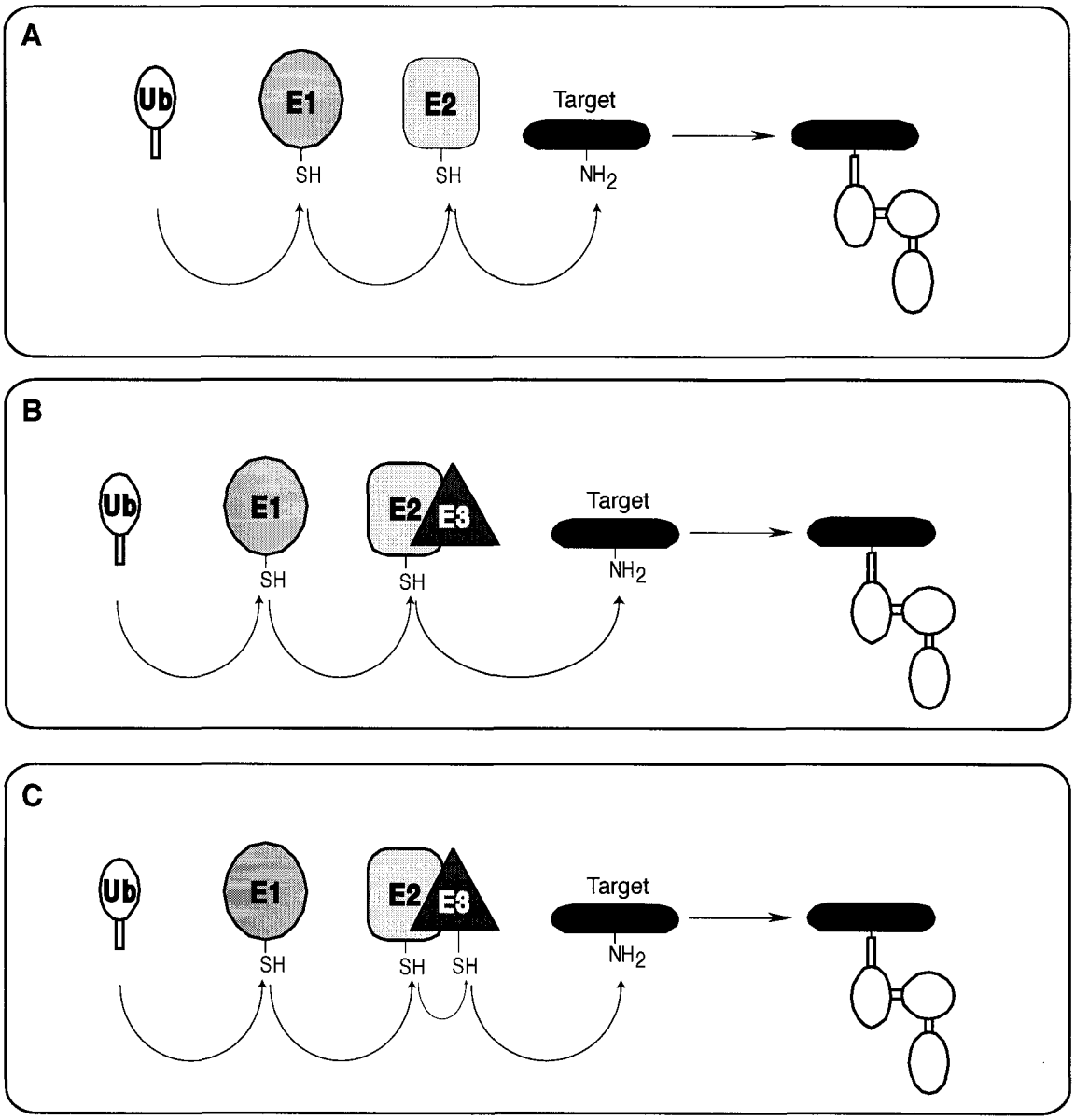

Figure 1.6. **Bucket Brigade Mechanism for Ub Chain Formation**
The three possible pathways that can lead to the formation of a multi-Ub chain on a target protein. **A**, the target protein is recognized directly by an E2 and the Ub chain is built by subsequent addition to the target. **B**, represents a situation where a complex is formed between an E2 and E3 which then results in the recognition of a target. In this situation, the E3 participates, only in target recognition and does not participate catalytically. **C**, demonstrates the direct involvement of the E3 as the terminal donator to the target protein. In this case, the E3 forms a thiolester with Ub and E2 is not involved in the transfer of Ub to the target.

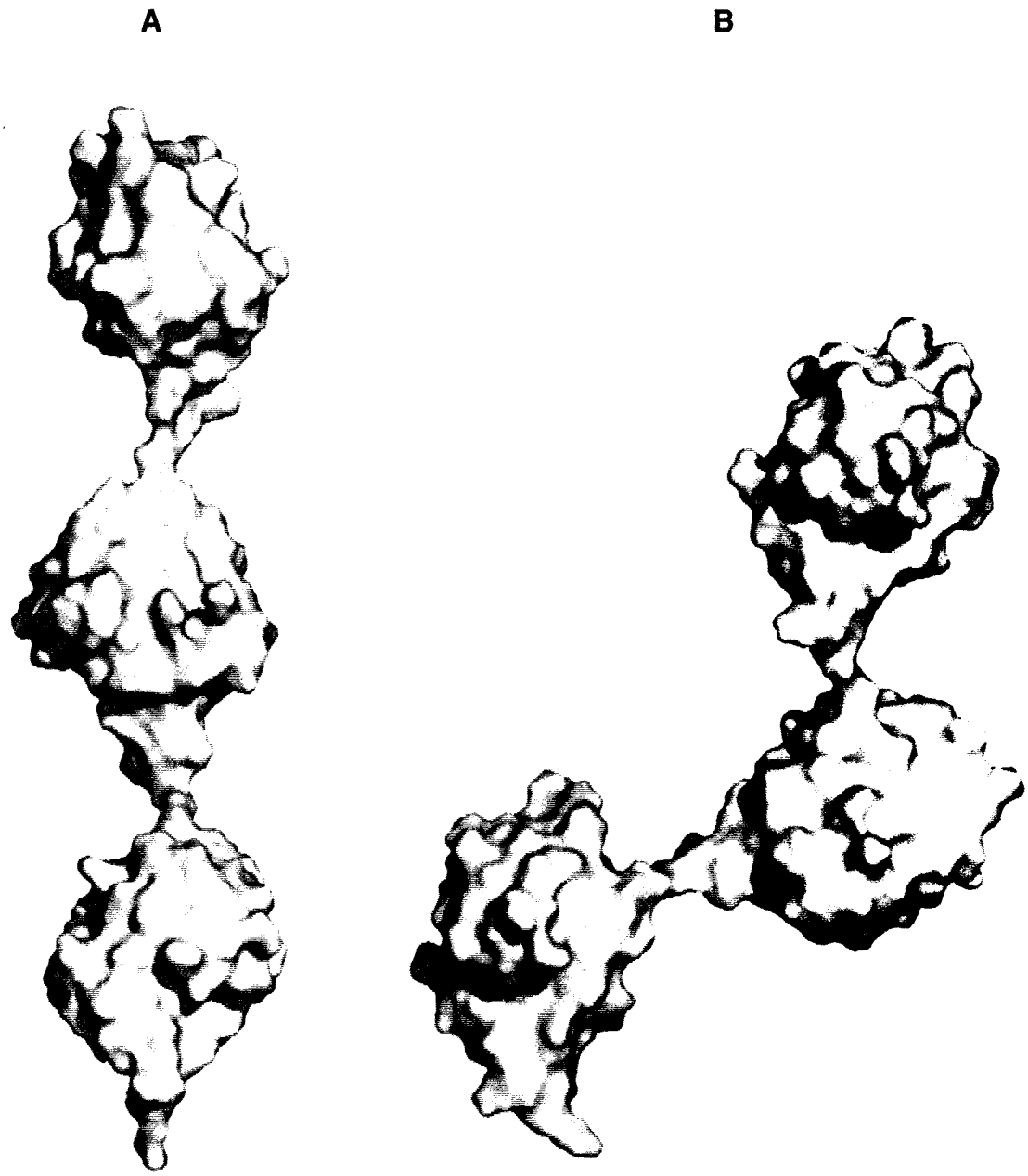

Figure 1.7. **Alternate Linkages of Ub Chains**
Connolly surface representations of two Ub chain variations. These images were generated by linking three molecules of Ub (1UBQ) at either Lys 63 (**A**) or Lys 48 (**B**). The yellow patches on each chain surface represents the position of the modified lysine residue. These structures are schematic representations of the potential, extended orientation that Ub chains may adopt. They are meant to demonstrate the variability that can be achieved and do not represent actual structures of these chains within the cell.

1.10 References

Arnason, T., & Ellison, M. J. (1994). Stress resistance in Saccharomyces cerevisiae is strongly correlated with assembly of a novel type of multiubiquitin chain. *Mol Cell Biol, 14(12)*, 7876-83.

Baboshina, O. V., & Haas, A. L. (1996). Novel multiubiquitin chain linkages catalyzed by the conjugating enzymes E2EPF and RAD6 are recognized by 26 S proteasome subunit 5. *J Biol Chem, 271(5)*, 2823-31.

Bachmair, A., Finley, D., & Varshavsky, A. (1986). In vivo half-life of a protein is a function of its amino-terminal residue. *Science, 234(4773)*, 179-86.

Baker, R. T., Smith, S. A., Marano, R., McKee, J., & Board, P. G. (1994). Protein expression using cotranslational fusion and cleavage of ubiquitin. Mutagenesis of the glutathione-binding site of human Pi class glutathione S-transferase. *J Biol Chem, 269(41)*, 25381-86.

Banerjee, A., Gregori, L., Xu, Y., & Chau, V. (1993). The bacterially expressed yeast CDC34 gene product can undergo autoubiquitination to form a multiubiquitin chain-linked protein. *J Biol Chem, 268(8)*, 5668-75.

Barral, Y., Jentsch, S., & Mann, C. (1995). G1 cyclin turnover and nutrient uptake are controlled by a common pathway in yeast. *Genes Dev, 9(4)*, 399-409.

Bartel, B., Wunning, I., & Varshavsky, A. (1990). The recognition component of the N-end rule pathway. *Embo J, 9(10)*, 3179-89.

Beal, R., Deveraux, Q., Xia, G., Rechsteiner, M., & Pickart, C. (1996). Surface hydrophobic residues of multiubiquitin chains essential for proteolytic targeting. *Proc Natl Acad Sci U S A, 93(2)*, 861-66.

Belleau, B., & Chevalier, R. (1968). The absolute conformation of chymotrypsin-bound substrates. Specific recognition by the enzyme of biphenyl asymmetry in a constrained substrate. *J Am Chem Soc, 90(24)*, 6864-66.

Chau, V., Tobias, J. W., Bachmair, A., Marriott, D., Ecker, D. J., Gonda, D. K., & Varshavsky, A. (1989). A multiubiquitin chain is confined to specific lysine in a targeted short-lived protein. *Science, 243(4898)*, 1576-83.

Ciechanover, A., Hod, Y., & Hershko, A. (1978). A heat-stable polypeptide component of an ATP-dependent proteolytic system from reticulocytes. *Biochem Biophys Res Commun, 81*, 1100-05.

Ciechanover, A., DiGiuseppe, J. A., Bercovich, B., Orian, A., Richter, J. D., Schwartz, A. L., & Brodeur, G. M. (1991). Degradation of nuclear oncoproteins by the ubiquitin system in vitro. *Proc Natl Acad Sci U S A, 88(1)*, 139-43.

Ciechanover, A., Elias, S., Heller, H., & Hershko, A. (1982). "Covalent affinity" purification of ubiquitin-activating enzyme. *J Biol Chem, 257(5)*, 2537-42.

Ciechanover, A., Heller, H., Katz-Etzion, R., & Hershko, A. (1981). Activation of the heat-stable polypeptide of the ATP-dependent proteolytic system. *Proc Natl Acad Sci U S A, 78(2)*, 761-65.

Cuervo, A. M., Gomes, A. V., Barnes, J. A., & Dice, J. F. (2000). Selective degradation of annexins by chaperone-mediated autophagy. *J Biol Chem, 275(43)*, 33329-35.

Deveraux, Q., Wells, R., & Rechsteiner, M. (1990). Ubiquitin metabolism in ts85 cells, a mouse carcinoma line that contains a thermolabile ubiquitin activating enzyme. *J Biol Chem, 265(11)*, 6323-29.

Deveraux, Q., Ustrell, V., Pickart, C., & Rechsteiner, M. (1994). A 26 S protease subunit that binds ubiquitin conjugates. *J Biol Chem, 269(10)*, 7059-61.

Di, M. S., & Priestle, J. P. (1997). Structure of the complex of leech-derived tryptase inhibitor (LDTI) with trypsin and modeling of the LDTI-tryptase system. *Structure, 5(11)*, 1465-74.

Dubiel, W., & Gordon, C. (1999). Another link in the polyubiquitin chain? *Curr Biol, 12(9)*, R554-R557.

Dubnoff, J.W. (1959). *Biochim Biophys Acta, 31*, 541-45.

Etlinger, J. D., & Goldberg, A. L. (1977). A soluble ATP-dependent proteolytic system responsible for the degradation of abnormal proteins in reticulocytes. *Proc Natl Acad Sci U S A, 74(1)*, 54-58.

Feldman, R. M., Correll, C. C., Kaplan, K. B., & Deshaies, R. J. (1997). A complex of Cdc4p, Skp1p, and Cdc53p/cullin catalyzes ubiquitination of the phosphorylated CDK inhibitor Sic1p. *Cell, 91(2)*, 221-30.

Finley, D., Ciechanover, A., & Varshavsky, A. (1984). Thermolability of ubiquitin-activating enzyme from the mammalian cell cycle mutant ts85. *Cell, 37(1)*, 43-55.

Finley, D., Ozkaynak, E., & Varshavsky, A. (1987). The yeast polyubiquitin gene is essential for resistance to high temperatures, starvation, and other stresses. *Cell, 48(6)*, 1035-46.

Finley, D., Sadis, S., Monia, B. P., Boucher, P., Ecker, D. J., Crooke, S. T., & Chau, V. (1994). Inhibition of proteolysis and cell cycle progression in a multiubiquitination-deficient yeast mutant. *Mol Cell Biol, 14(8)*, 5501-09.

Fujimuro, M., Sawada, H., & Yokosawa, H. (1997). Dynamics of ubiquitin conjugation during heat-shock response revealed by using a monoclonal antibody specific to multi-ubiquitin chains. *Eur J Biochem, 249(2)*, 427-33.

Gieffers, C., Dube, P., Harris, J. R., Stark, H., & Peters, J. M. (2001). Three-dimensional structure of the anaphase-promoting complex. *Mol Cell, 7(4)*, 907-13.

Glotzer, M., Murray, A. W., & Kirschner, M. W. (1991). Cyclin is degraded by the ubiquitin pathway. *Nature, 349(6305)*, 132-38.

Goldstein, G., Scheid, M., Hammerling, U., Schlesinger, D. H., Niall, H. D., & Boyse, E. A. (1975). Isolation of a polypeptide that has lymphocyte-differentiating properties and is probably represented universally in living cells. *Proc Natl Acad Sci U S A, 72(1)*, 11-15.

Granner, D. K., Hayashi, S., Thompson, E. B., & Tomkins, G. M. (1968). Stimulation of tyrosine aminotransferase synthesis by dexamethasone phosphate in cell culture. *J Mol Biol, 35(2)*, 291-301.

Gregori, L., Poosch, M. S., Cousins, G., & Chau, V. (1990). A uniform isopeptide-linked multiubiquitin chain is sufficient to target substrate for degradation in ubiquitin-mediated proteolysis. *J Biol Chem, 265(15)*, 8354-57.

Grossman, A., & Mavrides, C. (1967). Studies on the regulation of tyrosine aminotransferase in rats. *J Biol Chem, 242(7)*, 1398-405.

Gwozd, C. S., Arnason, T. G., Cook, W. J., Chau, V., & Ellison, M. J. (1995). The yeast UBC4 ubiquitin conjugating enzyme monoubiquitinates itself in vivo: evidence for an E2-E2 homointeraction. *Biochemistry, 34(19)*, 6296-302.

Haas, A., Reback, P. M., Pratt, G., & Rechsteiner, M. (1990). Ubiquitin-mediated degradation of histone H3 does not require the substrate-binding ubiquitin protein ligase, E3, or attachment of polyubiquitin chains. *J Biol Chem, 265(35)*, 21664-69.

Haas, A. L., & Rose, I. A. (1982). The mechanism of ubiquitin activating enzyme. A kinetic and equilibrium analysis. *J Biol Chem, 257(17)*, 10329-37.

Haas, A. L., Warms, J. V., Hershko, A., & Rose, I. A. (1982). Ubiquitin-activating enzyme. Mechanism and role in protein-ubiquitin conjugation. *J Biol Chem, 257(5)*, 2543-48.

Haas, A. L., Warms, J. V., & Rose, I. A. (1983). Ubiquitin adenylate: structure and role in ubiquitin activation. *Biochemistry, 22(19)*, 4388-94.

Hamilton, K. S., Ellison, M. J., Barber, K. R., Williams, R. S., Huzil, J. T., McKenna, S., Ptak, C., Glover, M., & Shaw, G. S. (2001). Structure of a

conjugating enzyme-ubiquitin thiolester intermediate reveals a novel role for the ubiquitin tail. *Structure (Camb), 9*, 897-904.

Haglund, K., Shimokawa, N., Szymkiewicz, I., & Dikic, I. (2002). Cbl-directed monoubiquitination of CIN85 is involved in regulation of ligand-induced degradation of EGF receptors. *Proc Natl Acad Sci U S A*, 99(19), 12191-96.

Handley, P. M., Mueckler, M., Siegel, N. R., Ciechanover, A., & Schwartz, A. L. (1991). Molecular cloning, sequence, and tissue distribution of the human ubiquitin-activating enzyme E1. *Proc Natl Acad Sci U S A, 88(1)*, 258-62.

Hatfield, P. M., Callis, J., & Vierstra, R. D. (1990). Cloning of ubiquitin activating enzyme from wheat and expression of a functional protein in Escherichia coli. *J Biol Chem, 265(26)*, 15813-17.

Hatfield, P. M., & Vierstra, R. D. (1992). Multiple forms of ubiquitin-activating enzyme E1 from wheat. Identification of an essential cysteine by in vitro mutagenesis. *J Biol Chem, 267(21)*, 14799-803.

Hershko, A., Ciechanover, A., Heller, H., Haas, A. L., & Rose, I. A. (1980). Proposed role of ATP in protein breakdown: conjugation of protein with multiple chains of the polypeptide of ATP-dependent proteolysis. *Proc Natl Acad Sci U S A, 77(4)*, 1783-86.

Hershko, A., Ganoth, D., Pehrson, J., Palazzo, R. E., & Cohen, L. H. (1991). Methylated ubiquitin inhibits cyclin degradation in clam embryo extracts. *J Biol Chem, 266(25)*, 16376-79.

Hershko, A., & Tomkins, G. M. (1971). Studies on the degradation of tyrosine aminotransferase in hepatoma cells in culture. Influence of the composition of the medium and adenosine triphosphate dependence. *J Biol Chem, 246(3)*, 710-14.

Hershko, A. (1997). Roles of ubiquitin-mediated proteolysis in cell cycle control. *Curr Opin Cell Biol, 9(6)*, 788-99.

Hershko, A., & Ciechanover, A. (1992). The ubiquitin system for protein degradation. *Annu Rev Biochem, 61*, 761-807.

Hershko, A., Ciechanover, A., & Rose, I. A. (1979). Resolution of the ATP-dependent proteolytic system from reticulocytes: a component that interacts with ATP. *Proc Natl Acad Sci U S A, 76(7)*, 3107-10.

Hershko, A., & Heller, H. (1985). Occurrence of a polyubiquitin structure in ubiquitin-protein conjugates. *Biochem Biophys Res Commun, 128(3)*, 1079-86.

Hershko, A., Heller, H., Elias, S., & Ciechanover, A. (1983). Components of ubiquitin-protein ligase system. Resolution, affinity purification, and role in protein breakdown. *J Biol Chem, 258(13)*, 8206-14.

Hershko, A., Leshinsky, E., Ganoth, D., & Heller, H. (1984). ATP-dependent degradation of ubiquitin-protein conjugates. *Proc Natl Acad Sci U S A, 81(6)*, 1619-23.

Hodgins, R., Gwozd, C., Arnason, T., Cummings, M., & Ellison, M. J. (1996). The tail of a ubiquitin-conjugating enzyme redirects multi-ubiquitin chain synthesis from the lysine 48-linked configuration to a novel nonlysine-linked form. *J Biol Chem, 271(46)*, 28766-71.

Huibregtse, J. M., Scheffner, M., & Howley, P. M. (1994). E6-AP directs the HPV E6-dependent inactivation of p53 and is representative of a family of structurally and functionally related proteins. *Cold Spring Harb Symp Quant Biol, 59*, 237-45.

Ikehata, H., Kaneda, S., Yamao, F., Seno, T., Ono, T., & Hanaoka, F. (1997). Incubation at the nonpermissive temperature induces deficiencies in UV resistance and mutagenesis in mouse mutant cells expressing a temperature-sensitive ubiquitin-activating enzyme (E1). *Mol Cell Biol, 17(3)*, 1484-89.

Johnson, E. S., Bartel, B., Seufert, W., & Varshavsky, A. (1992). Ubiquitin as a degradation signal. *Embo J, 11(2)*, 497-505.

Johnson, P. R., Swanson, R., Rakhilina, L., & Hochstrasser, M. (1998). Degradation signal masking by heterodimerization of MATalpha2 and MATa1 blocks their mutual destruction by the ubiquitin-proteasome pathway. *Cell, 94(2)*, 217-27.

Johnston, J. A., Johnson, E. S., Waller, P. R., & Varshavsky, A. (1995). Methotrexate inhibits proteolysis of dihydrofolate reductase by the N- end rule pathway. *J Biol Chem, 270(14)*, 8172-78.

Johnston, S. D., Enomoto, S., Schneper, L., McClellan, M. C., Twu, F., Montgomery, N. D., Haney, S. A., Broach, J. R., & Berman, J. (2001). CAC3(MSI1) suppression of RAS2(G19V) is independent of chromatin assembly factor I and mediated by NPR1. *Mol Cell Biol, 21(5)*, 1784-94.

Jones, E. W. (1991). Three proteolytic systems in the yeast saccharomyces cerevisiae. *J Biol Chem, 266(13)*, 7963-66.

Kamura, T., Conrad, M. N., Yan, Q., Conaway, R. C., & Conaway, J. W. (1999). The Rbx1 subunit of SCF and VHL E3 ubiquitin ligase activates Rub1 modification of cullins Cdc53 and Cul2. *Genes Dev, 13(22)*, 2928-33.

King, R. W., Peters, J. M., Tugendreich, S., Rolfe, M., Hieter, P., & Kirschner, M. W. (1995). A 20S complex containing CDC27 and CDC16 catalyzes the mitosis-specific conjugation of ubiquitin to cyclin B. *Cell, 81(2)*, 279-88.

Kornitzer, D., Raboy, B., Kulka, R. G., & Fink, G. R. (1994). Regulated degradation of the transcription factor Gcn4. *Embo J, 13(24)*, 6021-30.

Kulka, R. G., Raboy, B., Schuster, R., Parag, H. A., Diamond, G., Ciechanover, A., & Marcus, M. (1988). A Chinese hamster cell cycle mutant arrested at G2 phase has a temperature-sensitive ubiquitin-activating enzyme, E1. *J Biol Chem, 263(30)*, 15726-31.

Lake, M. W., Wuebbens, M. M., Rajagopalan, K. V., & Schindelin, H. (2001). Mechanism of ubiquitin activation revealed by the structure of a bacterial MoeB-MoaD complex. *Nature, 414(6861)*, 325-9..

Lee, N. (1956). The Induced Increase in the Tryptophan Peroxidase-Oxidase Activity of Rat Liver: Time Studies. *J Biol Chem, 219*, 211-20.

Li, F. N., & Johnston, M. (1997). Grr1 of Saccharomyces cerevisiae is connected to the ubiquitin proteolysis machinery through Skp1: coupling glucose sensing to gene expression and the cell cycle. *Embo J, 16(18)*, 5629-38.

Liu, Y., Mathias, N., Steussy, C. N., & Goebl, M. G. (1995). Intragenic suppression among CDC34 (UBC3) mutations defines a class of ubiquitin-conjugating catalytic domains. *Mol Cell Biol, 15(10)*, 5635-44.

Lisztwan, J., Marti, A., Sutterluty, H., Gstaiger, M., Wirbelauer, C., & Krek, W. (1998). Association of human CUL-1 and ubiquitin-conjugating enzyme CDC34 with the F-box protein p45(SKP2): evidence for evolutionary conservation in the subunit composition of the CDC34-SCF pathway. *EMBO J*, 17(2), 368-83.

Lopez-Otin, C., & Overall, C. M. (2002). Protease degradomics: A new challenge for proteomics. *Nat Rev Mol Cell Biol, 3(7)*, 509-19.

Mastrandrea, L. D., You, J., Niles, E. G., & Pickart, C. M. (1999). E2/E3-mediated assembly of lysine 29-linked polyubiquitin chains. *J Biol Chem, 274(38)*, 27299-306.

Maurizi, M. R. (1992). Proteases and protein degradation in Escherichia coli. *Experientia, 48(2)*, 178-201.

Mayer, A., Siegel, N. R., Schwartz, A. L., & Ciechanover, A. (1989). Degradation of proteins with acetylated amino termini by the ubiquitin system. *Science, 244(4911)*, 1480-83.

McGrath, J. P., Jentsch, S., & Varshavsky, A. (1991). UBA 1: an essential yeast gene encoding ubiquitin-activating enzyme. *Embo J, 10(1)*, 227-36.

Monia, B. P., Ecker, D. J., Finley, D., & Crooke, S. T. (1990). A human ubiquitin carboxyl extension protein functions in yeast. *J Biol Chem, 265(31)*, 19356-61.

Mori, M., Eki, T., Takahashi-Kudo, M., Hanaoka, F., Ui, M., & Enomoto, T. (1993). Characterization of DNA synthesis at a restrictive temperature in the temperature-sensitive mutants, tsFT5 cells, that belong to the complementation

group of ts85 cells containing a thermolabile ubiquitin-activating enzyme E1. Involvement of the ubiquitin-conjugating system in DNA replication. *J Biol Chem, 268(22)*, 16803-09.

Neurath, H. (1986). The versatility of proteolytic enzymes. *J Cell Biochem, 32(1)*, 35-49.

Nugroho, T. T., & Mendenhall, M. D. (1994). An inhibitor of yeast cyclin-dependent protein kinase plays an important role in ensuring the genomic integrity of daughter cells. *Mol Cell Biol, 14(5)*, 3320-28.

Ozkaynak, E., Finley, D., Solomon, M. J., & Varshavsky, A. (1987). The yeast ubiquitin genes: a family of natural gene fusions. *Embo J, 6(5)*, 1429-39.

Page, A. M., & Hieter, P. (1999). The anaphase-promoting complex: new subunits and regulators. *Annu Rev Biochem, 68*, 583-609.

Pickart, C. M. (1997). Targeting of substrates to the 26S proteasome. *Faseb J, 11(13)*, 1055-66.

Pickart, C. M., & Rose, I. A. (1985). Functional heterogeneity of ubiquitin carrier proteins. *J Biol Chem, 260(3)*, 1573-81.

Pitluk, Z. W., McDonough, M., Sangan, P., & Gonda, D. K. (1995). Novel CDC34 (UBC3) ubiquitin-conjugating enzyme mutants obtained by charge-to-alanine scanning mutagenesis. *Mol Cell Biol, 15(3)*, 1210-19.

Portig, I., Pankuweit, S., Lottspeich, F., & Maisch, B. (1996). Identification of stress proteins in endothelial cells. *Electrophoresis, 17(4)*, 803-08.

Ptak, C., Gwozd, C., Huzil, J. T., Gwozd, T. J., Garen, G., & Ellison, M. J. (2001). Creation of a pluripotent ubiquitin-conjugating enzyme. *Mol Cell Biol, 21(19)*, 6537-48.

Stellwagen, R. H. (1992). Involvement of Sequences Near Both Amino and Carboxyl Termini in the Rapid Intracellular Degradation of Tyrosine Aminotransferase. *J. Biol. Chem., 267*, 23713-21.

Rechsteiner, M. (1989). PEST regions, proteolysis and cell cycle progression. *Revis Biol Celular, 20*, 235-53.

Redman, K. L., & Burris, G. W. (1996). The cDNA for the ubiquitin-52-amino-acid fusion protein from rat encodes a previously unidentified 60 S ribosomal subunit protein. *Biochem J, 315(Pt 1)*, 315-21.

Redman, K. L., & Rechsteiner, M. (1989). Identification of the long ubiquitin extension as ribosomal protein S27a. *Nature, 338(6214)*, 438-40.

Sarin, A., Adams, D. H., & Henkart, P. A. (1993). Protease inhibitors selectively block T cell receptor-triggered programmed cell death in a murine T cell hybridoma and activated peripheral T cells. *J Exp Med, 178(5)*, 1693-700.

Scheffner, M., Werness, B. A., Huibregtse, J. M., Levine, A. J., & Howley, P. M. (1990). The E6 oncoprotein encoded by human papillomavirus types 16 and 18 promotes the degradation of p53. *Cell, 63(6)*, 1129-36.

Schimke, R.T., Sweeney, E.W. & Berlin, C.M. (1965). Studies of the Stability *in Vivo* and *in Vitro* of Rat Liver Tryptophan Pyrrolase. *J. Biol. Chem, 240(12)*, 4609-4620.

Schlesinger, D. H., Goldstein, G., & Niall, H. D. (1975). The complete amino acid sequence of ubiquitin, an adenylate cyclase stimulating polypeptide probably universal in living cells. *Biochemistry, 14(10)*, 2214-18.

Schulman, B. A., Carrano, A. C., Jeffrey, P. D., Bowen, Z., Kinnucan, E. R., Finnin, M. S., Elledge, S. J., Harper, J. W., Pagano, M., & Pavletich, N. P. (2000). Insights into SCF ubiquitin ligases from the structure of the Skp1-Skp2 complex. *Nature, 408(6810)*, 381-86.

Seufert, W., McGrath, J. P., & Jentsch, S. (1990). UBC1 encodes a novel member of an essential subfamily of yeast ubiquitin-conjugating enzymes involved in protein degradation. *Embo J, 9(13)*, 4535-41.

Simpson, M. V. The release of labeled amino acids from the proteins of rat liver slices. *J. Biol. Chem., 201*, 143-54.

Smyth, M. J., Browne, K. A., Thia, K. Y., Apostolidis, V. A., Kershaw, M. H., & Trapani, J. A. (1994). Hypothesis: cytotoxic lymphocyte granule serine proteases activate target cell endonucleases to trigger apoptosis. *Clin Exp Pharmacol Physiol, 21(1)*, 67-70.

Spence, J., Sadis, S., Haas, A. L., & Finley, D. (1995). A ubiquitin mutant with specific defects in DNA repair and multiubiquitination. *Mol Cell Biol, 15(3)*, 1265-73.

Squier, M. K., Miller, A. C., Malkinson, A. M., & Cohen, J. J. (1994). Calpain activation in apoptosis. *J Cell Physiol, 159(2)*, 229-37.

Stroud, R. M., Kossiakoff, A. A., & Chambers, J. L. (1977). Mechanisms of zymogen activation. *Annu Rev Biophys Bioeng, 6*, 177-93.

Swanson, R., & Hochstrasser, M. (2000). A viable ubiquitin-activating enzyme mutant for evaluating ubiquitin system function in Saccharomyces cerevisiae. *FEBS Lett, 477(3)*, 193-98.

Tanaka, K., Yoshimura, T., Kumatori, A., Ichihara, A., Ikai, A., Nishigai, M., Kameyama, K., & Takagi, T. (1988). Proteasomes (multi-protease complexes) as 20 S ring-shaped particles in a variety of eukaryotic cells. *J Biol Chem, 263(31)*, 16209-17.

Tobias, J. W., Shrader, T. E., Rocap, G., & Varshavsky, A. (1991). The N-end rule in bacteria. *Science, 254(5036)*, 1374-77.

Tongaonkar, P., Beck, K., Shinde, U. P., & Madura, K. (1999). Characterization of a temperature-sensitive mutant of a ubiquitin- conjugating enzyme and its use as a heat-inducible degradation signal. *Anal Biochem, 272(2)*, 263-69.

Treger, J. M., Heichman, K. A., & McEntee, K. (1988). Expression of the yeast UB14 gene increases in response to DNA-damaging agents and in meiosis. *Mol Cell Biol, 8(3)*, 1132-36.

van Nocker, S., & Vierstra, R. D. (1993). Multiubiquitin chains linked through lysine 48 are abundant in vivo and are competent intermediates in the ubiquitin proteolytic pathway. *J Biol Chem, 268(33)*, 24766-73.

Varshavsky, A., Bachmair, A., & Finley, D. (1987). The N-end rule of selective protein turnover: mechanistic aspects and functional implications. *Biochem Soc Trans, 15(5)*, 815-16.

Vijay-Kumar, S., Bugg, C. E., Wilkinson, K. D., & Cook, W. J. (1985). Three-dimensional structure of ubiquitin at 2.8 A resolution. *Proc Natl Acad Sci U S A, 82(11)*, 3582-85.

Voet, D., & Voet, J. G. (1995). *Biochemistry 2nd Edition*. New York, N.Y.: John Wiley and Sons.

von Arnim, A. G. (2001). A hitchhiker's guide to the proteasome. *Sci STKE, 2001(97)*, PE2.

Walden, H., Podgorski, M. S., & Schulman, B. A. (2003). Insights into the ubiquitin transfer cascade from the structure of the activating enzyme for NEDD8. *Nature, 422(6929)*, 330-34.

Walker, J. E., Eberle, A., Gay, N. J., Runswick, M. J., & Saraste, M. (1982). Conservation of structure in proton-translocating ATPases of Escherichia coli and mitochondria. *Biochem Soc Trans, 10(4)*, 203-06.

Watt, R., & Piper, P. W. (1997). UBI4, the polyubiquitin gene of Saccharomyces cerevisiae, is a heat shock gene that is also subject to catabolite derepression control. *Mol Gen Genet, 253(4)*, 439-47.

Wenzel, T., Eckerskorn, C., Lottspeich, F., & Baumeister, W. (1994). Existence of a molecular ruler in proteasomes suggested by analysis of degradation products. *FEBS Lett, 349(2)*, 205-09.

Wigle, D. T., & Dixon, G. H. (1970). Transient incorporation of methionine at the N-terminus of protamine newly synthesized in trout testis cells. *Nature, 227(259)*, 676-80.

Williams, M. S., & Henkart, P. A. (1994). Apoptotic cell death induced by intracellular proteolysis. *J Immunol, 153(9)*, 4247-55.

Wilson, D. B., & Dintzis, H. M. (1970). Protein chain initiation in rabbit reticulocytes. *Proc Natl Acad Sci U S A, 66(4)*, 1282-89.

Yennawar, N. H., Yennawar, H. P., & Farber, G. K. (1994). X-ray crystal structure of gamma-chymotrypsin in hexane. *Biochemistry, 33(23)*, 7326-36.

Yoshida, A., Watanabe, S., & Morris, J. (1970). Initiation of rabbit hemoglobin synthesis: methionine and formylmethionine at the N-terminal. *Proc Natl Acad Sci U S A, 67(3)*, 1600-07.

Zheng, N., Schulman, B. A., Song, L., Miller, J. J., Jeffrey, P. D., Wang, P., Chu, C., Koepp, D. M., Elledge, S. J., Pagano, M., Conaway, R. C., Conaway, J. W., Harper, J. W., & Pavletich, N. P. (2002). Structure of the Cul1-Rbx1-Skp1-F boxSkp2 SCF ubiquitin ligase complex. *Nature, 416(6882)*, 703-09.

Zhu, D. X., Zhang, A., Zhu, N. C., Xu, L. X., Deutsch, H. F., & Han, K. K. (1986). Investigations of primary and secondary structure of porcine ubiquitin. Its N epsilon-acetylated lysine derivative. *Int J Biochem, 18(5)*, 473-76.

Chapter 2

Mechanistic Insights into Ub Activation and Transfer to the Ubiquitin Conjugating Enzymes.[1]

2.1 Introduction

Ubiquitination involves a reaction cascade in which the small protein modifier ubiquitin (Ub) is transferred between multiple enzymes prior to its becoming conjugated to a target protein. Ubiquitin activating enzyme (E1 or Uba1) is responsible for the initial ATP dependent activation of Ub, which results in the formation of a high-energy thiolester bond between the carboxy terminus of Ub and a cysteine residue internal to Uba1 (Haas and Rose, 1982; Haas *et al.*, 1982; Ciechanover *et al.*, 1984). The formation of the high-energy thiolester bond between Uba1 and Ub allows for the transfer of Ub to a second enzyme in this pathway, a Ubiquitin conjugating enzyme (Ubc or E2). This transfer comprises a transthiolation reaction in which Ub is transferred from the Uba1 active site cysteine to the active site cysteine of E2 (Hershko, 1983).

Once Ub has become bound to E2, the subsequent transfer of Ub may occur in one of two ways. First, E2 may directly transfer Ub from its active site to an ε-amino group of a lysine residue within the target protein (Pickart and Rose, 1985; Pickart and Vella, 1988), or Ub may be transferred to a cysteine residue of a third protein in

---

1 Manuscript in preparation.

this pathway, a ubiquitin protein ligase (E3). E3 is then responsible for recognition and binding of target proteins resulting in the transfer of Ub to an internal lysine residue within the target protein itself (Hershko *et al.*, 1983; Hershko and Ciechanover, 1986).

The focus of this study was to determine the spatial organization of the two active sites within the *Saccharomyces cerevisiae* Uba1 and establish how they function in the activation and transfer of Ub to E2. Previous kinetic studies of this mechanism have determined the rate of ATP hydrolysis, formation of Ub-adenylate, formation of the Uba1~Ub thiolester and explored the transfer of Ub from Uba1 to E2 (Haas and Rose, 1982; Haas *et al.*, 1982; Haas *et al.*, 1983). In Chapter 4 a model of the Uba1 active site will be introduced and a possible mechanism of Ub transfer will be discussed. Here we describe the generation and purification of several Uba1 active site derivatives that aid in confirming the positions of the ATP binding and thiolester sites. These sites are predicted by sequence comparisons with other proteins involved in the activation of Ubiquitin Like Proteins (UBLs) (Chapter 4, section 4.1.3) and provides us with insight into the mechanism and structure of Uba1. In particular, this chapter provides biochemical evidence that the two active sites of Uba1 and the active site of an E2, Ubc1Δ (the catalytic core domain of Ubc1: Hamilton *et al.*, 2001), are spatially close and transfer between them all is possible.

2.2 Experimental Procedures

Plasmids and Strains

Escherichia coli expression plasmids for Ub and Ubc1Δ have been previously described (Hodgins *et al.*, 1996). Dr. Dan Finley (Harvard Medical School) generously provided the high copy, *Leu2* based, yeast expression vector containing the Uba1 coding region and the *S. cerevisiae* Uba1 deletion strain PJD325, sustained with the above-mentioned plasmid. The Uba1 coding

sequence includes codons for six histidine residues at the 3' end and is bounded by the *CUP1* promoter and the *CYC1* terminator.

The *E. coli* strain MC1061 (F- araD139 (ara-leu)7696 galE15 galK16 (lac)X74 rpsL (Strr) hsdR2 (rk-mk+) mcrA mcrB1) was used for PCR mutagenesis and plasmid biosynthesis (New England Biolabs). The *E. coli* strain BL21(DE3)pLysS (F- ompT hsdSB (rB-mB-) gal dcm (DE3) pLysS (CamR)) (Invitrogen) was used for the overexpression of Ubc1Δ and Ub. Wild type Uba1 and mutant forms of Uba1 plasmids were over-expressed in the *S. cerevisiae* strain MHY-501 (MATa his3-Δ200 leu2-3,112 ura3-52 lys2-801 trp1-1, gal2) (constructed by Dr. Mark Hochstrasser, University of Chicago), which is a copper resistant wild type strain.

Codon changes within the coding sequence of UBA1 were introduced using the polymerase chain reaction and oligonucleotides containing the mutant sequences. Codon changes included GGT to GTT resulting in a glycine to valine substitution at position 446 (uba1G446V), TGT to GCT resulting in a cysteine to alanine substitution at position 600 (uba1C600A) and TGT to AGT resulting in a cysteine to serine substitution also at position 600 (uba1C600S). *S. Cerevisiae* Uba1 and the active site derivatives were expressed in the yeast strain MHY501 (MATa *his3-Δ200 leu2-3,112 ura3-52 lys2-801 trp1-1 gal2*) (Papa and Hochstrasser, 1993). All of the high copy yeast expression plasmids, carrying the coding regions of the various Uba1 active site derivatives, are identical to the Uba1 expression plasmid, with the exception that they carry the appropriate codon modifications mentioned previously.

Plating Experiments

Viability of Uba1Δ yeast strains PJD325-UBA1A, PJD325-UBAS and PJD325-UBAV, containing each of the mutated plasmids, was tested using typical 5-fluoro-orotic acid (FOA) plating experiments. FOA is commonly used in these types of plasmid shuffling experiments, as it is a toxigenic substrate of the Ura3 enzyme. The Uba1Δ strain carrying a Ura3 based Uba1 expression plasmid (pUba1-Ura)

was transformed with the Leu2 based expression plasmids carrying either the wild type coding region for Uba1 or the various Uba1 active site derivatives uba1C600A, uba1C600S and uba1G446V. Cells were grown in liquid synthetic defined (SD) media lacking uracil and leucine. 10^5 cells were plated and streaked on fully supplemented SD plates containing 1mg/ml FOA, and on growth control plates containing supplemented SD media lacking both leucine and uracil.

Protein Expression and Purification

Expression plasmids for Uba1 and its active site derivatives were transformed into the yeast strain MHY501 and cells were plated onto SD media lacking leucine and grown at 30 °C until individual colonies appeared. One hundred ml of SD liquid media lacking leucine was then inoculated with a single colony from a transformation plate and the culture was grown overnight to an OD_{600} of 1.0. Cultures were diluted to an initial OD_{600} of 0.1 into 2L of liquid media and grown at 30 °C with shaking to an OD_{600} of 0.15. Copper sulfate was then added to a concentration of 100 μM to induce Uba1 expression from the *CUP1* promoter. Cultures were grown for an additional 12 hours at 30 °C with vigorous shaking, after which the cells were harvested by centrifugation.

The cell pellet was suspended in 2 volumes of buffer A (50 mM Tris (pH 7.5), 10 mM $MgCl_2$, 1M sorbitol, 1 mM DTT), the suspension was centrifuged and the pellet was re-suspended in 2 volumes of buffer A containing 1 mg zymolyase (Seikagaka Corp) per gram of packed cells. The cell suspension was incubated at 30 °C with gentle rocking for 1 hour to aid in the formation of spheroplasts. Spheroplasts were pelleted, suspended in buffer A, then centrifuged and re-suspended in 2 volumes of buffer B (80 mM Na_2HP0_4, 93 mM NaH_2PO_4, 4 M NaCl, pH 7.4). Two additional volumes of distilled water were added to promote lysis of the spheroplasts as a result of osmotic shock.

To ensure complete cell lysis, a 1:5 volume of acid washed glass beads (Biospec) was added to the spheroplast suspension in a 50 ml conical Falcon tube and the

cells were vortexed repeatedly. The resulting lysate was centrifuged at 3000 rpm to remove the glass beads and clarified by additional high speed centrifugation at 40,000 rpm. The supernatant was then filtered using a 0.45 μm low protein binding syringe tip filter (Millipore), to remove particulate matter that remained in suspension.

Clarified lysates were passed through a 1 ml HiTrap Chelating column (Pharmacia Biotech) charged with 2 ml of a 100 mM nickel sulfate solution. The lysate was re-circulated over the column for 1 hour at 4 °C at a constant flow rate of 1 ml/min using a peristaltic pump. To remove non-specifically bound proteins, the column was first washed with 5 ml of buffer B containing 10 mM imidazole, followed by 5 ml of buffer B containing 100 mM imidazole, and finally an additional 10 ml buffer B containing 10 mM imidazole. Histidine tagged Uba1 was eluted from the column with 5 ml of buffer B containing 500 mM imidazole.

Peak fractions from the 500 mM Imidazole elution were pooled and immediately loaded onto a Hi Load Superdex 75 16/60 FPLC column (Pharmacia) equilibrated with buffer C (50 mM HEPES (pH 7.5), 150 mM NaCl, 1 mM EDTA). Peak fractions were pooled and aliquots run on SDS-PAGE. Initial concentrations of Uba1 or its active site derivatives were determined by comparison to the density of BSA standards run on the same gel. The purified proteins were diluted to final concentrations of 150 μg/ml with a solution containing 50 μg/ml BSA and 10% v/v glycerol. Protein solutions were then divided into individual aliquots, flash frozen with liquid nitrogen and stored at -80 °C.

Expression and purification of Ubc1Δ and [^{35}S]Ub from *E. coli* have been described previously (Hodgins *et al.*, 1992; Ptak *et al.*, 1994).

Iodoacetamide Treatment of Uba1

Iodoacetamide is a compound that irreversibly reacts with sulfhydryl groups, thereby rendering them inactive in any subsequent chemical reactions. To promote the inactivation of wild type Uba1, 500 μg of purified Uba1 was incubated with a 1000x molar excess of iodoacetamide at 30 °C for 1 hour (Jones *et al.*, 1975; Haas *et al.*,

1982; Hershko *et al.*, 1983). The sample was then dialyzed overnight against 4 L of buffer C (50 mM HEPES (pH 7.5), 150 mM NaCl, 1 mM EDTA). Finally, the dialyzate was centrifuged and re-assayed for protein concentration as described in *Protein Expression and Purification.*

In vitro Ubiquitination Reactions

All ubiquitination assays, unless stated otherwise, were carried out in ubiquitination buffer consisting of 10 mM HEPES (pH 7.5), 5 mM $MgCl_2$, 40 mM NaCl, 5 mM ATP, protease inhibitors (Sigma Aldrich) (*antipain*, *aprotinin*, *chymostatin*, *leupeptin*, *pepstatin A* at 20 μg/ml and PMSF at 180 μg/ml). Inorganic pyrophosphatase (Sigma Aldrich) (0.6 units/ml) was included to facilitate the removal of PP_i that accumulated over the course of the reaction.

Each reaction contained 360 nM [^{35}S]-Ub and Uba1, uba1C600S, uba1C600A, or uba1G446V at a final concentration of 90 nM. Reactions were incubated at 30 °C for 60 min and immediately loaded on a Superdex 75 HR 10/30 gel filtration column (Pharmacia). Reaction products were eluted with buffer C at a constant flow rate of 1 ml/min. Fractions were collected every 0.5 min and the counts per minute (cpm) of [^{35}S]-Ub present in each fraction were determined by scintillation counting using a Beckman LS-6800 Liquid Scintillation counter. These values were used to generate elution profiles for the reaction products from each run.

Ubc1Δ~Ub Thiolester Formation Reactions with Uba1 Derivatives

The Ubc1Δ~Ub thiolester was generated using a reaction containing 10 nM wild type Uba1, 100 nM Ubc1Δ and 100 nM [^{35}S]Ub. The reaction mixture was incubated at 30 °C for 1 hour. To observe the transfer of Ub to Ubc1Δ from the mutant derivatives of Uba1, subsequent ubiquitination reactions contained equimolar amounts of Ubc1Δ, [^{35}S]Ub and Uba1 derivatives, each having a final concentration of 100 nM in the reaction. Reactions were incubated for 60 minutes at 30 °C, then passed over a Superdex 75 gel filtration column (Pharmacia Biotech Inc.) and treated as in the previous example of Ub adenylate formation.

Ub Chain Formation

In vitro ubiquitination reactions were carried out in ubiquitination buffer described above, in the presence of 100nM [^{35}S]Ub, 100nM Ubc1Δ, and 100nM of either Uba1, or uba1C600A. Reactions were incubated at 30 °C for 60 min, then stopped by the addition of 10% trichloroacetic acid (TCA) and centrifuged. Pellets were re-suspended in SDS buffer containing DTT and boiled for 10 min. The samples were then applied to a10% SDS polyacrylamide gel. Following electrophoresis, the gel was dried and visualized by autoradiography using a Fuji Film phosphoimager.

Purification and Stability of the Ubc1Δ~Ub Thiolester

Purified Ubc1Δ (1.2 μM), [^{35}S]Ub (1.2 μM) and wheat Uba1 (Hatfield and Vierstra, 1992) (8 nM) were added to a ubiquitination reaction to a final reaction volume of 1 ml. The reaction was incubated at 30 °C for 5 hr after which it was immediately loaded onto a Superdex 75 16/30 gel exclusion column equilibrated with buffer C containing 50 μg/ml BSA (Fraction V, Boehringer Mannheim). Reaction products were eluted from the column using the buffer C, and 1 ml fractions were collected.

The contents of specific peak fractions were verified using SDS-PAGE followed by autoradiography. Any Ubc1Δ~Ub thiolester present in these fractions would be cleaved by the DTT present in the SDS load mix and fractions containing only Ubc1Δ~Ub thiolester are easily identified. The stability of Ubc1Δ~Ub thiolester present in the peak fractions was tested by first pooling, and then concentrating this solution using centricon (Amicon) filtration. The concentrated sample was then frozen at -80 °C prior to further use. This sample was thawed and a 50 μl aliquot of this concentrate was retained for analysis by SDS-PAGE and autoradiography. The remaining concentrate was loaded onto a gel filtration column and an elution profile of those components of the concentrate containing [^{35}S]Ub generated as described above. In this way, it was found that the Ubc1Δ~Ub thiolester was stable enough to be purified and utilized in our reactions.

Back-transfer Reactions

Back-transfer reactions contained ubiquitination buffer and an equimolar amount (100nM) of purified Ubc1Δ~[^{35}S]Ub thiolester and Uba1, uba1C600S, uba1C600A, or uba1G446V. Reactions were incubated at 30 °C for 30 minutes and immediately loaded onto a Superdex 75 HR 10/30 gel filtration column. Elution profiles were generated by following [^{35}S]Ub as described in *In vitro Ubiquitination Reactions*.

Figure Creation

Please refer to Chapter 4, *Experimental Procedures* for a description of the creation of the Uba1 active site model and the computer hardware and software used in the creation of Figure 2.9. Hydrophobic and Electrostatic surface representations of the Uba1 active site model were created using GRASP (Nicholls *et al.*, 1991). Default settings were applied to the molecule when rendering both the surface and coloring schemes.

2.3 Results

Characterization of Uba1 Active Site Derivatives

The spatial relationship of the ATP binding site, specifically the Walker fold (residues 440-446), and the catalytic cysteine residue (residue 600) was explored by introducing specific point mutations at these positions. These mutants were then tested in ubiquitination assays for their ability to support ubiquitination reactions, both *in vitro* and *in vivo*. These substitutions included a single mutation within the putative ATP binding site (uba1G446V) and two mutations at the site of Ub-thiolester formation (uba1C600S and uba1C600A). Both Gly 446 and Cys 600 have been predicted to define critical residues for Uba1 directed Ub activation, and all of these substitutions were expected to render Uba1 null with respect to its ability to carry out Ub activation *in vivo* (McGrath *et al.*, 1991). This was confirmed using a plasmid

shuffling experiment which demonstrated that yeast expression plasmids bearing the coding sequences for uba1G446V, uba1C600S, or uba1C600A were unable to rescue a Uba1 deletion (pUba1-Ura) strain. This defect was established by the inability of mutant Uba1 containing cells to grow, upon introduction of FOA into the media, as compared to cells containing the wild type construct (see *Plating Experiments*) (Figure 2.1).

In vitro Activity of Uba1 Active Site Derivatives

While the inactivity of the Uba1 active site mutants *in vivo* was not unexpected, their ability to activate Ub to Ub-AMP adenylate was examined *in vitro*. To test the activity of each derivative, they were purified from yeast and used in ubiquitination reactions. To facilitate their purification, each derivative carried six histidine residues at its carboxy terminus (Hochuli *et al.*, 1987). This allowed the Uba1 mutants to be purified using nickel affinity chromatography, resulting in approximately 95% homogeneity based on SDS PAGE (Figure 2.2). The presence of the histidine tag at the carboxy terminus of each construct also provided a means of determining if each protein was fully expressed, as incomplete expression would yield no histidine tag and therefore no purified protein. An interesting observation was the presence of a low molecular weight band that was present in the purified Uba1 lane. The presence of this band may imply the proteolysis of Uba1 at a region that defines some stable domain, as it corresponds roughly to the size of truncated Uba1Δ (Chapter 4, Figure 15). This fragment would either have to occur following purification, or correspond to an amino terminal truncation due to the histidine tags presence on the carboxy terminus of Uba1. It most likely does not correspond to another protein that binds to Uba1 during the purification, as it is not seen in during the gel exclusion chromatography purification steps.

Following the purification of each Uba1 mutant, their ability to activate Ub *in vitro* was tested using ubiquitination assays (see *In vitro Ubiquitination Reactions*). Reactions containing Uba1 or one of the derivatives, uba1C600S, uba1C600A and uba1G446V, were performed in ubiquitination buffer containing [^{35}S]Ub. The

activity of each derivative was then assessed by following the incorporation of [^{35}S]Ub in to Uba1. Reactions were incubated for 1 hr. at 30 °C then passed over a Highload Superdex gel exclusion column. The amount of [^{35}S]Ub present in each column fraction was determined by scintillation counting and these values were plotted to generate an elution profile. Each profile, with the exception of uba1G446V, exhibited two peaks corresponding to free [^{35}S]Ub or, [^{35}S]Ub that has been incorporated into Uba1 (Figure 2.3A).

Based on the elution profiles, the ratio of bound Ub to the number of available active sites for wild type Uba1 was determined to be 1.6:2 (Figure 2.3B). This indicates that while not all of the Ub binding sites available were occupied, at least a fraction of the Uba1 population has two molecules of bound Ub, presumably one as adenylate and the other as thiolester. As expected, the uba1C600A mutant, having only one active site, exhibited a binding ratio of 0.7:1, consistent with occupation of the adenylate site only. Determination of the exact ratio of the two forms of Ub was not attempted.

uba1C600S Forms a Stable Ester with Ub

The uba1C600S derivative exhibited a bound Ub ratio of 1.2:2, indicating that a fraction of the uba1C600S population contains at least two bound molecules of Ub (Figure 2.3B). This result suggested the possibility that the uba1C600S substitution allows this derivative to retain its ability to synthesize Ub-AMP and to subsequently transfer Ub to the hydroxyl group of the serine residue at position 600, thus forming an Ub ester. Previous work using cysteine to serine substitutions at the active site of an E2, demonstrated the formation of a stable ester between Ub and E2, suggesting a similar effect to that of uba1C600S (Sung *et al.*, 1991; Sullivan and Vierstra, 1993).

To determine whether a serine ester was in fact being generated *in vitro,* ubiquitination reactions were once again used. Purified Uba1 or uba1C600S were incubated with [^{35}S]Ub in ubiquitination buffer for 1 hr. at 30 °C. Reactions were

subsequently treated with dithiothreitol (DTT), to disrupt formation of the Uba1~Ub thiolester, and samples were analyzed on SDS-PAGE followed by autoradiography to identify DTT insensitive reaction products containing [^{35}S]Ub. Figure 2.4 demonstrates that the uba1C600S mutant forms a ubiquitinated product that is not disrupted upon treatment with DTT. Furthermore, the conversion of uba1C600S into the Ub modified form was effectively quantitative, as determined by densitometry (not shown). This indicates that the ratio of 1.2:2 given in Figure 2.3B corresponds effectively to 100% of the serine 600 position being bound to Ub and only 20% of the ATP binding sites being filled with Ub-AMP.

By comparison, no DTT sensitive uba1C600A-Ub derivative was observed, due to its inability to form thiolester, and only a small amount of wild type Uba1-Ub conjugate was seen. A high molecular weight Uba1-Ub complex was consistently observed in these types of ubiquitination reactions. This may be due to an auto-ubiquitination event wherein Ub is transferred from the Uba1~Ub thiolester to some internal lysine residue within Uba1 itself (Figure 2.4). The presence of these high molecular weight Uba1 derivatives confirms previous reports of β-mercaptoethanol insensitive Uba1-Ub conjugates being formed using *in vitro* assays (McGrath *et al.*, 1991).

Ub Activation by uba1C600A and Chemically Modified Uba1

Unlike wild type Uba1 and uba1C600S, the uba1C600A mutant lacks a thiol or hydroxyl group at position 600 that is capable of accepting Ub from Ub-AMP. The fact that uba1C600A binds Ub at all, reflects its ability to chemically synthesize Ub-AMP (Figure 2.3A). Previous studies have used chemical agents, such as iodoacetamide, to block the active site cysteine of Uba1 (Haas *et al.*, 1982). Such chemical modifications were found to block Uba1~Ub thiolester formation, but not Ub-AMP synthesis. We expected that Ub activation by either uba1C600A or iodoacetamide treated Uba1 would be therefore equivalent. In fact, when Ub activation by uba1C600A is compared to that of iodoacetamide treated Uba1, both show equivalent levels of Ub binding, corresponding to an overall Ub:Uba1 active

site ratio of 0.7:1 (Figure 2.5A); a result comparable to the observations previously reported for iodoacetamide treated Uba1 (Haas *et al.*, 1982).

When similar reactions with iodoacetamide treated Uba1 and the uba1C600A mutant were carried out in the presence of DTT, no effect on either's ability to bind Ub was observed (Figure 2.5B). This was in direct contrast to wild type Uba1, which exhibits no Ub binding when reactions contain DTT (Figure 2.5B). Introducing DTT into a ubiquitination reaction results in the cleavage of the thiolester bond as it is formed. This situation results in the perpetual transfer of Ub to the active site cysteine, forming the thiolester bond, followed by its subsequent cleavage by DTT.

Direct Transfer of Ub from uba1C600A to a Ubiquitin Conjugating Enzyme

Not only can the relative levels of Ub binding to Uba1 be determined using a ubiquitination reaction, but these reactions can also be used to follow Ub transfer from Uba1 to an E2. As an example, a reaction containing [^{35}S]Ub, Uba1, Ubc1Δ that was incubated in ubiquitination buffer at 30 °C for 1 hr, followed by gel exclusion chromatography generated an elution profile consisting of three distinct peaks containing [^{35}S]Ub (Figure 2.6A) (Hodgins *et al.*, 1996). These peaks correspond to free [^{35}S]Ub (8.5 kDa), [^{35}S]Ub that has been incorporated into Uba1 (as Uba1~Ub thiolester Ub-AMP adenylate), and [^{35}S]Ub incorporated into Ubc1Δ (as Ubc1Δ~Ub). When Uba1 is omitted from these reactions, only a free Ub peak is observed confirming that formation of the Ubc1Δ~Ub peak is indeed Uba1 dependent (Figure .2.6A). To confirm that the Ubc1Δ~Ub peak corresponded to thiolester linked Ub, peak fractions were pooled, subjected to DTT treatment, and again run over a gel exclusion column. DTT treatment disrupts the thiolester bond, cleaving any Ub, resulting in a chromatogram that revealed only a free Ub peak (data not shown).

While the uba1C600S and uba1C600A derivatives retained the ability to form Ub-AMP, and in the case of uba1C600S to form an ester with Ub, neither derivative was expected to be capable of transferring Ub to Ubc1Δ. Not surprisingly, the

reaction containing uba1C600S exhibited no Ubc1Δ~Ub peak (Figure 2.6A). When uba1C600A was used under identical reaction conditions, no transfer was observed from the adenylate to Ubc1Δ (Figure 2.6A). However, the transfer of Ub to Ubc1Δ did occur when both uba1C600A and Ubc1Δ were present at equimolar concentrations (Figure 2.6B). Even so, the degree to which Ubc1Δ was converted to the Ubc1Δ~Ub form by uba1C600A was about four fold less than that converted by wild type Uba1 under identical conditions.

Gel filtration experiments were supported by observations made when reaction products from these experiments were subsequently analyzed using SDS polyacrylamide gel electrophoresis and visualized using autoradiography. The ability of Ubc1Δ~Ub to produce a Ub conjugate (Ubc1Δ-Ub) through an auto-ubiquitination reaction, had been previously demonstrated (Hodgins *et al.*, 1996). It is based upon this auto-ubiquitination reaction, that formation of Ubc1Δ-Ub is clearly seen in Figure 2.7. This result demonstrates that uba1C600A can stimulate the formation of Ubc1Δ~Ub, as evidenced by the presence of Ubc1Δ-Ub conjugate chains at least two Ub molecules in length.

Back-transfer of Ub from Ubc1Δ to Uba1

The trans-thiol transfer of Ub from the Uba1 active site to the Ubc1Δ active site is a spontaneous process and is energetically conserved (Hershko *et al.*, 1983). Due to the close proximity of the active sites of Uba1 and Ubc1Δ, suggested by the forward transthiolation reaction, we thought it possible that the reverse transfer of Ub may be equivalent to the forward transfer of Ub. Along the forward direction of the ubiquitination pathway Uba1 is responsible for transferring Ub to E2. If this reaction could be reversed, Ub would be back-transferred from the E2~Ub thiolester to the Uba1 active site cysteine, thereby regenerating the Uba1~Ub thiolester.

To facilitate the back-transfer reaction, Ubc1Δ~Ub was first generated and purified by coupling a ubiquitination reaction with gel exclusion chromatography as described above in *In vitro Ubiquitination Reactions*. Peak fractions containing Ubc1Δ~Ub

were pooled and incubated with ubiquitination buffer and an equimolar concentration of Uba1 for 30 min. Under these conditions, Ub was shown to become transferred from the Ubc1Δ~Ub thiolester to Uba1 by the appearance of a Uba1~Ub peak (Figure 2.8A). Treatment of fractions corresponding to the Uba1~Ub peak with DTT, which results in the disruption of the Uba1~Ub complex, followed by SDS PAGE resulted in the disappearance of the thiolester (data not shown).

As the reaction leading to the formation of the Uba1~Ub thiolester occurred efficiently in the presence of ATP, the lack of ATP on this mechanism was tested. When ATP was excluded from the back-transfer reaction (Figure 2.8A), there was a slight reduction in Uba1~Ub formed and the appearance of a free Ub peak. This free Ub peak was accompanied by an overall decrease in amount of both Uba1~Ub and Ubc1Δ~Ub thiolesters. The decrease in Uba1~Ub thiolester levels in the absence of ATP (Figure 2.8B) did not directly correspond to the reduction in amount of free Ub generated (Figure 2.8A). Rather, the free Ub generated corresponded to a reduction in the amount of Ubc1Δ~Ub thiolester observed in the absence of ATP. These observations suggest that in the absence of ATP, the Uba1~Ub thiolester is more susceptible to hydrolysis by comparison to back-transfer reactions when ATP is present. A greater degree of hydrolysis might result in further transfer of Ub from the Ubc1Δ~Ub thiolester to Uba1, accounting for the reduction in the amount of Ubc1Δ~Ub observed.

Because of the results obtained with Uba1 in the presence and absence of ATP, the ability of Uba1 to bind ATP was tested using uba1G446V. This mutant lacks the ability to form Ub adenylate and therefore to activate Ub (Figure 2.3B), but still contains the active site cysteine at residue 600. As such, it should retain the ability to form a thiolester with Ub at its active site when activated Ub is transferred from Ubc1Δ~Ub. This was confirmed using the same back-transfer reaction as described for wild type Uba1 under identical conditions. Back-transfer to uba1G446V was, however, approximately 1.5 to 2 fold less efficient than that observed for Uba1. Furthermore, the degree to which Ub was back-transferred to uba1G446V showed

no dependence on ATP (Figure 2.8B). This result reflects the inability of this derivative to employ the nucleotide binding site and therefore stabilize the formation of Uba1~Ub by binding ATP.

While the back-transfer reaction employing uba1G446V exhibited no dependence on the presence of ATP, there was no destabilization effect, as observed for wild type Uba1 in the absence of ATP, given that little if any free Ub was generated during the reaction (Figure 2.8A). This result is somewhat surprising, and further demonstrates the interplay between both halves of the Uba1 active site, wherein the structural integrity of the nucleotide binding site and the binding of ATP affect Uba1~Ub thiolester formation. These results provide supporting evidence for the stability of the Uba1~Ub thiolester as suggested by a model of the Uba1 nucleotide binding site (Chapter 4).

2.4 Discussion

The *S. cerevisiae* expression system described in *Experimental Procedures* is much more efficient than previously described methods of expressing active Uba1. Previously described purification schemes for native Uba1 produced only sub μM quantities of wheat (Hatfield and Vierstra, 1992) and bovine (Pickart personal communication) Uba1, which were far too low to be useful for the experiments discussed herein. Recombinant Uba1 expression in *E. coli* seemed to result in the production of principally inactive protein (C. Ptak, Personal Communication), likely due to its large size and the inherent difficulty for prokaryotic systems to produce multi-domain proteins (Edwards *et al.*, 2000). The over expression of Uba1 in *S cerevisiae* has enabled us to perform the *in vitro* experiments described in this chapter. Furthermore, observations that were made using these *in vitro* ubiquitination assays provide additional biochemical support for the Uba1 active site model described in Chapter 4.

Characterization of ATP Binding in the Uba1 Model

Sequence comparisons of *S. cerevisiae* Uba1, Uba2, Uba3 and *E. coli* MoeB have identified putative positions of key residues within the bipartite active site of Uba1 (Chapter 4, Figure 8). The Uba1 active site consists of a nucleotide (ATP) binding site that functions as the site of Ub-adenylate (Ub-AMP) formation, and a cysteine at position 600 that functions in Ub-thiolester formation (Hatfield and Vierstra, 1992). The nucleotide binding site contains a classical Walker fold (G-X-G-(A/G)-(G/L)-G) at residues 440-446 (Walker *et al.*, 1982; Wierenga and Hol, 1983).

In a model of the Uba1 active site (Chapter 4), the sulfur atom of the active site cysteine is ambiguously positioned over the center of the anionic ATP binding pocket. This provides the prospect for direct contact between a bound molecule of ATP and the active site cysteine. It would follow that if the activated adenylate form of Ub must become transferred to the active site cysteine to form the thiolester, then these two sites must be spatially close within Uba1. From this, we can theorize that the binding of a nucleotide would influence the ability of the active site to form thiolester or transfer Ub to an E2. Results obtained from ATP binding and ubiquitin activation assays of mutant forms of Uba1 suggested that the position of the active site cysteine would be more ordered in the presence of ATP. Results demonstrated here are in agreement with previous results that illustrated the requirement for ATP, not only in the activation of Ub, but also in its subsequent transfer to E2 (Pickart *et al.*, 1994).

Ub Activation by Uba1 Mutants

Ub activation generates two forms of Ub bound to Uba1, a non-covalent Ub-adenylate (Ub-AMP) and a covalently linked Ub-thiolester at the active site cysteine (Uba1~Ub) (Ciechanover *et al.*, 1981; Hershko *et al.*, 1981). When examining the incorporation of Ub into wild type Uba1, a ratio of 1.6 implies that approximately 20% of the Uba1 molecules contain only a single Ub moiety, most likely as the Uba1~Ub thiolester (Figure 2.3A) (Haas and Rose, 1982). The less than ideal ratio is most likely due to the concentrations of either free Ub or ATP within the reaction

being two low to push the equilibrium further to the right, resulting in vacant ATP and Ub binding sites. Another possible reason for a decrease in activity could be improperly folded protein as a result of protein purification and storage conditions.

Binding of Ub by uba1C600A

The ability of uba1C600A to form any complex with Ub (Figure 2.3A) is indicative of its ability to synthesize and bind Ub-AMP. Our results demonstrated that at least 70% of the ATP binding sites of the uba1C600A derivative were occupied (Figure 2.3B). DTT appears to disrupt the formation of the Uba1~Ub thiolester, thereby freeing Ub from the active site cysteine of Uba1 (Haas *et al.*, 1982). Thus, DTT may perpetuate a futile cycle of Ub-AMP synthesis, Ub transfer to the thiol site, and thiolester cleavage. This cycle is disrupted when an Ala residue is substituted for the active site Cys (residue 600). The presence of alanine in uba1C600A prevents Ub thiolester formation and renders the ubiquitination reaction insensitive to DTT, as only the Ub adenylate is able to form and can remain non-covalently bound to Uba1 (Figure 2.5B). We would therefore propose that the uba1C600A derivative, while capable of synthesizing Ub-AMP, can not transfer the activated Ub when alanine is substituted for cysteine at residue 600.

Binding of Ub by uba1C600S

The uba1C600S derivative also demonstrated the dependence of Ub-AMP synthesis on the presence of a thiol at the active site. We observed that uba1C600S bound a significantly lower amount of Ub relative to wild type Uba1, with ratios of 1.2 and 1.6 respectively (Figure 2.3B). Given that this derivative is quantitatively converted into Ub ester under the given conditions (Figure 2.4), this defect must be attributed to a reduction in the amount of Ub-AMP bound at the ATP site when an ester as opposed to a thiolester linked Ub is present. A similar defect has also been described in the Ub mutant ubG76A (Pickart *et al.*, 1994). When ubG76A is utilized in a similar reaction, the presence of the methyl side chain at the carboxy terminus of Ub was thought to interfere with further Ub-AMP binding at the

ATP site of Uba1. Together these observations indicate that the specific thiolester formed between the carboxy terminus (Gly 76) of Ub and the active site cysteine of Uba1 (residue 600) is required for the additional synthesis and/or binding of a second Ub-AMP molecule by Uba1.

If we assume that once Ub is activated it becomes transferred to the Uba1 active site cysteine, then any ratio greater than 1:2 would imply 100% occupation of the thiolester. The lower than ideal values for binding of Ub in all of the Uba1 mutants may be a consequence of competition between ATP, AMP, Ub, UB-AMP or Ub thiolester for the adenylate binding site. Preliminary results suggest that increasing the concentration of Ub in these reactions can shift the equilibrium to the right resulting in higher ratios for product species (not shown).

Back-transfer Reactions

The ability of uba1C600A to directly transfer from the Ub-AMP adenylate intermediate to the active site of Ubc1Δ provided us with direct evidence for the hypothesis that the three active sites of the Uba1/Ubc1 complex (the two active site cysteines and the ATP binding site) form a tight catalytic partnership. This was demonstrated by the appearance of the Uba1~Ub thiolester in reactions containing Ubc1Δ~Ub and Uba1, illustrating Ub transfer directly from the E2 to Uba1 (Figure 2.6). The presence of ATP in the back-transfer reactions seems to have a significant effect, not on the efficiency of Ub transfer, but on the stability of the Uba1~Ub thiolester following transfer to Uba1. Back-transfer reactions performed in the absence of ATP resulted in increased hydrolysis of Ub from the Uba1~Ub thiolester, while those performed in the presence of ATP showed very little free Ub (Figure 2.8A).

Ub Activation by uba1G446V

Not surprisingly, the Uba1 mutant, uba1G446V, was unable to catalyze the reaction between ATP and [^{35}S]-Ub, as shown by the absence of a Uba1/Ub peak in the elution profile for this mutant (Figure 2.3A). This result may be due to the inability of

uba1G446V to bind ATP, or its inability to catalyze the reaction due to misaligned substrates. Either reason supports the hypothesis that residues 440-446 function in some capacity at the site of Ub-AMP synthesis. Since uba1G446V is unable to utilize ATP in Ub activation, but still contained a functional active site cysteine, it was not unexpected that it would still accept pre-charged Ub via a back-transfer reaction (Figure 2.8). This mutation, while effectively rendering the enzyme null with regard to the ATP activation of Ub, seemed to have a minimal effect on the ability of Uba1 to form the thiolester.

The substitution of Gly 446 with valine would increase the hydrophobic character of the ATP binding site. This increase in hydrophobicity, of the adenylate-binding pocket, was demonstrated in the uba1G446V, at the position where the phosphate atoms of ATP are positioned upon binding (Figure 2.9). Dynamics experiments on this region suggest that this replacement has a predisposition for the occlusion of ATP from the binding site (data not shown). If this is the case, then the inactivity of uba1G446V may not simply be a result of a "misaligned" ATP molecule that cannot participate in the formation of Ub-AMP, but may be a result of its inability to bind ATP at all. Since uba1G446V is unable to utilize ATP in Ub activation, it was expected that the back-transfer of Ub to uba1G446V would mimic reactions employing Uba1 in the absence of ATP. In fact these two reactions proved to be quite different. In the case of Uba1, the absence of ATP appears to cause a cycle of Ub back-transfer from Ubc1Δ to form the Uba1~Ub thiolester, followed by hydrolysis of Ub from Uba1 to yield free Ub. This would be followed by an additional transfer of Ub from E2~Ub to Uba1 and an increase in the concentration of free Ub.

This mechanism would generate free Ub with an overall reduction in the amount of Ubc1Δ~Ub observed (Figure 2.8A). In the case of uba1G446V, there was a decrease in the amount of Uba1~Ub thiolester formed, but the absence of any free Ub. It appears that the uba1G446V substitution reduces the efficiency of the back-transfer reaction, but also stabilizes the thiolester on Uba1, suggesting that the

uba1G446V substitution causes a structural perturbation that must affect either the ATP binding site or the structure of the active site loop.

Preliminary dynamics experiments, presented in Chapter 4, provide a possible explanation for the instability of the Uba1~Ub thiolester as generated by the back-transfer reaction in the absence of ATP. In the presence of ATP, stabilization of the nucleotide binding site could limit solvent accessibility to thiolester linked Ub, thereby preventing the hydrolysis of Ub from the active site cysteine. This result might also explain why ATP and Ub-AMP stimulate Ub transthiolation from Uba1 to E2 (You and Pickart, 2001). The presence of ATP at the nucleotide binding site could also stabilize the active site loop once the Uba1~Ub thiolester has formed, thereby facilitating transthiolation by allowing this reaction to be favored over Ub hydrolysis in the presence of E2. However, the presence of Ub-AMP adenylate at the active site may act in a different mechanism, this time sterically, causing the loop to open, revealing the thiolester bond to E2.

Back-transfer results would suggest that as Ub becomes transferred to the Uba1 active site, the active site cysteine would become exposed for transfer to an E2. This conformation would expose the thiolester bond between Uba1 and Ub to increased rates of hydrolysis. This is also supported by the position of the active site cysteine residue in the structure of the Uba1 homologue, Uba3 (Chapter 4, Figure 6). This structure places the thiol group facing away from the nucleotide-binding site, and may be representative of a conformation that makes the thiolester bond accessible to the E2's. The fact that the active site in Uba3 must exist in at least two conformations is clear, as in its crystal structure, it is at least 32 Å removed from the nucleotide binding site. This implies that it has to move substantially closer to pick up the activated molecule of Ub, to form the thiolester.

In a closed conformation, Ub hydrolysis would not take place as readily, as the thiolester bond becomes sequestered in the active site of Uba1. In the absence of ATP at the active site of uba1G446V the Ub thiolester may be found in either of the two conformations, thus resulting in the lower levels of Ub hydrolysis observed in

Figure 2.8A. If this is the case, the increased levels of Ub hydrolysis seen with the wild type Uba1 in the absence of ATP can be explained by the loop occupying the open conformation when bound to Ub as the thiolester with no ATP present at the active site. The increased level of Ub transferred for the reactions that contained ATP may simply be a result of loop stabilization in the closed conformation and a slower rate of Ub hydrolysis following transfer from the Ubc1Δ~Ub thiolester.

The Ability of Uba1 Mutants to Transfer Ub to Ubc1Δ

The most exciting observation made throughout the course of this study was the ability of uba1C600A to transfer activated Ub directly to E2, bypassing the intermediate thiolester. Not only must the Uba1 and E2 thiol sites be close to one another, allowing for the normal Ub transthiolation reaction to occur, but the E2 thiol site must also be near the carboxy terminus of Ub, while Ub is in the Ub-AMP form. According to the Uba1 model that is presented in Chapter 4, upon binding of E2 by Uba1, all three active sites can come together to form a contiguous surface shared by both enzymes. A hypothetical model of the complex formed between Uba1 and Ubc1Δ implies that the active site cysteines of both molecules may be close enough to allow the transfer of Ub to either cysteine from the Ub-adenylate (Chapter 4, Figure 14B).

Examination of the structure of the scaffolds that were utilized during the construction of the Uba1 active site model raises a significant question regarding the transfer of Ub to E2. In their structure of MoeB/MoaD, Rajagopalan *et al.* (2001) demonstrated that in the Ub homologue, MoaD, the tail region would be threaded under a disordered loop at which point it contacts ATP bound at the nucleotide binding site of MoeB. Because a sulfur ion rather than a cysteine residue is used to activate MoeB, this may not pose a problem for *E. coli*. However, in the case of Uba1, following its activation, Ub becomes transferred to the active site cysteine and subsequently to E2. If Ub were bound to AMP while having the carboxy terminus threaded under the short loop, this transfer would not be possible without rotating the polypeptide backbone, not only through 180° pulling Ub through Uba1 itself.

Previous studies showed that the transfer of Ub from the thiol site of Uba1 to an E2 thiol group was stimulated by binding of either ATP or Ub-AMP at the ATP site in Uba1 (Pickart *et al.*, 1994). This suggests that at least in part, stimulation of Ub transfer from Uba1 to E2 is a consequence of Uba1~Ub thiolester stability in the presence of ATP and, by extension, Ub-AMP. These observations support our hypothesis that the binding sites in Uba1 must be spatially close to one another and may in fact define a contiguous surface. This also lends support to the hypothesis that the active site loop must undergo some conformational change upon binding Ub as the thiolester.

2.5 Conclusion

The construction of three active site mutants, and a model of Uba1's nucleotide binding site (Chapter 4), has provided a substantial amount of insight into its activation and transfer of Ub to the E2s. The model and biochemical results discussed here demonstrate the necessity for close spatial orientation of the active sites of both Uba1 and Ubc1. The direct transfer of Ub from Ub-AMP to Ubc1Δ (Figure 2.6) is the most substantial proof of this spatial arrangement. Corroboration of the influence ATP has upon the flexibility of the active site, within the Uba1 model, was demonstrated by the extent of Ub hydrolysis in the absence or presence of ATP. Unfortunately, we were unable to determine the relative rates of Ub hydrolysis for the Uba1 thiolester versus Ub-AMP, as transfer immediately follows formation of the Ub-AMP adenylate. Future experiments, using non-reactive Ub adenylate analogues, could determine if the presence of AMP-Ub at the ATP binding site does indeed stimulate Ub transfer to E2, and as a result hydrolysis of the thiolester linkage.

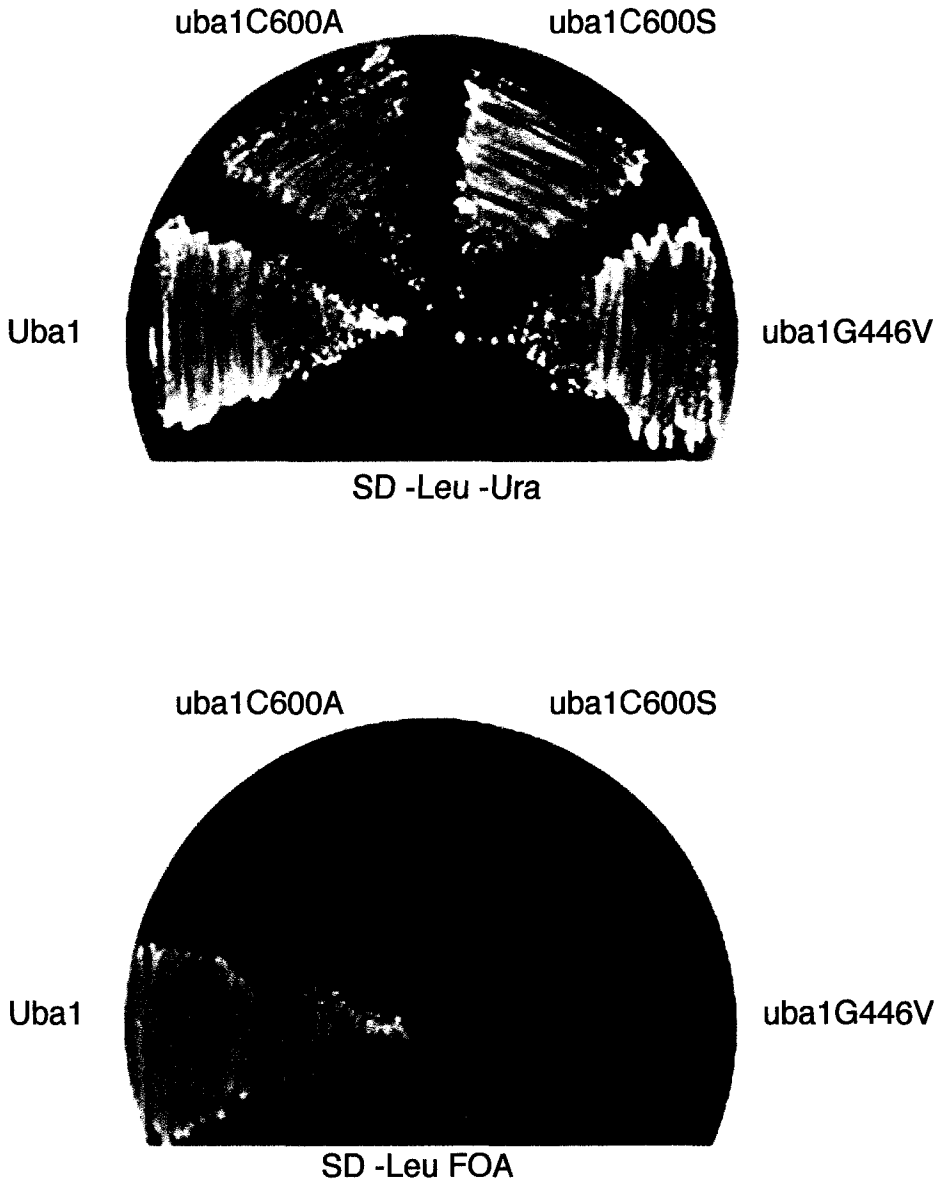

Figure 2.1. **Plating of Uba1 Active Site Derivatives**
The yeast UBA1 deletion strain (described in the *Experimental Procedures*) was rescued with a plasmid containing Wild Type UBA1 and the *URA* gene. To this strain, plasmids containing each of the mutations uba1C600A, uba1C600A, uba1G446V and wild type UBA1 with the *LEU* gene were added. These strains were then grown in liquid synthetically defined (SD) media lacking leucine and uracil. Equal amounts of each culture were then plated onto SD media lacking leucine and uracil or plated onto SD media also lacking leucine, but also containing 5-fluoro-orotic acid (FOA). As can be seen in this figure, only the wild type Uba1 is able to substitute for the Uba1 deletion. None of the Uba1 mutations are capable of supporting growth under these conditions.

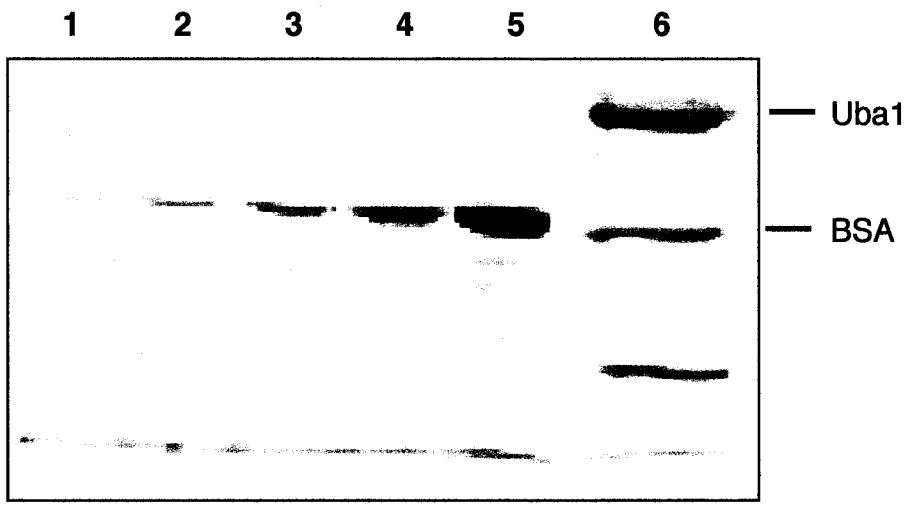

Figure 2.2. **Purification of Wild Type Uba1**
SDS polyacrylamide gel of the purified Uba1 and bovine serum albumin used to determine purified protein concentration. Samples were subjected to standard SDS-PAGE (12%), followed by densitometry to determine relative band densities for standard curve generation. Lanes **1-5** show a BSA gradient used for the determination of the final concentration of Uba1 in the preparation. Lane **6** shows the final stage of the purification of 6x His tagged Uba1. The lower band present in lane **6** may be a degradation product of Uba1 that corresponds to a proteolytically stable domain. BSA is present in the sample to stabilize the purified Uba1.

A

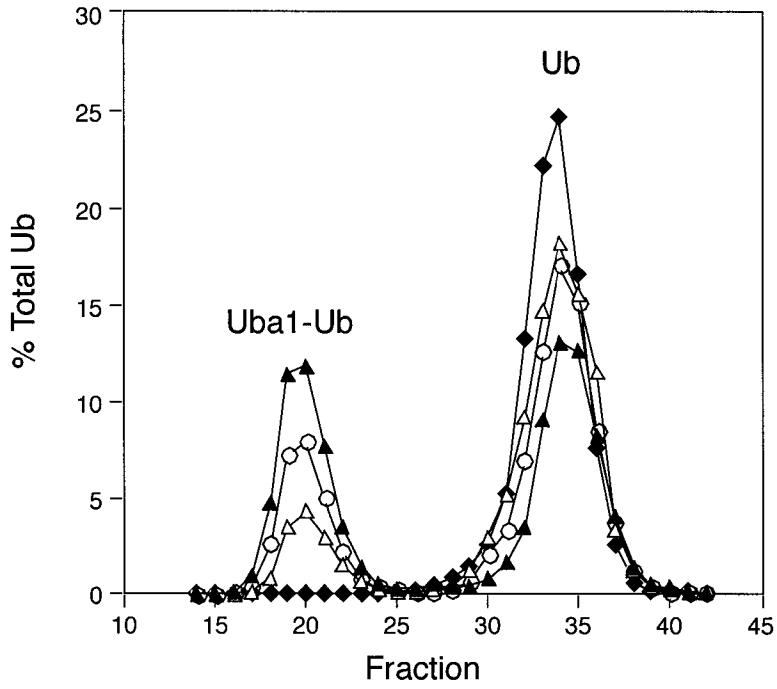

B

Uba1 Derivative	Bound Ub
Uba1	80% ±5
uba1G144V	0%
uba1C600S	60% ±3
uba1C600A	70% ±5

Figure 2.3. ***In vitro* Activity of Uba1 and its Active Site Derivatives**
In vitro ubiquitination reactions included 100nM [^{35}S]Ub, and 10nM of either Uba1, uba1G446V, uba1C600S, or uba1C600A. Reactions were incubated for 60 min. at 30 °C and run over a gel exclusion column. The amount of [^{35}S]Ub present within each fraction was determined by scintillation counting. **A**, the percentage of total [^{35}S]Ub counts present in each fraction was determined and plotted to give an elution profile for each reaction. The elution profiles shown are for the reactions which contained Uba1 (closed triangles), uba1G446V (closed diamonds), uba1C600S (open circles), and uba1C600A (open triangles). Peaks observed correspond to free [^{35}S]Ub (Ub), and [^{35}S]Ub incorporated into Uba1 or one of its derivatives (Uba1-Ub). **B**, the molar ratio of bound Ub to the total number of Ub binding sites on Uba1 (two sites for each of the uba1C600S and wt Uba1 and one for the uba1C600A). Results presented here are the average of three independent experiments.

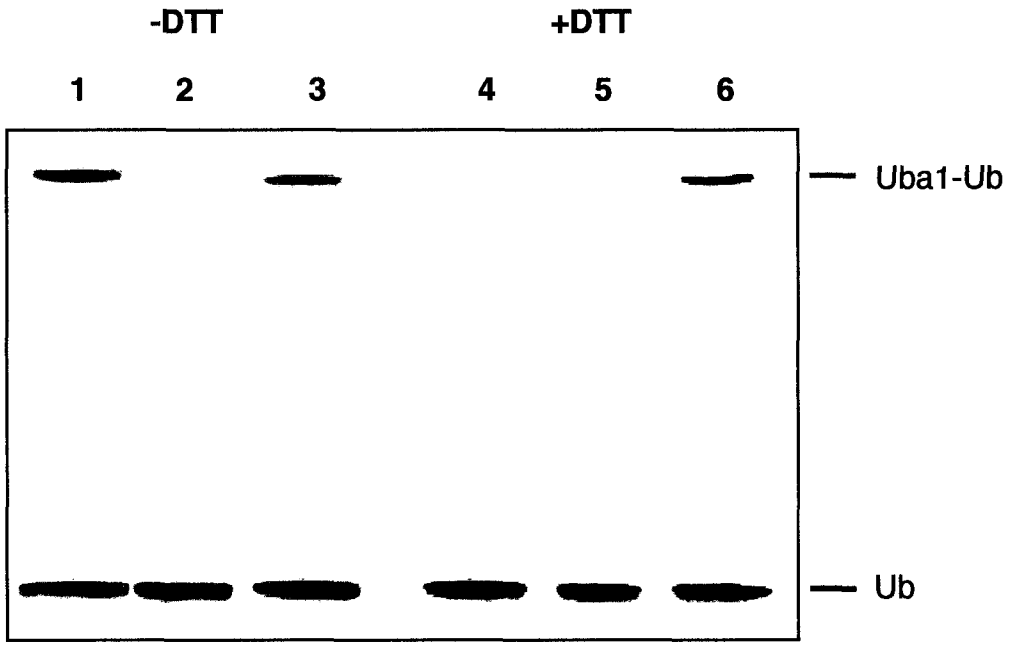

Figure 2.4. **uba1C600S Forms an Ester with Ub**
Shown is an autoradiograph of a 12% SDS polyacrylamide gel of in vitro ubiquitination reactions in which 100nM of [^{35}S]Ub was incubated in the presence of 10 nM of either Uba1 (lane **1**), uba1C600A (lane **2**), or uba1C600S (lane **3**) at 30 °C for 60 min. These same reactions were then treated with 100mM DTT and heated at 100 °C for 15 min. to disrupt any thiolester formed between Ub and any of the Uba1 derivatives (lanes **4-6** respectively). Bands corresponding to [^{35}S]Ub (Ub) and Uba1 derivatives covalently modified with [^{35}S]Ub (Uba1-Ub) are indicated. The high molecular weight band seen in lane **4** is indicative of an internal Ub linkage to Uba1 itself. The high molecular weight band seen in lane **6** is due to the formation of a DTT insensitive ester linkage between [^{35}S]Ub and the serine residue at the active site of uba1C600S.

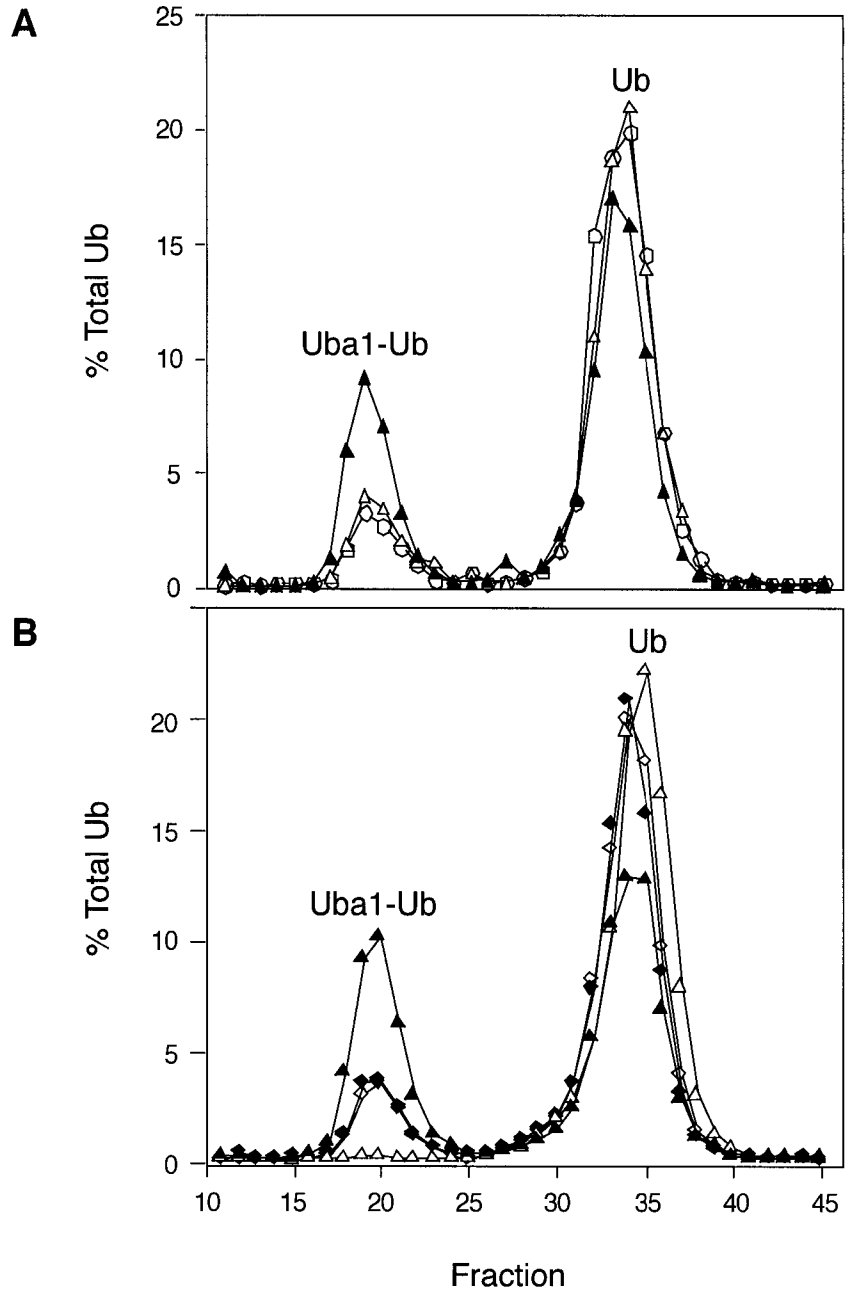

Figure 2.5. **Comparison of uba1C600A Ubiquitin Activation with that of Iodoacetamide Treated Uba1 and the Effect of DTT on these Reactions** Reaction conditions and generation of elution profiles were similar to those described for Figure 2.3. **A**, *in vitro* reactions contained either Uba1 (closed triangles), Uba1 pretreated with iodoacetamide (open circles), or uba1C600A (open triangles). **B**, *in vitro* reactions were carried out in the presence or absence of DTT and included Uba1 in the absence (closed triangles), or presence (open triangles) of DTT and, uba1C600A in the absence (closed diamonds), or presence (open diamonds) of DTT. Peaks observed correspond to free [^{35}S]Ub, and [^{35}S]Ub incorporated into Uba1 as the Ub-AMP conjugate or thiolester.

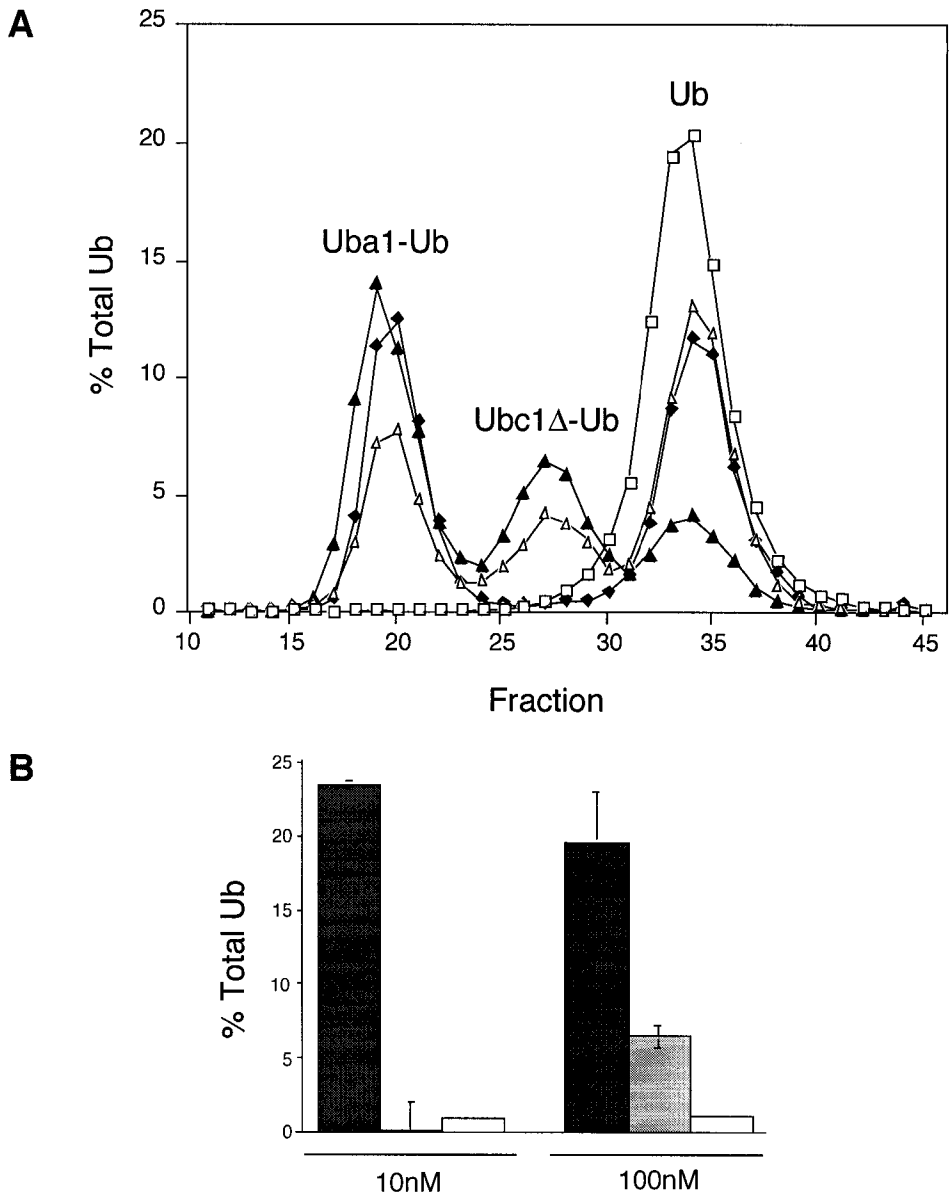

Figure 2.6. **Ubiquitin Transfer from uba1C600A to Ubc1Δ**
A, *in vitro* ubiquitination reactions were carried out in the presence of 100nM [^{35}S]Ub, 100nM Ubc1Δ, and 100nM of either Uba1, uba1C600S, or uba1C600A. Reactions were incubated at 30 °C for 60 min. and elution profiles for each reaction generated as described in Figure 2.5. Elution profiles shown are for reactions that lack Uba1 (open squares), or contain Uba1 (closed triangles), uba1C600S (closed diamonds), or uba1C600A (open triangles). Peaks observed correspond to free [35S]-Ub (Ub), [^{35}S]Ub incorporated into Ubc1, (Ubc1Δ~Ub) and [^{35}S]Ub incorporated into Uba1 or one of its derivatives (Uba1-Ub). **B**, a comparison of Uba1Δ~Ub thiolester formation in reactions containing Uba1 (black bars), uba1C600A (gray bars), or uba1C600S (white bars) at concentrations of either 10nM or 100nM. Bars represent the percentage of total Ubc1Δ added to each reaction that has been converted into Ubc1Δ~[^{35}S]Ub thiolester.

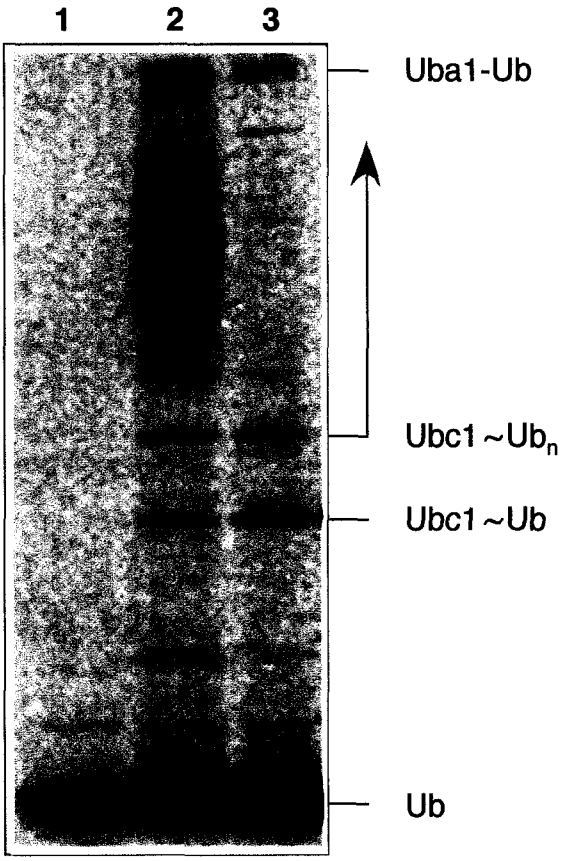

Figure 2.7. **Uba1 Activity Measured by Ub Chain Formation on Ubc1Δ**
In vitro ubiquitination reactions were carried out in the presence of 100nM [^{35}S]Ub, 100nM Ubc1Δ, and 100nM of either Uba1, or uba1C600A. Reactions were incubated at 30 °C for 60 min, then stopped by the addition of 10% trichloroacetic acid and centrifuged. Pellets were resuspended in SDS buffer and samples were applied to a 10% SDS polyacrylamide gel, followed by autoradiography. Lane **1** shows a reaction which contained only purified Ubc1Δ and [^{35}S]Ub. Lane **2** demonstrates a reaction containing wild type Uba1, Ubc1Δ and [^{35}S]Ub , while lane **three** shows a reaction which contains uba1C600A, Ubc1Δ and [^{35}S]Ub.

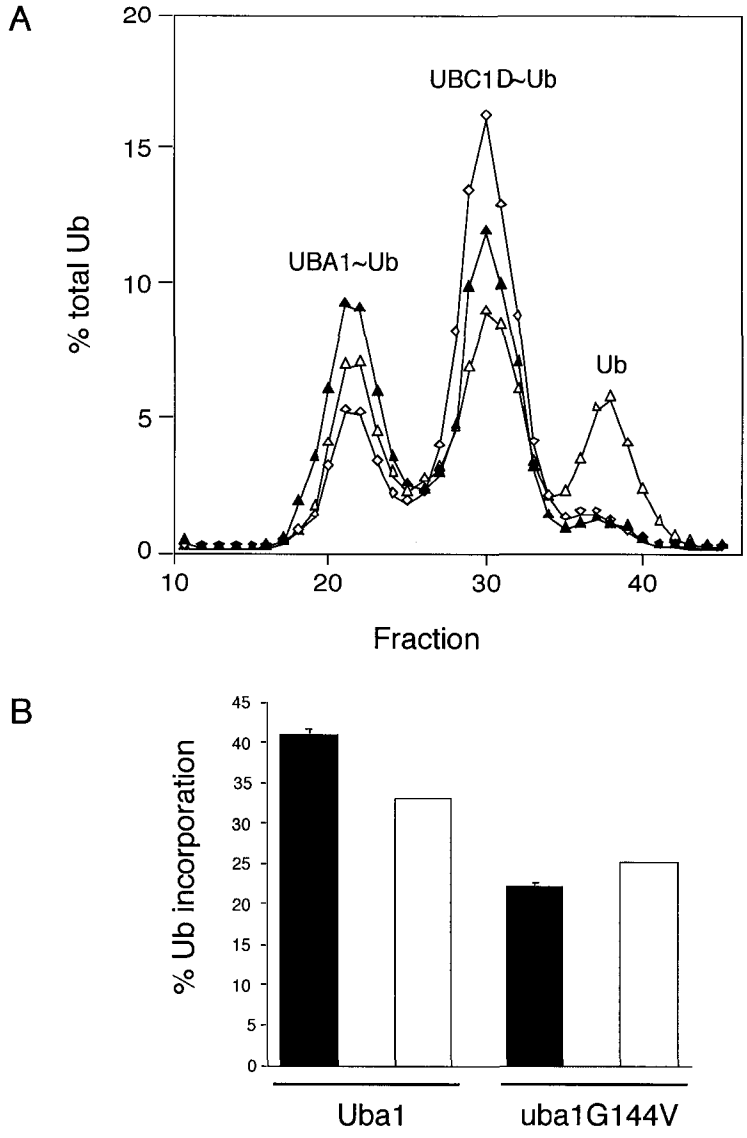

Figure 2.8. **Back-transfer of Ub from Ubc1Δ~Ub to Uba1 is ATP Dependent** **A**, included in each back-transfer reaction was 100nM Ubc1Δ~[^{35}S]Ub and either Uba1, or uba1G446V. Reactions that included Uba1 were carried out either in the presence of ATP (closed triangles) or in the absence of ATP (open triangles). The uba1G446V reaction (open diamonds) included ATP. Each reaction was run over a gel exclusion column to separate and identify reaction products. Peaks observed correspond to free [^{35}S]Ub (Ub), Ubc1Δ~[^{35}S]Ub thiolester and Uba1~[^{35}S]Ub thiolester. **B**, a comparison of the degree to which Ub is back transferred from Ubc1Δ~[^{35}S]Ub to either Uba1 or uba1G446V in the presence (black bars), or absence (white bars) of ATP.

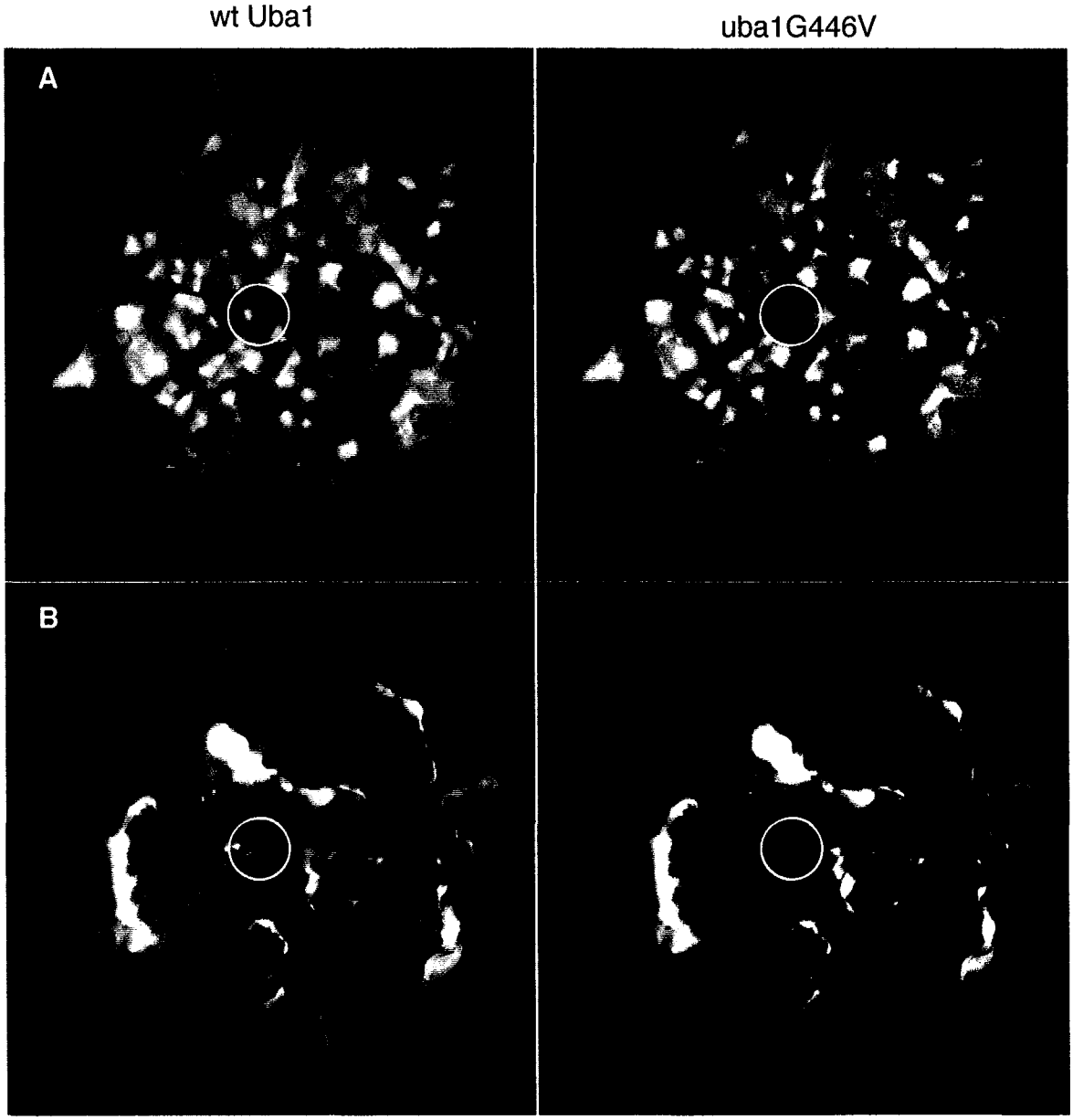

Figure 2.9. **Hydrophobic and Electrostatic Representations of the Uba1 and uba1G446V Active Sites**

Connelly surface representations, created with GRASP of the Uba1 active site model (Chapter 4), illustrating structures containing either glycine or valine at position 446 (white circle). **A**, hydrophobic surface residues are shown in green, while hydrophillic surface residues are blue. **B**, electrostactic residues are colored showing no change in the overall charge of the Uba1 surface. Negatively charged surface residues are colored red and positively charged residues are blue.

2.6 References

Ciechanover, A., Finley, D., & Varshavsky, A. (1984). The ubiquitin-mediated proteolytic pathway and mechanisms of energy- dependent intracellular protein degradation. *J Cell Biochem, 24(1)*, 27-53.

Ciechanover, A., Heller, H., Katz-Etzion, R., & Hershko, A. (1981). Activation of the heat-stable polypeptide of the ATP-dependent proteolytic system. *Proc Natl Acad Sci U S A, 78(2)*, 761-65.

Edwards, A. M., Arrowsmith, C. H., Christendat, D., Dharamsi, A., Friesen, J. D., Greenblatt, J. F., & Vedadi, M. (2000). Protein production: feeding the crystallographers and NMR spectroscopists. *Nat Struct Biol, 7 Suppl*, 970-72.

Haas, A. L., & Rose, I. A. (1982). The mechanism of ubiquitin activating enzyme. A kinetic and equilibrium analysis. *J Biol Chem, 257(17)*, 10329-37.

Haas, A. L., Warms, J. V., Hershko, A., & Rose, I. A. (1982). Ubiquitin-activating enzyme. Mechanism and role in protein-ubiquitin conjugation. *J Biol Chem, 257(5)*, 2543-48.

Haas, A. L., Warms, J. V., & Rose, I. A. (1983). Ubiquitin adenylate: structure and role in ubiquitin activation. *Biochemistry, 22(19)*, 4388-94.

Hamilton, K. S., Ellison, M. J., Barber, K. R., Williams, R. S., Huzil, J. T., McKenna, S., Ptak, C., Glover, M., & Shaw, G. S. (2001). Structure of a conjugating enzyme-ubiquitin thiolester intermediate reveals a novel role for the ubiquitin tail. *Structure (Camb), 9(10)*, 897-904.

Hatfield, P. M., & Vierstra, R. D. (1992). Multiple forms of ubiquitin-activating enzyme E1 from wheat. Identification of an essential cysteine by in vitro mutagenesis. *J Biol Chem, 267(21)*, 14799-803.

Hershko, A. (1983). Ubiquitin: roles in protein modification and breakdown. *Cell, 34(1)*, 11-12.

Hershko, A., & Ciechanover, A. (1986). The ubiquitin pathway for the degradation of intracellular proteins. *Prog Nucleic Acid Res Mol Biol, 33*, 19-56.

Hershko, A., Ciechanover, A., & Rose, I. A. (1981). Identification of the active amino acid residue of the polypeptide of ATP-dependent protein breakdown. *J Biol Chem, 256(4)*, 1525-28.

Hershko, A., Heller, H., Elias, S., & Ciechanover, A. (1983). Components of ubiquitin-protein ligase system. Resolution, affinity purification, and role in protein breakdown. *J Biol Chem, 258(13)*, 8206-14.

Hochuli, E., Dobeli, H., & Schacher, A. (1987). *J. Chromatogr., 411*, 177-84.

Hodgins, R., Gwozd, C., Arnason, T., Cummings, M., & Ellison, M. J. (1996). The tail of a ubiquitin-conjugating enzyme redirects multi-ubiquitin chain synthesis from the lysine 48-linked configuration to a novel nonlysine-linked form. *J Biol Chem, 271(46)*, 28766-71.

Hodgins, R. R., Ellison, K. S., & Ellison, M. J. (1992). Expression of a ubiquitin derivative that conjugates to protein irreversibly produces phenotypes consistent with a ubiquitin deficiency. *J Biol Chem, 267(13)*, 8807-12.

Jones, J. G., Otieno, S., Barnard, E. A., & Bhargava, A. K. (1975). Essential and nonessential thiols of yeast hexokinase. Reactions with iodoacetate and iodoacetamide. *Biochemistry, 14(11)*, 2396-403..

McGrath, J. P., Jentsch, S., & Varshavsky, A. (1991). UBA 1: an essential yeast gene encoding ubiquitin-activating enzyme. *Embo J, 10(1)*, 227-36.

Nicholls, A., Sharp, K., & Honig, B. (1991). *PROTEINS, Structure, Function and Genetics, 11(4)*, 281.

Papa, F. R., & Hochstrasser, M. (1993). The yeast DOA4 gene encodes a deubiquitinating enzyme related to a product of the human tre-2 oncogene. *Nature, 366(6453)*, 313-19.

Pickart, C. M., Kasperek, E. M., Beal, R., & Kim, A. (1994). Substrate properties of site-specific mutant ubiquitin protein (G76A) reveal unexpected mechanistic features of ubiquitin-activating enzyme (E1). *J Biol Chem, 269(10)*, 7115-23.

Pickart, C. M., & Rose, I. A. (1985). Functional heterogeneity of ubiquitin carrier proteins. *J Biol Chem, 260(3)*, 1573-81.

Pickart, C. M., & Vella, A. T. (1988). Ubiquitin carrier protein-catalyzed ubiquitin transfer to histones. Mechanism and specificity. *J Biol Chem, 263(29)*, 15076-82.

Ptak, C., Prendergast, J. A., Hodgins, R., Kay, C. M., Chau, V., & Ellison, M. J. (1994). Functional and physical characterization of the cell cycle ubiquitin- conjugating enzyme CDC34 (UBC3). Identification of a functional determinant within the tail that facilitates CDC34 self-association. *J Biol Chem, 269(42)*, 26539-45.

Sullivan, M. L., & Vierstra, R. D. (1993). Formation of a stable adduct between ubiquitin and the Arabidopsis ubiquitin-conjugating enzyme, UBC1. *J Biol Chem, 268(12)*, 8777-80.

Sung, P., Prakash, S., & Prakash, L. (1991). Stable ester conjugate between the Saccharomyces cerevisiae RAD6 protein and ubiquitin has no biological activity. *J Mol Biol, 221(3)*, 745-49.

Walker, J. E., Eberle, A., Gay, N. J., Runswick, M. J., & Saraste, M. (1982). Conservation of structure in proton-translocating ATPases of Escherichia coli and mitochondria. *Biochem Soc Trans, 10(4)*, 203-06.

Wierenga, R. K., & Hol, W. G. (1983). Predicted nucleotide-binding properties of p21 protein and its cancer-associated variant. *Nature, 302(5911)*, 842-44.

You, J., & Pickart, C. M. (2001). A HECT domain E3 enzyme assembles novel polyubiquitin chains. *J Biol Chem, 276(23)*, 19871-78.

Chapter 3

Structure of a Conjugating Enzyme-Ubiquitin Thiolester Complex Intermediate[1]

3.1 Introduction

The interface of the *Saccharomyces cerevisiae* Ubiquitin Conjugating Enzyme (Ubc1Δ) with Ubiquitin (Ub) bound as a thiolester at its active site, was determined by kinetically monitoring thiolester formation using ^{1}H-^{15}N Heteronuclear Single Quantum Coherence (HSQC) NMR spectroscopy. Using the previously determined X-ray structures of Human Ub (Vijay-Kumar *et al.*, 1987) and *S. cerevisiae* Ubc1Δ (Hamilton *et al.*, 2001), with the NMR determined surface interface as a guide, docking simulations were used to produce the first model of an E2~Ub thiolester intermediate.

Chapter 1, sections 6 through 8, introduced the concept of multi-Ub chain formation and its importance in target selection within the ubiquitin proteasome system. Chapter 4 will discuss the importance of understanding structural relationships between components of the Ub system and introduced a theoretical

---

1 Portions of the results presented in this chapter have been published: Katherine S. Hamilton, Michael J Ellison, Kathryn R. Barber, R. Scott Williams, John T. Huzil, Sean McKenna, Christopher Ptak, Mark Glover and Gary S. Shaw. *Structure of a Conjugating Enzyme-Ubiquitin Thiolester Intermediate Reveals a Novel Role for the Ubiquitin Tail,* Structure. *9*:897-904.

structure of Uba1. Here we describe generation of a model of the Ubc1Δ~Ub thiolester using information provided through NMR spectroscopy to determine their interaction.

E2 Structural Analysis

Because of their importance in target recognition and enzymatic transfer of Ub to target proteins, the E2s have met with exhaustive study and many from *S. cerevisiae* have had their tertiary structures solved by X-ray crystallographic analysis. To date, these include the core catalytic domain of Ubc1, referred to as Ubc1Δ (Hamilton *et al.*, 2001), Ubc2 (Worthylake *et al.*, 1998), Ubc 4 (Cook *et al.*, 1979), Ubc7 (Cook *et al.*, 1997) and Ubc13 (Moraes *et al.*, 2001) (VanDemark *et al.*, 2001), with new structures appearing in the literature often. Intense structural examination of the E2s has revealed that the core domain is conserved and that diverse target specificity may be generated by either carboxy or amino terminal extensions (Chapter 1, Figure 5). These extensions also alter their interactions with E3 proteins (Reiss *et al.*, 1989; Merkley and Shaw, 2003). The conserved "core" catalytic domain of E2 comprises a total of 150 residues (Figure 3.1) and includes the active site cysteine used to accept Ub from Uba1 to form the E2~Ub thiolester. One face of this domain is composed of four α helices, the opposite face is a four strand antiparallel β sheet (Chapter 1, Figure 4B). The thiolester forming cysteine residue is located on an unstructured loop that joins α helix 2 to β sheet 4.

E2~Ub Thiolester

The E2 active site cysteine performs two distinct roles. It accepts Ub in its activated form from Uba1 and transfers this Ub to either an E3 or a target protein. The collection of E2 and Ub structural information has been straightforward, but structural characterization of their association, the E2~Ub thiolester, has been elusive. This is because the thiolester bond is a transient intermediate in the Ub pathway (Haas *et al.*, 1982; Hodgins *et al.*, 1996). *In vitro*, the E2~Ub thiolester is formed easily, but undergoes rapid hydrolysis yielding free E2 and Ub (Hodgins *et al.*, 1996). The short-lived nature of the E2~Ub thiolester has

prevented three-dimensional determination by X-ray crystallography and NMR spectroscopy. The structure of the E2~Ub thiolester intermediate, however, is key to a comprehensive structural understanding of the spatial relationships among all the components of this system, including Uba1 (Chapter 4), the E3s and ultimately, target proteins.

This study combined NMR spectroscopy and molecular modeling to determine the first three-dimensional model of an E2~Ub thiolester complex. In the present work, data collected from NMR spectroscopy of *in situ* Ubc1Δ~Ub thiolester formation, has been utilized to construct a model of the interaction between Ub and E2.

3.1.2 Heteronuclear Single Quantum Coherence NMR spectroscopy

The NMR experiments presented in this chapter were used as a guide for creating the Ubc1Δ~Ub thiolester model. The collection of NMR spectra and their analyses was performed by Dr. Katherine Hamilton and is discussed briefly as a point of reference.

Certain nuclei have a property called spin. In many atoms such as [^{12}C] and [^{14}N], these spins are paired against each other, such that the nucleus of the atom has no overall spin. In other atoms such as [^{1}H] and [^{13}C], the nucleus possesses an observable spin. The energy levels of these nuclei become split in a magnetic field. Nuclei in lower energy levels can absorb energy when subjected to a pulse of radiation in the radiofrequency range of the electromagnetic spectrum. Because the nucleus is a spinning charge, it can be oriented by the magnetic field and it precesses around the direction of this field. The nucleus can only absorb energy if the frequency of the energy radiated is the same as the frequency at which the nucleus is precessing. This exchange of energy is called resonance. This resonant energy is characteristic of the type of nucleus being observed and the chemical environment of the nucleus. Excited nuclei eventually fall back to their ground states, emitting absorbed energy. Energy absorbed or emitted can be measured with a suitable detector. Thus, spectral information about the position and the surroundings of some of the

nuclei in a protein can be obtained by placing that protein in a magnetic field and subjecting it to a beam of radiofrequency.

As was suggested above, all protons have an observable spin. When a simple molecule such as methane is analyzed with NMR spectroscopy, using a frequency suitable to excite protons, only the four protons can be observed to absorb energy. As more complex molecules are studied, such as proteins, the spectra produced become more complex. Even in the smallest proteins, the number of protons and their interactions cause the signals to become exceedingly complex.

NMR and the Structural Determination of Proteins

For proteins having less than 100 residues, conventional homonuclear 2-dimensional (2D) NMR methods can be applied for the purpose of structural determination. It was not until the development of residual dipolar couplings and cross-correlated relaxation experiments that larger protein structures could be tackled by NMR (Riek *et al.*, 1999). As the number of residues increases, spectral analysis becomes increasingly difficult. The large number of protons in a protein causes signals to overlap. Also, large molecules tumble slowly causing peaks to broaden, decreasing the overall sensitivity of the NMR experiment (Wagner, 1993; Kay and Gardner, 1997; Clore and Gronenborn, 1998).

These obstacles do not preclude larger protein structures from being solved by NMR techniques. Overlapping peaks on NMR spectra can sometimes be resolved by increasing the dimensions of the data set, or by observing nuclei (with spin) other than protons, such as [^{15}N] or [^{13}C] (Wagner, 1993). This necessitates the use of uniformly [^{15}N] or [^{13}C]-labeled proteins, which are produced by expressing cloned proteins in bacterial systems on minimal media supplemented by [^{15}N]NH_4Cl or [^{13}C]-glucose as the sole nitrogen or carbon source.

Because [^{15}N] and [^{13}C] nuclei are much more insensitive than protons, polarization transfer experiments transfer magnetization (via heteronuclear

coupling) from [^{1}H] to [^{15}N] and/or [^{13}C], and finally back to the proton, where it can then be detected. A typical example of this type of experiment is the Insensitive Nuclei Enhanced by Polarization Transfer (INEPT) pulse sequence, which is used for practically all 2D, 3D and 4D heteronuclear NMR experiments. The HSQC pulse scheme, in very simple terms, employs an INEPT sequence to transfer [^{1}H] magnetization into antiphase [^{15}N] or [^{13}C] magnetization, and back again into the [^{1}H] (reverse INEPT) for detection.

NMR Spectroscopy as a Tool to Map Protein Interactions

Experimental results presented in this chapter utilized NMR spectroscopy to determine interactions between Ubc1Δ and Ub. When a protein interaction occurs, surface residues involved in the interaction undergo conformational changes to accommodate the other proteins. Such displacements result in a change of chemical environment for all the atoms within the interface. The interaction of Ub and UbcΔ to form the Ubc1Δ~Ub thiolester is an example of such an interaction. If spectra of [^{15}N]-Ub are collected, in the absence of other proteins, and spectra of [^{15}N]-Ub bound to unlabeled Ubc1Δ is then collected, an interpretable differential spectra is obtained (Figure 3.2A and B). Spectra such as these can then be examined and the differences in the spectra can determine what residues had been affected by the interaction of Ub with UbcΔ. This procedure was repeated for [^{15}N]-Ubc1Δ and unlabeled Ub to determine how surface residues change when the thiolester is formed (Figure 3.2C and D). This information, along with the crystallographically determined structures of Ubc1Δ and Ub allowed us to create a map of the surface residues involved in their interaction. Once the interacting surfaces on each molecule had been determined, they were used to model the interaction that occurs between them.

3.1.3 Simulations of Protein-Protein Interactions

The simulation of protein-protein or protein-ligand interactions is commonly referred to as docking. The computational methods that are applied to these simulations can range from the very simple to the extremely complex. An example of a simple docking simulation might involve first determining the

surface contours of each molecule, followed by the manipulation of each molecule to find the best fit by eye. We could then perform an inspection of the docking interactions, including such physical properties as hydrophobic and ionic character and the total occluded surface area, as an estimate of the potential binding character of the interaction. This method of docking is only as accurate as the investigator's intuition and, while intuition plays an important role in molecular modeling, the use of algorithms designed for the purpose of docking is much more useful.

Rigid-Body Methods

Rigid body docking methods, such as grid-based simulations, have proven to be extremely useful in reducing computational loads and increasing the number of solutions to docking problems (Luty *et al.*, 1995). This technique involves the simplification of a molecular pair to the smallest box that can surround each molecule. A grid corresponding to the properties of the underlying atoms is then created on the surface of the box. The physical description of each molecule is therefore defined as a series of points on the surface of each box. The number of points can vary, thereby increasing or decreasing the accuracy of the simulation. Although more points provide more accuracy, more computational power and time are required to obtain a solution. The creation of a grid substantially reduces the time required for each of these calculations. It is a crude estimate but provides the user with a picture of the overall energy of the interaction.

Monte Carlo Type Simulations

A Monte Carlo simulation entails allowing a ligand to "randomly walk" about the surface of a target. In this method of docking, the energy of the system is evaluated in an initial binding mode, and a random change is subsequently applied (Hart and Read, 1992). The energy of the system is then recalculated and, if the change leads to a decrease in energy, the new configuration is accepted as the new state of the system and the cycle is repeated. If the change causes an increase in the energy of the system, then a random choice is made to

either accept or reject this new conformation. Since there is some randomness to the generation of the final molecular complex and, since there are usually many protein-ligand conformations having similar energies, an ensemble of many structures is usually calculated with the hope that some of the structures will show the same binding mode. With extensive sampling, this procedure should yield a Boltzmann weighted distribution of the accessible states of the system.

Dynamic Protein-Protein Docking

Dynamic protein docking is also known as simulated annealing, and is roughly analogous to heating and slowly cooling a substance to obtain a strong crystalline structure (Clamp *et al.*, 1994; Cummings *et al.*, 1995). The simulated annealing process lowers the temperature by slow stages until the system "freezes" and no further changes occur. At each temperature, the simulation must proceed long enough for the system to reach a steady state or equilibrium, known as thermalization. To apply simulated annealing, a configuration is constructed by imposing a random displacement, using a Monte Carlo step (Goodsell and Olson, 1990; Hart and Read, 1992). If only good perturbations are accepted, as with iterative improvement, the final solution is likely to be a local minimum. In simulated annealing bad or "uphill" configurations are probabilistically accepted based on the temperature parameter. This is known as the Metropolis step, the fundamental procedure of simulated annealing (Metropolis *et al.*, 1953). Annealing gives the system the opportunity to jump out of local minima with a reasonable probability while the temperature is still relatively high.

There are now numerous software packages that will easily perform Grid and Dynamic based Monte Carlo type docking simulations. These include the ever-present Affinity package in Insight II (Accelyrs Inc.) and AutoDock, which is rapidly gaining popularity (Goodsell *et al.*, 1996). These packages are extremely useful in that they simplify the initial setup of the molecular systems with an easy to understand graphical user interface.

3.2 Experimental Procedures

Protein Purification

Purification of His tagged Uba1 was performed as described in Chapter 3 *Protein Purification.* Ub and Ubc1Δ were purified as described previously by Hodgins *et al.* (1996).

Thiolester reactions

UbcΔ1~Ub thiolester reactions were performed at 30 C *in situ*, as described by Hamilton *et al.* (2001).

3.2.2 Molecular Modeling

Hardware

All molecular calculations were performed on a Silicon Graphics Indigo2 IMPACT 10,000 workstation. Graphical representations of proteins were created on a G4 power Macintosh using PyMol for manipulation and rendering (Delano, 2002).

Software

Monte-Carlo Docking simulations were performed using the docking module in the program Insight II release 95.0 (Biosym Technologies, San Diego, California). Grid docking simulations were performed using the docking module in Insight II release 98.0. Following all docking simulations, molecular minimizations and dynamics were performed with the Discover 3 module in Insight II release 98.0. Surface areas were calculated using the program VADAR (D.S. Wishart, University of Alberta), which incorporates the ANAREA program (Richmond, 1984).

Structure Preparation

The structures of human Ub (1ubq; Vijay-Kumar *et al*, 1987) and the E2, Ubc1Δ (1FZY) (Hamilton *et al.*, 2001) were obtained from the Brookhaven Protein Data Bank. Ubc1Δ is a carboxy terminal truncation of *Saccharomyces cerevisiae*

Uba1 that corresponds to its catalytic core domain (Chapter 1, Figure 4B). Both proteins were imported into Insight II and default energy matrices were generated using the standard import commands for pdb files. Residue manipulations based on the primary sequence of Ubc1Δ were made using the Biopolymer module in Insight II. Hydrogen atoms were added at an experimental pH of 7.0 leaving the protein termini uncapped. Default bond orders for both molecules were fixed and the energy potentials were calculated then checked and fixed using a standard AMBER force field (Fox and Kollman, 1996; Weiner *et al.*, 1986). Separate minimization experiments were performed *in vacuo*, allowing only the hydrogen atoms freedom of motion. Subsequent Conjugate Gradient minimization simulations were then performed on each molecule; each molecule reached convergence in fewer than 1000 iterations.

Monte Carlo Docking and Simulated Annealing

Ubc1Δ and Ub were imported into a single environment, with Ubc1Δ configured as the *target* and Ub the *probe*. The *probe* is the molecule that is manipulated while holding the *target* fixed. An initial, random docking was attempted by separating both the "left" and "right" faces of Ubc1Δ into two distinct subsets for the simplification of docking calculations and analysis of results (Figure 3.3). Ub was then docked to either side of Ubc1Δ in separate Monte-Carlo energy comparison experiments. This was done by positioning the tail of Ub near the active site cysteine of Ubc1Δ and displacing Ub through 360° over the Ubc1Δ surface, while maintaining the position of the carboxy terminal glycine of Ub. An arbitrary angle was chosen with which to rotate Ub and another with which to displace Ub over the surface of Ubc1Δ (Figure 3.3). Simulated annealing runs were performed, followed by individual energy minimization calculations. A value of 30° was chosen for the displacement of Ub to reduce computational load but still give a reasonable data set. When the results were compared, a sub-set of structures having intramolecular energies below an arbitrary energy value were analyzed.

Following the initial docking experiments, data obtained from the NMR analysis was incorporated into the model. Residues I87, C88, L89, I91, L92, W96, S97, I100, A105, S108, Q114, S115 and A119, all corresponding to major NMR chemical shifts in the E2-Ub complex, were used to define the ubiquitin binding site on the right side Ubc1Δ. Residues that were shown to have a change in their chemical shifts on the "left" side of Ubc1Δ were excluded from the analysis due to the poor energies obtained in the initial docking experiments. A similar E2 binding site on Ub was defined using residues R42, L43, L48, V70, L71, R72, L73 and G76.

After the interface patches between Ub and Ubc1Δ were identified, a restrained docking experiment between them was performed. Subsets were once again created in Insight II; in this case they were based on the interfacial residues determined by the NMR experiments. Ub and Ubc1Δ were placed in close proximity, using these subsets to constrain the system, docking only these surfaces of Ub and Ubc1Δ. The tail of Ub was positioned so that it was oriented towards the active site cysteine of Ubc1Δ, thereby making this a trivial docking simulation. The Insight II docking module was then utilized to perform a restrained simulated annealing simulation to bring the two molecules to the lowest energy complex. With this experiment a Ubc1Δ~Ub complex which closely resembled the final model was generated. Next the backbone atoms of both molecules were fixed and a simple steepest descent energy minimization was performed on the side chain atoms. A distance restraint of 2 Å was introduced between the carboxy group of Gly 76 on Ub and the sulfur atom of Cys 88 on Ubc1Δ. This corresponds to a slightly longer than average distance for a sulfur to oxygen bond in a thiolester (actual calculated length from simulations was 1.73 Å). Final minimization and dynamics were then performed, on the eight residues of the carboxy terminus of Ub. After approximately 1000 iterations, the lowest energy complex was obtained and another conjugate gradient minimization was performed on the entire complex. Once this minimization experiment was complete, molecular dynamics were performed on the previously defined binding sites of the two molecules.

Molecular Dynamics

To perform the dynamics experiment, the backbone atoms in both molecules were fixed, allowing only 3 Å of movement through six degrees of freedom. Atoms found within 15 Å from either of the interacting surfaces of Ubc1Δ or Ub were excluded from this constraint and were given unlimited motion in the system. Dynamics simulations were performed at a temperature of 500 K for a total of 10 picoseconds. The lowest energy structures were obtained and analyzed for hydrogen bonding, occluded surface area, and inter and intra molecular energies. Once the initial minimization and dynamics were completed, the two molecules were covalently attached to form a single molecule. An isopeptide bond between the sulfur of Cys 88 on Ubc1 and the hydroxyl oxygen of the carboxy terminal Gly 76 on Ub was formed using the Biopolymer module in Insight II. A final round of minimization and dynamics was then performed on the entire structure, with the backbone residues fixed to avoid perturbing the final docked structure.

Atomic Coordinates

Atomic coordinates for the crystallographic structure of Ubc1 and the model for the Ubc1Δ~Ub thiolester have been deposited in the Protein Data Bank under accession code 1FXT.

3.3 Results

In our initial model of the Ubc1Δ~Ub thiolester the lowest energy values were obtained when Ub was docked on the "right" side of the E2 molecule (Figure 3.3). This region was found to be formed by a slight depression on the surface of Ubc1Δ, which was composed largely of hydrophobic residues. This region was later identified as the binding site for Ub as determined by the NMR spectra collected during the formation of the thiolester *in situ*.

Previous results obtained in our laboratory have demonstrated that an E2~Ub thiolester intermediate is formed when millimolar concentrations of Ub and yeast

Ubc1Δ are incubated in the presence of yeast Uba1, Mg^{2+} and ATP (Hodgins *et al.*, 1996). To eliminate the possibility of Ubc1 auto-ubiquitination and the formation of multi-ubiquitin chains, appropriate amino acid substitutions were introduced into Ub (K48R) and Ubc1Δ (K93R) (Gregori *et al.*, 1990; Hodgins *et al.*, 1996). Chemical shift perturbation results obtained by following the formation of the thiolester with HSQC NMR, combined with the crystal structures of both Ub and Ubc1Δ, provided the tools required to determine the first structure of an E2~Ub thiolester intermediate.

Collection of NMR Data

Figure 3.2 shows a comparison of regions of ^{1}H-^{15}N HSQC spectra for the [^{15}N]-Ub and [^{15}N]-E2 proteins in free and complexed forms. Upon E2-Ub thiolester formation there is an overall decrease in peak intensities resulting from the increased molecular mass of the covalent intermediate (24 kDa) compared to that of the E2 (16 kDa) or Ub (8 kDa). The intensity of several peaks decreased significantly. These peaks correspond to residues near the active site cysteine (Cys 88) in the E2 (Lys 74, Val 75, Ser 82, Leu 89), near the C-terminus of Ub (Val 70, Leu 71, Arg 72, Leu 73) and near other surface residues of the proteins. These observations are consistent with the placement of these residues at the protein-protein interface of the E2-Ub intermediate.

Residues in Ubc1Δ and Ub that exhibited the greatest peak intensity decrease upon thiolester formation were mapped to the x-ray crystallographic surfaces of human Ub (Vijay-Kumar *et al.*, 1985) and the catalytic domain of the Ubc1Δ from *S. cerevisiae* (Hamilton *et al.*, 2001) (Figure 3.4). The majority of affected residues are clustered together forming contiguous exposed surface patches on each protein. In the case of Ubc1Δ, the surface identified from ^{1}H-^{15}N HSQC experiments radiates to one side of the molecule from the active site and includes Cys 88. In the case of Ub (Figure 3.4B), this surface sits at the base of the globular domain, includes residues Arg 42, Leu 43 and Arg 48 and extends into the carboxy terminal tail including the thiolester-forming residue Gly 76. The surfaces identified on Ub and Ubc1Δ by NMR spectroscopy have properties

consistent with an interface formed between the proteins in the thiolester. Both patches cover similar surface areas and consist largely of hydrophobic residues.

Structure of the E2-Ub Intermediate

The Ubc1Δ-Ub footprint obtained from ^{1}H-^{15}N HSQC experiments is shown in Figure 3.4. This footprint was used in combination with multiple separate Monte Carlo calculations to dock Ub to Ubc1Δ. Initial docking experiments were done without the thiolester linkage. Later, the covalent bond between Cys 88 in Ubc1 and Gly 76 in Ub was modeled in. This greatly aided the docking procedure and limited the total number of possible Ubc1Δ~Ub complexes. The lowest-energy structures had the carboxy terminal tail of Ub wrapped around Ubc1Δ, with Gly 76 situated near the active site cys 88 residue of Ubc1Δ. In the E2-Ub thiolester model (Figure 3.5), residues Leu 71–Gly 76 in Ub position themselves in a shallow cleft on the surface of Ubc1Δ. This cleft is comprised of the Ubc1Δ residues Leu 89 – Ile 91 on one side and Asp 119 – Pro 121 on the other. Although no direct charge interactions are immediately apparent, two important regions of hydrophobic interactions are present; Leu 71 and Leu73 in Ub sandwich Ile 91 in Ubc1Δ, while Ile 44 and Val 70 in Ub interact with Ala 111 and Gln 114 in Ubc1Δ. The E2-Ub interface is also supported by several obvious hydrogen bonding interactions between the side chains of Glu 117 (Ubc1Δ) and Arg 72 (Ub), between the side chain of Asp 120 (Ubc1Δ) and the backbone nitrogen of Gly 75 (Ub), and between the carbonyl oxygen of Ala 111 (Ubc1Δ) with the side chain of Arg 42 (Ub).

Together, the side chain interface of the E2-Ub thiolester intermediate occupies approximately 1823 $Å^2$ of surface area comprising about 48% non polar components and 52% polar or charged side chains. Furthermore, residues at the interface, including Ile 44, Val 70, Leu 71 and Leu 73 in Ub along with Ala 111, Gln 114, Asn 119, and Asp 120 in Ubc1Δ, were among those with the largest peak-intensity changes observed in the NMR spectra (Figure 3.2).

3.4 Discussion

Several previous attempts have been made to determine the three-dimensional structures of E2-Ub and related complexes using NMR spectroscopy. Most notable have been the carboxy terminal hydrolases Uch-L3 (Wilkinson *et al.*, 1999) and YUH-1(Rajesh *et al.*, 1999; Sakamoto *et al.*, 1999). The solution of these interfaces has allowed the partial mapping of surfaces which probably resemble recognition sites for Ub on E2. A handful of other studies have also, unsuccessfully, attempted to map surface interactions of covalent E2-Ub homologues (Liu *et al.*, 1999) and non-covalent interactions between E2 (Ubc2) and Ub (Miura *et al.*, 1999).

The thiolester intermediate is sufficiently labile to preclude its purification in quantities sufficient to determine its three dimensional structure by either traditional NMR or X-ray crystallographic techniques. As an alternative, ^{1}H-^{15}N HSQC NMR spectrometry was used to monitor the formation of the Ubc1Δ~Ub thiolester intermediate. Spectra were acquired as a function of time from two reactions that contained catalytic amounts of Uba1 with either [^{15}N]-Ub and unlabeled Ubc1Δ or [^{15}N]-Ubc1Δ and unlabeled Ub. Building upon the NMR assignments of these proteins in their un-complexed forms, time-dependent changes in cross peak intensity that occur with thiolester formation were used to determine the interfacial regions between the proteins (Hamilton *et al.*, 2000b). This method has been shown to be extremely useful for *in situ* NMR reactions where sample dependent variations in environment are eliminated (Hamilton *et al.*, 2000a).

The surface region of Ub that was determined to interact with Ubc1Δ is similar to that which interacts with other proteins including the Ub hydrolase Uch-L3 (Johnston *et al.*, 1997), the human E2 HsUbc2b (Miura *et al.*, 1999), the 26S proteasome (Phillips *et al.*, 2001), and Uba1 (Burch and Haas, 1994) (Chapter 2). The Ubc1Δ patch contains residues Ser 97 and Ala 111. The mutants ubc1S97R and ubc1A111R reduced the ability of Ubc1Δ to form the thiolester in vitro (Ptak *et al.*, 2001). In addition, the Ubc1Δ A111R mutation strongly

attenuates the ability of Ubc1Δ to catalyze the formation of multi-Ub chains *in vitro*. These substitutions affect the general function of the E2~Ub thiolester, but have no effect on the catalytic transfer of Ub from Uba1 to E2.

Structure of the Ubc1~Ub thiolester

To form the covalent bond between the Ubc1Δ active site and the carboxy terminus of Ub, a modest conformational adjustment of the crystallographic form of Ub was required. This modification was not surprising, given the significant observed flexibility of the Ub carboxy terminus in solution as determined from ^{15}N and ^{13}C relaxation experiments (Powers *et al.*, 1991). The flexibility of the Ub tail may be a requirement for the binding of Ub to Uba1and Ubc1Δ and was utilized in the Ub-adenylate and Ub-thiolester models.

The putative interacting surfaces between Ubc1Δ and Ub are consistent with site-directed mutagenesis experiments (Figure 3.6). Residues 72-76 in the tail of Ub have been shown to be essential for its function (Wilkinson and Audhya, 1981). In the E2-Ub thiolester complex, the side chains of these residues account for nearly 300 $Å^2$ of contact surface at the thiolester interface. With the exception of Gly 75, each residue in this region of Ub has 40% of its side chain buried in the Ubc1Δ~Ub thiolester intermediate as compared to the un-complexed proteins. One of the residues in the tail of Ub that was shown to interact with Ubc1Δ is Arg 72. This residue has been shown to be critical for initial Uba1 binding and for the interaction of Ub with the Uch-L3 hydrolase (Johnston *et al.*, 1999).

The interacting surface for Ubc1Δ contains two distinct residues important to its function, Ser 97 and Ala 111. The mutation of Ubc1 Ser 97 to Arg and Ala 111 to Arg, produce an E2 that retains full capacity for thiolester formation but has lost its stress-related function in vivo (Ptak *et al.*, 2001). In addition, the A111R replacement strongly attenuates the ability to catalyze multi-Ub chains in vitro. These substitutions have no effect on the catalytic transfer of Ub from E1 to E2, implying that the Ubc1Δ surface occupied by Ub in the thiolester may be only required for downstream functions such as multi-Ub chain assembly and target recognition. Conversely, the replacements T73R and K74A in Ubc1Δ occur at

amino acid positions that are not at the Ubc1Δ~Ub interface in the thiolester (Opposite face in Ubc1 Figure 3.6B). These substitutions have no effect on thiolester formation, chain assembly, or *in vivo* properties of E2 (Ptak *et al.*, 2001).

Other similarities exist between residues in Ub involved at the Ubc1Δ~Ub interface and residues that are important for its activation by Uba1. For example, residues Leu 8, Ile 44, and Val 70 in Ub have been proposed as important for Uba1 binding (Burch and Haas, 1994). These residues also make intimate contacts in the E2-Ub thiolester complex. Furthermore, these residues also form a repeating surface patch in the multi-Ub chains that are implicated in binding to the Proteasome (Gregori *et al.*, 1990; Beal *et al.*, 1998; Fu *et al.*, 1998; Phillips *et al.*, 2001).

These results may indicate that the surface identified here is not essential for the transfer of Ub to Ubc1Δ as described in the model (Chapter 2). Alternate sites on the surface of Ubc1Δ may be responsible for the main interaction between Ubc1Δ and Uba1, with the surface identified here coming into play only after transfer has occurred and the Ubc1Δ~Ub thiolester has been displaced from the complex. The discussion in Chapter 4 describes similar binding motifs on the surfaces of Uba1 and Ubc1Δ indicating similar binding interactions with Ub. This may imply that Ub, upon being transferred to Ubc1Δ, may undergo a conformational switch that allows it to interact with the binding site described here.

A Glimpse of the E3-E2-Ub Ternary Complex

Understanding the structural relationship between the E2-Ub thiolester intermediate and the Ub protein ligases (E3s) is an important prerequisite for determining the mechanistic events leading to target recognition. There have recently been two structural reports of E2-E3 complexes. One is composed of the E2 protein HsUbc7 and the E3 protein E6AP, a member of the HECT class of E3s (Huang *et al.*, 1999). The other complex is composed of HsUbc7 and the E3 protein c-Cbl, a member of the RING-finger class of E3s (Zheng *et al.*, 2000). In both cases, specific and nearly identical non covalent interactions occur between

the E3 and E2 proteins. Because of the high degree of homology within the catalytic domains of all E2 proteins (Figure 3.1) the results from these experiments can be extrapolated to Ubc1Δ. Residues 60, 61, 63, 64, and 65 between β strands 3 and 4 (the L1 region), and residues 98 and 99 that are found prior to α helix 2 (the L2 region) make close contacts with the E3 proteins. Charge-charge contacts are also present between arg 6 and Lys 9 in α helix 1 of Ubc1Δ and E3. This indicates that the interaction of Ubc1Δ with an E3 protein should occur via the same intermolecular surface as other E2 proteins. However, it should be noted that the precise E3 that interacts with Ubc1Δ has yet to be identified. The similarities between Ubc1Δ in the E2~Ub thiolester intermediate and HsUbc7 in the E2-E3 complex allow the spatial relationship of the E2, E3, and Ub components of an E3-E2-Ub thiolester complex to be proposed for the first time (Figure 3.7). The three-dimensional structure UbcH7in the HsUbc7-c-Cbl complex was superimposed on the Ubc1Δ~Ub thiolester model described in the current work to provide a picture of the E3-Ubc1Δ~Ub ternary complex. This figure suggests a common interaction between the E3 protein and Ubc1Δ. In particular, the Ubc1Δ interface contains residues Arg 6 and Lys 9 in α helix 1, and residues found in both L1 and L2 regions. Such a structure may give clues to the transfer of Ub between E2 and E3 or between E2 and a target substrate.

As such, the model of the E2~Ub thiolester intermediate does not include any of the interactions important for E2-E3 recognition, indicating that E2 proteins have unique interactions with Ub and E3 proteins. Furthermore, in the E3-E2-Ub ternary complex, the Ub molecule is held adjacent to the E3 protein through contacts with E2. This tight association of proteins presents an attractive arrangement for Ub transfer to a target protein recruited by E3, one of the possible mechanisms for ubiquitin targeting.

3.5 Conclusion

As a tool for determining the interface between two proteins, NMR has become extremely useful in cases where traditional crystallography is not possible. The

structure discussed in this manuscript reveals the first glimpse of the surface recognition between Ub and an E2, providing invaluable insight into the three dimensional arrangement of Ub, E2 and E3 in complex. This structure also provides insight into the mechanism for Ub transfer from Uba1 to E2, determinants for the recognition of targets, and interactions with E3.

We are fortunate that mutational data from the surface of Ubc proteins correlates well with the regions previously determined to be important for their functions (Ptak *et al.*, 2001). From this data we can see positions on the surface of E2 in which conservative mutations have the greatest effect. These mutations will not only affect the binding of Ub to E2 but also interactions with other proteins such as Uba1, target proteins and E3s. Many of the residues correspond to residues that were mapped onto the surface of Ubc1Δ through NMR experiments presented here.

The validity of the thiolester model has been reinforced by experiments designed to address its biological and structural significance. Furthermore, this model has provided invaluable insight into the three dimensional arrangement of Ub relative to other protein components downstream in the ubiquitin system, such as the *HECT*-type (Huang *et al.*, 1999) and *ring-finger*-type E3 ternary complexes (Zheng *et al.*, 2000).

Figure 3.1. **Structure-based alignment of *S. cerevisiae* E2 Catalytic Domains** Three-dimensional structures of *S. cerevisiae* Ubc1 (Hamilton *et al.*, 2001), Ubc2 (Worthylake *et al.*, 1998), Ubc4 (Cook *et al.*, 1997), and Ubc7 (Cook *et al.*, 1997) and *Homo sapiens* Ubc9 (Tong *et al.* (1997)) were aligned by using the superimpose function contained within the viewer module of Insight II, version 95.0 (Molecular Simulations Inc.). Alignments were performed by using nine structurally conserved amino acid positions distributed throughout the length of each polypeptide (positions 17, 34, 49, 66, 77, 86, 96, 110, and 135 according to the numbering of *S. cerevisiae* Ubc4). The root mean square deviation for these four superimposed structures at the nine positions indicated equaled 0.83 Å. The resulting alignment served as the guide for the subsequent alignment of the remaining E2 catalytic domains.

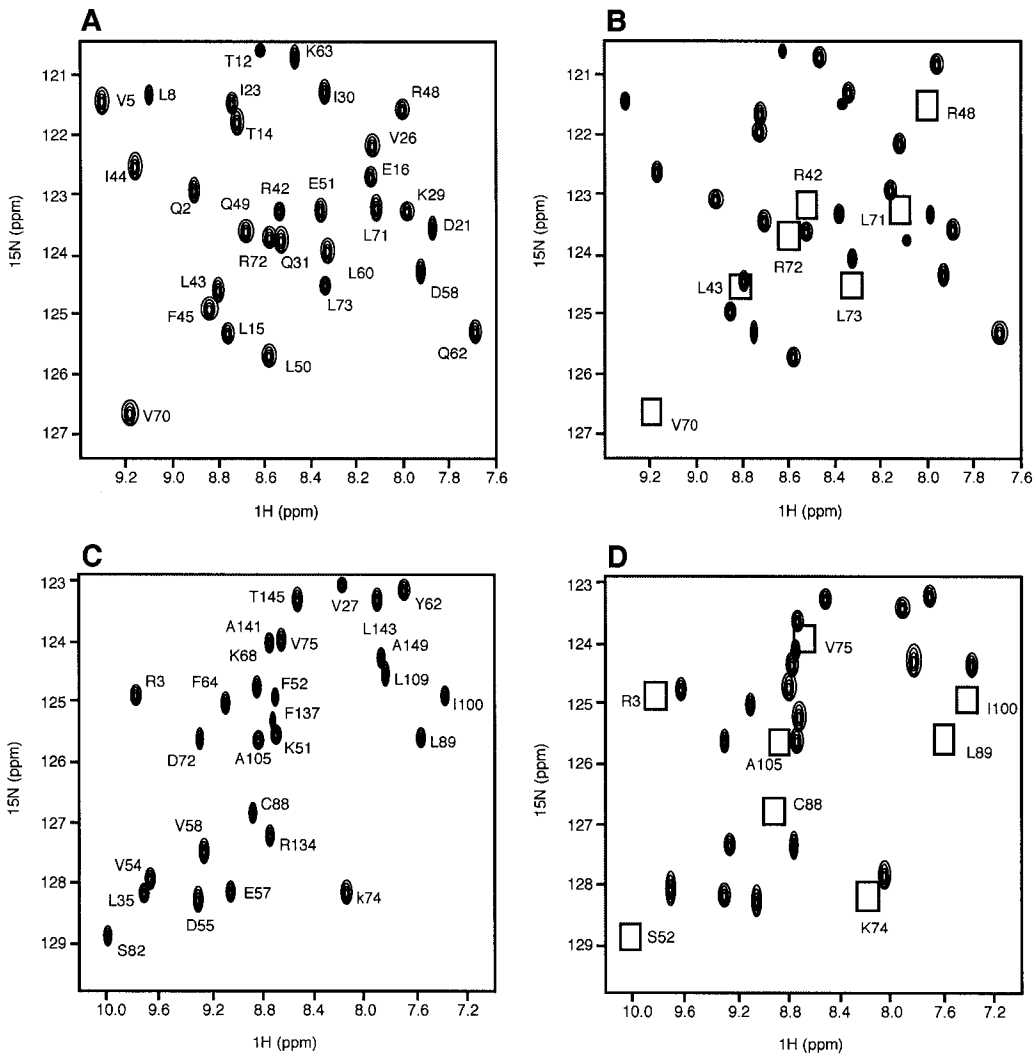

Figure 3.2. **E2-Ub Thiolester Formation Probed by NMR Spectroscopy** Selected regions of 500 MHz ^{1}H-^{15}N HSQC spectra of ^{15}N-Ub (A and B) and ^{15}N-Ubc1Δ (**C** and **D**) showing the effect of thiolester formation on peak intensity. **A**, ^{15}N-Ub and unlabeled Ubc1Δ collected prior to thiolester formation. **B**, the same sample with Uba1, ATP, and MgCl added to initiate thiolester formation and spectra collected after 1 hour. **C** and **D**, identical to **A** and **B** with the exception that ^{15}N-Ubc1Δ and unlabeled Ub were used. In both cases resonances are indicated with boxes (**B** and **D**) to indicate those that decreased in intensity when compared to those prior to thiolester formation (**A** and **C**) (Hamilton *et al.*, 2001).

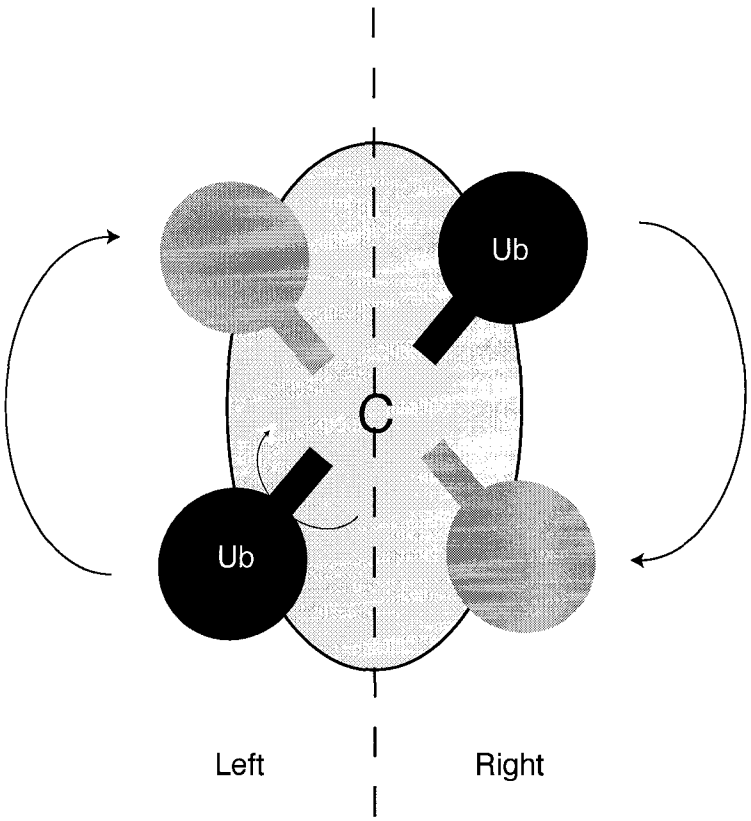

Figure 3.3. **Schematic Representation of Ub Docking to the Ubc1Δ Active Site** Hybrid Monte Carlo simulated annealing docking of Ub to Ubc1Δ was performed with a two step approach. Ubc1Δ was seperated into left and right subsets and Ub was placed onto its surface (dark grey) with its tail oriented towards the active site cysteine (C). Ub was then rotated through 180° to rest on the opposite face of Ubc1Δ active site (light grey). Throughout the displacement of Ub, it was rotated about its axis to explore all the available conformations. This procedure was then repeated for the other subset.

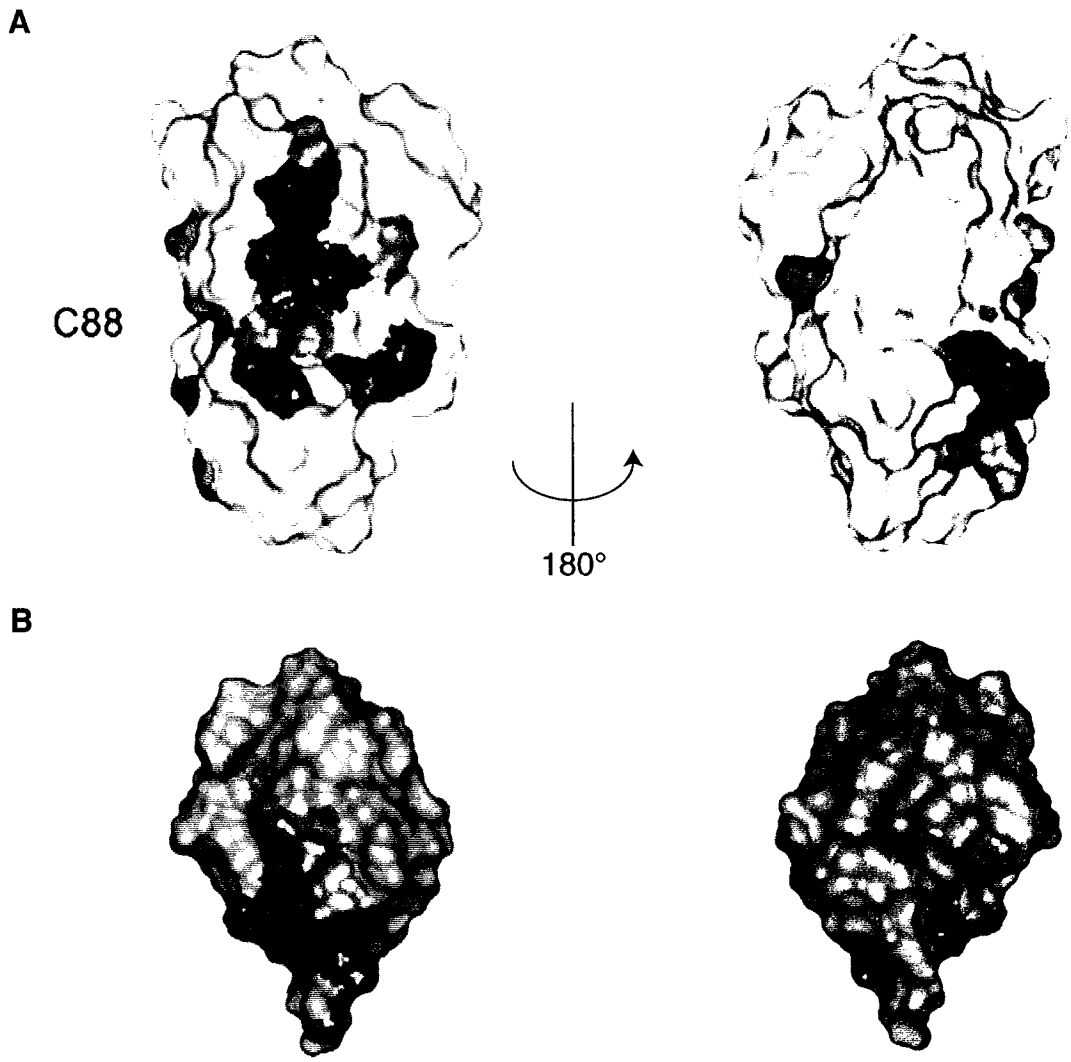

Figure 3.4. **NMR Determined Surface Patches on Ubc1Δ and Ub**
Connolly surface representations of Ubc1Δ (**A**) and Ub (**B**), depicting surfaces comprising residues affected by thiolester formation. Surfaces colored red indicate residues that had a peak intensity decrease of 90% in ^{1}H-^{15}N HSQC spectra as compared to spectra of the un-complexed proteins. Surfaces are also colored magenta to indicate those residues whose peak intensities decreased between 10% and 21% as compared to the un-complexed forms of these proteins. Each molecule is displayed in two orientations that are 180° from one another. The active site cysteine of Ubc1 (residue 88) can not be seen, but is illustrated by an arrow. From these images, the clustering of residues on the surface of each molecule is apparent.

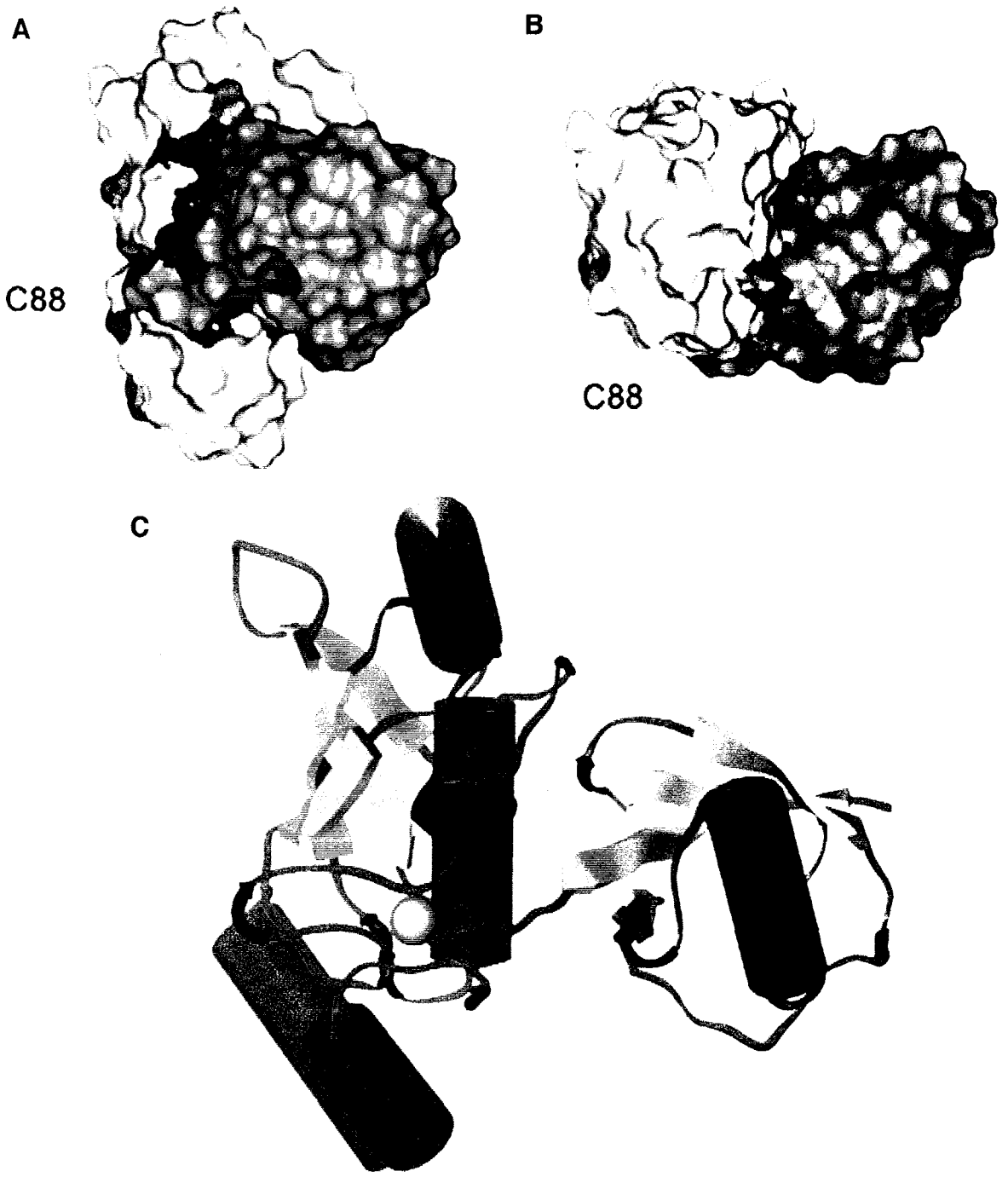

Figure 3.5. **Model of the Ubc1Δ-Ub Thiolester Intermediate**
This model was determined by Monte Carlo docking as described in *Monte Carlo Docking and Simulated Annealing*. The model shows (**A**) side and (**B**) end orientated views of α helix 2 (α**2**) in Ubc1Δ. Surface coloring is as in Figure 3.4. **C**, ribbon representation of the thiolester model, illustrating the underlying structural motifs within both Ubc1Δ and Ub, the orientation is as in **A**. The active site cysteine is shown as a yellow VDW sphere with the tail of Ub positioned directly above. Here the packing of ubiquitin's β sheet (yellow) with α helix 2 in Ubc1Δ (red) is clearly seen.

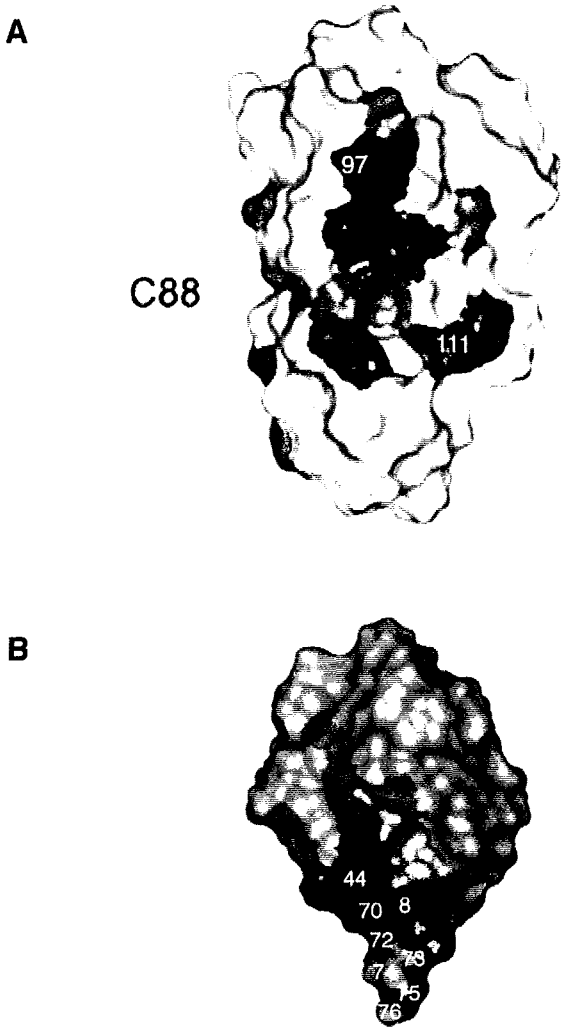

Figure 3.6. **Surface Mutations on Ubc1Δ and Ub Affecting *in vivo* Function** Mutational data for both Ubc1Δ (**A**) and Ub (**B**) are shown on the surfaces determined to interact by NMR spectroscopy. Coloring is as in Figure 3.4. **A**, as described in the text, residues Ser 97 and Ala 111 are implicated in the stress response *in vivo* (Ptak *et al.,* 2001). Mutations of alternate residues Thr 73 and Lys 74 (found on the opposite face) have no effect on Ubc1Δ function. **B**, similar residues found on the interacting face of Ub that also have an effect *in vivo*. Residues 72-76 in the tail of Ub are crucial for its function *in vivo* (Wilkinson *et al.*, 1981). The residues Leu 8, Ile 44 and Val 70 have been implicated in binding Uba1 (Burch *et al.*, 1994).

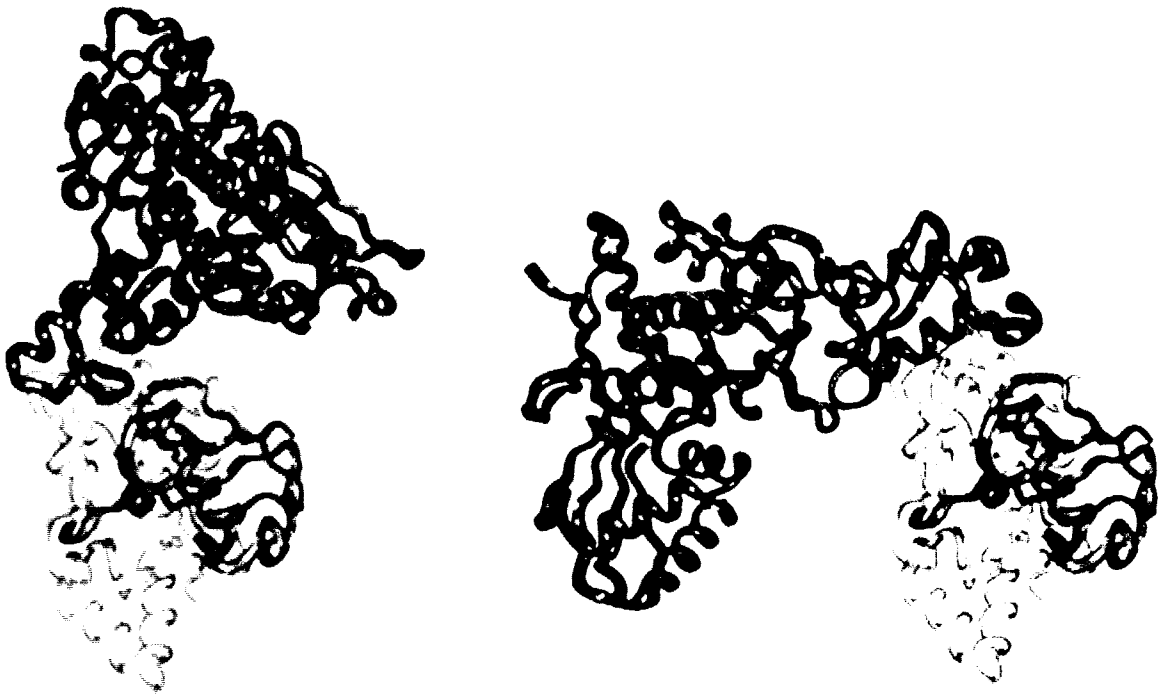

Figure 3.7. **Model of an E3/Ubc1~Ub Ternary Complex**
Key intermolecular contacts between the Ubc1Δ~Ub thiolester model and the E3s c-Cbl and E6AP were modeled and demonstrate the absence of any steric clashes between these E3s and Ub in the docked thiolester. Residues in Ubc1Δ (4-17, 22-26, 34-41, 50-58, 67-72, 104-113,123-132, and 135-147) that are conserved between Ubc1 and UbcH7 were used to perform a structural alignment. UbcH7 is the E2 present in the complexed structures of both c-Cbl (Zheng *et al.*, 2000) and E6AP (Huang *et al.*, 1999). In the E2-Ub model presented here the corresponding regions of UbcH7 in the UbcH7-c-Cbl or UbcH7-E6AP complex, were superimposed Ubc1Δ. The RMSD for this superposition in both cases was determined to be 3.0 Å. Following the superposition, the structure of UbcH7 was removed from both structures. The ribbon colors represent blue for either c-Cbl or E6AP, red for Ub, and white for Ubc1Δ.

3.6 References

Beal, R. E., Toscano-Cantaffa, D., Young, P., Rechsteiner, M., & Pickart, C. M. (1998). The hydrophobic effect contributes to polyubiquitin chain recognition. *Biochemistry, 37(9)*, 2925-34.

Burch, T. J., & Haas, A. L. (1994). Site-directed mutagenesis of ubiquitin. Differential roles for arginine in the interaction with ubiquitin-activating enzyme. *Biochemistry, 33(23)*, 7300-08.

Clamp, M. E., Baker, P. G., Stirling, C. J., & Brass, A. (1994). Hybrid Monte Carlo: an efficient algorithm for condensed matter simulation. *J Comput Chem, 15*, 838-46.

Clore, G. M., & Gronenborn, A. M. (1998). NMR structure determination of proteins and protein complexes larger than 20 kDa. *Curr Opin Chem Biol, 2(5)*, 564-70.

Cook, W. J., Martin, P. D., Edwards, B. F., Yamazaki, R. K., & Chau, V. (1997). Crystal structure of a class I ubiquitin conjugating enzyme (Ubc7) from Saccharomyces cerevisiae at 2.9 angstroms resolution. *Biochemistry, 36(7)*, 1621-27.

Cook, W. J., Suddath, F. L., Bugg, C. E., & Goldstein, G. (1979). Crystallization and preliminary x-ray investigation of ubiquitin, a non- histone chromosomal protein. *J Mol Biol, 130(3)*, 353-55.

Cummings, M. D., Hart, T. N., & Read, R. J. (1995). Monte Carlo docking with ubiquitin. *Protein Sci, 4(5)*, 885-99.

Delano, W. L. (2002). The PyMOL Molecular Graphics System. from http://www.pymol.org

Fox, T., & Kollman, P. A. (1996). The application of different solvation and electrostatic models in molecular dynamics simulations of ubiquitin: how well is the X-ray structure "maintained"? *Proteins, 25(3)*, 315-34.

Fu, H., Sadis, S., Rubin, D. M., Glickman, M., van, N., S., Finley, D., & Vierstra, R. D. (1998). Multiubiquitin chain binding and protein degradation are mediated by distinct domains within the 26 S proteasome subunit Mcb1. *J Biol Chem, 273(4)*, 1970-81.

Goodsell, D. S., Morris, G. M., & Olson, A. J. (1996). Automated docking of flexible ligands: applications of AutoDock. *J Mol Recognit, 9(1)*, 1-5.

Goodsell, D. S., & Olson, A. J. (1990). Automated docking of substrates to proteins by simulated annealing. *Proteins, 8(3)*, 195-202.

Gregori, L., Poosch, M. S., Cousins, G., & Chau, V. (1990). A uniform isopeptide-linked multiubiquitin chain is sufficient to target substrate for degradation in ubiquitin-mediated proteolysis. *J Biol Chem, 265(15)*, 8354-57.

Haas, A. L., Warms, J. V., Hershko, A., & Rose, I. A. (1982). Ubiquitin-activating enzyme. Mechanism and role in protein-ubiquitin conjugation. *J Biol Chem, 257(5)*, 2543-48.

Hamilton, K. S., Ellison, M. J., Barber, K. R., Williams, R. S., Huzil, J. T., McKenna, S., Ptak, C., Glover, M., & Shaw, G. S. (2001). Structure of a conjugating enzyme-ubiquitin thiolester intermediate reveals a novel role for the ubiquitin tail. *Structure (Camb), 9(10)*, 897-904.

Hamilton, K. S., Ellison, M. J., & Shaw, G. S. (2000a). Letter to the editor: 1H, 15N and 13C resonance assignments for the catalytic domain of the yeast E2, UBC1. *J Biomol NMR, 16(4)*, 351-52.

Hamilton, K. S., Ellison, M. J., & Shaw, G. S. (2000b). Identification of the ubiquitin interfacial residues in a ubiquitin-E2 covalent complex. *J Biomol NMR, 18(4)*, 319-27.

Hart, T. N., & Read, R. J. (1992). A multiple-start Monte Carlo docking method. *Proteins, 13*, 206-22.

Hodgins, R., Gwozd, C., Arnason, T., Cummings, M., & Ellison, M. J. (1996). The tail of a ubiquitin-conjugating enzyme redirects multi-ubiquitin chain synthesis from the lysine 48-linked configuration to a novel nonlysine-linked form. *J Biol Chem, 271(46)*, 28766-71.

Huang, L., Kinnucan, E., Wang, G., Beaudenon, S., Howley, P. M., Huibregtse, J. M., & Pavletich, N. P. (1999). Structure of an E6AP-UbcH7 complex: insights into ubiquitination by the E2-E3 enzyme cascade. *Science, 286(5443)*, 1321-26.

Johnston, S. C., Larsen, C. N., Cook, W. J., Wilkinson, K. D., & Hill, C. P. (1997). Crystal structure of a deubiquitinating enzyme (human UCH-L3) at 1.8 A resolution. *Embo J, 16(13)*, 3787-96.

Johnston, S. C., Riddle, S. M., Cohen, R. E., & Hill, C. P. (1999). Structural basis for the specificity of ubiquitin C-terminal hydrolases. *Embo J, 18(14)*, 3877-87.

Kay, L. E., & Gardner, K. H. (1997). Solution NMR spectroscopy beyond 25 kDa. *Curr Opin Struct Biol, 7(5)*, 722-31.

Liu, Q., Jin, C., Liao, X., Shen, Z., Chen, D. J., & Chen, Y. (1999). The binding interface between an E2 (UBC9) and a ubiquitin homologue (UBL1). *J Biol Chem, 274(24)*, 16979-87.

Luty, B. A., Wasserman, Z. R., Stouten, P. F. W., Hodge, C. N., Zacharias, M., & McCammon, A. (1995). A Molecular Mechanics/Grid Method for Evaluation of Ligand-Receptor Interactions. *J Comp. Chem., 16*, 454-64.

Merkley, N., & Shaw, G. S. (2003). Interaction of the tail with the catalytic region of a class II E2 conjugating enzyme. *J Biomol NMR, 26(2)*, 147-55.

Metropolis, N., Rosenbluth, A. W., Rosenbluth, M. N., & Teller, A. H. (1953). Equation of State Calculations by Fast Computing Machines. *J. Chem. Phys., 21*, 1087-92.

Miura, T., Klaus, W., Gsell, B., Miyamoto, C., & Senn, H. (1999). Characterization of the binding interface between ubiquitin and class I human ubiquitin-conjugating enzyme 2b by multidimensional heteronuclear NMR spectroscopy in solution. *J Mol Biol, 290(1)*, 213-28.

Moraes, T. F., Edwards, R. A., McKenna, S., Pastushok, L., Xiao, W., Glover, J. N., & Ellison, M. J. (2001). Crystal structure of the human ubiquitin conjugating enzyme complex, hMms2-hUbc13. *Nat Struct Biol, 8(8)*, 669-73.

Phillips, C. L., Thrower, J., Pickart, C. M., & Hill, C. P. (2001). Structure of a New Crystal Form of Tetraubiquitin. *Acta Crystallogr., Sect.D, 57*, 341.

Powers, R., Clore, G. M., Bax, A., Garrett, D. S., Stahl, S. J., Wingfield, P. T., & Gronenborn, A. M. (1991). Secondary structure of the ribonuclease H domain of the human immunodeficiency virus reverse transcriptase in solution using three-dimensional double and triple resonance heteronuclear magnetic resonance spectroscopy. *J Mol Biol, 221(4)*, 1081-90.

Ptak, C., Gwozd, C., Huzil, J. T., Gwozd, T. J., Garen, G., & Ellison, M. J. (2001). Creation of a pluripotent ubiquitin-conjugating enzyme. *Mol Cell Biol, 21(19)*, 6537-48.

Rajesh, S., Sakamoto, T., Iwamoto-Sugai, M., Shibata, T., Kohno, T., & Ito, Y. (1999). Ubiquitin binding interface mapping on yeast ubiquitin hydrolase by NMR chemical shift perturbation. *Biochemistry, 38(29)*, 9242-53.

Reiss, Y., Heller, H., & Hershko, A. (1989). Binding sites of ubiquitin-protein ligase. Binding of ubiquitin-protein conjugates and of ubiquitin-carrier protein. *J Biol Chem, 264(18)*, 10378-83.

Richmond, T. J. (1984). Solvent accessible surface area and excluded volume in proteins. Analytical equations for overlapping spheres and implications for the hydrophobic effect. *J Mol Biol, 178(1)*, 63-89.

Riek, R., Wider, G., Pervushin, K., & Wuthrich, K. (1999). Polarization transfer by cross-correlated relaxation in solution NMR with very large molecules. *Proc Natl Acad Sci U S A, 96(9)*, 4918-23.

Sakamoto, T., Tanaka, T., Ito, Y., Rajesh, S., Iwamoto-Sugai, M., Kodera, Y., Tsuchida, N., Shibata, T., & Kohno, T. (1999). An NMR analysis of ubiquitin recognition by yeast ubiquitin hydrolase: evidence for novel substrate recognition by a cysteine protease. *Biochemistry, 38(36)*, 11634-42.

Tong, H., Hateboer, G., Perrakis, A., Bernards, R., & Sixma, T. K. (1997). Crystal structure of murine/human Ubc9 provides insight into the variability of the ubiquitin-conjugating system. *J Biol Chem, 272(34)*, 21381-87.

VanDemark, A. P., Hofmann, R. M., Tsui, C., Pickart, C. M., & Wolberger, C. (2001). Molecular insights into polyubiquitin chain assembly: crystal structure of the Mms2/Ubc13 heterodimer. *Cell, 105(6)*, 711-20.

Vijay-Kumar, S., Bugg, C. E., & Cook, W. J. (1987). Structure of ubiquitin refined at 1.8 A resolution. *J Mol Biol, 194(3)*, 531-44.

Vijay-Kumar, S., Bugg, C. E., Wilkinson, K. D., & Cook, W. J. (1985). Three-dimensional structure of ubiquitin at 2.8 A resolution. *Proc Natl Acad Sci U S A, 82(11)*, 3582-85.

Wagner, G. (1993). Prospects for NMR of large proteins. *J Biomol NMR, 3(4)*, 375-85.

Wilkinson, K. D., Laleli-Sahin, E., Urbauer, J., Larsen, C. N., Shih, G. H., Haas, A. L., Walsh, S. T., & Wand, A. J. (1999). The binding site for UCH-L3 on ubiquitin: mutagenesis and NMR studies on the complex between ubiquitin and UCH-L3. *J Mol Biol, 291(5)*, 1067-77.

Wilkinson, K. D., & Audhya, T. K. (1981). Stimulation of ATP-dependent proteolysis requires ubiquitin with the COOH-terminal sequence Arg-Gly-Gly. *J Biol Chem, 256(17)*, 9235-41.

Worthylake, D. K., Prakash, S., Prakash, L., & Hill, C. P. (1998). Crystal structure of the Saccharomyces cerevisiae ubiquitin-conjugating enzyme Rad6 at 2.6 A resolution. *J Biol Chem, 273(11)*, 6271-76.

Zheng, N., Wang, P., Jeffrey, P. D., & Pavletich, N. P. (2000). Structure of a c-Cbl-UbcH7 complex: RING domain function in ubiquitin-protein ligases. *Cell, 102(4)*, 533-39.

Chapter 4

Homology Modeling of the Ubiquitin Activating Enzyme Nucleotide Binding Site: Insights into Ub Activation and Transfer to the Ubiquitin Conjugating Enzymes[1]

4.1 Introduction

Ubiquitin activating enzyme (E1 or Uba1) is responsible for the initial ATP dependent activation of Ubiquitin (Ub) by way of two separate reaction steps. First, upon binding one molecule of Ub and one molecule of ATP, Uba1 catalyzes the formation of a Ub-AMP (Ub-adenylate) intermediate, which remains non-covalently bound at the site of adenylate formation. The second step involves the direct transfer of this activated Ub to an active site cysteine within Uba1 (Cys 600 in *Saccharomyces cerevisiae* Uba1) (Haas *et al.*, 1982; Ciechanover *et al.*, 1984). Following the transfer to Uba1's active site cysteine, Ub becomes transferred to a Ubiquitin conjugating enzyme (Ubc or E2) that then catalyzes its subsequent conjugation to a target protein.

The current mechanism of Ub conjugation places Uba1 solely at the Ub activation step, after which it is not thought to participate following the transfer of Ub to an E2. Given that Uba1 is the only enzyme capable of activating Ub implies that it must interact with each of the numerous E2 proteins to facilitate the formation of the E2~Ub thiolester (Chapter 1) (McGrath *et al.*, 1991). Unfortunately, a structure for Uba1

---

1 Manuscript in preperation.

does not yet exist, and therefore a detailed understanding behind Ub activation and subsequent interaction with the additional components of the Ubiquitin system has not been possible. To address the lack of structural information for Uba1, we have utilized molecular modeling, coupled with key biochemical observations to postulate a mechanism that explains the activation of Ub by Uba1.

4.1.2 Structural History of the Ubiquitin System

The Ubiquitin system has provided researchers with a wealth of structural data. The first structure of Ub revealed a compact, globular fold that terminated in a flexible carboxy "tail", approximately five residues in length (Vijay-Kumar *et al.*, 1987) (Chapter 1, Figure 4A). The structure of this single molecule of Ub was quickly followed by the structures of recombinant Ub_2 and Ub_4 chains, synthesized *in vitro* (Cook *et al.*, 1992; Cook *et al.*, 1994). These structures reinforced the importance of Ub's extended carboxy terminus and identified the establishment of an isopeptide bond between a lysine side chain within Ub itself.

Numerous three dimensional structures of E2 molecules have also provided invaluable information and, currently, include: Ubc1 (Cook *et al.*, 1992; Hamilton *et al.*, 2001), Ubc2 (Worthylake *et al.*, 1998), Ubc4 (Cook *et al.*, 1993), Ubc7 (Cook *et al.*, 1997), Ubc9 (Tong *et al.*, 1997), Ubc10 (Lin *et al.*, 2002) and Ubc13 (Moraes *et al.*, 2001; VanDemark *et al.*, 2001). While none of these structures provided any empirical information regarding E2's interaction with Ub or Uba1, they did provide a platform from which the mechanisms required for protein Ubiquitination could be postulated. The first actual structure of an E2-E3 complex was that of E6AP, which is involved in the degradation of the tumor suppressor p53 (Huang *et al.*, 1999), this was followed by the structure of c-Cbl-UbcH7, which targets activated receptor tyrosine kinases (Zheng *et al.*, 2000) and finally a complex between Ubc13/Mms2, which is involved in *S. cerevisiae* DNA repair pathways (Moraes *et al.*, 2001; VanDemark *et al.*, 2001). As with the structures of the E2's themselves, none of these structures provided information on their interactions with Ub. The first information revealing the interactions between Ub and an E2 is

described here (Chapter 3) and involves the second step in the formation of the Ub conjugate, the Ubc1~Ub thiolester (Hamilton *et al.*, 2001). Even while none of the afore mentioned structures have provided any information with regards to the Ub interaction with Uba1, the existence of several homologous systems has enabled us to extrapolate several of the structural determinants involved in the activation of Ub.

4.1.3 Ubiquitin Like Proteins (UBLs)

Ub shares sequence and structural similarity with at least four different eukaryotic and two prokaryotic proteins (Yeh *et al.*, 2000; Lake *et al.*, 2001). These proteins have been grouped together in a diverse family and are collectively known as Ubiquitin Like proteins (UBL) (Table 4.1). Each of these proteins can be classified into one of two basic groups. The first group contains proteins that are involved in the activation of a single atom of elemental sulfur for its subsequent inclusion into some cofactor, while the second group is composed of proteins that become covalently conjugated to a protein that is involved in their activation. All of the UBL proteins undergo activation by way of a carboxy terminal glycine residue and many by way of a Gly-Gly motif, (see Chapter 1, section 1.5.1) in a reaction that is comparable to that of the activation of Ub (Haas *et al.*, 1983; Johnston *et al.*, 1997; Liakopoulos *et al.*, 1998; Furukawa *et al.*, 2000).

UBL	Ortholog	Activated by	Activated to
Ub	-	Uba1	cysteine
Rub1	Nedd8	Ula1/Uba3	cysteine
Smt3	Sumo	Aos1/Uba2	cysteine
Apg12	Hapg12	Apg7	cysteine
Urm1	-	Uba4	cysteine
MoaD	-	MoeB	sulfur
ThiS	-	ThiF	sulfur

Table 4.1. Ub and UBL proteins

Ubiquitin Like Proteins found in both *S. cerevisiae* and *Escherichia coli* with their H. sapiens orthologs. This table shows each of the UBLs and what protein or protein complex is responsible for its activation. UBLs are activated by a cysteine contained within the activating enzyme, or an atom of sulfur, coordinated by the activating enzyme. Each UBL is activated at a single glycine residue or a Gly-Gly motif that must be post-translationally processed prior to the activation of the UBL.

The first subset, and arguably the progenitors of the Ub system, include the UBLs ThiS (Reviewed by: Begley *et al.*, 1999) and MoaD (Reviewed by: Rajagopalan, 1996), components of the thiamine biosynthetic pathway and the molybdopterin biosynthetic pathway respectively. ThiS and MoaD are similar to Ub in tertiary structure having virtually identical protein folds (Figure 4.1); yet they share only nominal sequence identity (Figure 4.2). . The activation mechanisms for both MoeB and ThiS are similar to the activation of Ub. Both are activated through the formation of an adenylate, after which their carboxy terminal glycine residue becomes covalently bound to an atom of sulfur (Figure 4.3). While Ub becomes covalently

bound to the active site cysteine of Uba1, ThiS and MoeB act only as intermediate carriers for a single atom of sulfur, and following their activation, MoeB and ThiS donate this sulfur atom to proteins involved in the biosyntheses of molybdopterin and thiamine respectively (Xi *et al.*, 2001).

The second group of UBLs is composed of proteins that become covalently bound to targets through the formation an intermediate thiolester. Two proteins in this group, Rub1 in *S. cerevisiae* and Nedd8 in *Homo sapiens,* are involved in modification of the Skp1-cullin-F-box (SCF) complex through the recruitment of a Ubc4~Ub thiolester, which is thought to increase the overall efficacy of SCF. Nedd8-modified cullins can be found within SCF and cullin-2/elongin BC (CBC) E3 ubiquitin ligase complexes (Osaka *et al.*, 2000). The Rub1 and Nedd8 pathways appear to be directly involved in regulation of SCF activity or may specify a subset of its targets. Another protein in this group, Sumo1 (also known as Smt3), is found in mammalian and yeast cells and is involved specifically in cellular trafficking (Kretz-Remy and Tanguay, 1999). Sumo1 modification of target proteins is also involved in nuclear protein targeting, formation of sub-nuclear structures, regulation of transcriptional activities, DNA binding of transcription factors, and control of protein stability (Reviewed by: Kim *et al.*, 2002).

The activation of each UBL protein utilizes the energy contained within the phosphate bonds of ATP to activate their carboxy terminus, thereby creating a nucleophilic center that can then be attacked by a sulfur ion (either from the active site cysteine residue or a persulfate). The protein responsible for the activation of MoaD, in the molybdopterin biosynthetic pathway is known as MoeB (Leimkuhler *et al.*, 2001). MoeB does not have an active site cysteine like Uba1, but it shares a similar nucleotide binding motif and a high degree of homology with Uba1 (Figure 4.4). The thiamine biosynthetic pathway utilizes a similar protein, known as ThiF for the activation of the UBL, ThiS (Taylor *et al.*, 1998). This reaction is similar to that of MoaD activation, in that an atom of elemental sulfur becomes conjugated to ThiS.

Within the second group of UBL's, the activator of Rub1 is composed of a heterodimer of two proteins known as Ula1 and Uba3, which is also similar in sequence to Uba1 (Liakopoulos *et al.*, 1998). Interestingly, although Uba1 alone can activate Ub, Ula1 and Uba3 must form a complex to achieve the ATP dependent activation of Rub1. Sequence alignments between Uba1, Ula1 and Uba3 demonstrate that Ula1 shows similarity to the amino terminus of Uba1, while Uba3 corresponds to the Uba1 active site region and contains the nucleotide-binding site and active site cysteine residue (Figure 4.4). This observation may imply the presence of a recognition site for Rub1 in Ula1 and could be extrapolated to a recognition site for Ub in the amino terminus of Uba1. Sumo1, like Rub1, is activated for conjugation to other proteins by an analogous heterodimer that is composed of the two proteins Aos1 and Uba2 (Johnston *et al.*, 1997). The Aos1 and Uba2 sequences share strong similarities with Uba1; Aos1 corresponds, to the amino terminus of Uba1 and Uba2 to its carboxy terminus (Figure 4.4).

The identification and characterization of these homologous proteins has provided us with a starting point from which to begin an examination of the mechanism behind the Uba1 dependent activation of Ub. Recently, the structures of the two Uba1 like proteins, MoeB and Uba3 were deposited into the Brookhaven data base (Lake *et al.*, 2001; Walden *et al.*, 2003). Structural data from these proteins has presented us with the information required to compare their sequences and structures and generate a model of the Uba1 active site.

4.1.4 Protein Modeling

From the time that the first three-dimensional structure of a protein was determined, attempts have been made to predict secondary and tertiary structural information based only on primary amino acid sequence. Large quantities of independent experimental evidence have confirmed the hypothesis that a proteins tertiary structure is determined by its amino acid sequence; this subject is reviewed by Creighton (1992). While amino acid sequence may indeed be the key determinant of a protein's three dimensional structure, we now understand that a protein's

structural fold is also influenced by the cellular environment in which folding occurs. For instance, one clear example is the process of protein folding, as it is aided by additional proteins, known as chaperonins (Gething and Sambrook, 1992; Morimoto *et al.*, 1994; Hartl, 1996). If the process protein folding is not orchestrated in both a temporally and a spatially precise manner, the ultimate outcome will be an ineffectual protein. Even in the face of such a computationally complex problem, there are still techniques that we can use for predicting the folding pattern of a polypeptide chain.

Molecular Threading and Comparative Modeling

Some of the earliest attempts at modeling the three dimensional structures of proteins were based on their overall similarity to proteins whose crystal structures had been previously determined (Bing *et al.*, 1981). The basic principle behind this technique, known as molecular threading, is the assumption that two proteins that are essentially identical in amino acid sequence will also have similar tertiary structures. A threaded model is obtained by taking the coordinates of a previously determined protein structure and substituting in residues of a highly similar protein. This method can provide us with a quick, yet generally precise structure of a protein if a homologue of this protein has already had its structure solved by another method such as X-ray crystallography or NMR. The main drawback to molecular threading is the requirement for a template with an extremely high degree of homology to the target protein, making this method applicable to proteins within closely related families. This shortcoming can be overcome by utilizing an analogous technique, known as comparative or homology (Chothia and Lesk, 1986; Luthy *et al.*, 1992; Peitsch, 1996).

Homology modeling, instead of using a single protein scaffold, numerous structural motifs are pieced together to form the final comparative model. A scoring function assesses both the sequence identity and quality of the template that is being considered. The scores are ranked and the fold with the best score is assumed to be the one adopted by the sequence. As the description suggests, comparative modeling requires the availability of at least two structural homologues on which to

base a hypothetical model. Based upon this reasoning and the availability of the MoeB and Uba3 structures as templates, this method was chosen for the construction of the Uba1 active site model.

4.1.5 Building a Homology Model

The process of building a homology model is conceptually straightforward. First, the sequences of a group of proteins for which structural data has previously been determined are aligned against the sequence of a protein, which is to be modeled. This sequence alignment is used to construct an initial model by copying over main chain and side chain coordinates from the reference structures based on equivalent residues within the sequence alignment. Side chains must be approximated for any residues in the target that do not correspond to an identity in the alignment. This approximation must also be performed for any residues where the side chain conformation is thought to vary in the model, relative to the parent structure.

Identifying Homologues (Step 1)

Several computerized search methods are available to assist in identifying sequence homologues, the most common is the Basic Local Alignment Search Tool (BLAST) (Altschul *et al.*, 1990). However, a more accurate, iterative BLAST tool, PSI-BLAST provides better results when examining possible protein families (Altschul *et al.*, 1997). The first round of a PSI-BLAST search performs a standard protein-protein BLAST search. The program builds a position-specific scoring matrix (PSSM) from an alignment of the sequences that are returned. In the second iteration the PSSM becomes the query in the search. Any new database hits below the inclusion threshold are included in a new PSSM. The PSI-BLAST search is said to have converged when no more new database sequences are added in subsequent iterations.

Following the identification of homologues, subsequent sequence analysis methods are then employed to identify the proteins with sequence similarity to the target protein, for which three-dimensional structures are available. One such tool is the

Swiss Model server at http://www.expasy.org, which queries the Brookhaven Protein Databank for homologous proteins to any input sequence. Ideally several homologues, with sufficient sequence identity to the target, will exist which to develop a homology model will exist, with the accuracy of the model increasing as the number of template structures increases (Baker and Sali, 2001).

Aligning Sequences (Step 2)

Following the identification of suitable candidate structures, their sequences must be aligned with the target protein. There are many software packages for aligning sequences, many of which are available as free tools on the Internet. These programs evaluate sequences based on a combination of sequence identity, chemical similarity (e.g., polarity, size, charge) and observed sequence substitutions, with greater scores given to alignments with similar properties (Higgins and Sharp, 1988). These algorithms perform iterative comparisons of alignments, ultimately selecting the best fit based upon user-defined parameters. The best way to assess the accuracy of a given alignment is to compare it with alignments that have been derived from three-dimensional protein structures. Unfortunately, this assessment is possible only when working with a family of proteins for which some have three-dimensional structures available, ultimately making homology modeling redundant.

Identification of Structurally Conserved Regions (SCRs) (Step 3)

After the structures have been aligned with the target, structurally conserved regions (SCRs) are identified by determining the regions with the highest sequence identity and an average structure is built for these regions. Variable regions (VRs), in which each of the known structures differs in conformation, are also identified. Alternative modeling methods, such as loop database searches and *ab initio* construction must be applied to model variable regions of the target protein (Pabo and Suchanek, 1986; Bower *et al.*, 1997b).

Generating Coordinates for the Unknown Structure (Step 4)

When generating three-dimensional coordinates for an unknown structure, main chain atoms and side chain atoms need to be modeled in both SCRs and VRs. Modeling SCRs is straightforward; side chain coordinates can be directly copied into the model if the residue type in the unknown protein is identical or very similar to that in the known homologues. The contribution of each homologue in each SCR is then weighted based on extent of similarity with the unknown protein.

For VRs, a variety of approaches must be applied in assigning coordinates to the unknown structure. These regions generally correspond to loops on the surface of the protein. If a loop in one of the known structures is a good model for that of the unknown, then the main chain coordinates of the known structure can simply be copied to the target structure. However, when a good model for a loop cannot be found among known structures, fragment databases can be searched for loops in other proteins, which might provide suitable candidates for the target structure. This involves examining a residue range within the undefined loop and searching fragments for their ability to fit in the undefined region without making bad contacts with other atoms in the structure. Finally, the loop can be subjected to a conformational search to identify the lowest energy conformers (Ferguson and Raber, 1989).

4.2 Experimental Procedures

Hardware and Software

The model of Ubiquitin Activating Enzyme (Uba1) was generated using the Homology Modeling package provided in Molecular Operating Environment (MOE) (Chemcomp Inc.). All energy minimizations and dynamics calculations were performed in the Discover3 package provided with Insight II (Accelrys Inc). Conformational searches of the Ub tail peptide were performed using the MOE

stochastic conformation search tool. Sequence alignments were carried out, initially in MOE and were refined in MacVector (Accelrys Inc.)

All simulations were performed on an SGI O_2 Impact 12000 running IRIX version 6.5.2 (InsightII and MOE), a Pentium 4 1.6 GHz running Windows XP Professional (MOE) and a 866 MHz G4 Macintosh Running OSX (MacVector)..

The stereochemical quality of the Uba1 model was analyzed in Procheck (Morris *et al.*, 1992a; Laskowski *et al.*, 1993) and Ramachandran plots were generated in MOE (Ramachandran *et al.*, 1963; Morris *et al.*, 1992b). Surface areas of the Uba1 model, the structure of Ubc1Δ~Ub and the model of theUba1/Ubc1~Ub complex were calculated using GETAREA 1.1 (Fraczkiewicz and Braun, 1998), as this application seems to be the most capable of accurately calculating solvent accessible surface areas of multi-component protein complexes.

Figure Creation

All 3 dimensional representations were first created in MOE using an SGI O2, and pdb files were exported with all hydrogen atoms included. Figures were then created and ray-traced using PyMol (Delano, 2002) on a G4 power Macintosh running OS X. Some surface representations of the Uba1 active site model were generated with the Grasp software package (Nicholls *et al.*, 1991) and PyMOL (Delano, 2002) and ray-traced using PyMOL. Ray tracing parameters were configured as follows: orthoscopic and antialias were set to on, solvent radius (for surface generation) was set to 1.6, specular power 200, specular reflection 1.5. For figures created on white backgrounds, the depth cue and ray trace fog were turned off.

Template Selection

Selection of templates for constructing the model of the Uba1 active site was straightforward, as only the structures of the MoeB and Uba3 homologues had been published. The selection of these templates were, initially verified with the template analysis tool at ExPASy Swiss-Model (Schwede *et al.*, 2003). This search

provided three related structures of the *Escherichia coli* MoeB/MoaD protein complex: the *E. coli* MoeB/MoaD native structure (1JW9B), the *E. coli* MoeB/MoaD structure in complex with ATP (1JWAB) and the covalent acyl-adenylate bound form of MoeB from *E. coli* (1JWBB). Shortly after the publication of the MoeB structures, the structure of *H. sapiens* Uba3 (Walden *et al.*, 2003) (1NZY), another Uba1 homologue, became available.

Structure Preparation

The Uba1 core catalytic domain, specifically the nucleotide binding site, was modeled using the technique of homology, or comparative modeling using the native *E. coli* MoeB (1PJW9) (Lake *et al.*, 2001) and human Uba3 (1NZY) (Walden *et al.*, 2003) structures as templates. The pdb coordinates of MoeB and Uba3 were initially imported into Insight II and hydrogen atoms were added using the Biopolymer module. All bond descriptors were checked for accuracy and any errors found within specific atom types were correctly described. Following the initial preparation, a rapid round of steepest descent energy minimization was performed (1000 iterations) on each molecule while holding backbone atoms fixed. The backbone atoms were fixed, so as to not perturb the already defined crystal structures of the MoeB and Uba3 template proteins. Following this initial minimization, more refined Conjugate gradient and Newton based minimizations were performed on both molecules. A total of 10000 minimization steps were performed on an energetically free system, thereby enabling the global energy minimum for each molecule to be found. These initial minimization steps were performed, only to relieve any unfavorable conformations associated with crystal packing that may adversely affect dynamics simulations within the modeled protein.

Alignments

Energy minimized structures of MoeB and Uba3 were exported from Insight II into MOE and a structural alignment was produced (FIGURE 4.7). This was accomplished by performing an iterative structural overlay until the Root Mean

Squared deviation (RMS) between each of the structures was reduced to a minimum. The structural alignment was then used as a starting point for analysis using MacVector (Accelrys), into which the primary sequence of Uba1 was introduced. Each alignment was then scored for both sequence identity and homology, dividing the entire sequence of Uba1 into discrete parts. The best alignment resulted in the carboxy and amino extensions of Uba1 being removed to leave only the core catalytic domain, which contains the nucleotide-binding region (residues 417-595) (Figure 4.4).

Generation of the Uba1 Homology Model

The final alignment between MoeB, Uba3 and Uba1 was then imported from MacVector into the MOE Homology module. The initial Uba1 model was generated by utilizing SCRs from MoeB and Uba3 that best matched the target Uba1 nucleotide binding region (residues 417-595). The conserved regions were then assigned three-dimensional coordinates using a best intermediate scoring algorithm, each structure being evaluated by a residue packing quality function based upon which hydrophobic and hydrogen bonding opportunities are satisfied (Jaroszewski *et al.*, 1998). Intervening gaps within the model were assigned coordinates by generating random loops. A total of 14 surface loops were generated for each gap in the sequence of Uba1 (Rosenbach and Rosenfeld, 1995; Bower *et al.*, 1997a). Each loop then underwent energy minimizations and their RMS values were calculated. These values were then compared to choose the best placement for each of these surface loops.

Following selection of the surface loops, an energy minimization of the entire molecule was performed to relieve unfavorable conformations resulting from splicing of the loops. This minimization was kept short to maintain the overall structure of the original homology model; a total of 1000 Conjugate Gradient minimization steps were performed (Fletcher and Reeves, 1964; Powell, 1977). Following the energy minimization step, dynamics calculations were performed and a total of 50 independent structures were analyzed with an additional round of energy

minimization, looking for structures that did not fall into local energy minima. Of these 50 candidate structures, the lowest energy structure was chosen for the final model of the Uba1 active site. The final model was then inspected for reasonable bond stereochemistry through the generation of a Ramachandran plot, followed by evaluation with the quality control tool Procheck (not shown) (Ramachandran *et al.*, 1963; Laskowski *et al.*, 1993).

Stochastic Conformational Searches of Ub-adenylate and Ub-thiolester

To examine the potential binding sites for Ub on the surface of the Uba1 model, a Ub carboxy terminal peptide was created using the MOE protein builder module. This peptide was left in its extended conformation when imported into the Uba1 model. The tail region of Ub, which was modeled, corresponded to the last eight residues of Ub (L-V-L-R-L-R-G-G), which was previously determined to be the minimally active peptide length to produce an interaction with Uba1 (Jonnalagadda *et al.*, 1988). Conformational searches were performed on Ub as the acyl adenylate bound to AMP and Uba1, and Ub as the thiolester bound at the Uba1 active site cysteine. The positioning of AMP within the active site of the Uba1 model was based upon the MoeB/MoaD acyl-adenylate structure (1JWAB) (Lake *et al.*, 2001). In order to preserve the structure of the Uba1 model and obtain a representation of the energy associated with movement of the peptide within the active site, the atoms within the backbone of the Uba1 model were fixed during the conformational searches and only residues found within the Ub tail peptide were permitted to move. The RMS gradient for dihedral minimization was set at 100 and the delta for perturbations was set to 0.03 [-0.03/2, 0.03/2]. To provide the greatest number of structures for subsequent analyses, the energy cutoff between structures was set to 100 (E min + Ecutoff, where E min is the global minima of the system), and the failure limit was set to 100 consecutive failures. A total of 20,000 conformations, for both Ub-adenylate and Ub-thiolester, were screened for energy and stereochemical quality. The Ub carboxy terminal peptide and atoms

surrounding it were then energy minimized and evaluated for energy, bond angles and van der Waals clashes.

From this search, a thousand starting structures were then screened using a hybrid Monte Carlo dynamics run, to exclude any energetically instable complexes. This dynamics run was performed at a temperature of 450 K with 1000 equilibration steps and a time step of 0.03 picoseconds, a time step that approaches the upper limit for observing normal bond vibrations in this system (Schlick *et al.*, 1997). This dynamics simulation was performed for a total of 10,000 iterations, which resulted in an overall simulation time of approximately 300 picoseconds

Docking of Ubc1Δ to the Uba1-Ub~Ub Conjugate Thiolester

To simplify the docking problem, the Uba1/Ub_2 model was treated as a rigid surface to which Ubc1Δ was tethered by an artificial constraint (Figure 4.13). This constraint, of 15 Å, was based upon the required interaction between the active site cysteine residues and nucleotide binding site between Uba1 and Ubc1Δ. By including this restraint, the problem is reduced to three translational and three rotational degrees of freedom for Ubc1Δ. This is simplified further by limiting the length of the constraint to allow the transfer of Ub from each of the active sites. Initially, Ubc1Δ was positioned over the active site of Uba1 and was rotated through 360° about the z axis. This rotation was carried out at random distances above the active site of Uba1, while the relative intermolecular energies were monitored throughout this initial "rough" docking to determine the best fit between static surfaces of Uba1 and Ubc1Δ. Following the initial placement of Ubc1Δ on the surface of Uba1, it was manipulated through all available degrees of freedom while simultaneous energy minimization was performed. This involved the translational displacement Ubc1Δ in increments of approximately 5 Å through the x, y and z axes while rotating in increments of approximately 5° through these same axes. This iterative movement of Ubc1Δ, followed by energy minimization was performed until an energy minimum was reached (Figure 4.14A).

Dynamics of the Uba3, Cysteine Containing, Helical Domain

The entire Uba3 structure was subjected to a short 100 ps dynamics simulation to examine the conformational flexibility of the linker region between the nucleotide binding site domain an the active site cysteine containing helical domain. Dynamics were performed using a constant pressure, volume and temperature (PVT) simulation, where each dynamics step was followed by a short minimization and Monte Carlo dynamics step (Metropolis *et al.*, 1953; Hart and Read, 1992). The temperature for this simulation was set to 400 K and utilized the velocity method for temperature scaling. A snapshot of the simulation was saved every 100 ns and was analyzed using the Dynamics Animation module in MOE.

Uba1 Active Site Truncation (Uba1Δ)

To examine the potential for a minimally active Uba1 domain to activate Ub, a carboxy and amino terminal truncation was created. This truncated version of Uba1 corresponded to the region upon which the active site model was based. PCR primers for regions within the *S. cerevisiae* Uba1 coding sequence were created and used to generate a PCR fragment for the cloning of Uba1Δ. Primers corresponding to the 5' region of Uba1 at 1227 base pairs carried an Sst1 restriction site and the 3' region at 2256 base pairs carried a 6x His tag followed by a BglI restriction site (Grundy *et al.*, 1998). These primers were introduced into a PCR reaction containing full length Uba1 on a LEU based plasmid (PJD325) (Provided by Seth Sadis) and yielded a 1029 base pair product that was purified using agarose gel electophoresis. The resulting PCR product was digested with Sst1 and BglI restriction enzymes and ligated into the plasmid pTi37i (obtained from C. Ptak) that had been subjected to the same restriction endonuclease treatment. The resulting ligation mixture was then transformed into the *E. coli* strain MC1061 and colonies were selected using the antibiotic ampicillin.

Expression plasmids were transformed into the *E. coli* strain BL21 pGP1-2, which contains the thermally induced T7 polymerase plasmid (Tabor and Richardson, 1985). Colonies were selected on LB-ampicillin plates and transferred to liquid LB

broth containing 50 μg/ml ampicillin. Cells were grown at 30 °C to an initial absorbance of 0.4 at 590 nm. The culture was shifted to 42 C for one hour followed by 37 C for two hours. Cells were harvested by centrifugation, re-suspended in approximately 25 ml of buffer A (50 mM Tris-HCl (pH 7.5), 1 mM EDTA, 2mM DTT) and lysed using a French press. The lysate was centrifuged at 40,000 rpm for 1 hour using a Beckman Ti70 rotor. The supernatant was decanted and filtered through a low protein binding 0.22 μm syringe tip filter (Millipore).

Uba1Δ was purified using ion exchange and nickel affinity chromatography. The clarified cellular lysate was passed over a HiLoad Q sepharose 26/10 ion exchange column (Pharmacia) equilibrated with buffer A. Proteins were eluted from the column with a gradient of 0 – 2M NaCl, with the major protein peak eluting from the column at a concentration of 282 mM NaCl. Peak fractions were pooled, concentrated and dialyzed against phosphate buffer (10 mM Na_2HPO_4, 10 mM HaH_2PO_4, 500 mM NaCl). The dialysate was passed over a 1 ml Hitrap Chelating (Pharmacia) column charged with Ni^{2+} and equilibrated with phosphate buffer containing 10 mM imidazole. The column was washed with 1 ml of 10 mM imidazole, followed by 5 ml of 50 mM imidazole. The His tagged Uba1Δ was eluted with 1 ml of phosphate buffer containing 500 mM imidazole. The eluate was dialyzed into buffer consisting of 50 mM HEPES (pH 7.5), 150 mM NaCl, 1 mM EDTA, 1 mM DTT and 5% glycerol and stored at -20 C.

Uba1Δ Activity

The activity of the Uba1 active site truncation was tested using ubiquitination reactions. All ubiquitination assays, unless stated otherwise, were carried out in a buffer consisting of 10 mM HEPES (pH 7.5), 5 mM $MgCl_2$, 40 mM NaCl, 5 mM ATP, and protease inhibitors (*antipain*, *aprotinin*, *chymostatin*, *leupeptin*, *pepstatin A* at 20 μg/ml and PMSF at 180 μg/ml) (Aldrich Sigma). The ubiquitination buffer also included inorganic pyrophosphatase (0.6 units/ml) to facilitate the removal of pyrophosphate, which has been demonstrated to be an inhibitor of the ubiquitination reaction (Haas and Rose, 1982). Each reaction contained 360 nM [^{35}S]-Ub and

Uba1 or Uba1Δ at a final concentration of 90 nM. Reactions were incubated at 30°C for 60 min and immediately loaded on a Superdex 75 HR 10/30 gel filtration column (Pharmacia). Reaction products were eluted with buffer containing 50mM HEPES (pH 7.5), 150mM NaCl and 1mM EDTA at a constant flow rate of 1 ml/min. Fractions were collected every 0.5 min and the counts per minute (cpm) of [^{35}S]-Ub present in each fraction were determined by scintillation counting using a Beckman LS-6800 Liquid Scintillation counter. These values were used to generate elution profiles for the reaction products from each run.

4.3 Results

Homology modeling of the *S. cerevisiae* Uba1 active site domain, consisting largely of the adenylate binding site was performed using recently published structures of *E. coli* MoeB (Lake *et al.*, 2001) and *H. sapiens* Uba3 (Walden *et al.*, 2003) as scaffolds. Based upon potential Ub binding sites within this model, coupled with empirically derived data on Ub activation, we have probed the mechanism of Ub activation by Uba1.

Comparison of the Uba3 and MoeB Templates

Structurally, MoeB and *H. sapiens* Uba3 are very similar and a superimposition of their main chain atoms yeilds an RMSD of 1.4 Å (Figure 4.5A). However, there are two notable features within Uba3 that are absent from MoeB. First is a large, 80 residue α helical domain in Uba3 that contains the active site cysteine residue (Figure 4.6). This domain is entirely absent from the MoeB structure, which has only a short eight-residue loop that displayed low density values in its crystal structure. The second feature is a "Ubiquitin Like" domain contained at the carboxy terminus of Uba3 that is also not present within the MoeB structure (Walden *et al.*, 2003).

To examine the basis for these differences between Uba3 and MoeB and how this could influence the modeling of the *S. cerevisiae* Uba1, a comparison between the Human and yeast orthologs of Uba3 was performed. The *H. sapiens* Uba3 protein

was found to be significantly larger than its *S. cerevisiae* counterpart, having an amino terminal extension 46 residues in length and a carboxy terminal extension 90 residues in length (Figure 4.7A). Interestingly, the sequence within the Human Uba3, which corresponded to the 90 residue carboxy terminal extension, comprises the entire "Ub like" domain. Based upon the alignment between these Uba3s, we concluded that the yeast protein does not contain the Ub like domain that seems to be present in the Human ortholog. Since we were modeling the *S. cerevisiae* Uba1, and alignments between Uba3 and Uba1 within this region result in low sequence identity, we chose to omit this region from our model. This does not imply that we do not believe that this domain is not present in Uba1, but for the purposes of this modeling experiment, it was determined to not be essential.

Sequence Alignments Between Uba3 and MoeB and Uba1

Utilizing a structural superimposition of Uba3 and MoeB as a guide, an initial sequence alignment was produced using MOE. At first, a disconcerting feature of these alignments was identified in the emergence of low sequence identity towards the proteins carboxy termini. Up to, and including their active site cysteine containing regions, sequence identity was shown to be relatively good at 37% (Figure 4.7B). It is at this point, within the sequence of Uba3, that the 80 residue helical domain within begins. Surprisingly, even with this major difference between them, the extreme carboxy termini of both Uba3 and MoeB are still quite analogous in their tertiary structure. The entire region, following the helical domain, was shown to have an extremely low sequence identity of only 6%, yet still had an RMSD of 1.46 Å (Figure 4.5B). The structural alignment between Uba3 and MoeB was then used as a template upon which to assign the sequence alignment of Uba1. By first fixing the alignment that was constructed between Uba3 and MoeB and then performing a Clustal alignment on Uba1, using the PAM250 bias, we obtained the result observed in Figure 4.8.

The alignment between Uba1, Uba3 and MoeB resulted in significant similarities up to, and including, their active site cysteine residues. These similarities, as with the Uba3 and MoeB alignment, dropped significantly towards their carboxy termini.

Overall, alignments of the carboxy terminal region, up to the active site cysteine residues within Uba1 and Uba3 were 37%, indicating that they are satisfactory candidates for homology modeling (Baker and Sali, 2001). The sequence identity between Uba1 and MoeB in this same region drops to 24%, but the RMSD of 1.4 Å between the structures of MoeB and Uba3, would suggest that this protein is also a good candidate for basing homology modeling.

Prior to continuing with homology modeling, the first 46 residues from the amino terminus, and the last 90 residues from the carboxy terminus of the *H. sapiens* Uba3 structure were removed. This brought the sequence into line with that of *S. cerevisiae* Uba3, and MoeB. In addition to the 46 residues that were removed from the amino terminus of Uba3, as a result of the alignment of the Human and yeast orthologs, an additional 28 residues were also removed. This region was composed of a short helix-loop-helix in the Uba3 structure, but is completely absent from the MoeB structure (structure not shown).

Surface Comparison of Uba3 and MoeB

Following the preparation of structures for both Uba3 and MoeB, an examination of their characteristics was performed by superimposing Connelly representations of their surfaces (Figure 4.9). This superimposition, straightforwardly demonstrates that these two proteins share comparable surface qualities. These similarities can be specifically seen as a deep depression around the location of the nucleotide binding site, providing a pocket for the binding of ATP. In addition to this nucleotide binding pocket, the existence of two surface clefts that emerge from it is also clear. These clefts are approximately 8 Å across and 6 Å deep and could provide possible binding sites for the tail of Ub, one for the Ub adenylate and the other for binding Ub as the thiolester.

The Uba1 Model

Sequence comparisons of *S. cerevisiae* Uba1 with MoeB identified putative positions in Uba1 that may represent its bipartite active site. The active site consists of a nucleotide (ATP) binding site that functions as the site of Ub-adenylate (Ub-

AMP) synthesis, and a cysteine at residue 600 that forms the Ub-thiolester. The nucleotide binding site contains a Walker fold (G-X-G-(A/G)-(G/L)-G) between residues 440-446 (Walker *et al.*, 1982; Wierenga and Hol, 1983). Using the methods described in section 4.1.4 with Uba3 and MoeB as templates, we have created a model of the nucleotide binding site region that encompasses residues 417-595 of Uba1. Based on the higher level of sequence identity between Uba1 and Uba3 within this region, Uba3 was chosen as the primary template, using MoeB to average atomic positions in the model.

The model of Uba1 produced a compact globular structure, which contained the entire nucleotide binding site (Figure 4.10). Unfortunately, low sequence identity between Uba1 and the Uba3 and MoeB templates made it infeasible to produce sufficient alignments and therefore a model of the region that includes the active site cysteine residue and region that follows it. However, based on structural similarities between Uba3 and MoeB we can assume that this region is still composed of a large α helix, which makes up the carboxy terminal end of either the short loop in MoeB or the 80 residue helical domain in Uba3, and two β sheets which are found in a larger β sheet within the core of the protein (Figure 4.5B).

Structurally, the Uba1 model is made of a six stranded β sheets surrounded by α helices. The core catalytic domain is composed of two smaller domains, with the first made up of a four stranded, parallel β sheet and the second is a four stranded antiparallel β sheet. It is the second domain that is partially composed of the region of low sequence identity between Uba1 and the template proteins. A deep cleft in the surface of the model forms the nucleotide binding site. This model suggests that the active site cysteine of Uba1 is located on a surface exposed loop, of indeterminate length, which is bounded by two α helices that may help to maintain its overall structure. The amino terminal helix is found within the region of Uba1 for which we were able produce a model, but the carboxy terminal helix, as mentioned previously, could not be modeled.

Docking of Ub into the Active Site of Uba1

Following the initial homology modeling of the Uba1 active site, the initial binding location for Ub was obtained. This was accomplished by performing an exhaustive search of possible conformations of the Ub tail in the active site of Uba1. A peptide corresponding to the tail of Ub (L-V-L-R-L-R-G-G), as opposed to the entire protein, was chosen to reduce the computational load while performing the search. The fact that peptide fragments of Ub have only limited ability to support ATP:PPi exchange suggests that there is indeed a minimal recognition surface on Ub for its initial interaction with Uba1 (Ciechanover *et al.*, 1982; Jonnalagadda *et al.*, 1988). This surface is most likely contained on the globular core of Ub, not in its tail. However, the fact that at high concentrations this peptide, which contains the first 6 carboxy terminal residues can support ATP:PPi exchange suggests that there is, at least, some recognition for the tail alone. We felt that, based on these results, an eight residue peptide corresponding to the carboxy terminus of Ub would be sufficient for modeling its interactions with Uba1 active sites.

Random conformations of this Ub peptide were generated using a stochastic conformational search, which were then evaluated for relative potential energy. A stochastic conformational search generates conformations by randomly sampling local minima of the potential energy surface of a molecule. This method is similar to methods using random perturbation of Cartesian coordinates of atoms within the system (Ferguson and Raber, 1989), however the stochastic conformational search is based upon random rotations of bonds rather than manipulation of Cartesian coordinates.

The stochastic search of the Ub peptide produced an energy landscape on the surface of Uba1 and indicated preferred directions that the tail of Ub could adopt while bound to AMP at the active site (Figure 4.11). From this figure, it is clear that the peptide prefers orientations that place it, near a cleft, identified in the superimposition of Uba3 and MoeB (Figure 4.9). This cleft lies in a parallel orientation to the phosphate tail of ATP, when it is bound at the nucleotide-binding

site. This orientation places the tail of Ub in a favorable conformation, where following the formation of the phosphate ester bond with ATP, the adenylate bond between the peptide and AMP has an optimal angle of 105° (calculated 105.63°) and if the phosphodiester bond has a length of 1.6 Å (calculated 1.62 Å) (optimal lengths and angles were determined on *de novo* structures minimized in Insight II).

Uba1 Binds Two Molecules of Ub

Throughout the modeling of the Ub-AMP adenylate an immediate problem became apparent. Initial characterization of the Uba1 reaction mechanism has unequivocally demonstrated that there are two molecules of Ub activated for each molecule of Uba1 (Ciechanover *et al.*, 1981). The model of the Uba1 active site, when it is bound with a single molecule of Ub as the adenylate, does not afford sufficient space to accommodate two molecules of Ub. As such, the initial binding of Ub and formation of adenylate would occlude the binding of a second Ub and formation of a second activated Ub could not occur. A second molecule of Ub could, however, be accommodated if the first molecule were to reposition itself at a secondary binding site following the transfer of Ub to the active site cysteine residue and formation of the thiolester. A reasonable candidate for this secondary binding site is indicated by the position of the UBL MoaD in the crystal structure of the MoeB/MoaD complex (Figure 4.12) (Lake *et al.*, 2001).

Docking of the Uba1 Active Site and the Ubc1Δ~Ub Thiolester

Previous studies in our laboratory have generated a model of the Ubc1Δ~Ub thiolester using NMR foot printing and the crystal structures of Ub and a truncation of the E2 Ubc1, Ubc1Δ (Chapter 3) (Hamilton *et al.*, 2001). As Ub must be transferred from Uba1 to an E2, the availability of the Ubc1Δ~Ub thiolester structure afforded us the opportunity to create a model of the interaction between the Uba1 active site and the Ubc1Δ~Ub thiolester.

With two Ub molecules already modeled on the surface of Uba1, we assumed that free Ubc1Δ would orient itself to one of the Ub molecules at its Ub binding site. As

a constraint, the active site cysteine residue of Ubc1Δ was initially positioned above the nucleotide binding. This constraint was chosen as Ub must first become transferred from the nucleotide binding site to the active site cysteine of Uba1, when it then becomes transferred to E2. Results presented in Chapter 2 also demonstrated that Ub could become directly transferred from the Ub adenylate to the active site cysteine of Ubc1. The possible interactions between Uba1 and Ubc1Δ were limited to a maximum distance of 15 Å between their active sites (Figure 4.13). These assumptions, and the conformational search performed on Uba1 and the carboxy terminus of Ub, simplified this problem to two dimensions from a computationally difficult six dimensional problem. Following the completion of the docking experiments, a final round of energy minimization yielded a complex in which the intermolecular energy was approximately –300 Kcal/mol (Figure 4.14A). Most of the intermolecular contacts between the two molecules were found to be standard surface loop interactions (Miller, 1989), with one main loop helix contact between the carboxy terminal helix of Ubc1Δ and a surface loop (residues 475-491) of Uba1.

There was approximately 1200 $Å^2$ of occluded molecular surface area on each of Uba1 and Ubc1Δ. Of this, 400 $Å^2$ was comprised of polar residues and 800 $Å^2$ contained non-polar residues. Based on previous examples, these values for the interface interactions are comparatively low for a 130 kDa protein complex (Janin *et al.*, 1988; Miller, 1989). When the energy of interaction between Uba1 and the Ubc1Δ~Ub thiolester and the occluded surface area were compared to that of previous docking experiments performed on Ub_2 (Cummings *et al.*, 1995), we estimated that there is only a transient interaction between these two molecules, with a dissociation constant in the millimolar range. However, given that Ubc1Δ~Ub synthesis occurs readily under conditions where Ub, Uba1 and Ubc1Δ are present at nanomolar concentrations, it seems likely that the interaction surface generated here only represents a portion of the total interface between Uba1 and E2, given that the Uba1 model only consists of the active site region. Based upon the required movement of the Uba1 active site cysteine into a position that would permit the

transfer of the Ub adenylate to the thiolester, the positioning the sulfur atoms from the two active site cysteine residues was modeled. The possible positioning of the sulfur atoms in relation to the α phosphate of ATP can be seen as yellow VDW spheres in Figure 4.14B.

Position of the Active site Cys in Uba3 Template

The crystal structure of Uba3 places the active site cysteine residue at a position that is 33.5 Å from the nucleotide binding site and in particular the α phosphate of ATP. This would imply that for the formation of the Rub1 thiolester to occur, the active site cysteine would have to reposition itself closer into the nucleotide binding site. Initial dynamics experiments on the entire Uba3 complex suggest that the two linker regions that connect the helical domain to the nucleotide binding site permit the movement of this region towards the α phosphate of ATP (not shown).

Creation of a Recombinant Uba1 Active Site Truncation

To test the biochemical feasibility of our model, we created a truncated mutant of Uba1 (Uba1Δ) and expressed it in an *E. coli* over expression system. This recombinant Uba1Δ was truncated at amino and carboxy termini and corresponded to the middle portion of Uba1 that aligns with the MoeB homologue (Figure 4.4), and aligns loosely with our model of the active site domain. This truncation comprised residues 410-752 of the full-length *S. cerevisiae* Uba1, and includes the Walker fold motif found near residue 446 and the active site cysteine at residue 600. Expression and purification of Uba1Δ yielded a soluble, 35 kDa product that was readily purified by gel exclusion chromatography, suggesting that the protein was correctly expressed and folded (Figure 4.15A). Ubiquitination of Uba1Δ (as described in: *In vitro ubiquitination reactions*) did not produce Ub-AMP. After separation of products by gel exclusion chromatography, the only peak to appear on the chromatogram was that of free Ub (Figure 4.15B). Additional reactions containing Uba1Δ and Ub, that were subjected to SDS-page, as described by Hodgins *et al.* (1996) and in Chapter 2, also produced no discernable ubiquitination products.

4.4 Discussion

The accuracy of the Uba1 model can be examined through examination of modeling data correlated through the ExPASy Molecular Biology Server (Peitsch, 1996; Schwede *et al.*, 2003) (Chapter 6, Figure 1). Based on the degree of sequence identity, used in the creation of the Uba1 model, we could predict a mean resolution of approximately 4 Å. Even at such a low resolution, we are able to discern the macromolecular positioning of molecules interacting with Uba1 at its nucleotide-binding site and estimate molecular interactions therein. Since the alignments between Uba1 and Uba3, in the region modeled here, resulted in sequence identities of 37% we can be relatively confident in the position of key residues within its active site. Unfortunately, because of the low sequence identity of regions following the active site cysteine residues in Uba3 and Uba1, and the region of low density in the MoeB structure, we were unable to make any predictions with regard to residue positions in the carboxy terminus of Uba1. However, the alignment between Uba1 and Uba3 suggests that the active site cysteine residues of these two proteins may, nevertheless, occupy similar positions (Figure 4.8). Independently determined alignments within this region of additional Uba1 like proteins, also suggested that this may in fact be true for this short, yet key region within Uba1 (Walden *et al.*, 2001). These results suggest that the active site cysteine residue is located on a slightly longer loop than that seen in MoeB, but shorter than the 80 residue helical domain seen in Uba3 (Figure 4.8; Consensus only).

Orientation of Uba1 Active Sites (Sequence Alignments)

The active site domains of yeast Uba1, human Uba3 and *E. coli* MoeB are very similar in their sequence makeup. Based upon their eukaryotic origins, one would expect that the structure of Uba1 would be more similar to that of Uba3 than to the prokaryotic MoeB. This statement may be true over the complete sequence of

these proteins, but with respect to the active site regions an interesting observation was made. Alignments of many Uba like proteins reveal substantial conservation within adenylate binding regions, but considerable variability within regions containing the active site residues. For example, the active cysteine residue in yeast Uba3, as determined by its tertiary structure, is situated in a compact 80 residue helical domain (Figure 4.5). This is dramatically different from the same region within the structure of MoeB, which is composed of a short, disordered eight residue surface loop. The large differences seen in the active site cysteine containing regions, and the similarities within the nucleotide binding regions are likely due to the fact that all of these proteins are initially involved in similar reaction mechanisms. This initial reaction results in the hydrolysis of ATP to form an adenylate at the UBL's carboxy terminus. The difference arises within the mechanism, once the adenylate has been formed, resulting in the evolutionary divergence in sequences and structures.

In our model of the Uba1 core catalytic domain, we utilized the *H. Sapiens* Uba3 structure as the major template, with the exception of the 80 residue helical domain which contains the active site cysteine residue. Initially, a troubling aspect of the Uba3 and MoeB templates used in constructing the model was the appearance of low sequence identity between these proteins in the regions following their active site cysteine residues. Despite the significant decrease in sequence identity towards each proteins carboxy termini, both proteins are quite similar in their underlying structures. The region following the active site cysteine residues shows very low sequence identity between the structures of Uba3 and MoeB (7%) but an RMSD for this region is 1.46 Å for the main chain atoms (Figure 4.5B). The low sequence identity, yet similar structures provide us with a condition where we can propose that Uba1 would contain this short helix-sheet structure. However, we could not accurately model this region due to the inability to predict which portion of the Uba1 sequence would fit into this structure.

This region of low sequence identity also presented a problem when an attempt was made to predict the position of the active site cysteine residue in Uba1. The question as to whether or not Uba1 contains a large domain, as in Uba3, or a short

loop as in MoeB could not be definitively answered without better agreement within the sequences in this region. However, alignments between Uba1 and Uba3 suggested that this region within Uba1 might contain a small portion of the helical domain (Figure 4.8). A smaller active site domain in Uba1 would seem to be preferential, as the presence of a large helical domain within Uba1 would inhibit the simultaneous binding of two Ub molecules. In a reaction that is analogous to the activation of Ub by Uba1, activation of Rub1 by the Uba3/Ula1 heterodimer results in the formation of a 40 kDa complex (Liakopoulos *et al.*, 1998). This complex corresponds to only a single moiety of Rub1 conjugated to Uba3. To date, only the activation of a single molecule of Rub1 per Uba3/Ula1 heterodimer has been demonstrated (Bohnsack and Haas, 2003). The limited interaction of the Uba3/Ula1~Rub1 complex with only Ubc12 *in vivo* suggests that the surface differences between Uba1 and Ula1/Uba3 may also be significant (Liakopoulos *et al.*, 1998). Based on the requirement for the accommodation of two Ub molecules at the active site of Uba1, and the inability for Uba3 to provide the necessary binding surfaces, it would seem unlikely that this large 80 residue helical domain would be present in Uba1.

Activity of Uba1Δ

To examine the reasonableness for the existence of an active site domain within Uba1 a truncation of full length Uba1 was created. For ease of purification a 6 X His tagged version of Uba1Δ was made, and based upon sequence alignments (Figure 4.4), the tag was placed on the carboxy terminus. Our reasoning for this relates back to the activators of both Smt3p and Nedd8 whose sequences correspond to the amino terminal portion of Uba1. If Uba1 is composed of multiple domains, tagging the carboxy terminus should not interfere with Uba1Δ binding to Ub. This position also allowed us to determine if the truncation was being completely translated, as the His tag would not be present in any translationally disrupted products.

Unfortunately, reactions that contained the truncated form of Uba1 proved to be incapable of activating Ub. The inactivity of Uba1Δ reflects either its inability to

process Ub at the active site cysteine, or an inability to catalyze the formation of a Ub-adenylate. Although Uba1Δ contains both an active site cysteine and the ATP binding site, these may not be sufficient to promote Ub activation. Activation of the UBL proteins Smt3p and Nedd8 requires the presence of two proteins, first the protein that contains the active site residues, Uba2 and Uba3 respectively and second a protein that corresponds to the amino terminus of Uba1, Aos1 and Ula1 respectively (Johnston *et al.*, 1997; Liakopoulos *et al.*, 1998). Based on the requirements for the activation of Smt3 and Nedd8, we can hypothesize that a similar domain in Uba1 might exist that may act to recruit, or bind Ub for its activation. There is evidence that the active site region in Uba1 constitutes an independent domain. When purifying full length Uba1, bands corresponding to the approximate molecular weight of the Uba1Δ truncation have been detected on gels (Chapter 2, Figure 2). This suggests that this region of Uba1 may be a stable proteolytic fragment, supporting the idea that this region forms an independent domain within the structure of Uba1.

The Uba1 Model

The model of the Uba1 active site produced a compact three-dimensional structure that has obvious characteristics similar to both the Uba3 and MoeB structures (Figure 4.9). The most notable feature of this model is the deep anionic nucleotide-binding pocket that contains several conserved residues that likely participate in the catalytic activation of Ub (Figure 4.16). The nucleotide binding pocket has two surface clefts that protrude at 90° from one another to the edges of the molecule (Figure 4.9). The base of the nucleotide binding pocket contains a Walker fold (G-X-G-(A/G)-(G/L)-G) between residues 440-446 (Figure 4.10B) (Walker *et al.*, 1982; Wierenga and Hol, 1983).

While the Uba3 and MoeB templates have allowed us a measure of reliability in modeling the nucleotide-binding site, we are only able to speculate as to the position of the active site cysteine in this model. The underlying structure of MoeB would place the active site cysteine of Uba1 directly above the nucleotide binding

site and as such, in a position that is competent for attacking the activated carboxy terminus of Ub to form the thiolester. The underlying structure of Uba3 places the active site cysteine at the edge of the 80 residue helical domain (Figure 4.6). However, based on loose sequence alignments in this region, we can assume that the active site cysteine is located in similar positions in both of these molecules (Figure 4.8). In either situation, the active site cysteine would have to move into a position above the nucleotide-binding site, enabling it to pick up an activated molecule of Ub, resulting in the formation of the Ub thiolester.

Uba1 Reaction Mechanism

Based upon the creation of the Uba1 active site model, coupled with structural information from the MoeB/MoaD crystal structure, we have proposed a model of Uba1 directed ATP hydrolysis ultimately leading to the formation of the Uba1~Ub thiolester.

ATP Binding and Ub Adenylate Formation

The first step in the activation of Ub is the binding of ATP and formation of the Ub adenylate. There are several side chain candidates within the active site of Uba1 that could participate in the catalysis of Ub-AMP formation and its resulting transfer to the active site cysteine. While the model cannot give us the exact position of these side chains, we are able to speculate on their functionality. Structurally, Asp 130 in MoeB is thought to be responsible for the coordination of Mg^{2+} that, in turn, coordinates the oxygen atoms of the α and β phosphates of ATP in the MoeB/MoaD structure (Lake *et al.*, 2001). In the Uba1 model, this aspartic acid (Asp 544) lies along the amino terminal side of the active site cysteine domain and may contribute to loop stability when ATP occupies the nucleotide-binding pocket (Figure 4.16). The presence of additional, conserved asparagines within the nucleotide-binding site could provide a means for the catalytic stabilization of increasing negative charges during the nucleophilic attack at the α phosphate by the carboylate of Gly 76 in Ub (Vernet *et al.*, 1995). These residues would also have a similar function during the

formation of the Ub thiolester during the nucleophilic attack of the Ub adenylate by the thiol group of the active site cysteine residue.

Ub Binding to Uba1

The interaction of Ub at the binding site occupied by MoaD in the MoeB/MoaD structure would be one possibility for adenylate formation, however, the binding of Ub at an alternate binding site places the Ub tail in an improved conformation for the nucleophilic attack at ATP (Figure 4.11). In order for Ub to become activated by Uba1, it must become bound at the active site in a position that places its carboxy terminal glycine residue near the α phosphate of ATP. Examination of the MoeB/MoaD structure led us to conclude that the binding modes for Ub and MoaD on the surfaces of Uba1 and MoeB are probably different. In the structure of MoeB/MoaD, the tail of MoaD appears to thread itself under the surface "loop" to form the adenylate. This arrangement may be sterically feasible in the case of MoaD, as it is activated with a single atom of sulfur. However, during the activation of Ub by Uba1, Ub becomes transferred to the active site cysteine of Uba1, which is on the loop itself. In this process the Ub tail would become threaded under the active site, making it inaccessible to E2. However, a conformational search of the Ub tail, covalently linked to AMP and bound at the adenylate binding pocket, revealed an alternate conformation for the Ub tail. This alternate binding site was found to be perpendicular to the binding site that was identified on the surface of MoeB and overcomes the problem of E2 accessibility to Ub (Lake *et al.*, 2001).

Active Site Cysteine Movement

Alignments of the active site cysteine regions between Uba1 and Uba3 suggest that this region is at least 20 residues in length and contains a catalytic histidine residue that may be involved in the deprotonation of the active site cysteine (Figure 4.8; Figure 4.17) (Vernet *et al.*, 1995). A number of factors suggest that the active site cysteine residue within Uba1 would sit at a position above the nucleotide-binding site and must undergo a conformational switch in order to bring it into a position that is capable of accepting Ub to form the UB thiolester. First is the

presence the highly disordered loop in the structure of MoeB. The fact that this disordered loop aligns to the region of Uba1 that contains the active site cysteine implies some evolutionarily, conserved purpose to maintain the flexibility of this loop. The presence of the long linkers that connect the nucleotide binding domain and the helical domain in Uba3 also points to the conservation of backbone flexibility within this region.

Thiolester formation and a Helix-loop-helix switch

The ability for the activated Ub adenylate to become transferred to the active site cysteine residue, resulting in the formation of the thiolester, is an obvious requirement in both Uba1 and Uba3 (Haas *et al.*, 1982; Gong *et al.*, 1999). The position of the active site cysteine residue, as seen in the Uba3 structure, places the thiol group a distance of 31.5 Å from the α phosphate of ATP at the nucleotide binding site (Figure 4.6). Because the active site cysteine residue is contained in the helical domain, it follows that this domain must undergo some sort of conformational shift to bring the active site cysteine into position to form the thiolester.

The nucleotide binding domain and active site cysteine domain, in Uba3, are linked by two short sections of polypeptide chain, giving rise to an elongated van der Waals cavity. What connection these structures have on the mechanism of the active site of Uba1 has yet to be determined, but one could hypothesize that it could act as a clamp, bringing the active site cysteine residue into the nucleotide-binding site. Initial dynamics simulations of the helical domain in Uba3 demonstrated that while the overall structure of the protein remains stable, the helical domain of Uba3, due to its presence on two large linker regions, could occupy a large region of space. This could result in the occlusion of Ub, ATP or both to the nucleotide binding pocket. When this domain exists in an open conformation, the nucleotide binding site is accessible to ATP and Ub, while in a closed conformation any binding with an E2 would be occluded until the thiolester has been formed and the switch has been opened.

Uba3 Helical Domain

At physiological pH, the thiol group of cysteine is only partially deprotonated, as its pKa is 8.5. In order for the active site cysteine residue to form the Ub thiolester readily, it must first become completely deprotonated. The deprotonation of residues, such as cysteine, normally occurs via a mechanism that utilizes a general base, such as histidine, to strip the hydrogen from the sulfur atom, thereby forming the nucleophile. MoeB contains only three histidine residues, none of which are found within the active site domain, a similar situation also exists for Uba3, which also contains no general bases in its active site. In the case of MoeB, the catalytic residues which result in the formation of the MoaD thiocarboxylate have been hypothesized to be found in the sulfurtransferase that binds to MoeB and donates the sulfur atom (Rajagopalan, 1996). In Uba3 there is no such sulfurtransferase, however, the presence of the helical domain may be an evolutionarily adaptation, which incorporates the sulfurtransferase into Uba3 itself, thereby increasing the efficiency of this reaction over that of the mechanism of MoeB.

The suggestion that E3s and E2s supply key catalytic residues during the formation of the thiolester and isopeptide bond is not new (Pickart, 2001). The 80 residue helical domain in Uba3 contains two histidine residues, one of which is conserved between Uba1 and all of the Uba1 like proteins (Figure 4.8). This histidine is located in a short helix-loop-helix and is structurally close to the active site cysteine residue and as there is no catalytic histidine within the nucleotide binding site of Uba3, this histidine may participate in the deprotonation of the cysteine residue (Figure 4.17). Upon binding Ub and ATP, this large domain could close over the nucleotide binding site, thereby bringing the active site cysteine into a position that can accept the Ub from the adenylate. This movement into the nucleotide binding site could occur concomitantly with a conformational rearrangement of the helical domain to provide His 227 in Uba3 or His 611 in Uba1 with access to the proton on the thiol group.

A Second Ub Must be Accommodated at the Uba1 Active Site

The canonical reaction mechanism of Uba1 involves the hydrolysis of two equivalents of ATP to form Uba1 that is charged with two molecules of Ub (Haas *et al.*, 1982). This implies that the active site of Uba1 must be capable of accommodating a second molecule of Ub while still bound to the first. When looking at the structures of the Uba3 and MoeB templates it is clear that the presence of two surface clefts suggest another Ub binding site (Figure 4.9). Comparing the Ub-AMP binding site to the position of MoaD in the MoeB/MoaD structure, MoaD would occupy the surface cleft that is perpendicular to the cleft into which we have placed the Ub adenylate. This suggested that when Ub is bound to Uba1 as the thiolester, it could exist in the conformation as seen in the MoeB/MoaD structure.

We suggest that the displacement of Ub from one binding site to the other would follow the formation of the thiolester, implying a rotation of the active site cysteine. This rotation is suggested by our initial dynamics experiments of Uba3 and would serve two purposes: first, the displacement of Ub from its initial binding site and second, the release of AMP. This displacement would reset Uba1 for binding new molecules of ATP and Ub to bind and allow the formation of a second Ub-adenylate.

Uba1/Ubc1 Complex

With two Ub molecules positioned on the surface of Uba1, we wanted to examine the possible interactions between Uba1 and an E2 to further understand the mechanism of Ub transfer between them. Since the location of Ub on the surface of Ubc1Δ had already been determined, we were looking for an alignment that was compatible with both the Ub-Ubc1 interaction and the Ub-Uba1 interactions. We reasoned that Uba1 and E2 would share complementary surface characteristics, so we prepared a surface representation that contained conserved residues in each molecule (Figure 4.18). These conserved residues are in agreement with the final positioning of Ubc1Δ on the surface of Uba1, such that the Ub contained at the "secondary" binding site is poised for transfer to E2. Interestingly, the conserved

residues form distinct patches on the surface of each molecule, while not interfering with the putative binding sites for either of the Ub molecules.

While docking experiments with models, such as this, are not necessarily accurate as to internal side chain interactions, bulk molecular interactions can still be predicted. Based upon the high degree of similarity between the two template structures, with an RMSD of 1.4 Å, and the fact that we were docking the structure of the E2~Ub thiolester to this highly conserved nucleotide binding site we felt confident that by excluding the active site cysteine domain we could determine the approximate location of the active site cysteine of E2 on this surface Uba1. The position, as described here, for Ubc1Δ on the surface of Uba1 would not clash with the position of the helical domain in the Uba3 template, if this were indeed the structure that the active site domain of Uba1 adopts. In this location on the surface of Uba1, Ubc1Δ would in fact be accommodated within the large van der Waals cavity that is formed between the nucleotide and active site cysteine domains in Uba3 (Figure 4.5).

While there were no immediately observable interacting structural motifs between the Uba1 model and Ubc1Δ, portions of the Uba1 molecule are quite obviously missing and may provide scaffolding for additional interactions. It should also be noted that the interaction between Uba1 and E2 is thought to be transient due to a lack of observed contacts (Hershko *et al.*, 1983), and additional surfaces of interaction may actually not be necessary. Both faces of Uba1 and Ubc1 share similar hydrophobic characteristics; however, both surfaces display a relatively unspectacular distribution of random charges, which may also contribute to the transient interaction between the two. It may indeed be the presence of Ub covalently bound to Uba1 that provides the main recognition surface for the E2s through its hydrophobic surface patch. Additionally, the position of Ub on the surface of Ubc1Δ, as determined by NMR spectroscopy, is not occluded in this model and could readily become transferred from the secondary binding site on Uba1 to the site on Ubc1Δ, as seen in Figure 4.14A. The key feature of this arrangement is that it places the two active sites of Uba1 and the active site of Ubc1

in close proximity, a constraint that has been demonstrated experimentally (Chapter 2, Figure 6).

Uba1 Surface Mutations and the Impact on Ub Interaction

Several temperature sensitive Uba1 alleles have been identified in mammalian cell lines (Finley *et al.*, 1984; Kulka *et al.*, 1988; Deveraux *et al.*, 1990; Mori *et al.*, 1993). Unfortunately none of these mutants have been characterized according to their sequences. In addition, most systematic deletions and mutations of Uba1 have proven to be lethal to the organisms that contained them. Recently, a viable Uba1 mutant was discovered (Swanson and Hochstrasser, 2000). This mutant does not bring any useful information to our model of the Uba1 active site, as it is a promoter mutant and therefore affects only the rate of Uba1 transcription. While our model does not include any of the regions of Uba1 that have been altered in the creation of these temperature sensitive mutations, the inability of Uba1Δ to activate Ub suggests that these domains must be required for either Ub recognition or activation by Uba1. This observation is also supported by the requirement of multi-enzyme complexes for the activation of UBL proteins.

A number of mutations within *H. sapiens* Uba3 have been created, by others, to map locations of Nedd8 interactions (Walden *et al.*, 2003). The effects these mutations on Nedd8 activation have been considered with respect to the binding of Ub on our Uba1 model. The mutation of residue Ile 127 in Uba3 did not appear to affect adenylation or thiolester formation with Nedd8, which agrees with our model in that there are no contacts between Ub and Uba1 in this area. Mutations of Tyr 331 and 333, and Phe 335 were shown to have dramatic effects on the formation of Nedd8-adenylate. As we were unable to model this region within Uba1, it was impossible to assign this region. However, depending on the length of the active site cysteine domain in Uba1, these residues could be located in the floor of the primary Ub binding site, or within the helix that constrains the amino terminal side of the active site domain. As such, these residues would affect the general stability of Uba3, and therefore binding of Rub1 and formation of the adenylate. This may also

be the case for mutations of residues Leu 206 and Tyr 207, as these residues are located within the helical domain itself how they might affect adenylate structure is difficult to determine, except for an effect on the movement of this domain into the nucleotide binding site. Mutations of Uba3 residues within the area that corresponds to the linker regions between the nucleotide binding site and the helical domain, Thr 217, Asp 331 and Ile 289, appear to affect Nedd8-thiolester formation, while not affecting the formation of Nedd8-adenylate.

Mutations of the carboxy terminus of Ub have demonstrated a requirement for glycine to be present to support the dual mode charging of Ub at the Uba1 active site. Mutations of the Ub carboxy terminus do not seem support ATP:PPi exchange (Ecker *et al.*, 1987), however, Hodgins *et al.* (1992) have demonstrated that ubG76A is a competent substrate for activation by Uba1 *in vitro*. Substitution of the carboxy terminal glycine residue with alanine leads to activation of only a single Ub molecule (Pickart *et al.*, 1994). The two surface clefts may be unable to accommodate the larger side chain of alanine, or there may be some inhibition of Ub displacement from the primary to the secondary binding site. Mutations within the core domain of Ub, that did not significantly alter the Ub tertiary structure, were shown to have little effect on interactions with Uba1 (Ecker *et al.*, 1987). Of all the Ub mutants created, only alteration of His 68 showed slight inhibition of Ub thiolester formation. The effect of His 68 may be due to its location within the hydrophobic patch formed by the β sheet structure of Ub (Chapter 1, Figure 4A). This patch was shown to form the interacting surface with our model of Uba1 and Ubc1 (Hamilton *et al.*, 2001).

4.5 Conclusion

The Uba1 active site model produced a picture of the central domain of Uba1 and provided us with valuable tool to investigate the mechanism of Ub activation. The central postulate of this model is that the Ub-adenylate and the Ub-thiolester are formed at the same location on the surface of Uba1. The model exhibits two surface clefts on Uba1, one that can accommodate the tail of Ub when it is bound as the

adenylate and the other can accommodate the tail of Ub when it is bound as the thiolester (Figure 4.9). Because of low sequence identity between Uba1 and the MoeB and Uba3 templates, we were unable to propose a position for the active site cysteine residue. However, the requirement for the active site cysteine to approach the Ub adenylate, prior to formation of the thiolester, suggests that a conformational change within this region must take place.

Using these results we have proposed a simple mechanism for the simultaneous activation of two molecules of Ub at the active site of Uba1. Upon binding of ATP and Ub ATP becomes hydrolyzed, resulting in the activation of Ub to the adenylate. Following the activation of Ub, the active site cysteine residue and a catalytic histidine must enter the nucleotide binding site, providing a situation which allows Ub to become transferred to the active site cysteine (Haas *et al.*, 1982). Concurrently with the dissociation of AMP, the first molecule of Ub, now bound as the thiolester, rotates into the secondary binding site, thereby freeing the primary Ub binding site and placing Ub into its secondary binding (Figure 4.9). As Ub rotates outward, the simultaneous binding of a second molecule of Ub and a second ATP occurs, resulting in the formation of a second Ub-adenylate and a dually charged Uba1 species. The first Ub molecule is now a suitable target for interaction with the E2 proteins, which can accept Ub from the Uba1~Ub thiolester. Recharging of the Uba1~Ub thiolester can then immediately occur because of the presence of the second Ub adenylate at the active site. This model of the Uba1 active site, as it is presented here is consistent with the experimentally determined observations, of Ub activation, made by our laboratory and others.

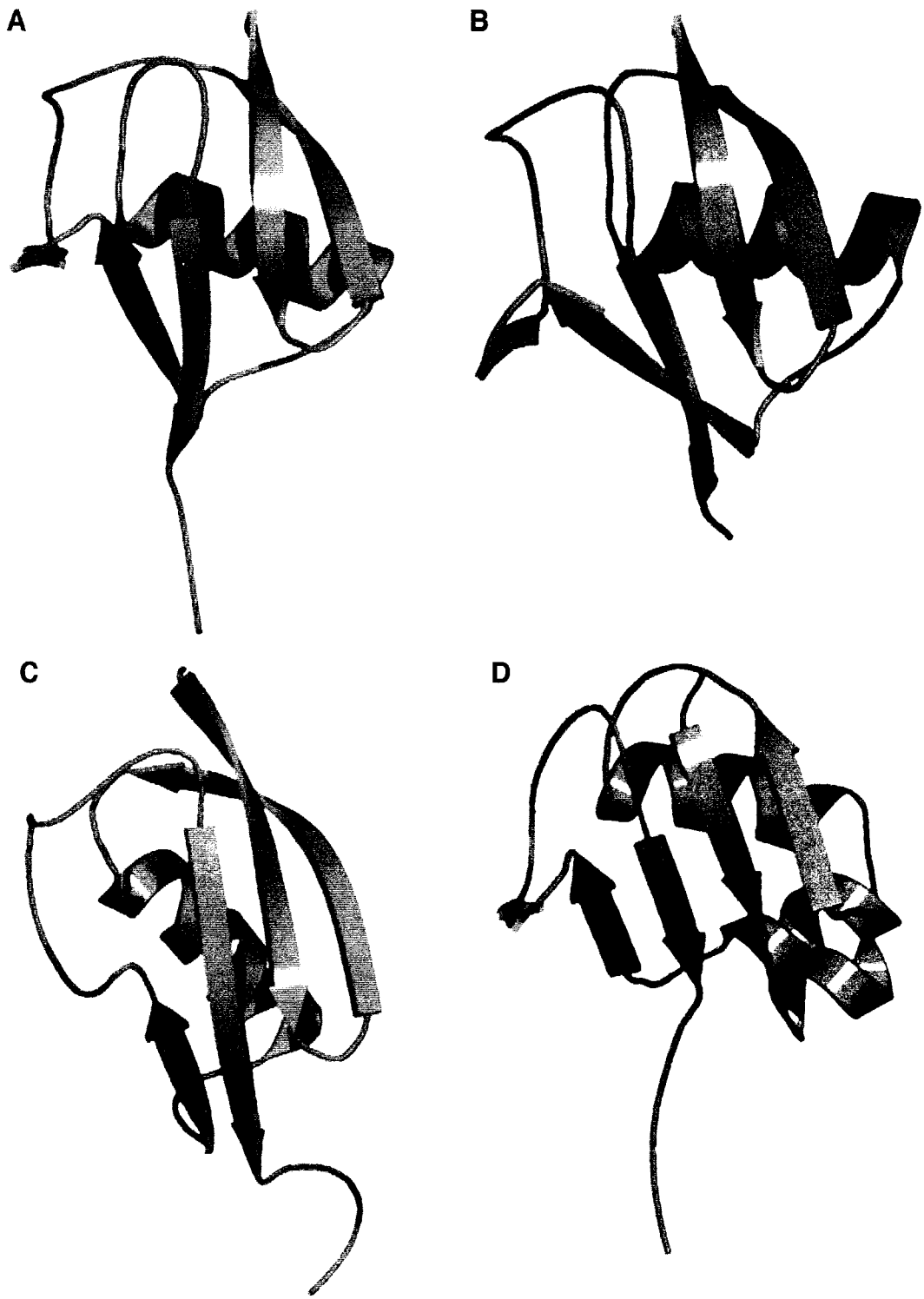

Figure 4.1. **Structures of Ub and UBL Proteins**
Cartoon representations of Ubiquitin (**A**) and the UBL proteins Rub1 (**B**), Sumo (**C**) and MoaD (**D**). The structures of these proteins demonstrates the high degree of similarity between Ub and UBL protein folds. The *H. sapiens* Ub (pdb-id 1UBQ) and Sumo (1A5R) proteins along with the *S. cerevisiae* Rub1 (1BTO) and *E. Coli* MoaD (1JWD) are all oriented with the β sheet to the front of the image.

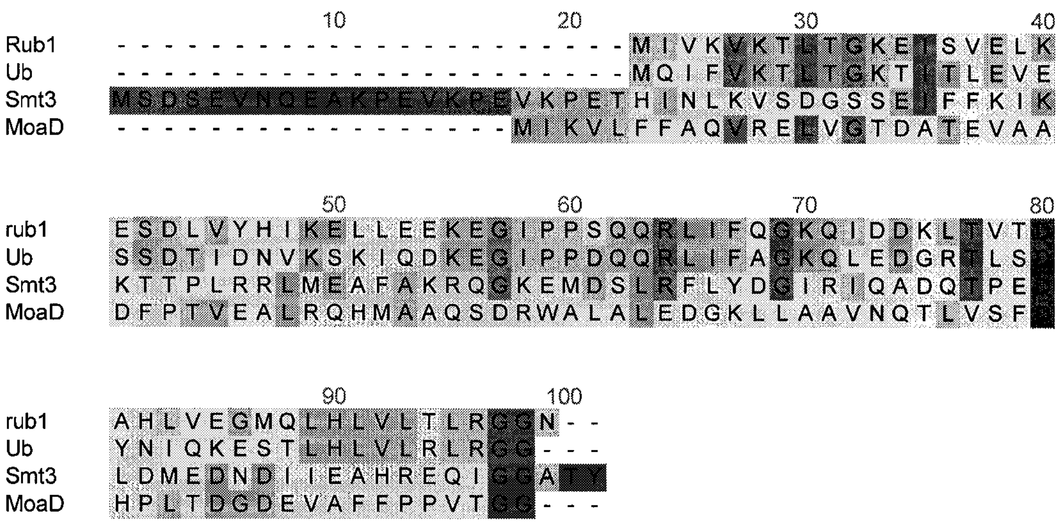

Figure 4.2. **Sequence Alignment of Ub and UBL Proteins**
Sequence alignment of *S. cerevisiae* Ub, Rub1 and Smt3 with *E. coli* MoeB. This alignment demonstrates sequence identities of 53%, 17% and 16% for Rub1, Smt3 and MoaD respectively, along the entire sequence of Ub. Light gray shading indicates similar residues, or identical within two of the sequences while dark gray indicates similar or identical residues within three or more of the sequences. All of the proteins share an identical Gly-Gly motif, where their activation occurs. Both Smt3 and Rub1 contain a carboxy terminal extension that must be processed prior to their activation, exposing the gly-gly motif (Lee *et al.*, 1999). Smt3 also contains a large unstructured amino terminal extension for which a definitive function has yet to be established (Bayer *et al.*, 1998).

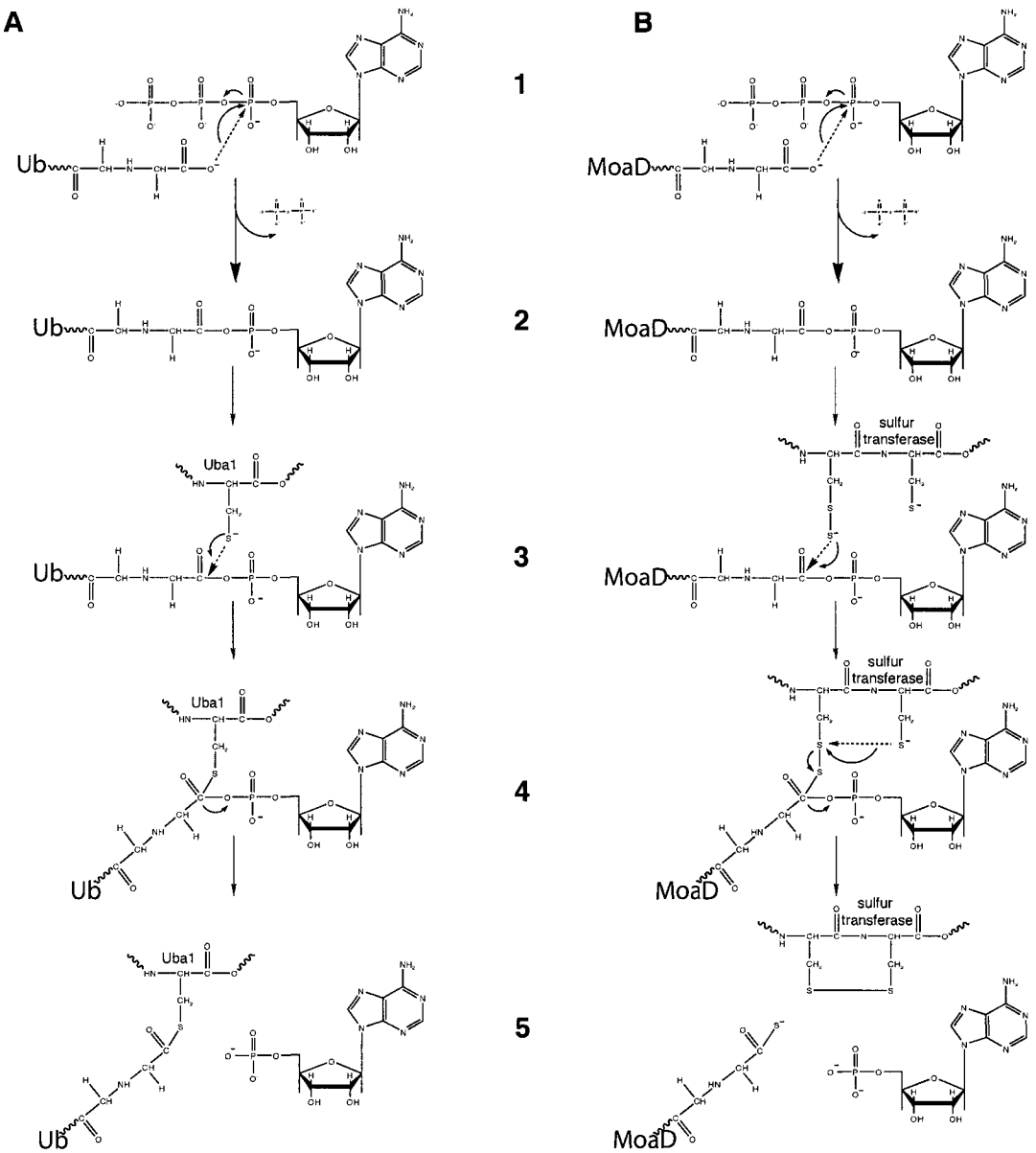

Figure 4.3. **Similarities Between Ub and MoaD During Activation**
The similar reaction mechanisms of Ub (**A**) and MoeB (**B**) activation are shown here as simple Lewis Structures. **1-2**, The first step in the activation of Ub or MoaD involves their conversion to a carboxy terminal acyl adenylate at the active sites of Uba1 or MoeB respectively. **3**, once activated, the carbonyl carbon of the phophate ester undergoes a nucleophilic attack from an active site thiol, forming a tetrahedral intermediate (**4**). In Ub activation, this thiol is from an active site Cys residue within Uba1, while MoaD activation occurs through the binding of a sulfurtransferase to the activator MoeB, which donates a sulfur atom to MoaD. **5**, The tetrahedral intermediate then collapses, releasing AMP and in the case of MoeB activation, also MoeB. During the activation of Ub, it remains bound to Uba1 as the thiolester (adapted from: Haas *et al.*, 1982; Rajagopalan *et al.*, 1997).

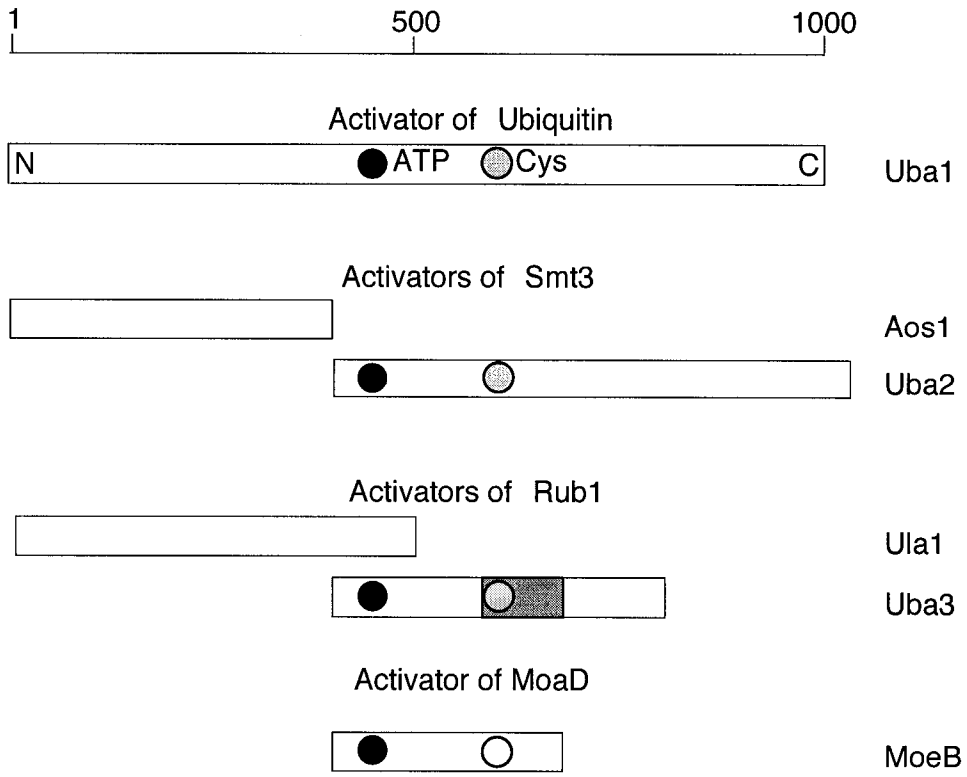

Figure 4.4. **Schematic Alignment of Uba1 and the Activators of Rub1, Smt3 and MoaD**

A schematic representation of the alignments produced for the modeling of the Uba1 active site. Full length Uba1 was aligned against the activators of Smt3, Rub1 and MoaD. Activation of Smt3 requires the presence of two proteins, Aos1 and Uba2 which correspond to the amino and carboxy termini of Uba1 respectively (Johnson, et al, 1997). Rub1 requires the presence of Ula1 and Uba3 prior to its activation (Liakopoulos et al, 1998), while MoaD requires only MoeB (Leimkuhler et al, 2001). The scale at the top of the figure illustrates the approximate number of amino acids in each protein. The ATP binding motif is represented by a black circle and the active site cysteine by a gray circle. There is a cysteine residue present in MoeB (white circle), but it does not function in the activation of MoaD (Rajagopalan et al, 2001). The gray box in Uba3 illustrates the position of the eighty residue α helical domain that is seen in its three dimensional structure (Walden et al, 2003).

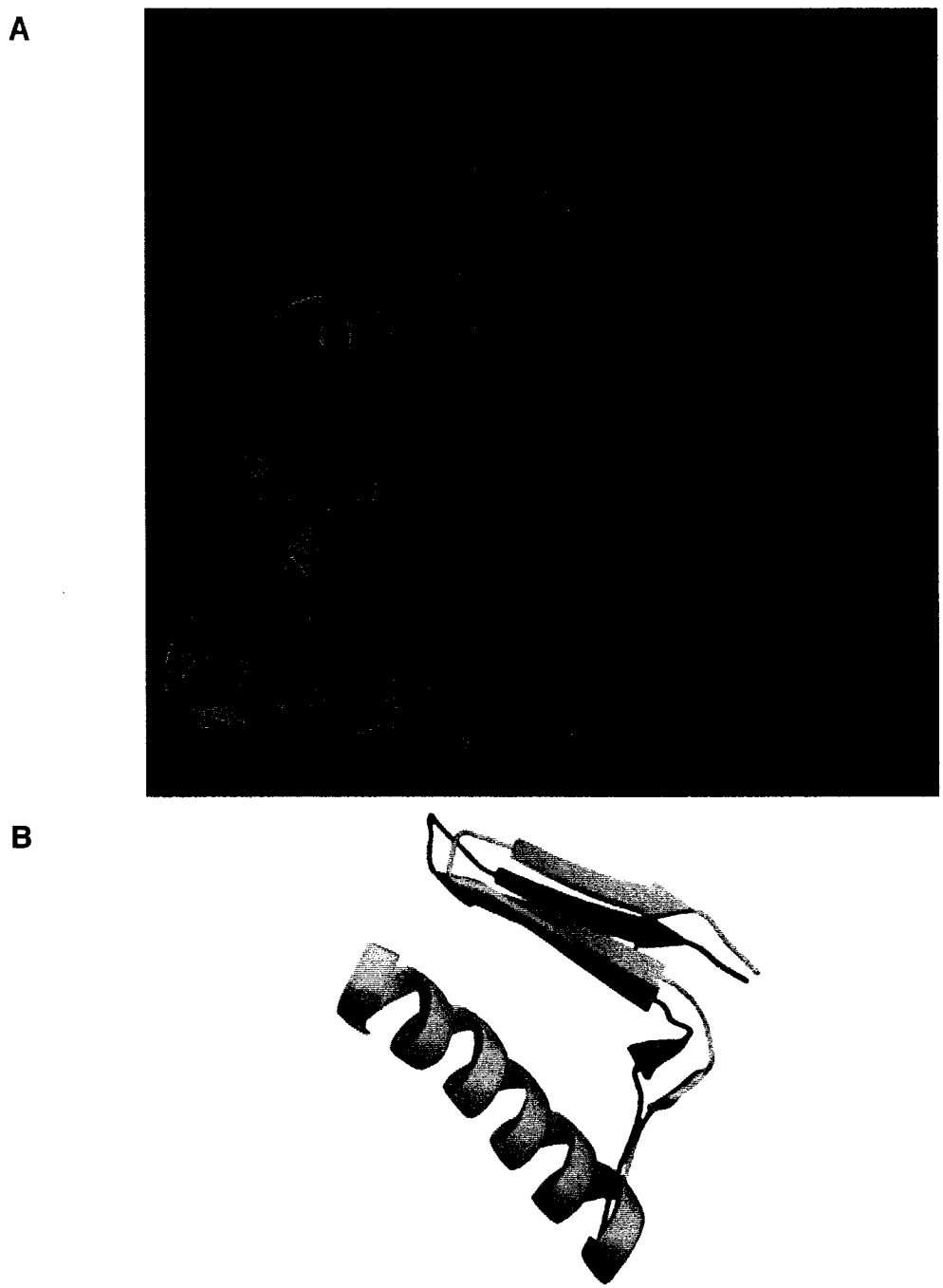

Figure 4.5. **Superimposition of Uba3 and MoeB structures**
A, the structures of Uba3 (pdb - 1NGV) red and MoeB (pdb - 1JW9) green were superimposed using the MOE homology package. The superimposition of all main chain atoms resulted in an RMSD of 1.40 Å and a structural alignment that was based upon this superimposition yielded 24% identity over the entire length of both proteins. **B**, the region of Uba3 and MoeB that follows their active site regions. In Uba3 this region occurs, carboxy terminally, following the 80 residue helical domain, while in MoeB it occurs after the disordered region in the crystal structure. The sequence identity of the region preceding (B) is 34%, and while the sequence identity of this region is only 7%, the RMSD is still low at 1.46 Å.

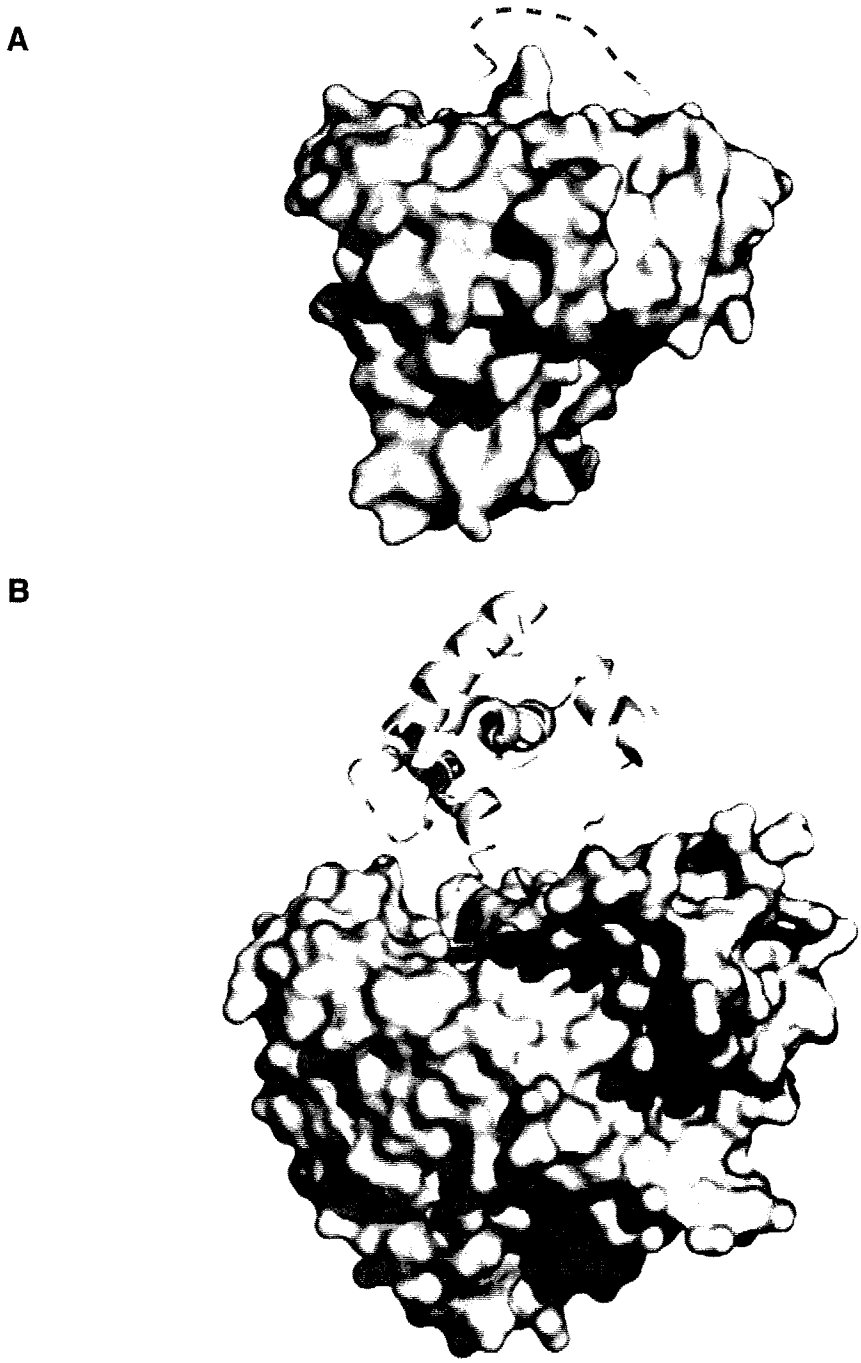

Figure 4.6. **Structural Comparison of MoeB and Uba3**
The two templates used in the construction of the Uba1 model are shown here as Connolly surfaces with ribbons representing the active site domains. **A**, the structure of *E. coli* MoeB (pdb-id 1JW9 Lake *et al.*, 2000). The region that makes up the active site loop is shown as a red dotted line, as there was no density for this region present in this structure. **B**, the structure of *H. sapiens* Uba3 (pdb-id 1NGV Walden *et al.*, 2003) with the large eighty residue helical domain represented as ribbons. The location of the active site cysteine is shown as a yellow stick.

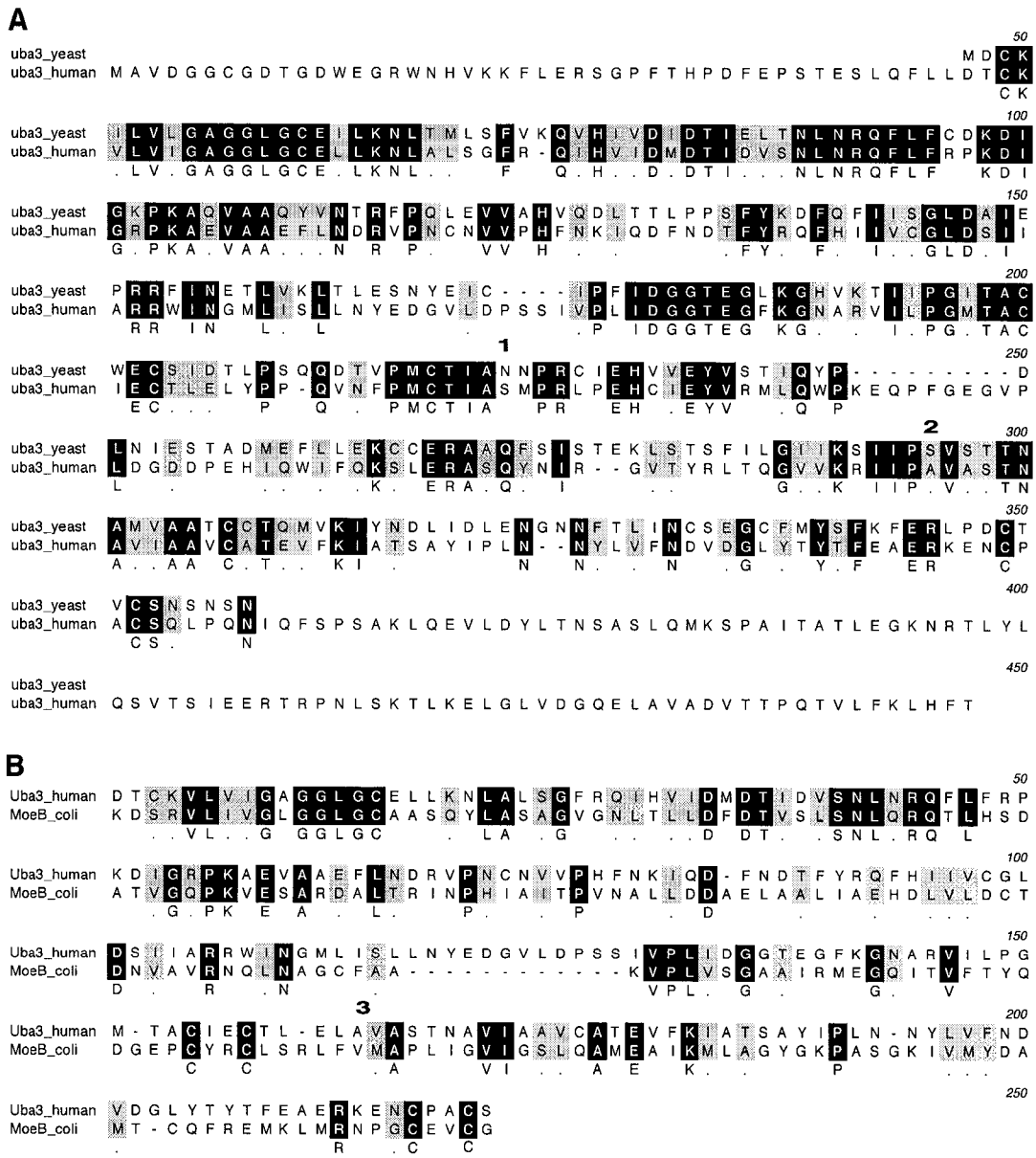

Figure 4.7. **Sequence Alignments Uba3 and MoeB**
A, Sequence alignment of the *H. sapiens* and *S. cerevisiae* Uba3 orthologs. This alignment illustrates the amino and carboxy terminal extensions within *H. sapiens* Uba3, as compared to the *S. cerevisiae* protein. (**1**) denotes the position where the alignments between Uba1 and Uba3 show a loss in identity (Figure 4.9). This is also the position, within Uba3 where the cysteine containing helical domain begins (Figure 4.5). (**2**) represents the position where the helical domain in Uba3 ends and the alignment with MoeB continues. **B**, structural alignment of *H. sapiens* Uba3 and *E. coli* MoeB, based on the region of Uba3, above, and the structures of Uba3 (pdb - 1NVG) and MoeB (pdb - 1JWD). This superimposition gave an rmsd of 1.4 Å over all main chain atoms. (**3**) The 80 residue helical domain that is present in Uba3, but not in MoeB has been omitted.

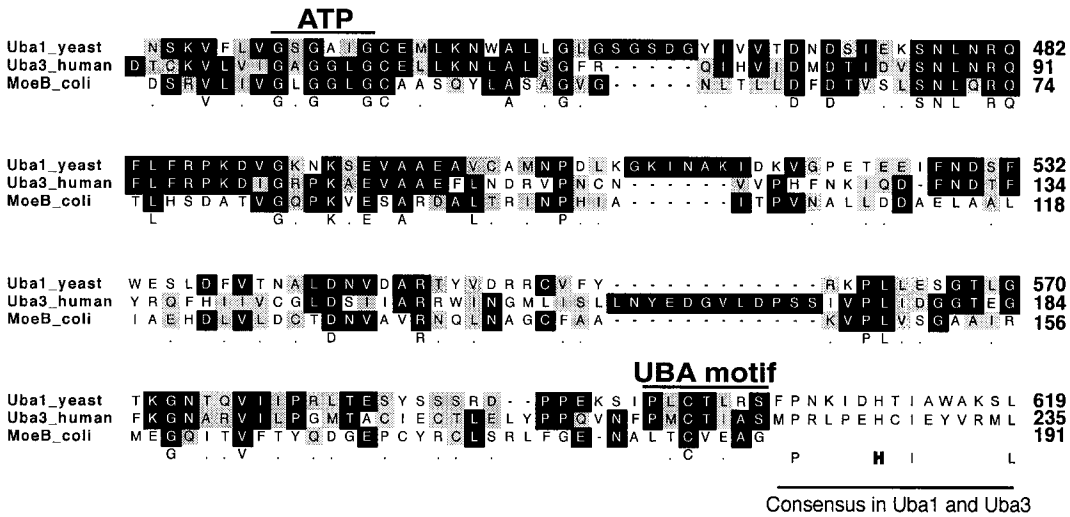

Figure 4.8. **Sequence Alignment Between Uba1, Uba3 and MoeB**
Displayed here are sequences corresponding to the active site regions of *S. cerevisiae* Ubiquitin Activating Enzyme (Uba1), the Smt3p Activating Enzyme (Uba3) and the activator of *E. coli* MoaD (MoeB). These alignments were generated using the structural alignment between Uba3 and MoeB (Figure 4.7) and were then used in the creation of the Uba1 active site model. The putative nucleotide binding motif is represented by (**ATP**) and the **UBA** motif contains the active site cysteine residues of Uba1 and Uba3. The last 15 residues of Uba1 and Uba3 (**Consensus only**) represent a region between these two proteins that is absent in the sequence of MoeB. This region contains a conserved His residue (**H**) that may be involved in the deprotonation of the active site cysteine, prior to the formation of the thiolester.

Figure 4.9. **Superimposed Surfaces of Uba3 and MoeB**
Based upon the structural superimposition in Figure 4.6, Connelly surfaces were generated to demonstrate the surface qualities of MoeB and Uba3. The helical domain within Uba3 has been omitted and the broken peptide bonds are represented by red stars. This figure looks down upon the nucleotide binding site, into which has a molecule of ATP (sticks) is positioned. The orientation of the phosphate atoms is illustrated by the fuchsia spheres. MoeB (gray surface) and Uba3 (gold surface) share three distinct surface qualities. First, is the deep pocket that makes up the nucleotide binding site. Second and third, are two deep clefts (shown by red arrows) which may act as channels to accept the tail of Ub, either as the adenylate or thiolester.

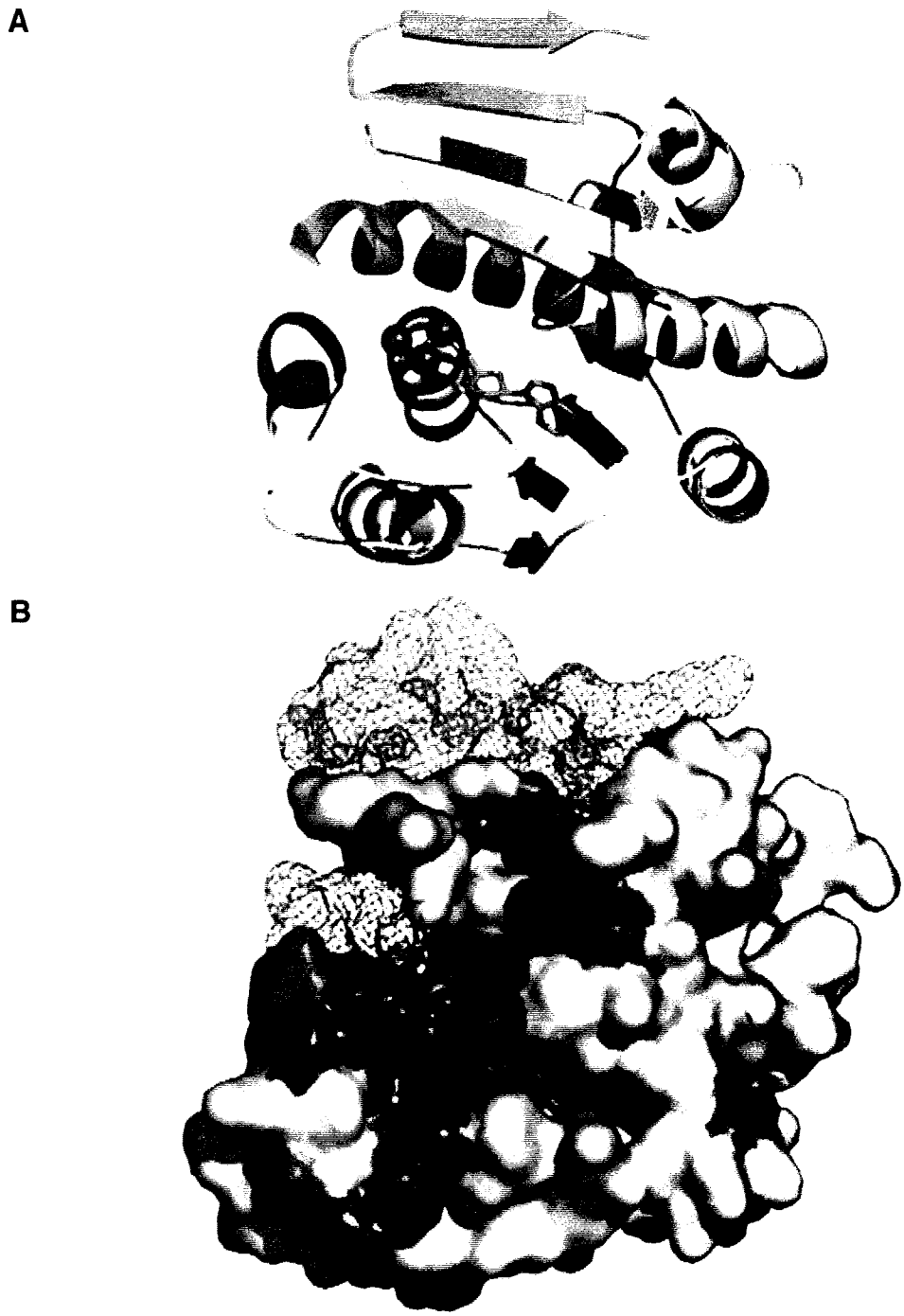

Figure 4.10. **Uba1 Homology Model**
Using the structures of Uba3 and MoeB, a homology model of the nucleotide binding site of Uba1 was constructed. **A**, ribbon diagram of the Uba1 active site, red ribbons represent identical residues and pink ribbons represent similar residues. A molecule of ATP (sticks and fuchsia spheres) has been superimposed into the nucleotide binding site using the structure of the ATP bound MoeB as a template. The green ribbon illustrates a region of low sequence identity between Uba3 and MoeB, and for this reason was not modeled. **B**, Surface representation of **A** illustrating that the majority of the nucleotide site is present in the model.

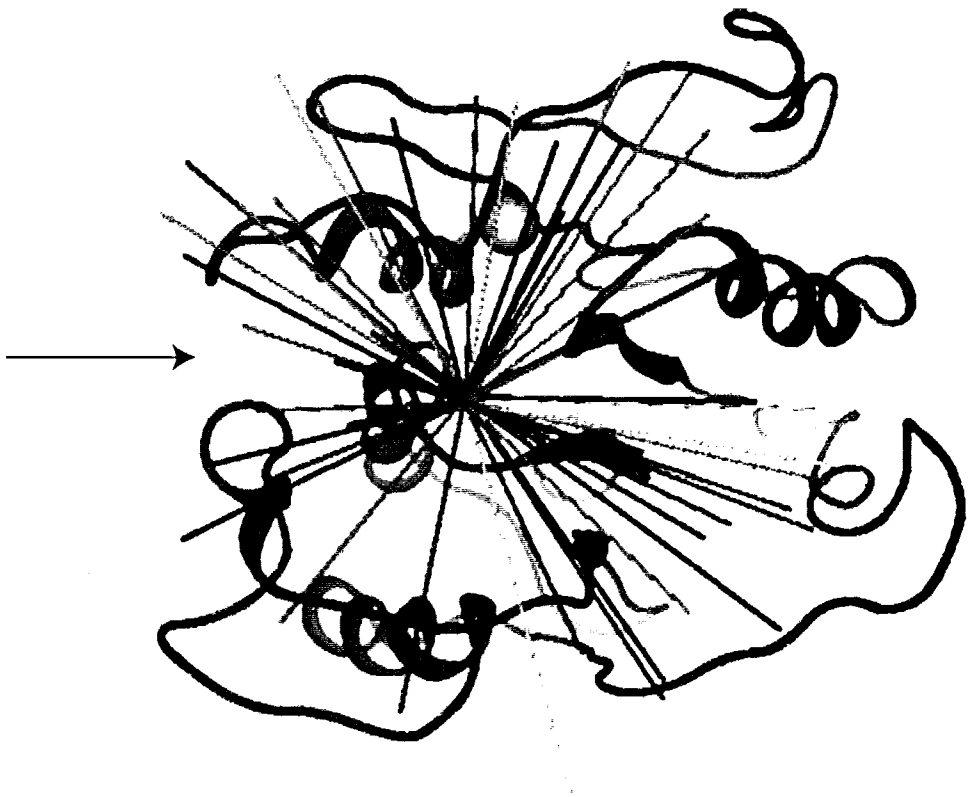

Figure 4.11. **Stochastic Confirmational Search of the Uba1 Active Site** The Uba1 active site model was imported into MOE and all backbone atoms were fixed. This simulation included an eight residue peptide, corresponding to the carboxy terminus of Ub, that was covalently linked to AMP and the Ub-AMP bound at the nucleotide binding pocket. This image shows Uba1 from a view looking down onto the active site. Based upon alignments of MoeB and Uba3 (Figure 4.9), a putative position for the active site cysteine is represented as a yellow space filling van der Waals sphere. Colored vectors, each originating above the α phosphate of AMP, represent the average of each conformation that the Ub tail adopted over the course of the simulation. Coloring of the vectors represents the potential energy of each conformation, red having the highest energy, followed by fuchsia, aqua and finally royal blue representing the lowest energy. The arrow represents the position a cleft in the surface of the model (Figure 4.6) and the location of the lowest energy conformations of the Ub peptide.

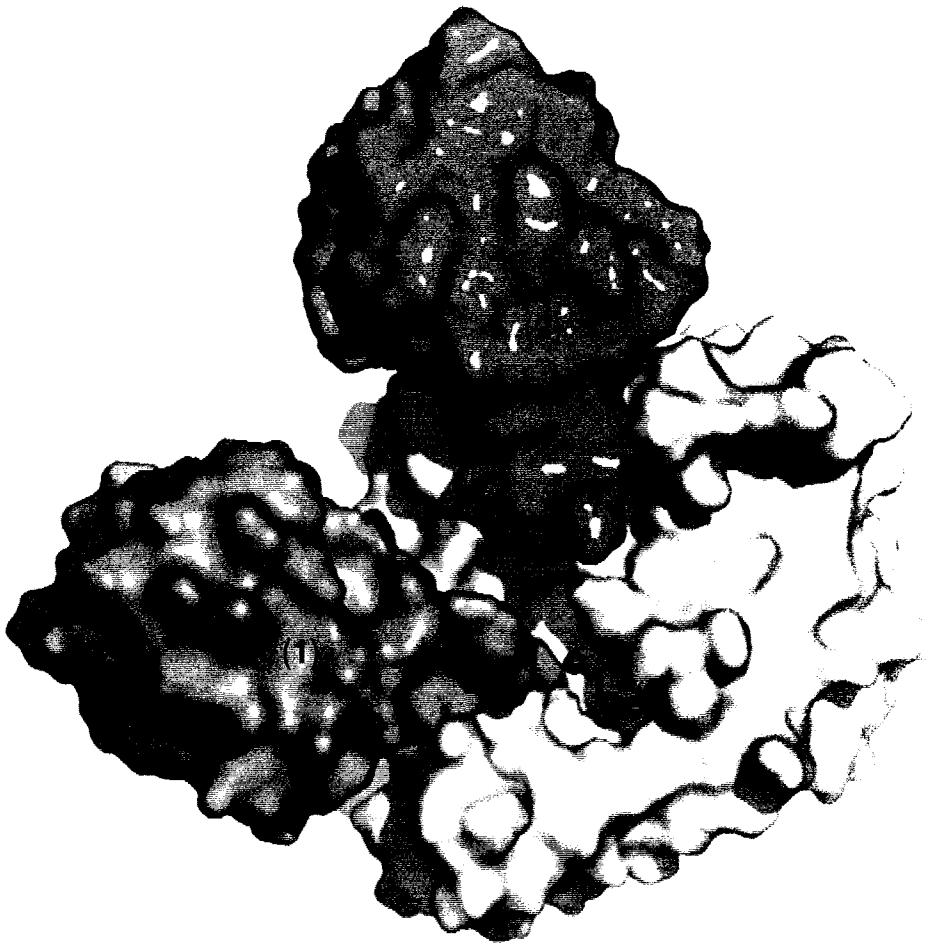

Figure 4.12. **Potential Positions of Ub on the Model of Uba1**
Illustrated here are the potential binding sites for the activated Ub adenylate and Ub thiolester on the surface of Uba1. The Uba1 model (white) is shown with the Ub-AMP adenylate (**1**) bound at the nucleotide binding site (AMP is drawn as fuchsia sticks). The tail of the Ub adenylate occupies one of the surface clefts that emanates from the nucleotide binding site (Figure 4.9). A second Ub binding site on the surface of Uba1 is suggested by the position of the UBL, MoaD, in the structure of the MoeB/MoaD complex (**2**). The tail of this Ub occupies a second surface cleft that eminates from the nucleotide binding site.

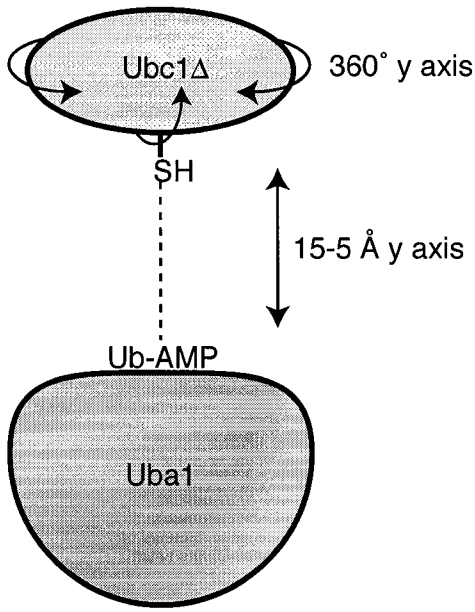

Figure 4.13. **Schematic Representation of Ubc1 Docking to Uba1**
The docking of Ubc1Δ to the surface of Uba1 involved manipulation through three degrees of freedom. Treating the active site of the Uba1 model as a fixed surface, the Ubc1Δ structure was manipulated so its active site cysteine residue was in a position such that it would enable a transthiolation reaction to occur. The Ubc1Δ was then moved to a position approximately 15 Å above the surface of Uba1. Docking involved the systematic movement of Ubc1Δ towards the active site of Uba1, while rotating it through 360° about the y axis, with slight perturbations in rotations about the x and z axes. The intermolecular energy between Uba1 and Ubc1Δ was monitored throughout this process, providing an energy landscape leading to the docked complex. Additional docking simulations were performed, using the positions of Ub on the surface of Uba1 as a guide for Ubc1Δ positioning. As we already knew the positions of Ub on the surface of Uba1 and the position of Ub on the surface of Ubc1Δ (Hamilton *et al.*, 2001) we could reduce the docking problem by one degree of freedom, forgoing the 360° rotation about the y axis. Both docking schemes yielded similar structures, with Ubc1Δ poised to accept Ub from the secondary binding position.

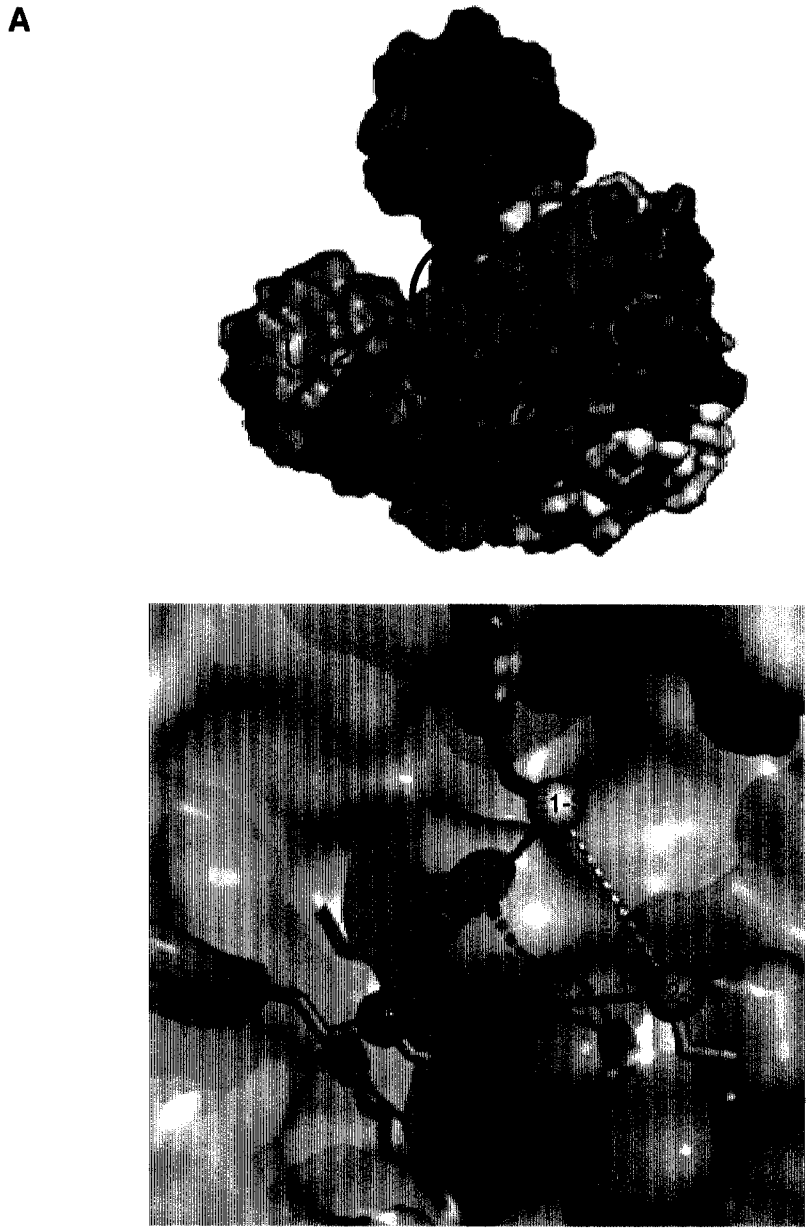

Figure 4.14. **Model of Uba1-Ub2-Ubc1Δ interaction**
A, illustrates the interaction between the Uba1 homology model (white surface), bound with two molecules of Ub (light green, Ub-AMP and dark green, Ub thiolester) with Ubc1Δ (blue surface) (pdb-id 1FXT (Hamilton *et al.*, 2001). The red patch on the surface of E2 represents the domain that was found to interact with Ub through NMR spectroscopy of the E2~Ub thiolester complex (Chapter 3). **B**, cut away view of the interaction of the active sites of Uba1 and Ubc1Δ, as expanded from the black circle in panel A. The ATP molecule can be seen as green sticks with the α phosphate a magenta VDW sphere. The tails of Ubiquitin are shown as light green and dark green tubes (as above). The transparent blue surface is that of Ubc1Δ and the two active site sulfur atoms are shown as yellow VDW spheres packed into the center of the complex. Distances between the two active sites and the α phosphate of ATP are shown as dashed lines.

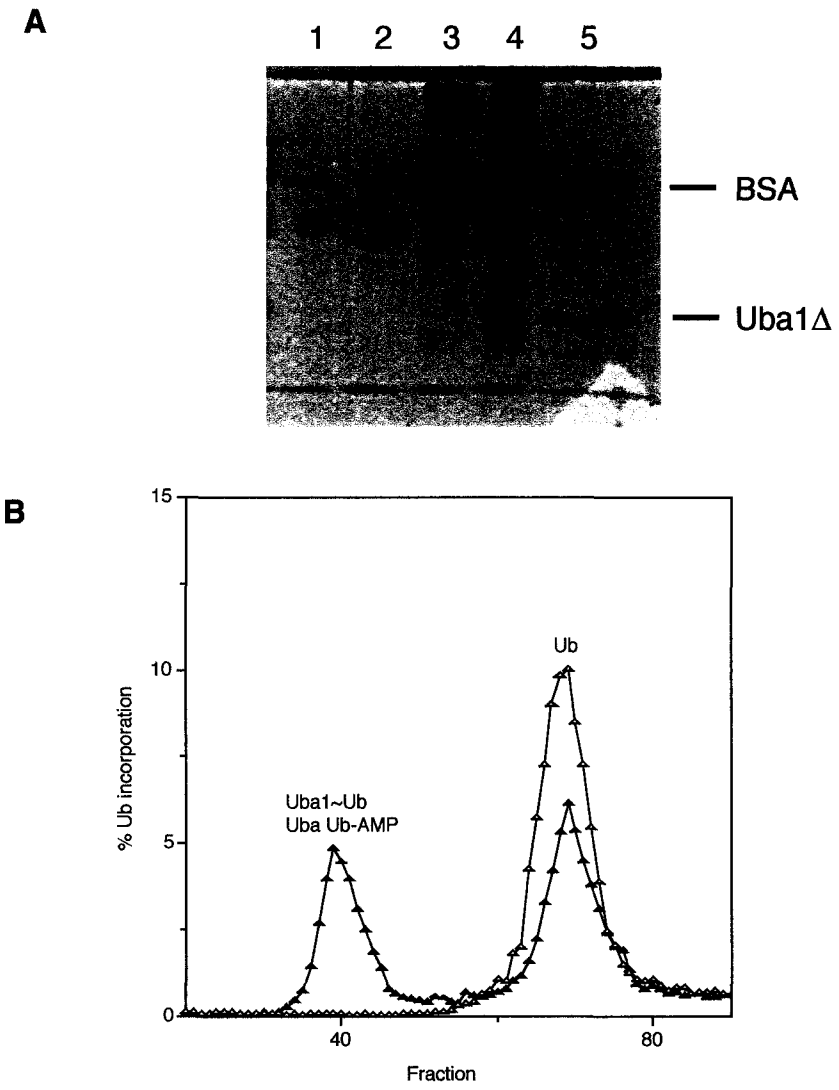

Figure 4.15. **Purification and Activity of Uba1Δ**
A, quantification of recombinant Uba1Δ by SDS-PAGE, following purification by nickel affinity chromatography. BSA standards, used for quantification of purified protein, can be seen in lanes one to four. Lane five shows purity of Uba1Δ with added BSA as a stabilizer during purification. **B**, the activity of Uba1Δ was assayed using a ubiqutination reaction containing [^{35}S] labeled Ub, as described in *Experimental Procedures*. Reactions containing wild type Uba1 are shown as closed triangles and Uba1Δ as open triangles.

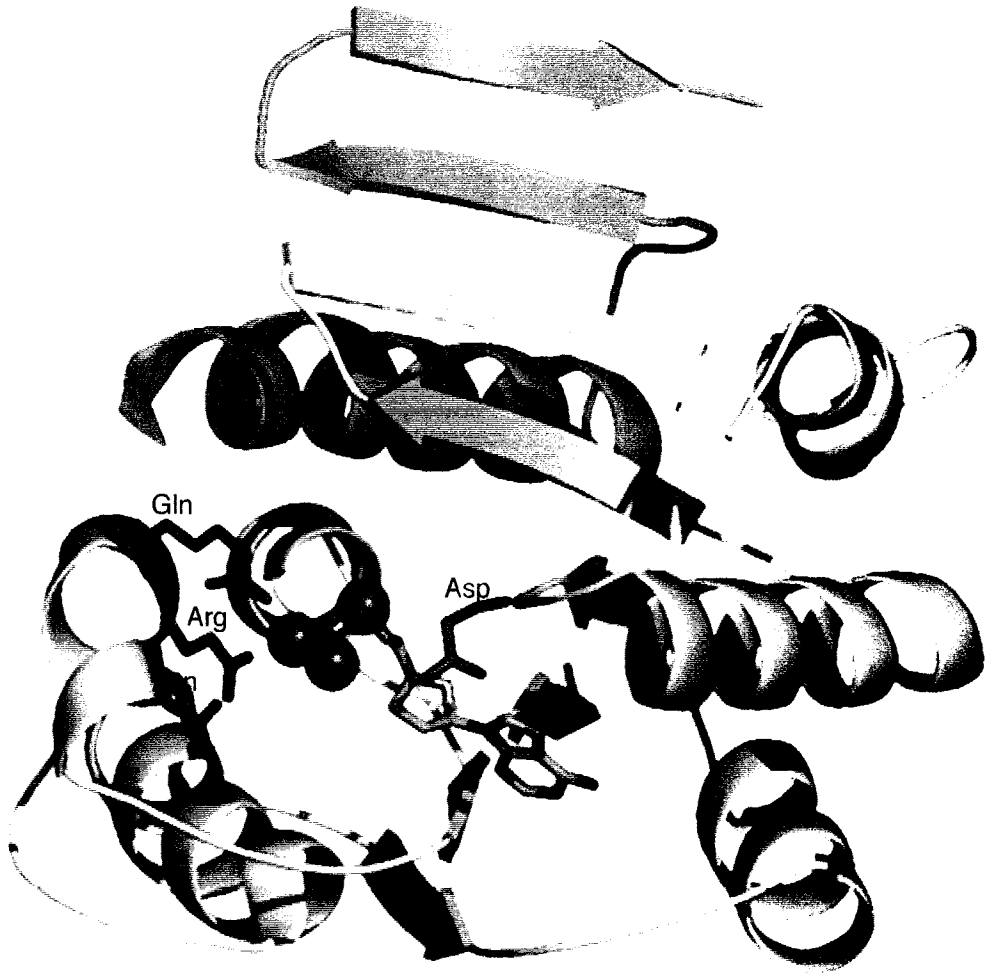

Figure 4.16. **Conserved Residues Within the Uba1 Nucleotide Binding Site** Shown here is the Uba1 homology model, with four putative, catalytic residues shown as red sticks. First, Asp 544 has been postulated to be involved in the coordination of magnesium, which has been suggested to be involved in binding ATP (Lake *et al.*, 2001). Also shown are the residues Asn 478, Arg 481 and Gln 482 which comprise a highly conserved region within Uba1, Uba1 and MoeB. These residues may be involved in stabilizing the negative charges during the nucleophilic attack at the α phosphate of ATP.

Figure 4.17. **Role of Conserved Histidine in Thiolester Formation**
This ribbon diagram of Uba3 clearly illustrates the position of the 80 residue helical domain and the location of the active site cysteine residue (**1**). The green ribbon, within the helical domain, corresponds to sequence similarities between Uba3 and Uba1 that are absent from MoeB (Figure 4.9). A conserved histidine (**2**) sits within this domain and may play a role in the deprotonation of the active site cysteine residue (**1**), following a confirmational change in this domain during formation of the thiolester.

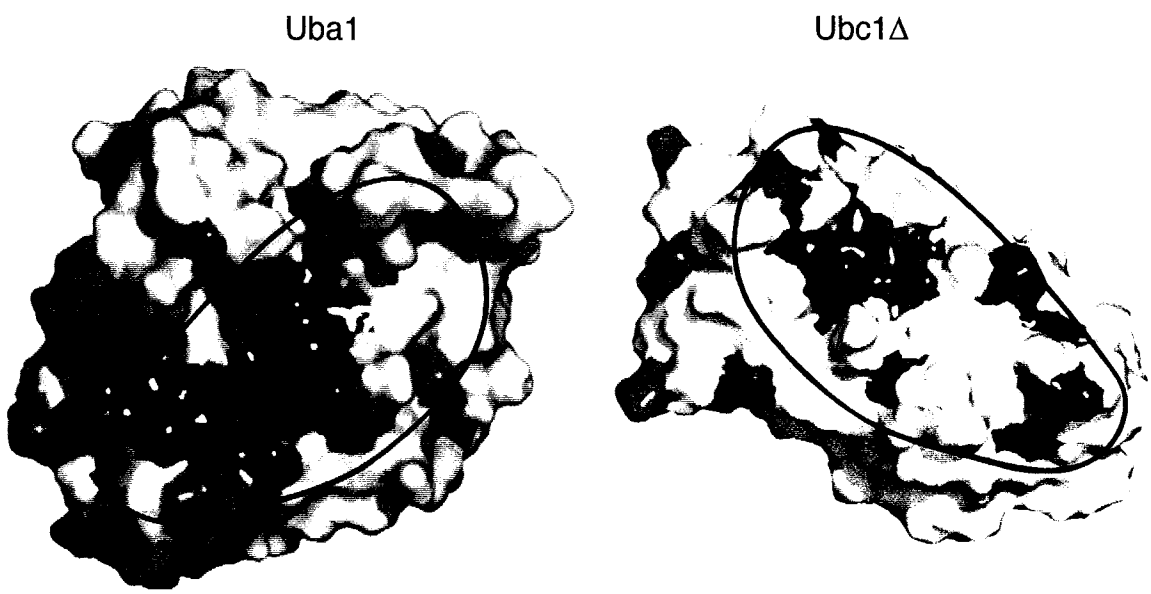

Figure 4.18. **Identical and Homologous Residues Found on the Interface of the Docked Uba1/Ubc1Δ Complex**
Connolly surface representations of the Uba1 active site model and Ubc1Δ. Ubc1Δ has been rotated 180° and displaced from its position in the docked structure. The black outline represents the regions on both molecules that participate in their interactions. The Uba1 active site loop is shown as a blue tube, with Cys 600 colored yellow. The active site cysteine of Ubc1Δ is also colored yellow. Residues corresponding to identities in the alignment of Uba1 with other UBL activators (Figure 4.4) are colored red and homologous residues are colored violet. The same coloring scheme has been applied to the residues in Ubc1Δ, based on structural alignments of all the E2s in *S. cerevisiae* (Ptak *et al.*, 2001).

4.6 References

Altschul, S. F., Madden, T. L., Schaffer, A. A., Zhang, J., Zhang, Z., Miller, W., & Lipman, D. J. (1997). Gapped BLAST and PSI-BLAST: a new generation of protein database search programs. *Nucleic Acids Res, 25(17)*, 3389-402.

Altschul, S. F., Gish, W., Miller, W., Myers, E. W., & Lipman, D. J. (1990). Basic local alignment search tool. *J Mol Biol, 215(3)*, 403-10.

Appleyard, M. V., Sloan, J., Kana'n, G. J., Heck, I. S., Kinghorn, J. R., & Unkles, S. E. (1998). The Aspergillus nidulans cnxF gene and its involvement in molybdopterin biosynthesis. Molecular characterization and analysis of in vivo generated mutants. *J Biol Chem, 273(24)*, 14869-76.

Bachmair, A., Finley, D., & Varshavsky, A. (1986). In vivo half-life of a protein is a function of its amino-terminal residue. *Science, 234(4773)*, 179-86.

Baker, D., & Sali, A. (2001). Protein structure prediction and structural genomics. *Science, 294(5540)*, 93-96.

Begley, T. P., Xi, J., Kinsland, C., Taylor, S., & McLafferty, F. (1999). The enzymology of sulfur activation during thiamin and biotin biosynthesis. *Curr Opin Chem Biol, 3(5)*, 623-29.

Bayer, P., Arndt, A., Metzger, S., Mahajan, R., Melchior, F., Jaenicke, R., & Becker, J. (1998). Structure determination of the small ubiquitin-related modifier SUMO-1. *J Mol Biol, 280(2)*, 275-86.

Bing, D. H., Laura, R., Robison, D. J., Furie, B., Furie, B. C., & Feldmann, R. J. (1981). A computer-generated three-dimensional model of the B chain of bovine alpha-thrombin. *Ann N Y Acad Sci, 370*, 496-510.

Bohnsack, R. N., & Haas, A. L. (2003). Conservation in the mechanism of Nedd8 activation by the human AppBp1-Uba3 heterodimer. *J Biol Chem*,

Bower, M.,, Cohen, F.,, & Dunbrack, R. (1997a). Prediction of protein side-chain rotamers from a backbone-dependent rotamer library: a new homology modeling tool. *Journal of Molecular Biology, 267*, 1268-82.

Bower, M. J., Cohen, F. E., & Dunbrack, R. L. J. (1997b). Prediction of protein side-chain rotamers from a backbone-dependent rotamer library: a new homology modeling tool. *J Mol Biol, 267(5)*, 1268-82.

Chothia, C., & Lesk, A. M. (1986). The relation between the divergence of sequence and structure in proteins. *EMBO J, 5(4)*, 823-26.

Ciechanover, A., Elias, S., Heller, H., & Hershko, A. (1982). "Covalent affinity" purification of ubiquitin-activating enzyme. *J Biol Chem, 257(5)*, 2537-42.

Ciechanover, A., Finley, D., & Varshavsky, A. (1984). The ubiquitin-mediated proteolytic pathway and mechanisms of energy- dependent intracellular protein degradation. *J Cell Biochem, 24(1)*, 27-53.

Ciechanover, A., Heller, H., Katz-Etzion, R., & Hershko, A. (1981). Activation of the heat-stable polypeptide of the ATP-dependent proteolytic system. *Proc Natl Acad Sci U S A, 78(2)*, 761-65.

Clamp, M.E., Baker, P.G., Stirling, C.J., Brass, A. (1994). Hybrid Monte Carlo: an efficient algorithm for condensed matter simulation. *J Comput Chem, 15*, 838-46.

Cook, W. J., Jeffrey, L. C., Carson, M., Chen, Z., & Pickart, C. M. (1992). Structure of a diubiquitin conjugate and a model for interaction with ubiquitin conjugating enzyme (E2). *J Biol Chem, 267(23)*, 16467-71.

Cook, W. J., Jeffrey, L. C., Kasperek, E., & Pickart, C. M. (1994). Structure of tetraubiquitin shows how multiubiquitin chains can be formed. *J Mol Biol, 236(2)*, 601-09.

Cook, W. J., Jeffrey, L. C., Sullivan, M. L., & Vierstra, R. D. (1992). Three-dimensional structure of a ubiquitin-conjugating enzyme (E2). *J Biol Chem, 267(21)*, 15116-21.

Cook, W. J., Jeffrey, L. C., Xu, Y., & Chau, V. (1993). Tertiary structures of class I ubiquitin-conjugating enzymes are highly conserved: crystal structure of yeast Ubc4. *Biochemistry, 32(50)*, 13809-17.

Cook, W. J., Martin, P. D., Edwards, B. F., Yamazaki, R. K., & Chau, V. (1997). Crystal structure of a class I ubiquitin conjugating enzyme (Ubc7) from Saccharomyces cerevisiae at 2.9 angstroms resolution. *Biochemistry, 36(7)*, 1621-27.

Creighton, T. E. (1992). *Protein Folding*. New York, New York: W. H. Freeman.

Cummings, M. D., Hart, T. N., & Read, R. J. (1995). Monte Carlo docking with ubiquitin. *Protein Sci, 4(5)*, 885-99.

Delano, W. L. (2002). The PyMOL Molecular Graphics System. from http://www.pymol.org

Deveraux, Q., Wells, R., & Rechsteiner, M. (1990). Ubiquitin metabolism in ts85 cells, a mouse carcinoma line that contains a thermolabile ubiquitin activating enzyme. *J Biol Chem, 265(11)*, 6323-29.

Ecker, D. J., Butt, T. R., Marsh, J., Sternberg, E. J., Margolis, N., Monia, B. P., Jonnalagadda, S., Khan, M. I., Weber, P. L., Mueller, L., & et, a. (1987). Gene synthesis, expression, structures, and functional activities of site-specific mutants of ubiquitin. *J Biol Chem, 262(29)*, 14213-21.

Ferguson, D. M., & Raber, D. J. (1989). A New Approach to Probing Conformational Space with Molecular Mechanics Random Incremental Pulse Search. *J. Am. Chem. Soc., 111*, 4371-78.

Finley, D., Ciechanover, A., & Varshavsky, A. (1984). Thermolability of ubiquitin-activating enzyme from the mammalian cell cycle mutant ts85. *Cell, 37(1)*, 43-55.

Fletcher, R., & Reeves, C. C. J. (1964). *Computer Journal, 7*, 81-84.

Fraczkiewicz, R., & Braun, W. (1998). Exact and efficient analytical calculation of the accessible surface areas and their gradients for macromolecules. *J. Comp. Chem., 1998*, 319.

Furukawa, K., Mizushima, N., Noda, T., & Ohsumi, Y. (2000). A protein conjugation system in yeast with homology to biosynthetic enzyme reaction of prokaryotes. *J Biol Chem, 275(11)*, 7462-65.

Gething, M. J., & Sambrook, J. (1992). Protein folding in the cell. *Nature, 355(6355)*, 33-45.

Gong, L., & Yeh, E. T. (1999). Identification of the activating and conjugating enzymes of the NEDD8 conjugation pathway. *J Biol Chem, 274(17)*, 12036-42.

Grundy, J. E., Wirtanen, L. Y., & Beauregard, M. (1998). Addition of a poly-(6X) His tag to Milk Bundle-1 and purification using immobilized metal-affinity chromatography. *Protein Expr Purif, 13(1)*, 61-66.

Haas, A. L., & Rose, I. A. (1982). The mechanism of ubiquitin activating enzyme. A kinetic and equilibrium analysis. *J Biol Chem, 257(17)*, 10329-37.

Haas, A. L., Warms, J. V., Hershko, A., & Rose, I. A. (1982). Ubiquitin-activating enzyme. Mechanism and role in protein-ubiquitin conjugation. *J Biol Chem, 257(5)*, 2543-48.

Haas, A. L., Warms, J. V., & Rose, I. A. (1983). Ubiquitin adenylate: structure and role in ubiquitin activation. *Biochemistry, 22(19)*, 4388-94.

Hamilton, K. S., Ellison, M. J., Barber, K. R., Williams, R. S., Huzil, J. T., McKenna, S., Ptak, C., Glover, M., & Shaw, G. S. (2001). Structure of a conjugating enzyme-ubiquitin thiolester intermediate reveals a novel role for the ubiquitin tail. *Structure (Camb), 9(10)*, 897-904.

Hart, T. N., & Read, R. J. (1992). A multiple-start Monte Carlo docking method. *Proteins, 13*, 206-22.

Hartl, F. U. (1996). Molecular chaperones in cellular protein folding. *Nature, 381(6583)*, 571-79.

Hershko, A., Heller, H., Elias, S., & Ciechanover, A. (1983). Components of ubiquitin-protein ligase system. Resolution, affinity purification, and role in protein breakdown. *J Biol Chem, 258(13)*, 8206-14.

Higgins, D. G., & Sharp, P. M. (1988). CLUSTAL: a package for performing multiple sequence alignment on a microcomputer. *Gene, 73(1)*, 237-44.

Hill, C. P., Johnston, N. L., & Cohen, R. E. (1993). Crystal structure of a ubiquitin-dependent degradation substrate: a three-disulfide form of lysozyme. *Proc Natl Acad Sci U S A, 90(9)*, 4136-40.

Hodgins, R., Gwozd, C., Arnason, T., Cummings, M., & Ellison, M. J. (1996). The tail of a ubiquitin-conjugating enzyme redirects multi-ubiquitin chain synthesis from the lysine 48-linked configuration to a novel nonlysine-linked form. *J Biol Chem, 271(46)*, 28766-71.

Hodgins, R. R., Ellison, K. S., & Ellison, M. J. (1992). Expression of a ubiquitin derivative that conjugates to protein irreversibly produces phenotypes consistent with a ubiquitin deficiency. *J Biol Chem, 267(13)*, 8807-12.

Huang, L., Kinnucan, E., Wang, G., Beaudenon, S., Howley, P. M., Huibregtse, J. M., & Pavletich, N. P. (1999). Structure of an E6AP-UbcH7 complex: insights into ubiquitination by the E2-E3 enzyme cascade. *Science, 286(5443)*, 1321-26.

Janin, J., Miller, S., & Chothia, C. (1988). Surface, subunit interfaces and interior of oligomeric proteins. *J Mol Biol, 204*, 155-64.

Jaroszewski, L.,, L., R., Zhang, B., & Godzik, A. (1998). Fold Prediction by a hierarchy of sequence, threading, and modeling methods. *Protein Science, 7*, 1431-40.

Johnston, S. C., Larsen, C. N., Cook, W. J., Wilkinson, K. D., & Hill, C. P. (1997). Crystal structure of a deubiquitinating enzyme (human UCH-L3) at 1.8 A resolution. *Embo J, 16(13)*, 3787-96.

Jonnalagadda, S., Ecker, D. J., Sternberg, E. J., Butt, T. R., & Crooke, S. T. (1988). Ubiquitin carboxyl-terminal peptides. Substrates for ubiquitin activating enzyme. *J Biol Chem, 263(11)*, 5016-19.

Kawakami, T., Chiba, T., Suzuki, T., Iwai, K., Yamanaka, K., Minato, N., Suzuki, H., Shimbara, N., Hidaka, Y., Osaka, F., Omata, M., & Tanaka, K. (2001). NEDD8 recruits E2-ubiquitin to SCF E3 ligase. *EMBO J, 20(15)*, 4003-12.

Kim, K. I., Baek, S. H., & Chung, C. H. (2002). Versatile protein tag, SUMO: its enzymology and biological function. *J Cell Physiol, 191(3)*, 257-68.

Kretz-Remy, C., & Tanguay, R. M. (1999). SUMO/sentrin: protein modifiers regulating important cellular functions [In Process Citation]. *Biochem Cell Biol, 77(4)*, 299-309.

Kulka, R. G., Raboy, B., Schuster, R., Parag, H. A., Diamond, G., Ciechanover, A., & Marcus, M. (1988). A Chinese hamster cell cycle mutant arrested at G2 phase has a temperature-sensitive ubiquitin-activating enzyme, E1. *J Biol Chem, 263(30)*, 15726-31.

Lake, M. W., Wuebbens, M. M., Rajagopalan, K. V., & Schindelin, H. (2001). Mechanism of ubiquitin activation revealed by the structure of a bacterial MoeB-MoaD complex. *Nature, 414(6861)*, 325-9..

Laskowski, R. A., MacArthur, M. W., Moss, D. S., & Thornton, J. M. (1993). PROCHECK: a program to check the stereochemical quality of protein structures. *J. Appl. Cryst., 26*, 283-91.

Leimkuhler, S., Wuebbens, M. M., & Rajagopalan, K. V. (2001). Characterization of Escherichia coli MoeB and its involvement in the activation of molybdopterin synthase for the biosynthesis of the molybdenum cofactor. *J Biol Chem, 276(37)*, 34695-701.

Liakopoulos, D., Doenges, G., Matuschewski, K., & Jentsch, S. (1998). A novel protein modification pathway related to the ubiquitin system. *Embo J, 17(8)*, 2208-14.

Lin, Y., Hwang, W. C., & Basavappa, R. (2002). Structural and functional analysis of the human mitotic-specific ubiquitin-conjugating enzyme, UbcH10. *J Biol Chem, 277(24)*, 21913-21.

Luthy, R., Bowie, J. U., & Eisenberg, D. (1992). Assessment of protein models with three-dimensional profiles. *Nature, 356(6364)*, 83-85.

McGrath, J. P., Jentsch, S., & Varshavsky, A. (1991). UBA 1: an essential yeast gene encoding ubiquitin-activating enzyme. *Embo J, 10(1)*, 227-36.

Metropolus, N., Rosenbluth, A. W., Rosenbluth, M. N., & Teller, A. H. (1953). Equation of State Calculations by Fast Computing Machines. *J. Chem. Phys., 21*, 1087-92.

Miller, S. (1989). The structure of interfaces between subunits of dimeric and tetrameric proteins. *Protein Eng, 3*, 77-83.

Mizushima, N., Noda, T., Yoshimori, T., Tanaka, Y., Ishii, T., George, M. D., Klionsky, D. J., Ohsumi, M., & Ohsumi, Y. (1998). A protein conjugation system essential for autophagy. *Nature, 395(6700)*, 395-98.

Moraes, T. F., Edwards, R. A., McKenna, S., Pastushok, L., Xiao, W., Glover, J. N., & Ellison, M. J. (2001). Crystal structure of the human ubiquitin conjugating enzyme complex, hMms2-hUbc13. *Nat Struct Biol, 8(8)*, 669-73.

Mori, M., Eki, T., Takahashi-Kudo, M., Hanaoka, F., Ui, M., & Enomoto, T. (1993). Characterization of DNA synthesis at a restrictive temperature in the temperature-sensitive mutants, tsFT5 cells, that belong to the complementation group of ts85 cells containing a thermolabile ubiquitin-activating enzyme E1. Involvement of the ubiquitin-conjugating system in DNA replication. *J Biol Chem, 268(22)*, 16803-09.

Morimoto, R. I., Tissieres, A., & Georgopolous, C. (1994). The Biology of Heat Shock Proteins and Molecular Chaperones. In Morimoto, R. I., Tissieres, A., & Georgopolous, C.(pp. 1-30). Cold Spring Harbor, NewYork: Cold Spring Harbor Laboratories Press.

Morris, A. L., MacArthur, M. W., Hutchinson, E. G., & Thornton, J. M. (1992a). Stereochemical quality of protein structure coordinates. *Proteins, 12*, 345-64.

Morris, A. L., MacArthur, M. W., Hutchinson, E. G., & Thornton, J. M. (1992b). Stereochemical quality of protein structure coordinates. *Proteins, 12(4)*, 345-64.

Nicholls, A., Sharp, K., & Honig, B. (1991). *PROTEINS, Structure, Function and Genetics, 11(4)*, 281.

Osaka, F., Saeki, M., Katayama, S., Aida, N., Toh-E, A., Kominami, K., Toda, T., Suzuki, T., Chiba, T., Tanaka, K., & Kato, S. (2000). Covalent modifier NEDD8 is essential for SCF ubiquitin-ligase in fission yeast. *EMBO J, 19(13)*, 3475-84.

Pabo, C. O., & Suchanek, E. G. (1986). Computer-aided model-building strategies for protein design. *Biochemistry, 25(20)*, 5987-91.

Peitsch, M. C. (1996). ProMod and Swiss-Model: Internet-based tools for automated comparative protein modeling. *Biochem Soc Trans, 24(1)*, 274-79.

Pickart, C. M. (2001). Mechanisms underlying ubiquitination. *Annu Rev Biochem, 70*, 503-33.

Pickart, C. M., Kasperek, E. M., Beal, R., & Kim, A. (1994). Substrate properties of site-specific mutant ubiquitin protein (G76A) reveal unexpected mechanistic features of ubiquitin-activating enzyme (E1). *J Biol Chem, 269(10)*, 7115-23.

Powell, M. J. D. (1977). *Mathematical Programming, 12*, 241-54.

Rajagopalan, K. V. (1996). Biosynthesis of the molybdenum cofactor. *Escherichia coli and Salmonella: Cellular and Molecular Biology, 1*, 674-79.

Ramachandran, G. N., Ramakrishnan, C., & Sasiekharan, V. (1963). Stereochemistry of Polypeptide Chain Configuration. *Journal of Molecular Biology, 7*, 95-99.

Ripoll, D. R., & Scheraga, H. A. (1989). The multiple-minima problem in the conformational analysis of polypeptides. III. An electrostatically driven Monte Carlo method: tests on enkephalin. *J Protein Chem, 8(2)*, 263-87.

Rosenbach, D., & Rosenfeld, R. (1995). Simultaneous modeling of multiple loops in proteins. *Protein Sci, 4(3)*, 496-505.

Schlick, T., Barth, E., & Mandziuk, M. (1997). Biomolecular dynamics at long timesteps: bridging the timescale gap between simulation and experimentation. *Annu Rev Biophys Biomol Struct, 26*, 181-222.

Schwede, T., Kopp, J., Guex, N., & Peitsch, M. C. (2003). SWISS-MODEL: an automated protein homology-modeling server. *Nucleic Acids Res, 31(13)*, 3381-85.

Swanson, R., & Hochstrasser, M. (2000). A viable ubiquitin-activating enzyme mutant for evaluating ubiquitin system function in Saccharomyces cerevisiae. *FEBS Lett, 477(3)*, 193-98.

Tabor, S., & Richardson, C. C. (1985). A bacteriophage T7 RNA polymerase/promoter system for controlled exclusive expression of specific genes. *Proc Natl Acad Sci U S A, 82(4)*, 1074-78.

Tanida, I., Tanida-Miyake, E., Ueno, T., & Kominami, E. (2001). The human homolog of Saccharomyces cerevisiae Apg7p is a Protein-activating enzyme for multiple substrates including human Apg12p, GATE-16, GABARAP, and MAP-LC3. *J Biol Chem, 276(3)*, 1701-06.

Taylor, S. V., Kelleher, N. L., Kinsland, C., Chiu, H. J., Costello, C. A., Backstrom, A. D., McLafferty, F. W., & Begley, T. P. (1998). Thiamin biosynthesis in Escherichia coli. Identification of this thiocarboxylate as the immediate sulfur donor in the thiazole formation. *J Biol Chem, 273(26)*, 16555-60.

Tong, H., Hateboer, G., Perrakis, A., Bernards, R., & Sixma, T. K. (1997). Crystal structure of murine/human Ubc9 provides insight into the variability of the ubiquitin-conjugating system. *J Biol Chem, 272(34)*, 21381-87.

Vakser, I. A. (1995). Protein docking for low-resolution structures. *Protein Eng, 8*, 371-77.

VanDemark, A. P., Hofmann, R. M., Tsui, C., Pickart, C. M., & Wolberger, C. (2001). Molecular insights into polyubiquitin chain assembly: crystal structure of the Mms2/Ubc13 heterodimer. *Cell, 105(6)*, 711-20.

Vernet, T., Tessier, D. C., Chatellier, J., Plouffe, C., Lee, T. S., Thomas, D. Y., Storer, A. C., & Menard, R. (1995). Structural and functional roles of asparagine 175 in the cysteine protease papain. *J Biol Chem, 270(28)*, 16645-52.

Vijay-Kumar, S., Bugg, C. E., & Cook, W. J. (1987). Structure of ubiquitin refined at 1.8 A resolution. *J Mol Biol, 194(3)*, 531-44.

Walden, H., Podgorski, M. S., & Schulman, B. A. (2003). Insights into the ubiquitin transfer cascade from the structure of the activating enzyme for NEDD8. *Nature, 422(6929)*, 330-34.

Walker, J. E., Eberle, A., Gay, N. J., Runswick, M. J., & Saraste, M. (1982). Conservation of structure in proton-translocating ATPases of Escherichia coli and mitochondria. *Biochem Soc Trans, 10(4)*, 203-06.

Weiner, S. J., Kollman, P. A., Nguyen, D. T., & Case, D. A. (1986). An All Atom Force Field for Simulations of Proteins and Nucleic Acids. *J. Comp. Chemistry, 7*, 230.

Wierenga, R. K., & Hol, W. G. (1983). Predicted nucleotide-binding properties of p21 protein and its cancer-associated variant. *Nature, 302(5911)*, 842-44.

Worthylake, D. K., Prakash, S., Prakash, L., & Hill, C. P. (1998). Crystal structure of the Saccharomyces cerevisiae ubiquitin-conjugating enzyme Rad6 at 2.6 A resolution. *J Biol Chem, 273(11)*, 6271-76.

Wymore, T., Nicholas, H. B., & Hempel, J. (2001). Molecular dynamics simulation of class 3 aldehyde dehydrogenase. *Chem Biol Interact, 130-132(1-3)*, 201-7..

Xi, J., Ge, Y., Kinsland, C., McLafferty, F. W., & Begley, T. P. (2001). Biosynthesis of the thiazole moiety of thiamin in Escherichia coli: identification of an acyldisulfide-linked protein--protein conjugate that is functionally analogous to the ubiquitin/E1 complex. *Proc Natl Acad Sci U S A, 98(15)*, 8513-18.

Yeh, E. T., Gong, L., & Kamitani, T. (2000). Ubiquitin-like proteins: new wines in new bottles. *Gene, 248(1-2)*, 1-14.

Zagrovic, B., Snow, C. D., Khaliq, S., Shirts, M. R., & Pande, V. S. (2002a). Native-like mean structure in the unfolded ensemble of small proteins. *J Mol Biol, 323(1)*, 153-64.

Zagrovic, B., Snow, C. D., Shirts, M. R., & Pande, V. S. (2002b). Simulation of folding of a small alpha-helical protein in atomistic detail using worldwide-distributed computing. *J Mol Biol, 323(5)*, 927-37.

Zagrovic, B., Sorin, E. J., & Pande, V. (2001). Beta-hairpin folding simulations in atomistic detail using an implicit solvent model. *J Mol Biol, 313(1)*, 151-69.

Zheng, N., Wang, P., Jeffrey, P. D., & Pavletich, N. P. (2000). Structure of a c-Cbl-UbcH7 complex: RING domain function in ubiquitin-protein ligases. *Cell, 102(4)*, 533-39.

Chapter 5

Uba1's Role in Multi-Ubiquitin Chain Formation

5.1 Introduction

For any protein to become degraded by the ubiquitin system, it must first be recognized by the proteasome (Hough and Rechsteiner, 1986; Hough *et al.*, 1986; Gregori *et al.*, 1990). This requires the protein to first become tagged with a chain of ubiquitin (Ub) molecules in a reaction cascade that begins with the activation of Ub by the Ubiquitin Activating Enzyme (Uba1) (Haas and Rose, 1982; Haas *et al.*, 1982; Ciechanover *et al.*, 1984; Chau *et al.*, 1989). The current hypothesis places Uba1 in the role of Ub activation and the subsequent transfer of this activated Ub to a ubiquitin conjugating enzyme (Ubc or E2) (Hershko, 1983). The formation of the Ub chain and recognition of target proteins is then believed to occur independently of Uba1, through the action of the E2 and, in some cases a ubiquitin protein ligase (E3).

The ability for Ub to form a chain is made possible by the fact that, Ub is itself included among known ubiqutination targets. Ubiquitin molecules are linked to each other through the formation of an isopeptide bond to an internal lysine residue (Chapter 1, Figure 7) (Zhu *et al.*, 1986; Chau *et al.*, 1989; Spence *et al.*, 1995). While the typical mechanism of Ub chain formation involves the conjugation of Ub to a target protein, *in vitro* studies have shown that the conjugation of free Ub to a previously activated Ub can lead to the formation of free chains (Chen and Pickart, 1990; van Nocker and Vierstra, 1991). These Ub chains are then competent for activation at the primary Ub's carboxy terminus by Uba1 and can subsequently be transferred to an E2 (Chen and Pickart, 1990).

This result implies that these free Ub chains are not constructed on target proteins, as they are found in their unbound state. In addition to their production *in vitro*, these un-conjugated Ub chains have also been reported in the cytoplasm of *S. cerevisiae*, suggesting that similar reaction mechanisms exist *in vivo* (Haldeman *et al.*, 1995). This description alludes to the complexity that is inherent within the mechanism of protein ubiqutination.

While the precise mechanism for Ub chain building has yet to be elucidated, studies have shown that Ubc1Δ, a carboxy terminal deletion of *S. cerevisiae* Ubc1, is capable of auto-ubiqutination, and the generation of a multi-Ub chain linked to an internal lysine residue (residue 93) on Ubc1Δ (Hodgins *et al.*, 1996). While this reaction has been shown to occur independently of Uba1, data presented here, show that the presence of Uba1 significantly increases the rate of this reaction. This suggests interplay between the active sites of Uba1 and Ubc1Δ that allows the intermolecular transfer of Ub between the two proteins during Ub chain building. The presence of short, target independent, Ub chains and the ability of Uba1 to activate them and facilitate their transfer to an E2, also imply that Uba1 may not simply be responsible for the activation of single Ub molecules. Uba1 would then play another role in Ub chain formation, activating short chains, commonly found within the cytoplasm, and through some yet unknown mechanism facilitate their conjugation to a growing chain found on an E2 (Johnson 1995, Johnson 1992, Chau 1989 Rechsteiner 1986).

Experiments introduced in this chapter along with results presented in Chapter 3, suggest that Uba1 and Ubc1Δ form a high molecular weight complex that may participate in the construction of Ub chains *in vivo*. The presence of such a complex is not surprising, since Ub must become transferred between Uba1 and Ubc1Δ in order to form the Ub~Ubc1Δ thiolester (Chapter 2). We suggest two possible mechanisms for the formation of multi-Ub chains. The first involves the intermolecular transfer of Ub between Uba1 and Ubc1 and the creation of a Ub chain upon either molecule which can then be transferred to a target protein, or alternatively, the catalytic participation of Uba1 in the conjugation of subsequent Ub moieties to the growing chain.

5.2 Experimental Procedures

Plasmids and Strains

Please see Chapter 2, *Plasmids and Strains* for a description of all *S. cerevisiae* and *E. coli* plasmids and strains used throughout this chapter.

Protein Expression and Purification

Please see Chapter 3, *Protein Expression and Purification* for a description of the expression and purification methods for Uba1, uba1C600A, uba1G446V, Ubc1Δ and Ub. The expression and purification of recombinant Ub_{C48} has been previously described by Gregori et al. (1990).

Formation of the Uba1~[^{35}S]Ub Thiolester

The Uba1~[^{35}S]Ub thiolester was prepared as described in Chapter 3, *Back-transfer Reactions*, with two exceptions. First, reactions contained 300 nM Ubc1Δ~[^{35}S]Ub and 300 nM Uba1. Second, following completion of the reaction, samples were loaded onto a Superdex 75 16/30 gel exclusion column equilibrated with buffer C (50 mM HEPES (pH 7.5), 150 mM NaCl, 1 mM EDTA). Peak fractions (fractions 15 to 25) were analyzed using SDS-PAGE containing DTT, to cleave thiolester, and visualized using autoradiography. Peaks containing the labile Uba1~Ub thiolester were pooled and concentrated by Centricon (Amicon) filtration to a final concentration of 200 nM, as determined by scintillation counting.

Purification and Stability of the Ubc1Δ~[^{35}S]Ub, Ubc1Δ~Ub and Ubc1Δ~Ub_{C48} Thiolesters

Ubc1Δ~Ub thiolester was purified as described in Chapter 3, *Purification and stability of the Ubc1Δ~Ub thiolester*, with the exception that either Ub, [^{35}S]Ub or Ub_{C48} were used as the Ub source.

Formation of Ubc1Δ-Ub and Ubc1Δ-Ub_{C48} Conjugates

Purification of the mono-ubiqutinated Ubc1Δ-Ub conjugates (Ubc1Δ-Ub, Ubc1Δ-Ub_{C48}) was identical to the method used in *Ubc1Δ~Ub Thiolester Purification* except for the following alterations. First, either Ub or Ub_{C48} (a Ub mutant in

which the canonical internal lysine residue has been changed to a cysteine) were used in place of [^{35}S]Ub. Second, the reactions were incubated at 30°C for 16 hours rather than 5 hours. Following incubation, DTT was added to the reactions to a final concentration of 100 mM in order to cleave any thiolester present. The reaction was then incubated for an additional hour, at 30°C, in the presence of DTT and loaded onto a Superdex 75 16/30 gel exclusion column equilibrated with buffer C. The same buffer C, was then used to elute the sample from the Superdex column. Peak fractions (fractions 64-67) were analyzed by SDS-PAGE to determine those that contained Ubc1Δ-Ub conjugates. The fractions were then pooled and concentrated by Centricon filtration and assayed for protein concentration using a standard BCA colorimetric assay (Pierce).

Iodoacetamide Treatment of Ubc1Δ-Ub Conjugates

Iodoacetamide acetylates sulfhydryl groups, rendering them inactive. To promote inactivation of the Ubc1Δ-Ub conjugate following its purification, described in *Formation of Ubc1Δ-Ub Conjugates*, approximately 200 μg of purified conjugate was incubated with a 1000x molar excess of iodoacetamide at 30 °C for 1 hour (Jones *et al.*, 1975; Haas *et al.*, 1982; Hershko *et al.*, 1983). The sample was then dialyzed for 3 hours against 4 L of buffer C (50 mM HEPES (pH 7.5), 150 mM NaCl, 1 mM EDTA). The dialyzate was then concentrated using 10,000 mw cutoff Centricon centrifuge tubes and the protein concentration was determined as described in *Protein Expression and Purification.*

In vitro Ubiquitination Reactions

Ubiquitination assays, unless stated otherwise, were carried out in ubiqutination buffer consisting of: 10 mM HEPES (pH 7.5), 5 mM $MgCl_2$, 40 mM NaCl, 5 mM ATP, and protease inhibitors (*antipain*, *aprotinin*, *chymostatin*, *leupeptin*, *pepstatin A* at 20 μg/ml and PMSF at 180 μg/ml). The ubiqutination buffer also included inorganic pyrophosphatase (0.6 units/ml) to remove PPi, which has been shown to inhibit the ubiquitination reaction (Haas and Rose, 1982).

Ubc1Δ~Ub Thiolester Chain Formation

Reactions were performed in ubiqutination buffer, with or without ATP. The reactions contained 100 nM purified Ubc1Δ~[^{35}S]Ub and 10 nM Uba1. Reactions were incubated at 30 C for 12 hours, after which they were stopped by addition of a 1/10th volume of ice-cold trichloroacetic acid (TCA). Samples were then centrifuged and the supernatant was decanted. The pellet was suspended in SDS load mix that contained DTT to disrupt thiolester and leave only conjugated Ub species. Samples were then boiled for 10 minutes and ubiquitinated proteins separated by SDS PAGE. Following electrophoresis, the gel was dried and visualized by autoradiography using a Fuji Film phosphoimager.

Time Course of Ub Chain Formation

Three separate reactions were performed, as in *Ubc1Δ~Ub Thiolester Chain Formation*, with the exception that one reaction was performed in ubiqutination buffer lacking Mg^{2+} and one was performed in ubiqutination buffer lacking Mg^{2+} and ATP. Aliquots were removed after 0, 1, 2, 4, 8 and 12 hours. Immediately following their removal from the reaction mixture, aliquots were processed as in *Ubc1Δ~Ub Thiolester Chain Formation*. In this case protein pellets were not suspended in SDS load buffer, but were frozen at -80 C. After all the time points had been collected, the frozen samples were thawed and resuspended in SDS load mix and subjected to SDS PAGE and autoradiography.

Densitometry of Ub Gels

Densitometry analysis of gels containing [^{35}S]Ub was performed to compare the quantity of Ub in the Ubc1Δ-Ub conjugate to the quantity of Ub in Ub chains (Figure 5.2). The gel was scanned using a Fuji Film phosphoimager, the scan was imported into MacBas (Fuji Film) and the relative density of each band was measured. The density in each lane was totaled and used to calculate the amount of Ub in each band. The clean laddering of Ub chains, made it easy to calculate the ratio of Ub in Ubc1Δ-Ub to Ub in the remainder of the chain. The total density for each species was calculated and plotted in Figure 5.3.

Transfer of Ub from Uba1~[^{35}S]Ub to Ub Chains

Reactions demonstrating the transfer of [^{35}S]Ub from Uba1 to Ub chains were performed in a similar way to that described above, *Ubc1Δ~Ub Thiolester Chain Formation*. The Uba1~[^{35}S]Ub thiolester was purified using a back transfer reaction as described previously. Reactions were performed in ubiquitination buffer with 100 nM Ubc1Δ~Ub thiolester or Ubc1Δ-Ub conjugate. Reaction times were 1 hour at 30 °C, after which they were treated as in *Ubc1Δ~Ub Thiolester Chain Formation*.

5.3 Results

Stimulation of Ub Chain Formation by Uba1

If Ubc1Δ~[^{35}S]Ub is concentrated and left to react with itself, an auto-ubiqutination reaction occurs, resulting in the formation of Ubc1Δ-[^{35}S]Ub conjugate, demonstrating Ubc1's role as both an E2 and target in the Ub system (Figure 5.1, lane 1) (Hodgins *et al.*, 1996). Figure 5.1 clearly demonstrates the stimulation of Ub chain formation upon addition of Uba1 to reactions containing only purified Ubc1Δ~[^{35}S]Ub thiolester. When Uba1 was introduced into a reaction containing only the Ubc1Δ~[^{35}S]Ub thiolester in ubiquitination buffer, there was a significant increase in the length and number of Ub chains formed (Figure 5.1, lane 2). This reaction resulted in the construction of Ub chains on Ubc1Δ of at least eight molecules in length. If an identical reaction is performed to that in lane 2, but ATP is omitted from the ubiquitination buffer, there is a slight decrease in the number of Ub molecules added into these chains (Figure 5.1, Lane 3).

The decrease of Ub chain formation following the omission of ATP from the reaction cocktail led us to investigate the role of ATP in this reaction. The effect of ATP and Mg^{2+} on the transfer of Ub from Uba1 to E2 was demonstrated in Chapter 2 (Pickart *et al.*, 1994). To determine if ATP or Mg^{2+} was capable of altering the ability of Uba1 to facilitate multi-Ub chain formation, we performed a series of time course reactions. These reactions contained Uba1 and the Ubc1~[^{35}S]Ub thiolester under three conditions: 1) the presence of both Mg^{2+} and

ATP, 2) the absence of Mg^{2+} and 3) the absence of both Mg^{2+} and ATP. Figure 4.2A represents standard ubiqutination reactions, which produced chains of at least eight Ub in length following a 12 hour reaction. Reactions that did not contain Mg^2 or ATP, led to slightly reduced chain lengths of six Ub and an overall decrease in band intensity, indicating lower overall amounts of Ub (Figure 5.2B and C).

To resolve small differences in the levels of [^{35}S]Ub incorporated into Ub chains, densitometry was performed on the gel produced in Figure 5.2. The density of each band was measured and the amount of [^{35}S]Ub incorporated into the Ubc1Δ-[^{35}S]Ub conjugate and Ub chains was calculated as described in *Densitometry of Ub Gels*, the results of these calculations are displayed in Figure 5.3. The analysis of the densitometry results revealed an interesting phenomenon regarding the participation of Uba1 and the requirement of ATP and Mg^{2+} in the formation of the Ubc1Δ-Ub conjugate and in the stimulation of higher molecular weight Ub chains. The absence of both ATP and Mg^{2+} resulted in approximately 10% conversion from the Ubc1Δ~Ub thiolester to the Ubc1-Ub conjugate following the 12 hour reaction (Figure 5.3A). This value increased to 15% when Mg^{2+} is added to the reaction and to 20% when both Mg and ATP were present. While there is a large variability in the levels of the Ubc1Δ-[^{35}S]Ub conjugate upon addition of ATP and Mg^{2+}, this effect is more dramatic with respect to the formation of Ub chains (Figure 5.2B). There is a significant enhancement in the overall formation of Ub chains when ATP and Mg^{2+} are both present in the reaction, increasing more than two fold.

The Effect of Uba1 Mutants on Ub chain Formation

To accurately test the effect that Uba1 and ATP play on the formation of Ub chains we needed to use Uba1 that is incapable of either catalyzing the hydrolysis of ATP or transferring activated Ub to the active site cysteine. To accomplish this, we used the Uba1 mutants uba1C600A and uba1G446V (Chapter 2) in standard ubiquitination reactions. Figure 4.4 illustrates reactions containing either 10 nM of either Uba1, uba1C600A or uba1G446V and 100 nM Ubc1Δ~[^{35}S]Ub thiolester in the presence or absence of ATP. The formation of

Ub chains is similar to that shown in Figure 4.1 when Uba1 is introduced into the (Figure 5.4, lanes 1 and 4). Reactions containing uba1G446V, the mutant of Uba1 that is unable to catalyze the formation of the Ub-adenylate, show similar results to that of Uba1 experiments lacking ATP (Figure 5.4, lane 3). Uba1G446V reactions with and without ATP resulted in chains of approximately four Ub molecules in length, slightly shorter than the Ub chains found in reactions containing Uba1, but lacking ATP (Figure 5.4, lane 4). Uba1C600A, a Uba1 mutant in which the active site cysteine has been changed to alanine, reactions resulted in the increased formation of the Ubc1Δ-[^{35}S]Ub conjugate in reactions lacking ATP and in formation of chains at least two Ub molecules in length in reactions containing ATP (Figure 5.4, lanes 2 and 5). All of the Uba1 or mutant Uba1 containing reactions resulted in the production of free Ub_2 chains, that is chains not linked to either Ubc1Δ or Uba1, as evidenced by the faint band present on SDS gels.

Following Ub Incorporation into the Ub Chain with Ub_{myc}

While the Uba1 stimulation of Ub chain formation with the Ubc1Δ~Ub thiolester is evident from the previous experiments, the actual path that activated Ub is taking was not clear. To test if the Ub is coming from Uba1 or if it is internally transferred from Ubc1Δ, reactions were spiked with Ub_{myc}. Ub_{myc} carries the 1.5 kDa myc epitope at its amino terminus (Lohnas *et al.*, 1998) and has been previously demonstrated to support Ub chain formation (C. Ptak personal communication). This form of Ub is useful for following Ub inclusion into chains as it alters the banding pattern normally observed in ubiquitination reactions. Figure 5.5 demonstrates that upon addition of cold Ub_{myc} to reactions containing Uba1 and Ubc1~[^{35}S]Ub, the normal banding pattern changes to represent the inclusion of the higher molecular weight Ub_{myc}. Ub_{myc} can be seen as a band of slightly higher molecular weight than the normal Ub chain, resulting in the presence of two bands for each additional Ub in the chain. As expected, the Ubc1Δ-Ub conjugate contained only wild type [^{35}S]Ub, as demonstrated by the presence of only one band. All chains corresponding to two or more Ub molecules contained both the wild type [^{35}S]Ub and Ub_{myc}. As with reactions in

Figure 5.1, reactions containing Uba1 produced Ub chains approximately 7 Ub molecules in length (Figure 5.5, lane 1). Reactions containing ubc1C600A produced chains of only two Ub molecules in length (Figure 5.5, lane 2).

Inhibition of Ub Chains Following Iodoacetamide Treatment of Ubc1Δ-Ub

The result illustrating Uba1's ability to stimulate the addition of activated Ub to the growing multi-Ub chain, we thought that Uba1~Ub would also stimulate the formation of Ub chains. We tested purified Uba1~[^{35}S]Ub for its ability to facilitate the transfer Ub to purified Ubc1Δ-Ub conjugate. Uba1 supports Ub chain building on the Ubc1Δ-Ub conjugate (Figure 5.6, lane 1), however this is to a lesser extent than it supports chain building with the Ubc1Δ~Ub thiolester. This result provided the evidence required to proceed with similar reactions on iodoacetamide treated Ubc1Δ-Ub conjugates. These reactions would enable us to determine what role the active site of Ubc1Δ plays in the formation of Ub chains and if chains would be built when Ubc1Δ was not present. Figure 5.6, lane 2, clearly demonstrates the formation of Ub chains on the Ubc1Δ-Ub conjugate following inactivation of the Ubc1Δ active site cysteine with iodoacetamide. This indicates that the Ub chain is still built in the absence of the E2 active site and the Uba1 active site is the only site that the newly added Ub molecules can come from for inclusion in the chain.

We could observe the complete inhibition of Ub chain formation when Ub_{C48} was used instead of wild type Ub in the formation of Ubc1Δ-Ub conjugates; see *Formation of Ubc1Δ-Ub and Ubc1Δ-Ub_{C48} Conjugates*. In Ub_{C48} the normal lysine 48 on which the canonical Ub chain is constructed (Chau *et al.*, 1989), is replaced with cysteine. Ub_{C48} has been demonstrated to be a competent substrate for the formation of multi-Ub chains and as such should work in the chain building reactions described here (Gregori *et al.*, 1990). Reactions containing the Ubc1Δ-Ub_{C48} conjugate and Uba1~[^{35}S]Ub maintained their ability, at a reduced level, to form multi-Ub chains (Figure 5.6, lane 4). The chains were approximately three Ub molecules in length and contained less radiolabel than reactions containing wild type Ub. Treatment of active site cysteines with iodoacetamide resulted in their inactivation in ubiquitination reactions (Chapter

2). Pre-treatment of the Ubc1Δ-Ub_{C48} conjugate with iodoacetamide and its use in reactions with Uba1~[^{35}S]Ub resulted in the complete inhibition of Ub chain formation (Figure 5.6 lane 5).

5.4 Discussion

One role of Uba1 in the ubiquitin system has been clearly defined; it is required for the activation of Ub (Haas *et al.*, 1982; Haas *et al.*, 1983). Because the initial step in the activation of Ub is the formation of a Ub-AMP intermediate, there is an obvious requirement for ATP in this reaction (Haas and Rose, 1982). Once activated, Ub becomes competent for ligation to a target protein and then recognition by the proteasome, the protease responsible for degradation of Ub tagged proteins (Driscoll and Goldberg, 1990). However, before Ub becomes a specific target for the proteasome, a Ub chain must first be constructed (Chapter 1, Figure 7) (Chau *et al.*, 1989)(Nickel and Davie, 1989)(Beal *et al.*, 1996).

The path to Ub chain formation is thought to proceed by the standard "bucket brigade" mechanism (Chapter 1, Figure 6). This involves the transfer of Ub from Uba1 to an E2, which recognizes the target protein and ligates Ub to it. Once bound to the target, Ub becomes a substrate for the subsequent addition of Ub to one of its own internal lysine residues (Chau *et al.*, 1989). In this way, Ub chain formation is thought to occur after Ub has been transferred to the E2 or E3 proteins in this pathway.

The role of the E2 in the formation of Ub chains is clearly demonstrated by reactions containing purified Ubc1Δ~Ub thiolester. Standard ubiquitination reactions performed by Hodgins *et al.* (1996) demonstrate that Ubc1Δ can act as both an E2 and as a target protein. High concentrations of Ubc1Δ~Ub thiolester were shown to stimulate the autocatalytic transfer of Ub to an internal lysine within Ubc1Δ itself, resulting in the formation of a Ubc1Δ-Ub conjugate. Following formation of the Ubc1Δ-Ub conjugate, the production of Ub chains is able to occur by an, as yet uncharacterized mechanism. While the formation of multi-Ub chains in these reactions does not require the presence of Uba1, except for the initial activation of Ub, experiments presented here demonstrate that the

addition of Uba1 to the Ubc1Δ~Ub thiolester stimulates the formation of Ub chains (Figure 5.1).

Uba1 Stimulates Ub Chain Formation

Reactions in Figure 5.1 revealed a dramatic increase in the formation of Ub chains upon addition of Uba1 to a reaction containing the Ubc1Δ~Ub thiolester. In the absence of ATP there is a clear reduction in the number of Ub chains formed (Figure 5.1 lane 3). This decrease of Ub molecules introduced into Ub chains is most likely due to destabilization of the Uba1 active site cysteine (Chapter 4). In back-transfer reactions (Chapter 2, Figure 8), Ub is transferred from the Ubc1Δ thiolester back to the active site cysteine of Uba1. Back transfer reactions performed in the absence of ATP resulted in increased hydrolysis of Ub. The instability of the active site loop on Uba1, in the absence of ATP (Chapter 2, Figure 9), may block binding of Ub by the active cysteine, favoring hydrolysis of the Ub. The overall loss of activated Ub would result in a decrease in chain formation. In the presence of ATP there is very little free Ub apparent in the back transfer reaction. Stabilization of the active site loop may prevent hydrolysis of Ub and/or allow the reactivation of hydrolyzed Ub. Increased recycling of Ub, in the presence of ATP, would also result in the enhancement of Ub chain building.

Not only were these observations made with Uba1, but addition of the Uba1 mutants, uba1C600A or uba1G446V also resulted in a marked increase in the formation of Ub chains in the presence and absence of ATP (Figure 5.4). Compared to Uba1, chain building was slightly decreased in the presence of uba1G446V (Figure 5.4, lane 3), a Uba1 mutant that was previously shown to be incapable of activating Ub, but which could still accept activated Ub from Ubc1Δ~Ub (Chapter 2, Figure 8). Since uba1G446V cannot synthesize the Ub-adenylate (Chapter 2, Figure 3), these results suggest a role for the active site cysteine of Uba1 in the formation of Ub chains. Reactions containing uba1G446V, either in the presence or absence of ATP, were capable of stimulating Ub chain formation to equivalent levels of Uba1 reactions lacking ATP (Figure 5.4 lanes 3 and 6). Uba1C600A had only a limited ability to stimulate Ub

chain formation (Figure 5.4), suggesting a role for the Uba1 active site in the transfer of Ub from the Ubc1Δ~Ub thiolester to the growing Ub chain.

The time course presented in Figure 5.2 further demonstrates the involvement of Uba1 in the formation of multi-Ub chains and the importance of both ATP and Mg^{2+} in this reaction. Pickart *et al.* (1994) had previously demonstrated the involvement of ATP and Mg^{2+} in the stimulation of Ub from Uba1 to an E2. Results presented here show an overall decrease in the length and number of Ub chains formed when either Mg^{2+} or ATP are omitted from the reactions containing Ubc1Δ~Ub thiolester and Uba1 (Figure 5.2). While we have demonstrated the involvement of ATP in the stability of the Uba1 active site Cys (Chapter 4), the comparable formation of Ubc1Δ-Ub conjugate under conditions lacking either Mg^{2+} or ATP and Mg^{2+} is puzzling. We would expect that these reactions would display results similar to the levels of chain formation. The stimulation of Ubc1Δ-Ub conjugate formation in the absence of ATP and Mg^{2+}, as opposed to only Mg^{2+} may be due to ATP stabilization of the active site loop (Chapter 2), or may be a result of increased back transfer of Ub back onto the Uba1 active site Cys (Chapter 2, figure 8).

The absence of Ub chains in reactions containing Ubc1Δ~Ub thiolester and lacking Uba1 (Figure 5.1, lane 1 and 7) may be due to the significantly decreased concentrations of thiolester used in these reactions (Hodgins *et al.*, 1996). The auto-ubiqutination and formation of multi-Ub chains on Ubc1Δ itself was shown to require concentrations of Ubc1Δ~Ub thiolester in the micromolar range. All reactions presented in this chapter used Ubc1Δ~Ub at nanomolar concentrations. At these low concentrations of Ubc1~Ub thiolester, it is common to see only the intramolecular transfer of Ub from the Ubc1~Ub thiolester to its internal Lys 93 residue (Personal observation; Figure 5.1, lane 1).

Free Ub_2 Chains

All chain building reactions, which included Uba1 or a Uba1 mutant, resulted in an increase in the number and length of Ub chains, but also resulted in the formation of free Ub_2 chains. Free Ub_2 chains are seen as a faint band just

above the free Ub band on SDS gels. These free Ub_2 conjugates may be a by-product of the Uba1 stimulation of Ub chain formation, as they are only observed upon inclusion of Uba1 to these reactions. The presence of free Ub_2 chains has been observed following ubiqutination reactions *in vitro* (Discussed here) and *in vivo* (van Nocker and Vierstra, 1993). As Ubs are transferred between the active sites of Uba1 and E2, it is easy to imagine a Ub molecule becoming conjugated to another while it is still bound at an active site cysteine. This would result in the formation of a thiolester bound Ub_2 conjugate, the hydrolysis of which would produce a free Ub_2 molecule.

The appearance of the free Ub_2 chains seems to be independent of ATP, or even the presence of a Uba1 active site (Figure 5.4), but still requires the presence of Uba1 itself. This may suggest a role for their transfer to the active site of Uba1 for ultimate inclusion in a growing Ub chain on Ubc1Δ . While the formation of free Ub_2 chains may not require the presence of the Uba1 active site cysteine residue, the actual mechanism of Ub chain formation seems to hold a place for it.

Direction of Ub Transfer

All of the experiments conducted with Ubc1Δ~[^{35}S]Ub thiolester have used Ub that was already covalently linked to Ubc1Δ. These experiments did not allow us to follow the path that Ub was taking when as it became conjugated to the Ub chain. From the experiments conducted with free Ub_{myc} (Figure 5.5) it is clear that free Ub is preferentially included in the growing Ub chain. Each band in the gel represents an additional Ub that has been added on to the growing chain. This is a series of steps that starts with the formation of the Ubc1Δ-Ub conjugate. The only [^{35}S]Ub in this reaction, and therefore the only species that we can observe on the gel, is found on Ubc1Δ as the Ub thiolester. For this reason, we are unable to observe any Ub_{myc} that has been incorporated as the initial Ubc1Δ-Ub conjugate and we only observe the Ubc1Δ-[^{35}S]Ub. All of the higher molecular weight Ub chains contain two bands, one corresponding to chains having wild type Ub and the higher of the two containing Ub_{myc}. From the band corresponding to the Ubc1Δ-Ub_2, we can infer that the Ub_{myc} is preferentially being added to the chain because of the greater density of the higher molecular

weight band, which contains one [^{35}S]Ub and one Ub_{myc}. Once the Ubc1Δ-[^{35}S]Ub conjugate is formed, the Ub_{myc}, which is only found only as the thiolester on Uba1, would become transferred as opposed to the [^{35}S]Ub that is found on the Ubc1Δ as the thiolester. The difference in band density between the Ubc1Δ-[^{35}S]Ub-Ub_{myc} and the Ubc1Δ-[^{35}S]Ub_2 require a large population of the Ubc1Δ-[^{35}S]Ub being utilized to form a Ubc1Δ-[^{35}S]Ub-Ub_{myc} conjugate, as the Ub_{myc} is unlabeled and can not contribute to the increase in radiolabel in the higher band.

While it is not specifically clear what ratios of Ub:Ub_{myc} are present in the bands corresponding to chains of three Ub molecules and greater, it is clear that the higher molecular weight chains in each band are made preferentially over the lower molecular weight chains. This, again, implies that the Ub_{myc} is preferentially introduced into the chain, as opposed to [^{35}S]Ub. This effect, while not as obvious, also occurs when the uba1C600A is used in these reactions (Figure 5.5, lane 2). However, the absence of the active site cysteine significantly decreased the length of chains generated in this reaction, as was seen in the reactivities of this mutant in Chapter 3. These results suggest that Ub that has been activated by Uba1 and is present as the Uba1~Ub thiolester, and to a lesser extent the Ub-AMP adenylate, becomes preferentially conjugated to the growing Ub chain.

Active Sites Involved in Chain Building

Results provided throughout this chapter point to a distinct role for the active site(s) of Uba1 in the formation of Ub chains. Evidence for the catalytic role of the Uba1 active site cysteine was reinforced by results obtained with the uba1C600A mutant (Figure 5.4). As was shown in Chapter 2, Figure 6, the uba1C600A active site mutant is capable of activating and transferring Ub from its adenylate binding site directly onto the active site cysteine of Ubc1Δ, bypassing its own active site residue, which has been mutated to alanine. When uba1C600A was substituted for wild type Uba1 in ubiquitination reactions containing purified Ubc1Δ~Ub thiolester, we see an increased production of Ubc1Δ-Ub conjugate and the formation of a Ub chain two molecules in length (Figure 5.4 lane 2). The uba1G446V mutant is capable of stimulating Ub chain formation to a greater extent (Figure 5.4, lanes 3 and 6, suggesting that the

active site cysteine on Uba1 enhances the formation of Ub chains, and that the formation of Ub chains is not dependent on the ATP binding site on Uba1.

We have clearly demonstrated that the active site of Ubc1Δ may not necessarily play a major role in the formation of Ub chains when Uba1 is present in the reaction. The presence of Ub chains in reactions containing Ubc1Δ-Ub conjugate that had been pre-treated with iodoacetamide unmistakably illustrates the direct involvement of Uba1 in the assembly of the chain (Figure 5.6, lane 2). In this case, the Ub can come only from the active site on Uba1, as the active site of Ubc1 is irreversibly blocked by treatment with iodoacetamide. As Ub molecules are added to the growing Ub chain by Uba1, they are added preferentially to Lys 48, as elongation is blocked when Ub_{C48} was utilized in these reactions (Figure 5.6, lane 3). The formation of Ub chains is completely inhibited when a reaction containing Ub_{C48} reaction is performed on Ubc1Δ-Ub_{C48} which was pre-incubated with iodoacetamide. This would imply that, with no acceptor cysteine or lysine residue for Ub, it must remain bound to the Uba1 as the thiolester.

These results point to a definitive catalytic role for the active sites of Uba1 in the formation of Ub chains on E2s. While a catalytically inactive Uba1 molecule may not be capable of stimulating chain formation to the extent of wild type Uba1, its role in formation of the Ubc1Δ-Ub conjugate and limited Ub chains is still evident (Figure 5.4). Uba1 may act to bring multiple molecules of Ubc1Δ together, thereby simulating the experiments performed by Hodgins *et al.* (1996), where Ubc1Δ~Ub at high concentrations results in the auto ubiqutination phenomenon. A second possibility is that Uba1 is actually participating catalytically in the formation of Ub chains, either by the transfer of Ub to the active site of Ubc1Δ, or directly to the Ub within the growing chain.

5.5 Conclusion

Recently, identification of the mouse embryo strain A31N has provided results that question the idea that the role of Uba1 is solely the activation of Ub for transfer to an E2, that is, that Uba1 plays no role in the targeting or formation of

Ub chains (Chowdary *et al.*, 1994; Salvat *et al.*, 2000). This cell line was shown to have a defect in Uba1. When grown at a non-permissive temperature, numerous proteins including p53, c-jun and histone 2A accumulated, presumably as a result of not becoming ubiquitinated and therefore degraded. While the accumulation of these specific targets was demonstrated, normal ubiquitination in these cells was not significantly impaired. This result suggests that there may be alternate mechanisms that enable Uba1 to recognize or target directly.

The results presented here point to a more involved role for Uba1 than has previously been postulated. Two main points should be taken from the experiments discussed here. First, Uba1 acts in an ATP and Mg^{2+} dependent fashion to stimulate the formation of Ub chains on the E2 Ubc1Δ (Figures 5.1 and 5.2). This stimulation, while enhanced in the presence of ATP and Mg^{2+} is not dependent on the presence of an activated Ub at the adenylate site (Figure 5.4) and is more likely stimulated by the presence of the Uba1 thiolester. Second, the Uba1 active site cysteine is directly involved in the formation of Ub chains on Ubc1Δ. There is no evidence that Uba1 is capable of conjugating Ub to an internal lysine on a target itself, but Uba1 is indeed capable of conjugating Ub to a growing Ub chain. Treatment of Ubc1Δ-Ub conjugate with iodoacetamide, effectively blocking its active site cysteine, stopped Ub chain formation (Gregori *et al.*, 1990). The introduction of Uba1 into these reactions results in the stimulation of Ub chain formation. This addition occurring, preferentially, at lysine 48 on Ub, at least when Ubc1Δ is the target (Figure 5.6).

The direct involvement of Uba1 in the Ub chain building mechanism would enable this reaction to occur at a faster rate, resulting in the increased degradation of those proteins for which this is required. If chain building were to only occur via the "Bucket Brigade" mechanism, where Ub must first become transferred to an E2 before being added to the chain, the bottle-neck in target construction of the chain be this transfer. Experiments presented in this chapter provide evidence for the catalytic role of Uba1 in the formation of Ub chains and point to a new mechanism for the rapid degradation of a certain subset of target proteins.

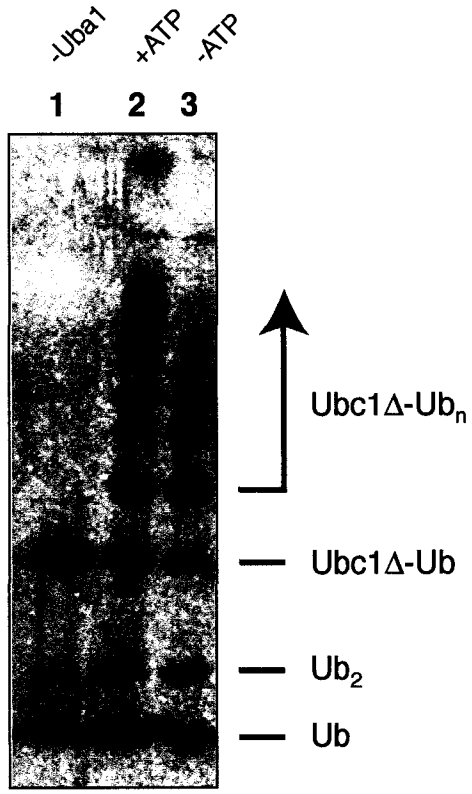

Figure 5.1. **Uba1 Stimulation of Ub Chain Formation**
Ubc1Δ~[^{35}S]Ub thiolester was purified as in Chapter 2, *Experimental Methods* and added to reactions containing Uba1 in the presence or absence of ATP. In lane **1**, 100 nM Ubc1Δ~[^{35}S]Ub thiolester was added to ubiquitination buffer and incubated for 12 hours at 30 °C. Reaction products were precipitated with TCA and resuspended in load mix containing DTT. Samples were subjected to SDS-PAGE and viewed by autoradiography. Lane **2** is identical to lane **1** with the exception that 10 nM Uba1 was added to the reaction prior to the 12 hour incubation. Lane **3** is identical to lane **2** with the exception that ATP was omitted from the ubiquitination buffer.

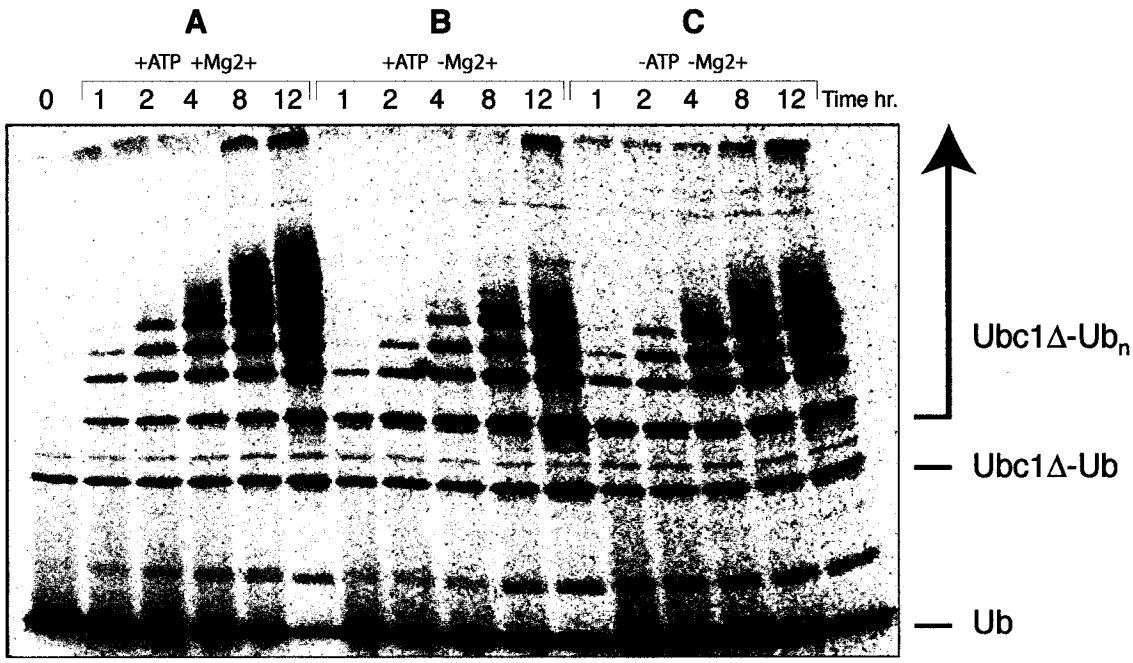

Figure 5.2. **ATP and Mg^{2+} influence on Ub Chain Building**
Time course reactions demonstrating the requirement for ATP and Mg^{2+} for efficient formation of Ub chains on Ubc1Δ. Reactions contained 100 nM Ubc1Δ~[^{35}S]-Ub and 10 nM Uba1 and were processed for a total of 12 hours. Aliquots were removed from the reaction at time points of 0, 1, 2, 4, 8 and 12 hours. Upon removal from the reaction, aliquots were processed as in Figure 4.1 and were visualized using autoradiography. **A**, reactions processed in standard ubiqutination reaction buffer containing ATP and Mg^{2+}. **B**, reactions processed in ubiqutination buffer lacking Mg^{2+}. **C**, reactions processed in ubiqutination buffer lacking both ATP and Mg^{2+}.

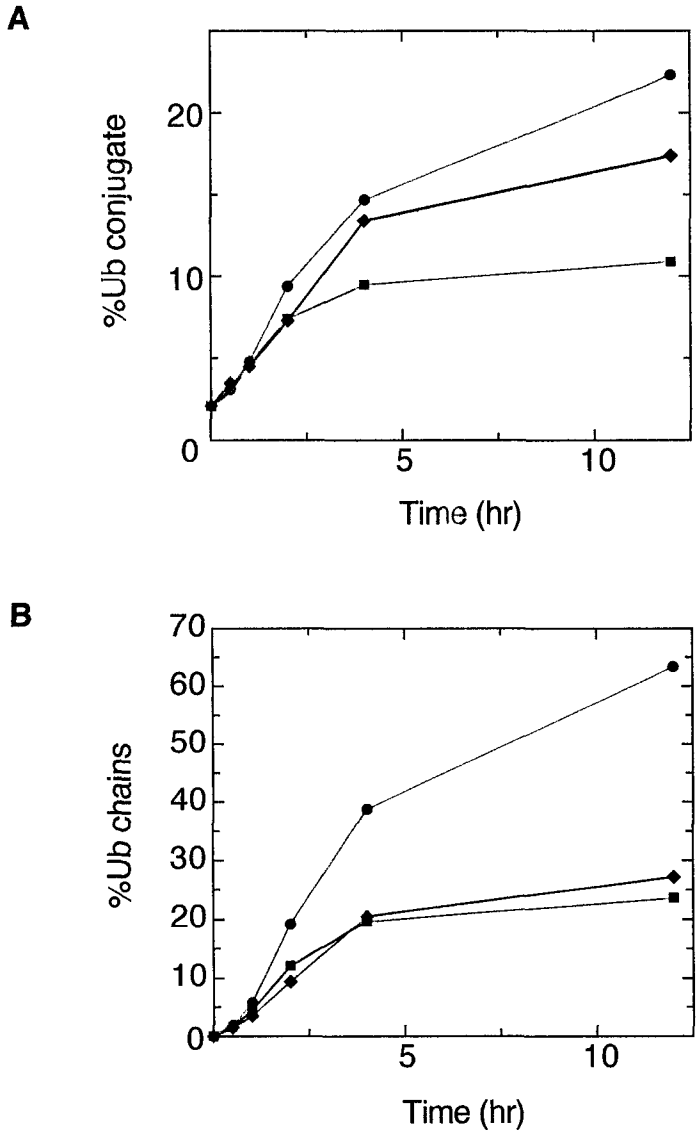

Figure 5.3. **Comparison of [^{35}S]-Ub as Ubc1Δ-Ub Conjugate or Ub Chains** The autoradiograph in Figure 5.2 was scaned and analyzed using densitomitry. Red lines correspond to reactions containing both Mg^{2+} and ATP, green lines correspond to reactions containing only ATP and black lines represent reactions containing neither ATP or Mg^{2+}. **A**, the total amount of Ubc1Δ-[^{35}S]Ub conjugate present in each lane. The total density of each lane was used to determine the average density per Ub contained in the reaction. This was then used to estimate the amount of conjugate present in each of the individual bands. **B**, uses identical methodology as in panel A with the exception that only the [^{35}S]Ub incorporated into multi-Ub chains was measured.

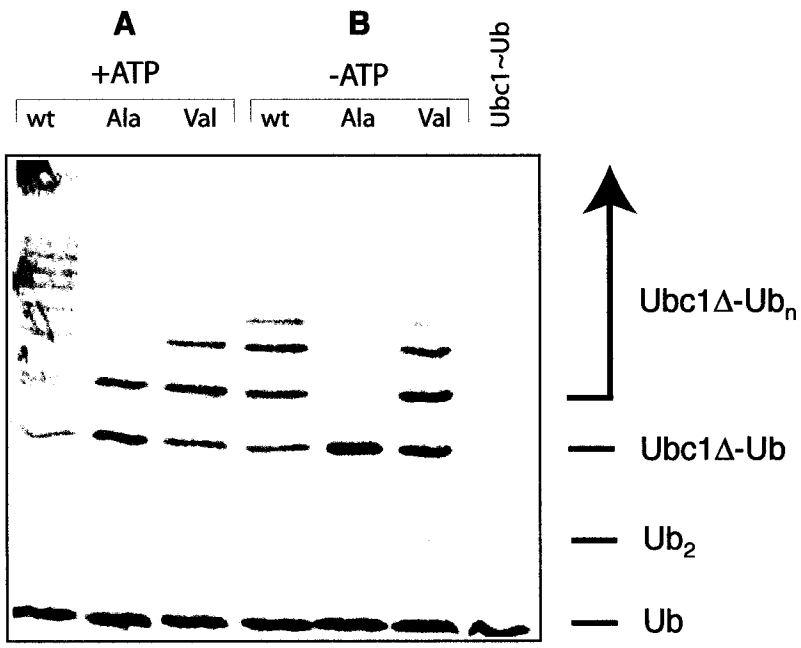

Figure 5.4. **Stimulation of Ub chain Formation by Uba1 and Uba1 mutants** Reactions containing 10 nM Uba1 and 100 nM Ubc1Δ~[^{35}S]Ub were incubated at 30 °C for 1 hour. After incubation, reactions were treated as in Figure 5.1 and products visualized using autoradiography. Uba1, uba1C600A (Ala) and uba1G446V (Val) were tested for their ability to support Ub chain formation. **A**, reacions were performed in standard ubiqutination buffer. **B**, reactions were performed in ubiqutination buffer that lacked ATP. The lane labeled Ubc1~Ub contained only Ubc1Δ~[^{35}S]Ub as a control for conjugate formation in the absence of Uba1 (Ptak *et al.*,1996).

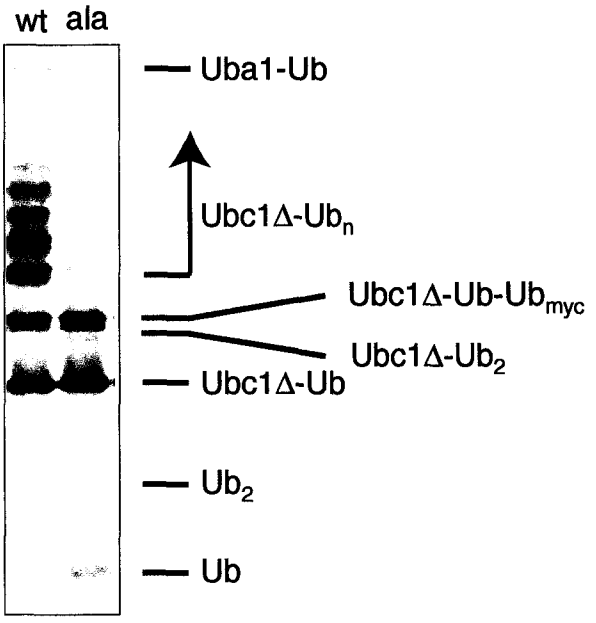

Figure 5.5. **Following the Movement of Ub into multi-Ub chains**
Ubc1Δ~[^{35}S]Ub was purified as described in Chapter 2 and introduced into reactions containing Ub$_{myc}$ (an epitope tagged version of Ub) and either (wt) Uba1 or (ala) uba1C600A. Each reaction contained 10 nM Uba1 or uba1C600A, 100 nM Ubc1Δ~[^{35}S]Ub and 100 nM Ub$_{myc}$ which was included to follow Ub incorporation into newly formed Ub chains. The myc epitope has a molecular mass of 1.5 kDa and inclusion into Ub chains is seen as laddering above normal band positions as illustrated in Figure 5.1. All reactions were performed in ubiqutination buffer, for 60 min at 30 °C. Following completion of the reaction, samples were treated as in Figure 5.1 and were visualized using autoradiography.

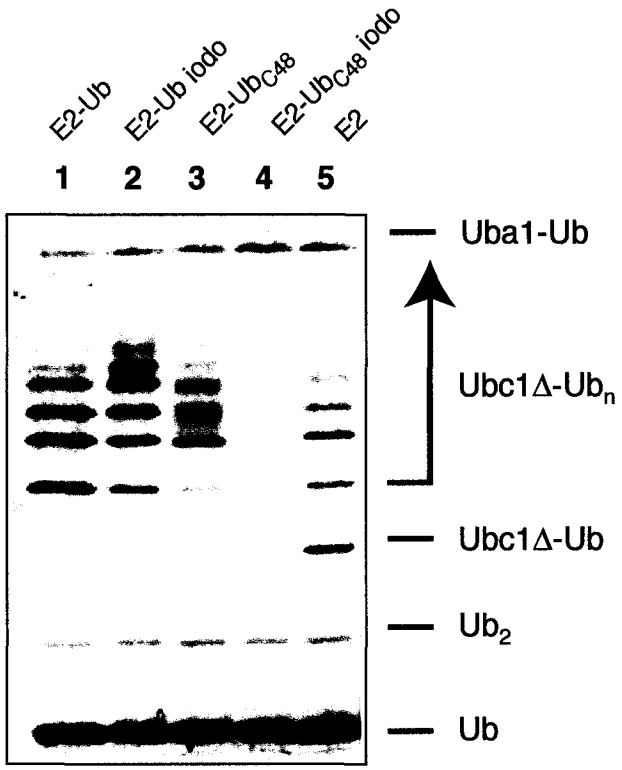

Figure 5.6. **Assembly Direction of Multi-Ub Chain Building**
Uba1~[^{35}S]Ub thiolester was prepared using a back transfer reaction as described in Chapter 2, *Experimental Methods*. The Uba1 thiolester was then tested for its ability to transfer activated [^{35}S]Ub to either the Ubc1Δ-Ub conjugate or an iodoacetamide inactivated species. Reactions contained 50 nM Uba1~[^{35}S]Ub and 25 nM of either Ubc1Δ~Ub thiolester or the Ubc1Δ-Ub conjugates. Iodoacetamide treated conjugates were purified as described in *Experimental Methods* and Ubc1Δ~Ub thiolester was purified as described in Chapter 2. Reactions were performed in ubiqutination buffer for 1 hour at 30 °C. Following completion of the reaction, samples were treated as in Figure 4.1 and were visualized by autoradiography. Lane **1** contains Ubc1Δ-Ub conjugate. Lane **2** contains Ubc1Δ-Ub conjugate that was pre-incubated with iodoacetamide. Lane **3** contains Ubc1Δ-Ub$_{C48}$ conjugate,Ub$_{C48}$ is still capable of forming Ub chains at this position, but treatment with iodoacetamide completely blocks its activity (Gregori *et al.*, 1990). Lane **4** contains Ubc1Δ-Ub$_{C48}$ conjugate that was pre-incubated with iodoacetamide. Lane **5** contains only Ubc1Δ.

5.6 References

Beal, R., Deveraux, Q., Xia, G., Rechsteiner, M., & Pickart, C. (1996). Surface hydrophobic residues of multiubiquitin chains essential for proteolytic targeting. *Proc Natl Acad Sci U S A, 93(2)*, 861-66.

Chau, V., Tobias, J. W., Bachmair, A., Marriott, D., Ecker, D. J., Gonda, D. K., & Varshavsky, A. (1989). A multiubiquitin chain is confined to specific lysine in a targeted short-lived protein. *Science, 243(4898)*, 1576-83.

Chen, Z., & Pickart, C. M. (1990). A 25-kilodalton ubiquitin carrier protein (E2) catalyzes multi-ubiquitin chain synthesis via lysine 48 of ubiquitin. *J Biol Chem, 265(35)*, 21835-42.

Chowdary, D. R., Dermody, J. J., Jha, K. K., & Ozer, H. L. (1994). Accumulation of p53 in a mutant cell line defective in the ubiquitin pathway. *Mol Cell Biol, 14(3)*, 1997-2003.

Ciechanover, A., Finley, D., & Varshavsky, A. (1984). The ubiquitin-mediated proteolytic pathway and mechanisms of energy- dependent intracellular protein degradation. *J Cell Biochem, 24(1)*, 27-53.

Driscoll, J., & Goldberg, A. L. (1990). The proteasome (multicatalytic protease) is a component of the 1500-kDa proteolytic complex which degrades ubiquitin-conjugated proteins. *J Biol Chem, 265(9)*, 4789-92.

Gregori, L., Poosch, M. S., Cousins, G., & Chau, V. (1990). A uniform isopeptide-linked multiubiquitin chain is sufficient to target substrate for degradation in ubiquitin-mediated proteolysis. *J Biol Chem, 265(15)*, 8354-57.

Haas, A. L., & Rose, I. A. (1982). The mechanism of ubiquitin activating enzyme. A kinetic and equilibrium analysis. *J Biol Chem, 257(17)*, 10329-37.

Haas, A. L., Warms, J. V., Hershko, A., & Rose, I. A. (1982). Ubiquitin-activating enzyme. Mechanism and role in protein-ubiquitin conjugation. *J Biol Chem, 257(5)*, 2543-48.

Haas, A. L., Warms, J. V., & Rose, I. A. (1983). Ubiquitin adenylate: structure and role in ubiquitin activation. *Biochemistry, 22(19)*, 4388-94.

Haldeman, M. T., Finley, D., & Pickart, C. M. (1995). Dynamics of ubiquitin conjugation during erythroid differentiation in vitro. *J Biol Chem, 270(16)*, 9507-16.

Hershko, A. (1983). Ubiquitin: roles in protein modification and breakdown. *Cell, 34(1)*, 11-12.

Hershko, A., Heller, H., Elias, S., & Ciechanover, A. (1983). Components of ubiquitin-protein ligase system. Resolution, affinity purification, and role in protein breakdown. *J Biol Chem, 258(13)*, 8206-14.

Hodgins, R., Gwozd, C., Arnason, T., Cummings, M., & Ellison, M. J. (1996). The tail of a ubiquitin-conjugating enzyme redirects multi-ubiquitin chain synthesis from the lysine 48-linked configuration to a novel nonlysine-linked form. *J Biol Chem, 271(46)*, 28766-71.

Hough, R., Pratt, G., & Rechsteiner, M. (1986). Ubiquitin-lysozyme conjugates. Identification and characterization of an ATP-dependent protease from rabbit reticulocyte lysates. *J Biol Chem, 261(5)*, 2400-08.

Hough, R., & Rechsteiner, M. (1986). Ubiquitin-lysozyme conjugates. Purification and susceptibility to proteolysis. *J Biol Chem, 261(5)*, 2391-99.

Jones, J. G., Otieno, S., Barnard, E. A., & Bhargava, A. K. (1975). Essential and nonessential thiols of yeast hexokinase. Reactions with iodoacetate and iodoacetamide. *Biochemistry, 14(11)*, 2396-403..

Lohnas, G. L., Roberts, S. F., Pilon, A., & Tramontano, A. (1998). Epitope-specific antibody and suppression of autoantibody responses against a hybrid self protein. *J Immunol, 161(12)*, 6518-25.

Nickel, B. E., & Davie, J. R. (1989). Structure of polyubiquitinated histone H2A. *Biochemistry, 28(3)*, 964-68.

Pickart, C. M., Kasperek, E. M., Beal, R., & Kim, A. (1994). Substrate properties of site-specific mutant ubiquitin protein (G76A) reveal unexpected mechanistic features of ubiquitin-activating enzyme (E1). *J Biol Chem, 269(10)*, 7115-23.

Salvat, C., Acquaviva, C., Scheffner, M., Robbins, I., Piechaczyk, M., & Jariel-Encontre, I. (2000). Molecular characterization of the thermosensitive E1 ubiquitin-activating enzyme cell mutant A31N-ts20. Requirements upon different levels of E1 for the ubiquitination/degradation of the various protein substrates in vivo. *Eur J Biochem, 267(12)*, 3712-22.

Spence, J., Sadis, S., Haas, A. L., & Finley, D. (1995). A ubiquitin mutant with specific defects in DNA repair and multiubiquitination. *Mol Cell Biol, 15(3)*, 1265-73.

van Nocker, S., & Vierstra, R. D. (1991). Cloning and characterization of a 20-kDa ubiquitin carrier protein from wheat that catalyzes multiubiquitin chain formation in vitro. *Proc Natl Acad Sci U S A, 88(22)*, 10297-301.

van Nocker, S., & Vierstra, R. D. (1993). Multiubiquitin chains linked through lysine 48 are abundant in vivo and are competent intermediates in the ubiquitin proteolytic pathway. *J Biol Chem, 268(33)*, 24766-73.

Zhu, D. X., Zhang, A., Zhu, N. C., Xu, L. X., Deutsch, H. F., & Han, K. K. (1986). Investigations of primary and secondary structure of porcine ubiquitin. Its N epsilon-acetylated lysine derivative. *Int J Biochem, 18(5)*, 473-76.

Chapter 6

Summary and Conclusions

6.1 Introduction

This thesis examines the mechanism of Ub activation and chain formation through the action of the eukaryotic protein, Uba1. We began by constructing two key Uba1 active site mutants, one at the catalytic cysteine residue (600) and the other at a conserved glycine that is found within a classical ATP binding motif (446) known as a Walker fold (Walker *et al.*, 1982) (Chapter 2). As expected, the nucleotide binding site mutant uba1G446V was not capable of activating Ub through the formation of adenylate, but was able to accept Ub through a transthiolation reaction at its active site cysteine. Conversely, the active site cysteine mutant, uba1C600A, was capable of activating Ub to the adenylate, but was not capable of forming the Ub thiolester. Using these mutations in standard Ubiqutination reactions with the E2, Ubc1Δ, we have determined that the active site cysteines of these proteins can be arranged in such a way as to allow the transfer of Ub directly from the Ub-AMP to either active site on Uba1 or the E2, Ubc1. This observation demonstrates that the two active sites of Uba1 and the active site of Ubc1 are close together during some point in the reaction, a result that served as an important constraint in our subsequent modeling experiments.

The construction of a Uba1 active site homology model has allowed us to propose the location of two Ub binding sites on its surface, one that accommodates Ub as the adenylate and the other as the thiolester. This model also provided insight into the possible positioning of the active site cysteine residue. We hypothesize that the active site cysteine is found on a surface loop,

of indeterminate length, at position that sits above the nucleotide-binding site (Chapter 4). More specifically, the active site cysteine must approach the α phosphate of ATP, thereby allowing the formation of the Ub thiolester. The potential for movement of the active site cysteine residue was demonstrated using dynamics experiments of the 80 residue cysteine containing domain in Uba3. These experiments illustrated that the two linker regions that connect the nucleotide and active site cysteine domains are quite flexible within a simulation and can accommodate the conformational shift from an open to a closed active site, thereby bringing the active site cysteine residue into close proximity with the bound Ub adenylate.

Using the model of Uba1 and the structure of a Ubc1~Ub thiolester, the potential for an interaction between the active site cysteines in these two proteins was examined (Chapters 3 and 5), to produce a model that was consistent for the observed transfer of Ub directly from the adenylate-binding site to the active site cysteine residue of Ubc1. Finally, using similar methods to those used in determining the mechanistic role of the Uba1 active sites in Ub activation, Uba1's role in the formation of Ub chains was explored (Chapter 4).

6.2 Uba1 Model and Active Site Arrangement

When building a molecular model of a protein, the ultimate goal is to have it agree with the actual molecular structure of the protein in question. But as often is the case, we do not have much structural data with which to compare these models. We must therefore define the error within a model by considering its sequence identity to empirically derived structures of homologous proteins. Figure 6.1 compares the reliability of homology models with the RMS differences between the final positions of α carbons within the model itself and those of corresponding atoms in the templates. Models with high sequence identity to template structures will generally produce more reliable results with lower RMS values to actual structures. Even without an empirically derived structure for comparison, we can often immediately recognize problems in a model. These

errors present themselves immediately as exposed hydrophobic residues or out-of-range Φ and Ψ angles, as determined by a Ramachandran plot (Ramachandran *et al.*, 1963). That said, often a simple visual inspection of the underlying arrangement of residues will provide some degree of validity to a homology model.

Chapter 4 discussed the creation of such a model, which provided us with only a limited view of the nucleotide-binding domain of Uba1. In this model, we suggest that the Ub-adenylate and the Ub-thiolester are formed at proximal positions on the surface of Uba1. Dynamics experiments on the 80 residue helical domain of Uba3 suggest that it could exist in either an "open" or "closed" conformation, providing access for Ub and ATP to their binding sites (Chapter 4, Figure 17). While it is not known if this domain is present in Uba1, it stands to reason that at least some portion of it must comprise Uba1's active site. This is clear due to the structural conservation of the regions surrounding it in the structures of the Uba3 and MoeB templates. Future experiments are obviously required to validate this mechanism and determine the actual physical structure of this domain at each step of Ub activation.

In addition to the modeling experiments that were carried out on the Uba1 active site loop, we created several active site mutants of the Uba1 active sites. In particular, the mutants uba1C600A and uba1G446V, provided a considerable amount of insight into the activation of Ub and the interplay between the two Uba1 active sites. Experiments with these Uba1 mutants substantiated the necessity for the close spatial organization of the active sites between Uba1 and Ubc1Δ. This was demonstrated by the direct transfer of Ub from Ub-AMP to Ubc1Δ in a reaction that occurred in the absence of any bound Uba1 thiolester, such as with the uba1C600A mutant (Chapter 2, Figure 6).

6.3 Uba1 Involvement In Ub Chain Formation

Results presented in Chapter 5 suggest a catalytic role for Uba1 in the mechanism of Ub chain construction. Two significant effects were observed while examining Uba1's involvement in Ub chain building. The first was the increased rate of chain formation upon inclusion of Uba1 in ubiquitination reactions (Chapter 5, Figure 1). Second, was the direct catalytic involvement of the Uba1 active site cysteine (cys 600) in this reaction (Chapter 5, Figure 6). Since tagging with a Ub chain is a prerequisite for protein degradation, the direct involvement of Uba1 in the Ub chain building mechanism would enable this reaction proceed more rapidly following the initial addition of Ub to a target by an E2.

6.4 A Model of Ub Activation and Chain Building

A model of Ub activation by Uba1 can be suggested, based upon the results obtained in Chapters 2, 3 and 4 (Figure 6.2). The model presented in Chapter 4 accounts for the requirement that Uba1 must be capable of activating and binding two molecules of Ub simultaneously (Haas and Rose, 1982). Ub enters the primary binding site, with its carboxy terminal glycine in position to become activated by ATP. The primary Ub binding site consists of a groove terminating in the ATP binding site that contains the Walker Fold motif at its base (Walker *et al.*, 1982). Immediately following the activation of Ub, Ub must be displaced from the primary binding site, resulting in the release of AMP and PPi. The Ub tail then enters the secondary binding site, which is perpendicular to the primary binding site. A second Ub can then enter the primary binding site, where it then becomes activated by a second molecule of ATP in a reaction identical to the activation of the first molecule of Ub, which now sits at the secondary binding site.

Domains in Uba3 and MoeB

One of the most challenging issues encountered while building the Uba1 active site model, were the differences between the two templates used in its construction. Both MoeB and Uba3 share similar folds within a common nucleotide-binding domain within their structures (Lake et al., 2001; Walden et al., 2003). However, Uba3 contains a large eighty residue domain constrained at the same position as the much smaller loop in MoeB. Several alignments within the active site regions of Uba3, MoeB and Uba1, were unable to distinguish where the active site cysteine in Uba1 would be positioned (Chapter 4, Figure 8). The only conclusion that we were able to make was that the active site cysteine residue must sit at a location, which enables its movement into the nucleotide binding site to pick up the activated Ub adenylate.

An additional structural motif found in Uba3 was the presence of a domain, which is similar to the fold of Ub (Walden *et al.*, 2003). We were unable to determine if Uba1 contains a corresponding Ub like domain, as sequence homology in this region is extremely weak. Alignments between the Human and Yeast orthologs of Uba3 demonstrate that this domain is not present in the *S. cerevisiae* Uba3 (Chapter 4, Figure 7). However, the presence of this domain, or the potential for Ub being located at this site would not hinder the positioning of Ubc1Δ on our model (Chapter 4). If the Ub like domain in Uba3 is an evolutionary addition and Uba1 does not contain such a domain, this site may constitute a third binding site for Ub on the surface of Uba1 (Figure 6.2). The presence of a third Ub binding domain on Uba1 could enable it to participate in Ub chain formation. While we did not include this domain in our model, due to lack of homology, this region could enable Uba1 to bind Ub that has become conjugated to an E2, or for that matter a target protein. The arrangement of three ubiquitins bound closely on the interacting surfaces of Uba1 and E2, may provide the opportunity for direct conjugation between Ub molecules at lysine 48 residues. This binding arrangement may also explain the presence of free Ub_2 chains in all chain-building reactions that contain Uba1 (Chapter 2). While this model of Ub

activation is preliminary and still requires substantial biochemical investigation, evidence presented here suggests an alternate role for Uba1 in this pathway.

6.5 The interaction Between Uba1 and Ubc1Δ

As a tool for determining the interface between two proteins, NMR has become extremely useful in cases where traditional crystallography is not possible. Using the structure of the Ubc1Δ~Ub thiolester, presented in Chapter 3, we were able to produce a low-resolution model of its interaction with Uba1 and speculate on the mechanism of Ub transfer. These modeling experiments were validated by experiments demonstrating the interplay between the three Ub binding sites (two cysteine and one nucleotide) contained in this complex (Chapter 2, Figure 6). The structure of the Ubc1Δ~Ub thiolester also reveals the first glimpse of the surface recognition between Ub and an E2, providing insight into the three dimensional arrangement of the Ub/E2/E3 complex (Chapter 3, Figure 7).

6.6 Future Directions

NMR Studies of the Ub Interface with Uba1

An obvious experimental goal is to obtain a three dimensional structure of Uba1, or its active site domain. Recently NMR techniques have been developed that allow the investigator to obtain structural information on proteins of approximately 80 kDa in molecular weight (Tugarinov and Kay, 2003)(Tugarinov *et al.*, 2002). NMR studies of the Ubc1Δ~Ub thiolester provided valuable information regarding interactions between E2 and Ub. Work in our laboratory has correlated Ub interactions with additional E2 proteins, Ubc13 and Mms2 (McKenna *et al.*, 2003a; McKenna *et al.*, 2003b). NMR studies have also determined the binding pattern of Ub to the ubiquitin-interacting motif found in the proteasome (Fisher *et al.*, 2003). Uba1 may not be amenable to study by NMR because of its large size and the difficulty in purifying large amounts of this protein; Ub however has no such limitations. As we have already assigned residues involved in Ub

interaction with Ubc1Δ, purification of sufficient quantities of Uba1 may allow the interacting surfaces of Ub with Uba1 to be mapped. The Uba1 mutants, described in Chapter 2, could be used to study the specific binding positions of Ub on Uba1, ubaC600A for the Ub-AMP site and uba1G446V for the Ub-thiolester site. Experiments, such as these, can provide additional evidence to support the presence of two, or even three, independent Ub binding sites on Uba1 (Chapter 4)

Uba1 Truncations

The multiple domain structure of Uba1 has been suggested by the presence of homologs to Uba1 that involved in the activation of UBL proteins. Initial experiments performed on a truncation that corresponds to the active site of Uba1, resulted in the observation that it was incapable of activating Ub (Chapter 2, Figure 15). This result may suggest a role for either the amino or carboxy terminus of Uba1 in the recognition or activation of Ub. The activators of *S. cerevisiae* Rub1 and Smt3 are proteins that correspond to the active site region of Uba1 (Chapter 2, Figure 4). For the activation of either Rub1 or Smt3 to occur, a protein that is homologous to the amino terminus of Uba1 must be present (Liakopoulos *et al.*, 1998; Johnson *et al.*, 1997). In addition to the two domains corresponding to the amino and active site regions of Uba1, Uba2, the activator of Rub1, also lacks a region that corresponds to Uba1's carboxy terminus. Amino and carboxy terminal truncations of Uba1, corresponding to these regions may provide information about their interactions with both Ub and E2.

Uba1 Kinetics

The precise rate of Ub activation by Uba1 have been determined previously, using studies designed to observe the hydrolysis of ATP to AMP and PPi (Haas et al., 1982). Unfortunately, the techniques used here were unable to provide information regarding the rate of ATP hydrolysis upon the formation of the Ub-thiolester versus Ub-AMP. The use of filter binding assays could increase accuracy of the kinetic experiments discussed in Chapter 3. These experiments would involve measuring the actual incorporation into Ub of AMP from [α^{32}P]ATP,

thereby facilitating the quantitation of bound Ub-AMP. The rate of ATP hydrolysis could also be determined by measuring the release of [^{32}P]Pi from [γ^{32}P]ATP using methods such as thin layer chromatography (Sadis and Hightower, 1992).

Uba1 Surface Mutations

The mutations that were created in the active site cysteine and nucleotide-binding site were able to provide a biochemical rationale for the modeling of Ub activation by Uba1. These mutations were specifically produced to validate the active sites of Uba1 and did not provide data on specific binding interactions between Ub and Uba1. Mutations in residues lining the predicted Uba1/Ub interface could differentiate among those residues that interfere with Ub-adenylate formation, initial Ub interaction, transfer to Ubc1Δ or transfer to the internal cysteine of Uba1 itself. For that matter, surface mutations on the surface of Ub, specific to regions shown to interact with Uba1 in our model, would provide information lending more precision to the model of their interaction.

Using the Uba1 homology model as a guide, we have selected four key mutations that would enable us to test the predicted placement of Ub on its surface (Figure 6.3). The first mutation occurs within the secondary Ub binding site, as identified in the structure of MoaD/MoeB (Chapter 4, Figure 12). A conserved glycine (Gly 567) sits at the base of this surface cleft, its lack of a side chain, presumably providing a path for the tail of Ub. A conservative mutation to the slightly larger side chain of alanine should provide us with data regarding the availability of this site for formation of the Ub thiolester. If this site were the location of thiolester formation, we would expect to see an overall decrease in that species during standard Ubiquitination reactions. However, if this site was actually the location of both adenylate and thiolester formation, then we would expect to see a decrease in the formation of both species. Results in Chapter 2 described the differentiation between Ub bound to Uba1 as either the adenylate or thiolester and as such could be used as a measure of this mutants effect on either reaction.

Due to the lack of sequence identity in the amino terminal portion of Uba1, it is difficult to assign specific mutations within the primary binding site (Figure 4.10). As such, we suggest mutations in conserved residues that line the side of this cleft. Asn 477 and Gln 482 are residues that may participate in coordinating the tail of Ub as it binds the primary binding site, but may also be involved in the catalytic mechanism of both Ub adenylate and thiolester formation. While these mutations may not enable us to distinguish the two binding sites, in the absence of adenylate formation, coupled with the mutation at Gly 567, should enable us to decipher which binding site is responsible for adenylate formation.

An important feature of cysteine proteases in general is the high nucleophilicity of the sulfur atom within the active site cysteine residue. This is due to the fact that at ph values where the enzyme is active, the sulfur is present as the thiolate anion. The mechanism of Ub thiolester formation and formation of the thiolate ion, a reaction that is analogous to that of proteolysis within the cysteine proteases, would most likely occur through the action of a catalytic histidine residue that is found within the active site (Yuan *et al.*, 1996; Gubba *et al.*, 2000). Interestingly, neither Uba3 nor MoeB contain a catalytic histidine residue within their nucleotide binding sites. Furthermore, MoeB does not contain a histidine that could participate catalytically in the formation of the thiolate, and additional catalytic residues are most likely supplied by the sulfurtransferase that binds MoeB. Uba3 contains a histidine residue within the 80 residue helical domain and upon movement of the active site cysteine into the nucleotide binding site may be capable of participating catalytically in the formation of the Nedd8 thiolester (Chapter 4, Figure 17). This histidine residue is also present in Uba1 as well as in several other Uba1 like proteins (Walden *et al.*, 2003) and could be responsible for the deprotonation of the catalytic cysteine residues. We propose that the creation of an alanine mutation of His 611 in *S. cerevisiae* Uba1 could lead to a general decrease in the formation of thiolester, but not to a decrease in Uba1's ability to synthesize the Ub-adenylate. This mutant could be tested under reaction conditions similar to those used throughout Chapter 2.

6.7 Conclusion

As biochemical research progresses, understanding of enzyme catalysis and the intricate interactions and dynamics between protein components must remain a priority. This is clearly true in the new field of proteomics, where the ultimate goal is to understand how each protein participates in a complex network of interactions. In some ways, this thesis can be viewed as an indication of the biochemical and technological challenges presented by such a goal. A variety of conceptually different techniques have been used to create a model of Ub activation by Uba1 and its subsequent transfer to an E2. These techniques include: 1) molecular biology, for the creation of specific mutations within the active sites of Uba1; 2) genetics, to observe the affect of these mutations *in vivo*; and 3) biochemistry, to study the *in vitro* behavior of the mutated Uba1 proteins. Computer simulations allowed us to create a model, while the other techniques described above allowed us to validate the model. As the number of known protein structures grows and the information collected about them increases, these techniques must be used together to provide a complete picture of both protein structure and function.

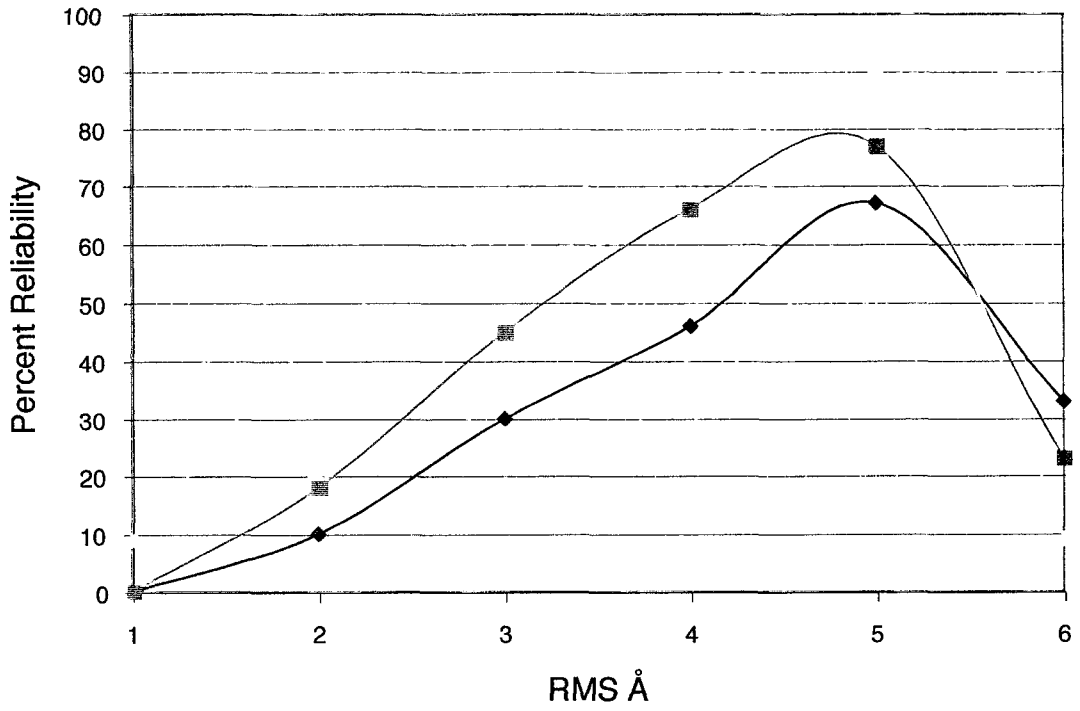

Figure 6.1. **Reliability of Homology Models**
Data derived from the Swiss3D server (Schwede *et al.*, 2003) illustrating the reliability of homology models as a function of their root mean squared values to empirically derived structures. Diamonds represent models generated based upon sequences with 25-29% identity. Squares represent models generated based upon sequences with 30-39% identity. Triangles represent models based upon sequences with 40-49% identity. This plot clearly shows higher reliability at lower RMS values with greater sequence identity.

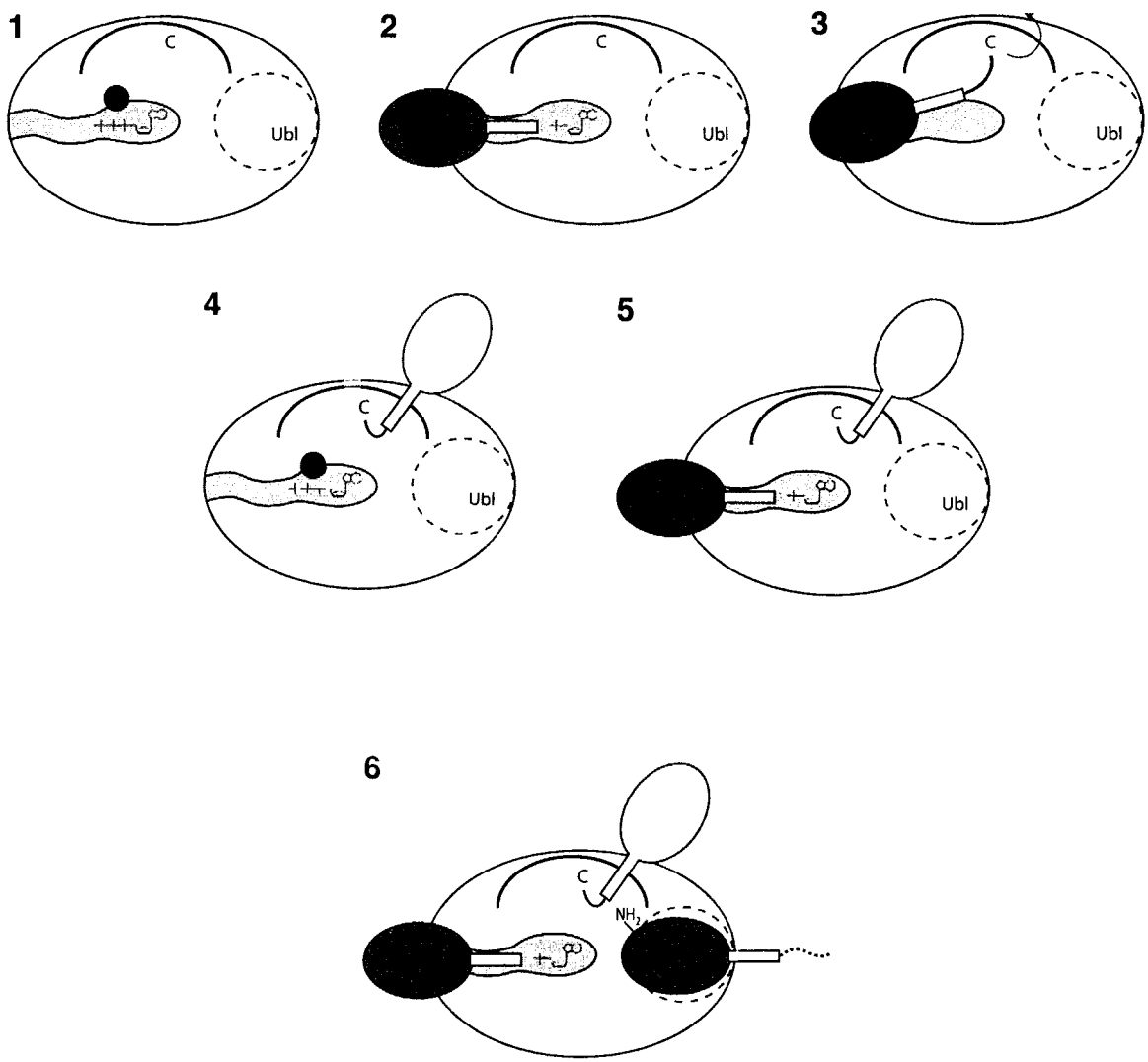

Figure 6.2. **Model of Ub Activation by Uba1**
Ub activation occurs by way of a six step sequence of events. First, binding of ATP and Mg^{2+} prepares the primary Ub binding site for accepting Ub (red) (**1**) The bound ATP then undergoes a dehydration reaction with the carboxy terminal glycine of Ub (**2**) The immediate transfer of Ub to the active site cysteine then occurs and Ub becomes displaced into the secondary binding site (yellow) (**3**) This is followed by the binding of a second ATP and Mg^{2+} (**4**) and another molecule of Ub at the primary binding site (red) (**5**) At this point Uba1 is fully charged with two molecules of activated Ub, one as the thiolester and one as the Ub-AMP adenylate. (**6**) represents the possible orientation of a third molecule of Ub (blue) to become conjugated to the activated Ub at an internal lysine reside resulting in the formation of Ub_2 chains. The tertiary binding site may be located at the position of the Ub like domain found in Uba3 (grey circle Ubl) (Walden *et al.*, 2003).

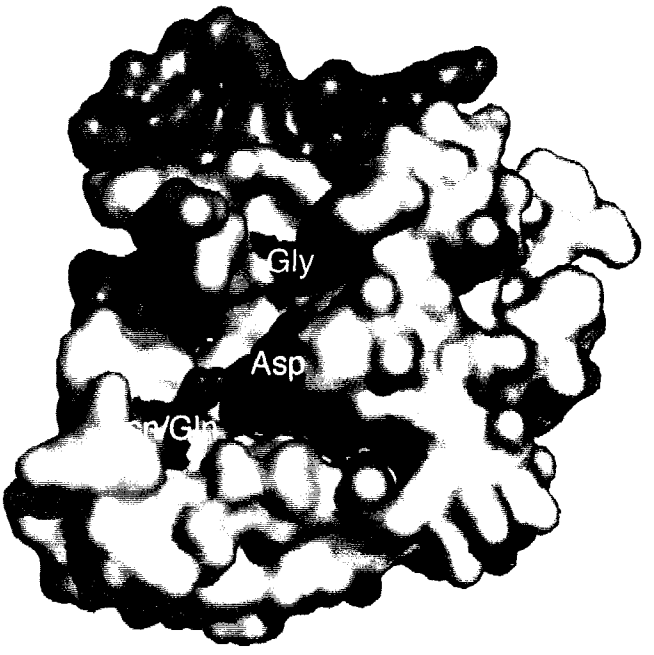

Figure 6.3. **Uba1 Mutagenisis**
The Uba1 active site model is shown in grey, with ATP bound at the nucleotide binding site (fuschia). Potential mutagenisis targets on the surface of Uba1 are highlighted in red. These residues have been chosen based on their positions within the nucleotide binding site and the binding sites for Ub. These positions include Asn 477 and Gln 482, which have been suggested to participate in the catalysis of Ub adenylate formation. Residue 567 would introduce a glycine to alanine mutation, to examine the role of the secondary binding site in the formation of adenylate and thiolester. Finally Asp 130 in MoeB was shown to coordinate magnesium and could therefore be involved in the binding of ATP at the nucleotide binding site.

6.8. References

Fisher, R. D., Wang, B., Alam, S. L., Higginson, D. S., Robinson, H., Sundquist, W. I., & Hill, C. P. (2003). Structure and Ubiquitin Binding of the Ubiquitin-interacting Motif. *J Biol Chem, 278(31)*, 28976-84.

Gubba, S., Cipriano, V., & Musser, J. M. (2000). Replacement of histidine 340 with alanine inactivates the group A Streptococcus extracellular cysteine protease virulence factor. *Infect Immun, 68(6)*, 3716-19.

Haas, A. L., & Rose, I. A. (1982). The mechanism of ubiquitin activating enzyme. A kinetic and equilibrium analysis. *J Biol Chem, 257(17)*, 10329-37.

Haas, A. L., Warms, J. V., & Rose, I. A. (1983). Ubiquitin adenylate: structure and role in ubiquitin activation. *Biochemistry, 22(19)*, 4388-94.

Hamilton, K. S., Ellison, M. J., Barber, K. R., Williams, R. S., Huzil, J. T., McKenna, S., Ptak, C., Glover, M., & Shaw, G. S. (2001). Structure of a conjugating enzyme-ubiquitin thiolester intermediate reveals a novel role for the ubiquitin tail. *Structure (Camb), 9(10)*, 897-904.

Hodgins, R., Gwozd, C., Arnason, T., Cummings, M., & Ellison, M. J. (1996). The tail of a ubiquitin-conjugating enzyme redirects multi-ubiquitin chain synthesis from the lysine 48-linked configuration to a novel nonlysine-linked form. *J Biol Chem, 271(46)*, 28766-71.

Johnson, E. S., Schwienhorst, I., Dohmen, R. J., & Blobel, G. (1997). The ubiquitin-like protein Smt3p is activated for conjugation to other proteins by an Aos1p/Uba2p heterodimer. *Embo J, 16(18)*, 5509-19.

Lake, M. W., Wuebbens, M. M., Rajagopalan, K. V., & Schindelin, H. (2001). Mechanism of ubiquitin activation revealed by the structure of a bacterial MoeB-MoaD complex. *Nature, 414(6861)*, 325-9..

Liakopoulos, D., Doenges, G., Matuschewski, K., & Jentsch, S. (1998). A novel protein modification pathway related to the ubiquitin system. *Embo J, 17(8)*, 2208-14.

McKenna, S., Hu, J., Moraes, T., Xiao, W., Ellison, M. J., & Spyracopoulos, L. (2003a). Energetics and Specificity of Interactions within Ub.Uev.Ubc13 Human Ubiquitin Conjugation Complexes. *Biochemistry, 42(26)*, 7922-30.

McKenna, S., Moraes, T., Pastushok, L., Ptak, C., Xiao, W., Spyracopoulos, L., & Ellison, M. J. (2003b). An NMR-based model of the ubiquitin-bound human ubiquitin conjugation complex Mms2.Ubc13. The structural basis for lysine 63 chain catalysis. *J Biol Chem, 278(15)*, 13151-58.

Ramachandran, G. N., Ramakrishnan, C., & Sasiekharan, V. (1963). Stereochemistry of Polypeptide Chain Configuration. *Journal of Molecular Biology, 7*, 95-99.

Sadis, S., & Hightower, L. E. (1992). Unfolded proteins stimulate molecular chaperone Hsc70 ATPase by accelerating ADP/ATP exchange. *Biochemistry, 31(39)*, 9406-12.

Schwede, T., Kopp, J., Guex, N., & Peitsch, M. C. (2003). SWISS-MODEL: an automated protein homology-modeling server. *Nucleic Acids Res, 31(13)*, 3381-85.

Tugarinov, V., & Kay, L. E. (2003). Quantitative NMR studies of high molecular weight proteins: application to domain orientation and ligand binding in the 723 residue enzyme malate synthase G. *J Mol Biol, 327(5)*, 1121-33.

Tugarinov, V., Muhandiram, R., Ayed, A., & Kay, L. E. (2002). Four-dimensional NMR spectroscopy of a 723-residue protein: chemical shift assignments and secondary structure of malate synthase g. *J Am Chem Soc, 124(34)*, 10025-35.

Walden, H., Podgorski, M. S., & Schulman, B. A. (2003). Insights into the ubiquitin transfer cascade from the structure of the activating enzyme for NEDD8. *Nature, 422(6929)*, 330-34.

Walker, J. E., Eberle, A., Gay, N. J., Runswick, M. J., & Saraste, M. (1982). Conservation of structure in proton-translocating ATPases of Escherichia coli and mitochondria. *Biochem Soc Trans, 10(4)*, 203-06.

Yuan, L., Nelson, B. A., & Caryl, G. (1996). The catalytic cysteine and histidine in the plant acyl-acyl carrier protein thioesterases. *J Biol Chem, 271(7)*, 3417-19.